ORIGIN AND SIGNIFICANCE OF CLAY MINERALS IN MESOZOIC SHALES OF THE SCOTIAN BASIN

by

Gregory Strathdee

A Thesis Submitted to Saint Mary's University, Halifax, Nova Scotia,
in Partial Fulfillment of the Requirements for the
Degree of Master of Science in Applied Science

September 4, 2012, Halifax, Nova Scotia

Approved:	Dr. Georgia Pe-Piper Supervisor Department of Geology
Approved:	Dr. Michael Parsons External Examiner Environmental Geochemistry, NRC Geological Survey of Canada (Atlantic)
Approved:	Dr. David J.W. Piper Supervisory Committee Member Bedford Institute of Oceanography
Approved:	Dr. Jason Clyburne Supervisory Committee Member Department of Chemistry & Environmental Science
Approved:	Dr. Kevin Vessey Dean of Graduate Studies
Date:	September 4, 2012

Origin and Significance of Clay Minerals in Mesozoic Shales of the Scotian Basin

By Greg Strathdee

ABSTRACT

Upper Jurassic–Lower Cretaceous shales of the Scotian Basin, offshore Nova Scotia, are a primary source of hydrocarbons and of the basinal fluids that affected diagenesis of sandstone reservoirs. This study documents and interprets variability in provenance, early diagenesis and burial diagenesis of clay minerals. A total of 108 shale samples from 16 wells in the Scotian Basin were analyzed with X-ray diffraction using bulk random sidepack and <2 µm oriented mounts.

The observed uniformity of clays present, including abundant mixed-layer clays, reflects detrital supply from the Canadian Shield and the Appalachian orogen, followed by trends of burial diagenesis known in other basins. Climate variability is masked by diagenetic processes. Enhanced supply from the Meguma Terrane in the Hauterivian-Aptian is marked by higher Mg chlorite and muscovite, erosion of volcanic products yielded smectite, whereas rapid denudation of inboard metamorphic terranes is recorded in the Albian by higher illite crystallinity.

ACKNOWLEDGEMENTS

I would like to thank my supervisors Dr. David J.W. Piper and Dr. Georgia Pe-Piper for all their advice and guidance which provided me the tools and knowledge to make this project a success.

Thanks to my committee Dr. David J.W. Piper, Dr. Georgia Pe-Piper and Dr. Jason Clyburne, for their time and guidance.

Guidance and support from Owen Brown of the Geological Survey of Canada (Bedford Institute of Oceanography) was instrumental in preparing the samples for XRD analysis. His time, energy and lab space were very much appreciated. Thanks to Bill LeBlanc of the Geological Survey of Canada (Bedford Institute of Oceanography) for providing his time to run the analyses. Thanks to Wayne Prime of the Geological Survey of Canada (Bedford Institute of Oceanography) for providing his time to repair multiple computer problems.

Thanks to the Geological Survey of Canada for providing a workspace for me to complete this project. Thanks to the Canada-Nova Scotia Offshore Petroleum Board for providing the samples that this project is based on.

I would like to dedicate this work to my daughter Asha Rhiannon Strathdee who was born in the middle of this project. She added a level of difficulty to completing this that I never expected but at the same time the joy of having her and the prospects of life after this project are more exciting than words can describe.

A special thanks to my partner and "baby mama", Mandy MacLean who unfortunately was virtually a single mom during the last three to four months of this project but has done an amazing job in supporting me and caring for our beautiful daughter. This would not have been possible without you. Thanks to Granny Mac for all the help and to my family for all their support and encouragement throughout my education.

TABLE OF CONTENTS

LIST OF TABLES

LIST OF FIGURES

CHAPTER 1: INTRODUCTION

1.1 INTRODUCTION

The Scotian Basin is a series of plateaus and sub-basins located off the eastern coast of Canada (Figure 1.1). The Mesozoic shales (primarily the Mid Jurassic to Mid Cretaceous) of the Scotian Basin are the primary source of oil and gas to offshore petroleum reservoirs in Jurassic limestones and Cretaceous sandstones (Bell & Campbell, 1990) (Figure 1.2). Compaction of these shales influenced the composition of the basinal fluids that affected diagenesis of sandstones. The mineralogical composition of the shales in the Scotian Basin is not well known. Understanding clay minerals can lead to a better understanding of paleoclimates, depositional environments, provenance, oil and gas reservoir quality, oil and gas generation and migration and thermal conditions with burial.

The composition of clays deposited in a basin depends on detrital supply, mostly through rivers. Clay minerals that are supplied by rivers have two main sources. They can be directly reworked from older shales, if from a more mountainous region. In this case, the clay mineral composition is inherited. They can also be transported from weathered products such as soil, if the source region is more flat. In this case the composition would reflect weathering conditions and climate. There are many factors that influence the composition of minerals in a sedimentary basin. This study examines three factors that had a major influence on the mineral composition of the Mid Jurassic to Mid Cretaceous clays of the Scotian Basin; detrital input, early diagenesis and burial diagenesis.

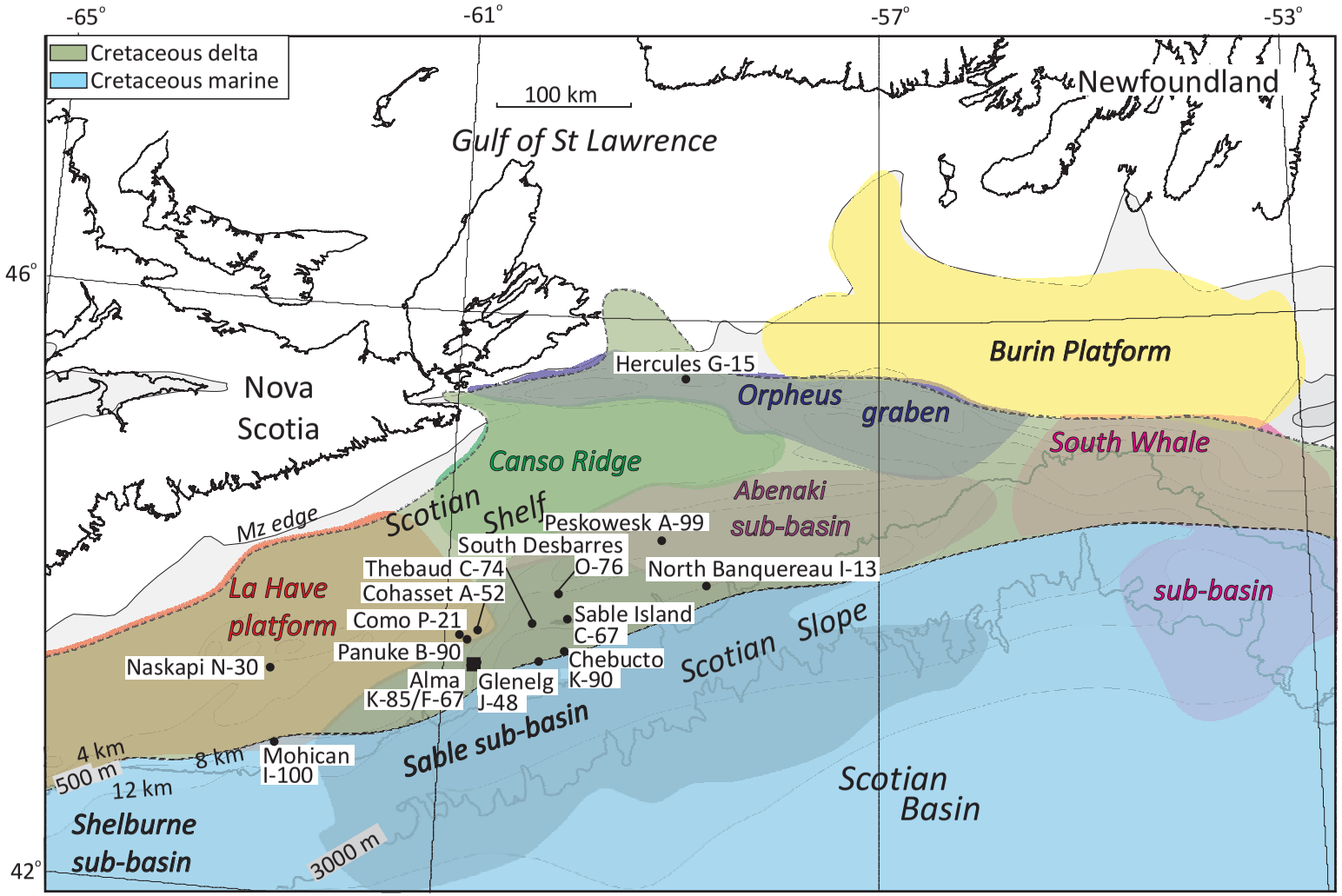

Figure 1.1: Map showing well locations in the Scotian Basin.

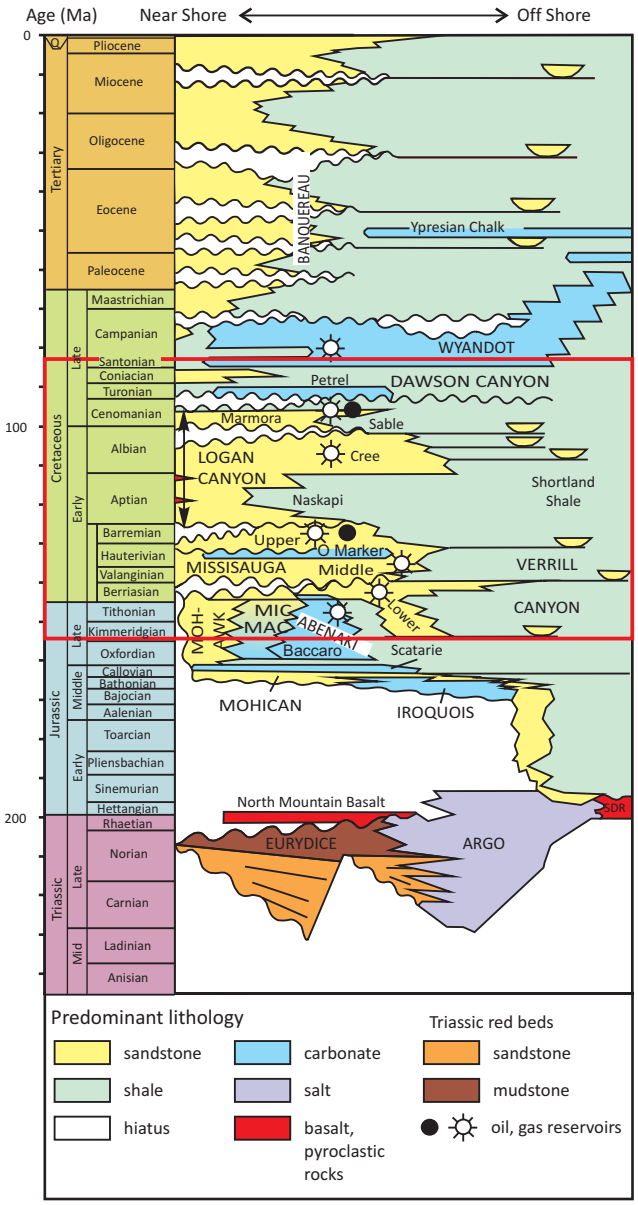

Figure 1.2: Scotian basin stratigraphy, based on data from OETR (2011) and compiled by D.J.W Piper (pers. comm. 2012). The red box indicates the interval investigated in detail.

The early diagenesis of clay minerals, which is facies dependant, is influenced by the water composition at the time of burial and shortly thereafter. Meteoritic water (which is typically more acidic due to the decay of organic compounds) produces more kaolinite (Potter, et al., 1980); odinite (verdine facies) will form in marine water with high Fe (Odin, 1990); saline environments and evaporitic settings will produce palygorskite and sepiolite (Shoval and Zlatkin, 2009. The water temperature and acidity can influence how the detrital minerals alter.

Burial diagenesis is the final step in the process that gives the composition found today. To understand this process two factors are important: a) The deeper the clays are buried the higher the temperature and pressure, leading to the recrystallization of minerals stable at the new temperature and pressure. Examples are the berthierine to chlorite transition starting at 90°C (Aagaard et al., 2000) and the smectite to illite transition beginning between 50-60°C (Hoffman & Hower, 1979); b) The composition of the pore fluid that travels through the system. For example, illite diagenesis in the Jeanne d'Arc Basin offshore Newfoundland is enhanced by the passage of deep K-bearing fluids (Abid & Hesse, (2007). If basinal shales are of varying composition, this may affect pore fluids that pass through reservoir rocks.

1.2 CLAY MINERALS AND DIAGENESIS

Sedimentary rocks cover most of the earth's surface with 60% of those being shale (Way, 1973). A major source of clay minerals is from weathering of silicate minerals, formed at high temperatures and high pressures, that are unstable at the

earth's surface. Other sources include: abrasion by continental ice sheets during major glaciations; altered volcanic ash; dust from continental deserts; and pulverized and ingested sediment by organisms (Potter, Maynard & Pryor, 1980). Some clay minerals like gibbsite, smectites, and kaolinite can form as precipitates in the void spaces of soil from groundwater (Potter, Maynard & Pryor, 1980). This, in turn, can then be eroded and deposited in basins.

Climate is also a factor in clay formation. Kaolinite appears less likely to form in arid conditions, but will form in humid conditions as long as minerals like feldspar, muscovite, or biotite are present. Volcanic rocks exposed to tropical conditions will produce the greatest volume of clay minerals because of the relatively unstable minerals in a very porous formation that may have a high flux of water and high temperatures. In general the higher the relief and rainfall, the greater the production of clay (Potter, et al., 1980). Mudrocks in sedimentary basins can contain mature clay mineral assemblages that have formed from the deposition of clay minerals created by weathering and shallow diagenesis (Merriman, 2005). During initial deposition of sediment, weathering and mineral authigenesis are accelerated during the processes of digestion, ingestion and excretion of sediment by worms and other organisms (McIlroy et al., 2003). These authors found that during digestion, chlorite was preferentially destroyed and chlorite and muscovite experienced peak broadening when analyzed by XRD. The worms produced neoformed minerals, which potentially could form the antecedent of diagenetic clay minerals, such as berthierine.

Three stages of basin maturity, in terms of clay mineral evolution, has been identified (Merriman, 2005) using the correlation of clay reaction progress, organic thermal maturity indicators, the Kubler Index of illite, and hydrocarbon zones (Merriman & Kemp, 1996; Merriman & Frey, 1999) (Figure 1.3). (1) Immature basins contain predominantly neoformed and inherited clays in the shallow diagenetic zone. These clays have not passed through the oil window. (2) Mature basins typically have neoformed and inherited clays partially transformed due to deep diagenesis. The sediment in these types of basins is found in the oil and gas window. The Scotian Basin is an example of this stage. (3) Supermature basins are where deformation is an integral part in the final stages of transformation of metastable diagenetic and inherited clays to equilibrium assemblages of white micas and chlorite. This deformation is due to the early onset of regional metamorphism and this type of basin is typically void of hydrocarbon potential (Merriman, 2005).

The Kubler Index is the measurement of the full width at half height of the 10 Å illite peak. It is the measurement of illite crystallinity with the lower values signifying more crystalline illite and the higher values signifying less crystalline illite. The Kubler Index is typically used as a measure of metamorphism with burial.

1.3 PREVIOUS RESEARCH ON SHALES IN THE SCOTIAN BASIN

Cassou et al. (1977) published the first account of clay mineralogy of Scotian Basin shales. In the Scotian Basin there is a strong correlation between the beginning of the 'oil diagenetic zone' and the transformation of montmorillonite into illite and mixed-

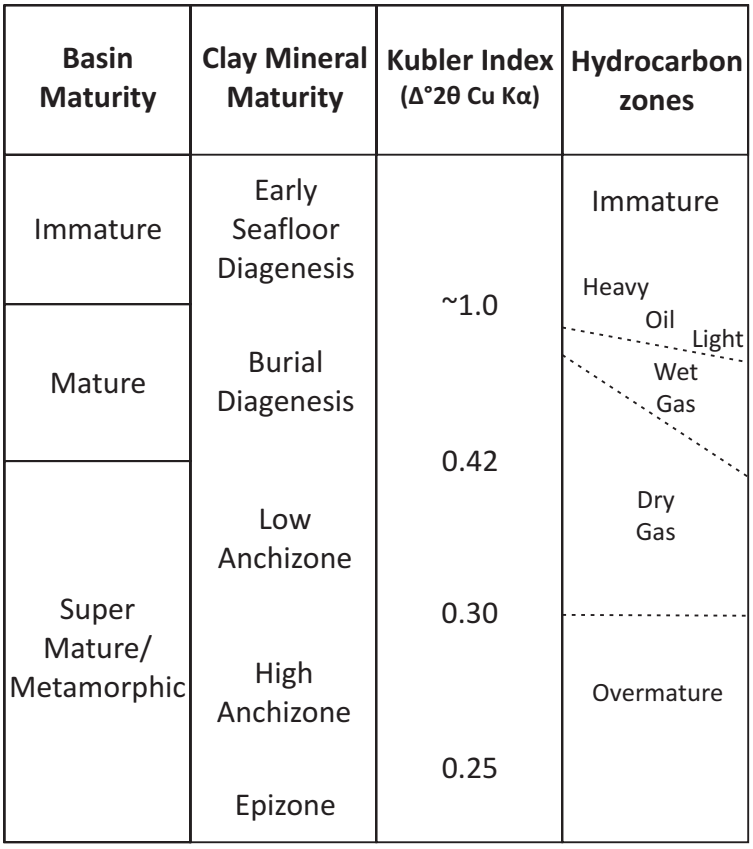

Figure 1.3: Basin maturity chart (data from Merriman & Kemp, 1996)

layered clay minerals (Cassou et al., 1977). This signifies the discharge of a significant quantity of fluid (hydrocarbons and formation waters) from both organic and mineral phases after a given amount of compaction (Cassou et al., 1977).

Wadden (2003) investigated clay mineralogy of Cretaceous shales in the Scotian Basin. Four wells were chosen for this study: Alma F-67, Chebucto K-90, Glenelg J-48 and Thebaud C-74. Using quantitative analysis of X-ray diffraction data, Wadden (2003) attempted to determine the abundance of each clay mineral. Although the sample number is too low to be definitive, there are some interesting claims that require further investigation.

The abundance of certain clay minerals directly relates to the stratigraphic level and burial depth of the sample in the basin (Wadden, 2003). Fe-chlorite is most abundant in the Mississauga Formation, with lesser amounts in the Naskapi and Cree members. Mg-chlorite is commonly more abundant at high stratigraphic levels in the Scotian Basin (Wadden, 2003). There is limited data in this study, however, it is most obvious in the Thebaud C-74 well, where Mg-chlorite is higher in the Logan Canyon Formation than the Mississauga Formation. Mg-chlorite is also present in the Mississauga Formation in Alma F-67. Wadden (2003) also found that smectite decreases down well, disappearing at the onset of overpressure, and kaolinite decreases markedly at the overpressure zone.

The Chaswood Formation is a Lower Cretaceous fluvial sandstone–mudstone succession and is time equivalent to the offshore deltaic rocks of the Scotian Basin that make up the Mississauga and Logan Canyon Formations (Stea & Pullan, 2001; Pe-Piper

et al., 2005). The most common clay minerals in the overbank mudrocks of the Chaswood Formation are illite and kaolinite, followed by vermiculite and vermiculite mixed layer clays (Piper et al., 2009). These clay minerals were identified through < 2 µm X-ray diffraction analysis and the non-clay minerals found in this fraction are quartz, goethite, rutile, dolomite, siderite, pyrite and hematite (Piper et al., 2009). No significant amounts of chlorite were found in the Chaswood Formation (Piper et al., 2009) and it is thought to be relatively rare in the Chaswood Formation (Pe-Piper et al., 2005). In the ultisols in the Chaswood Formation overbank mudrocks kaolinite increases downward from dissolution of illite (Piper et al., 2009). Oxidation of organic matter below the paleo-water table by bacteria is thought to have facilitated the increased amounts of vermiculite, mica/vermiculite mixed layer, and kaolinite/vermiculite mixed layer clays (Piper et al., 2009).

Multiple sources of the onshore Chaswood Formation have been identified from Nova Scotia, New Brunswick and Quebec. These include: the Grenville Terrane (Canadian Shield) and the Carboniferous sedimentary rocks and crystalline Appalachian rocks of the Meguma, Avalon, Gander, Dunnage, and Humber Terranes (Gobeil et al., 2006; Pe-Piper & MacKay, 2006; Piper et al., 2007; Strathdee, 2010). Cretaceous aged sediments in the Scotian Basin have been found to have similar sources as the Chaswood Formation with the addition of sources from western Newfoundland and Labrador (Triantafyllidis et al., 2010; Piper et al., 2012) (Figure 1.4).

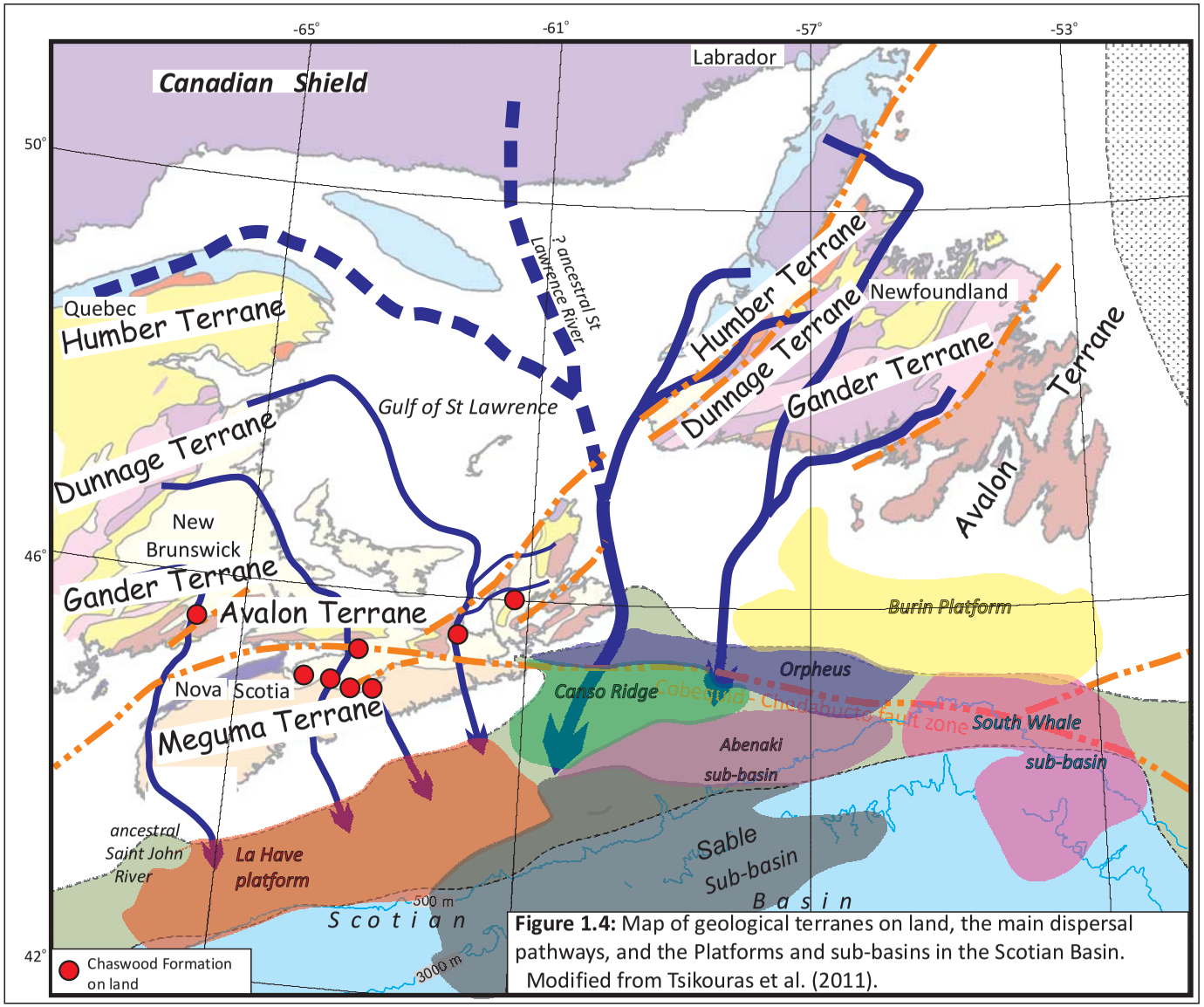

Figure 1.4: Map of geological terranes on land, the main dispersal pathways, and the Platforms and sub-basins in the Scotian Basin. Modified from Tsikouras et al. (2011).

1.4 X-RAY DIFFRACTION (XRD)

1.4.1 PRINCIPLES OF X-RAY DIFFRACTION

Clay minerals are typically considered to be particles that are less than <2 µm in diameter, and cannot be identified through petrographic analysis. X-ray diffraction is typically used to identify clay minerals and is the basis of this thesis. X-ray diffraction uses X-rays to produce a pattern of the key crystallographic planes that diffract X-rays (Carroll, 1970). By knowing these patterns, the minerals that comprise >5% of the sample can be identified. The orientation of the clay grains is important because for most clays, the mass absorption coefficient does not differ to a great extent. The mass absorption coefficient is a measurement of the strength of the absorption of light of a substance at a given wavelength per mass unit. Oriented clay mounts analyzed by XRD have patterns that show the basal (d) spacings (001) of the minerals, which give periodicities normal to the plane along the c axis. Humidity, glycolation, cations in interlayer positions, dehydration and acid treatment are several of the parameters that can cause this dimension to vary. The XRD patterns of non-oriented mounts are the hkl spacings. The hk spacings are found in all minerals, except the triclinic class, and are the a and b directions of the unit cell (Carroll, 1970).

1.4.2 X-RAY DIFFRACTION MOUNTING TECHNIQUES

When studying clay-rich rocks (claystones, mudstones and marls), XRD analysis has proven to be the best way to determine mineral content and abundance (Srodon et al., 2001). There are several methods used for XRD analysis of clays (as described by Moore & Reynolds, 1997); the glass slide method (<2 µm oriented), the smear mount

method (random), and the sidepack mount method (random). The <2 µm analysis is further enhanced by employing solvation and heat treatments.

The oriented <2 µm method is an oriented mount that accentuates the 00l diffractions and accentuates clays rather than silts (Moore & Reynolds, 1997). The <2 µm method cannot be used for quantitative analysis. The main challenges associated with the <2 µm method are the tendency for the clay particles to orient themselves and a lack of accurate diffraction intensities at medium to high diffraction angles due to the thinness of the clay film (Moore & Reynolds, 1997). The use of the <2 µm method facilitates the identification of clay minerals by enhancing the clay mineral basal spacings.

The findings from this method will be compared with the whole rock geochemistry of the samples to determine variations in the input of clays (detrital or authigenic) in time and space in the Scotian Basin.

Srodon et al. (2001) has developed the Sidepack method of clay XRD analysis. Through his study he tested grinding times and methods and found that using a McCrone Micronizing Mill for five minutes was the best way to reduce all the mineral components to a size of <20 microns. Methanol is the best liquid to use for grinding because it dries rapidly and helps avoid swelling in the shale. This is the best method for quantitative XRD analysis on clay bearing rocks (Srodon et al., 2001). This method was used in this study as well, to help determine the variations in the input of clays in the basin and the effect of burial on clay mineralogy.

Kleeberg et al. (2008) found that sidepack mounts of mineral powders after wet grinding in a micronizing mill will not produce randomly oriented grains; which contradicts the results of Srodon et al. (2001). Kleeberg et al. (2008) found that the initial methods (like those applied by Srodon et al. (2001)) worked well, save for a few minor changes. The key difference is the mounting procedure; Kleeberg et al. (2008) showed that by 'spray-drying' their samples and then loading them into mounts, perfect grain randomness was achieved. After examining the sidepack results of this study and of previously unpublished sidepack results, this study finds that the method of Srodon et al. (2001) is appropriate for quantitative clay analyses.

Solvation and heat treatment of <2 μm samples helps to characterize the clay minerals. Glycolation treatment is a way to refine your identification of clay minerals that contain water in their crystal structure. This treatment removes moisture from the sample, including humidity from the air. Smectite clays will swell when moist and this can lead to misleading interpretations in the XRD patterns (Frost & Rintoul, 1996). Bradley (1945) was the first to recognize the diagnostic absorption of ethylene glycol by smectite. This method can be used to help identify key minerals in the smectite, vermiculite and the expandable mixed layer clays. Heating the samples and analyzing the sample after each heat treatment is another way to refine your analysis. The peaks of some minerals will become more intense or less intense with each heat treatment. The peaks may also shift slightly to a higher or lower 2θ position compared to the air dried sample analysis. The temperatures used in this thesis are 110°C, 300°C, 500°C, and 650°C.

1.4.3 X-RAY DIFFRACTION REPRODUCIBILITY OVER TIME

In 2010 it was found that the detector for the XRD at the Geological Survey of Canada (Atlantic) was losing resolution and needed to be replaced. Several potential issues came to mind when considering variability and errors with sample preparation and analysis: 1) How reliable is the data from the X-ray diffractometer over time as the detector ages? 2) Variations and errors in creating the different types of mounts for the samples. 3) Variations and errors in picking and identifying the mineral peaks. 4) Problems with overlapping peaks in low 2θ range of bulk random sidepack samples. These issues will be further discussed in Chapter 5.

1.5 OBJECTIVES AND APPROACH

The purpose of this study is to investigate three key variables in the compositional change of Mesozoic shales of the Scotian Basin: detrital input, early diagenesis and burial diagenesis.

Sixteen wells from the Scotian Basin were selected for this study: Alma F67; Alma K-85; Chebucto K-90; Cohasset A-52; Como P-21; Glenelg J-48; Hercules G-15; Mohican I-100; Naskapi N-30; North Banquereau I-13; Panuke B-90; Peskowesk A-99; Sable Island C-67; South Desbarres O-76; Thebaud C-74 and Thebaud I-93 (Figure 1.1). 108 Clay samples were collected from multiple depths in each well ranging from the Late Jurassic to the Late Cretaceous (Table 1.1). The original hypothesis was that shales of the same age/stratigraphy should have the same or very similar detritus. Many of the shales that were deposited at different times have been buried at different rates and are now

Table 1.1: List of samples and details from the Scotian Basin

Well	Depth (m)	Age (Ma)	Geological Time Scale	Formation	Type	Geochem
Alma F-67	1190.00	72	Campanian	Banquereau Fm	Cuttings	No
Alma F-67	1750.00	100	Albian	Logan Canyon (Sable Mb)	Cuttings	No
Alma K-85	2449.40	110	Albian	Logan Canyon (Cree Mb)	C-Core	Yes
Alma K-85	2453.85	110.2	Albian	Logan Canyon (Cree Mb)	C-Core	Yes
Alma K-85	2455.00	110.4	Albian	Logan Canyon (Cree Mb)	C-Core	Yes
Alma K-85	2456.40	110.6	Albian	Logan Canyon (Cree Mb)	C-Core	Yes
Alma K-85	2456.50	110.8	Albian	Logan Canyon (Cree Mb)	C-Core	Yes
Alma K-85	2458.15	111	Albian	Logan Canyon (Cree Mb)	C-Core	Yes
Alma K-85	2460.75	111.2	Albian	Logan Canyon (Cree Mb)	C-Core	Yes
Alma K-85	2878.90	125	Barremian-Aptian	Mississauga Upper Mb	C-Core	Yes
Alma K-85	2880.22	125.25	Barremian	Mississauga Upper Mb	C-Core	Yes
Alma K-85	2888.26	125.5	Barremian	Mississauga Upper Mb	C-Core	Yes
Alma K-85	2904.15	125.75	Barremian	Mississauga Upper Mb	C-Core	Yes
Alma K-85	2906.78	126	Barremian	Mississauga Upper Mb	C-Core	Yes
Alma K-85	2912.04	126.25	Barremian	Mississauga Upper Mb	C-Core	Yes
Alma K-85	2919.00	126.5	Barremian	Mississauga Upper Mb	C-Core	Yes
Alma K-85	2919.45	126.5	Barremian	Mississauga Upper Mb	C-Core	Yes
Alma K-85	2920.30	126.6	Barremian	Mississauga Upper Mb	C-Core	Yes
Alma K-85	2931.87	126.75	Barremian	Mississauga Upper Mb	C-Core	Yes
Alma K-85	3038.00	127.5	Barremian	Mississauga Upper Mb	C-Core	Yes
Alma K-85	3039.88	127.75	Barremian	Mississauga Upper Mb	C-Core	No
Alma K-85	3044.60	128	Barremian	Mississauga Upper Mb	C-Core	Yes
Alma K-85	3047.90	128.2	Barremian	Mississauga Upper Mb	C-Core	Yes
Alma K-85	3068.15	128.4	Barremian	Mississauga Upper Mb	C-Core	Yes
Alma K-85	3071.80	128.6	Barremian	Mississauga Upper Mb	C-Core	Yes
Alma K-85	3089.05	128.8	Barremian	Mississauga Upper Mb	C-Core	Yes
Alma K-85	3090.15	129	Hauterivian-Barremian	Mississauga Upper Mb	C-Core	Yes
Alma K-85	3093.80	129.1	Hauterivian-Barremian	Mississauga Upper Mb	C-Core	Yes
Alma K-85	3104.10	130	Hauterivian	Verrill Canyon Fm	C-Core	Yes
Alma K-85	3104.70	130	Hauterivian	Verrill Canyon Fm	C-Core	Yes
Chebucto K-90	1690.00	58.6	Paleocene	Banquereau Fm	Cuttings	Yes
Chebucto K-90	2220.00	99.8	Albian	Logan Canyon (Marmora Mb)	Cuttings	Yes
Chebucto K-90	2470.00	100	Albian	Logan Canyon (Marmora Mb)	Cuttings	Yes
Chebucto K-90	3780.00	126.5	Barremian	Logan Canyon (Cree Mb)	Cuttings	Yes
Chebucto K-90	4370.00	130.2	Hauterivian-Barremian	Mississauga Fm	Cuttings	Yes
Chebucto K-90	4420.00	130.25	Hauterivian-Barremian	Mississauga Fm	Cuttings	Yes
Chebucto K-90	4585.00	130.3	Hauterivian-Barremian	Mississauga Fm	Cuttings	Yes
Chebucto K-90	4750.00	130.4	Hauterivian-Barremian	Mississauga Fm	Cuttings	Yes
Chebucto K-90	5120.00	130.9	Hauterivian	Mississauga Fm	Cuttings	Yes
Chebucto K-90	5230.00	131	Hauterivian	Mississauga Fm	Cuttings	Yes
Cohasset A-52	2072.90	109	Albian	Logan Canyon (Cree Mb)	C-Core	Yes
Cohasset A-52	2074.72	109	Albian	Logan Canyon (Cree Mb)	C-Core	Yes
Cohasset A-52	2123.52	110	Albian	Logan Canyon (Cree Mb)	C-Core	Yes
Cohasset A-52	2138.22	111	Albian	Logan Canyon (Cree Mb)	C-Core	Yes
Cohasset A-52	2418.75	119	Aptian	Logan Canyon (Naskapi Mb)	C-Core	Yes
Cohasset A-52	2597.05	125	Barremian-Aptian	Mississauga Upper Mb	C-Core	Yes
Como P-21	2188.75	125.5	Barremian-Aptian	Mississauga Upper Mb	C-Core	Yes
Como P-21	3065.72	149	Berriasian	Mississauga Middle Mb	C-Core	Yes
Glenelg J-48	1405.00	44.8	Ypresian-Lutetian	Banquereau Fm	Cuttings	No
Glenelg J-48	3250.00	114	Aptian	Logan Canyon (Naskapi Mb)	Cuttings	No
Glenelg J-48	3645.00	125.1	Barremian-Aptian	Mississauga Upper Mb	Cuttings	No
Glenelg J-48	3860.00	125.3	Barremian-Aptian	Mississauga Upper Mb	Cuttings	No
Glenelg J-48	4030.00	125.5	Barremian	Mississauga Upper Mb	Cuttings	No
Glenelg J-48	4385.00	125.8	Barremian	Mississauga Middle Mb	Cuttings	No
Glenelg J-48	4740.00	137	Valanginian	Verrill Canyon Fm	Cuttings	No
Hercules G-15	371.86	99.6	Albian-Cenomanian	Logan Canyon (Marmora Mb)	Cuttings	No
Hercules G-15	646.18	99.65	Albian-Cenomanian	Logan Canyon (Cree Mb/Pyro)	Cuttings	No
Mohican I-100	2533.24	138	Valanginian	Mississauga Middle Mb	C-Core	No
Mohican I-100	2539.94	138	Valanginian	Mississauga Middle Mb	C-Core	No
Mohican I-100	2541.23	138	Valanginian	Mississauga Middle Mb	C-Core	No
Naskapi N-30	1469.10	128	Barremian	Mississauga Upper Mb	C-Core	Yes
North Banquereau I-13	3248.80	117	Aptian	Logan Canyon (Naskapi Mb)	C-Core	Yes

North Banquereau I-13	3249.65	117	Aptian	Logan Canyon (Naskapi Mb)	C-Core	Yes
Panuke B-90	2097.27	110.5	Albian	Logan Canyon (Cree Mb)	C-Core	Yes
Panuke B-90	2235.37	118.5	Aptian	Logan Canyon (Naskapi Mb)	C-Core	Yes
Panuke B-90	2241.57	119.1	Aptian	Logan Canyon (Naskapi Mb)	C-Core	Yes
Panuke B-90	2245.78	119.5	Aptian	Logan Canyon (Naskapi Mb)	C-Core	Yes
Panuke B-90	2247.20	119.7	Aptian	Logan Canyon (Naskapi Mb)	C-Core	Yes
Panuke B-90	2255.49	120.5	Aptian	Logan Canyon (Naskapi Mb)	C-Core	Yes
Panuke B-90	2256.56	120.6	Aptian	Logan Canyon (Naskapi Mb)	C-Core	Yes
Panuke B-90	2278.21	122.8	Aptian	Logan Canyon (Naskapi Mb)	C-Core	Yes
Peskowesk A-99	2209.25	109.4	Albian	Logan Canyon (Cree Mb)	C-Core	Yes
Peskowesk A-99	2213.57	109.4	Albian	Logan Canyon (Cree Mb)	C-Core	Yes
Peskowesk A-99	2215.78	109.4	Albian	Logan Canyon (Cree Mb)	C-Core	Yes
Peskowesk A-99	2219.03	109.5	Albian	Logan Canyon (Cree Mb)	C-Core	Yes
Peskowesk A-99	2221.69	109.6	Albian	Logan Canyon (Cree Mb)	C-Core	Yes
Peskowesk A-99	2228.42	109.7	Albian	Logan Canyon (Cree Mb)	C-Core	No
Peskowesk A-99	2479.35	125.2	Barremian-Aptian	Mississauga Upper Mb	C-Core	Yes
Peskowesk A-99	2488.85	125.4	Barremian-Aptian	Mississauga Upper Mb	C-Core	Yes
Peskowesk A-99	2492.62	125.5	Barremian-Aptian	Mississauga Upper Mb	C-Core	Yes
Peskowesk A-99	2927.36	134.6	Valanginian	Mississauga Middle Mb	C-Core	Yes
Peskowesk A-99	2940.90	135	Valanginian	Mississauga Middle Mb	C-Core	Yes
Peskowesk A-99	2947.43	135.2	Valanginian	Mississauga Middle Mb	C-Core	Yes
Peskowesk A-99	3806.51	149	Tithonian	Mic Mac Fm	C-Core	No
Peskowesk A-99	3812.64	149	Tithonian	Mic Mac Fm	C-Core	No
Sable Island C-67	2474.18	108.6	Albian	Logan Canyon (Cree Mb)	C-Core	Yes
Sable Island C-67	2830.45	122.8	Aptian	Logan Canyon (Naskapi Mb)	C-Core	Yes
Sable Island C-67	2835.42	123	Aptian	Logan Canyon (Naskapi Mb)	C-Core	Yes
Sable Island C-67	3373.45	142.6	Berriasian	Mississauga Middle Mb	C-Core	Yes
Sable Island C-67	4089.87	148.5	Tithonian	Mississauga Lower Mb	C-Core	Yes
South Desbarres O-76	3815.10		Tithonian	Mississauga Lower Mb	C-Core	Yes
South Desbarres O-76	5956.80		Kimmeridgian	Mic Mac Fm	C-Core	Yes
Thebaud C-74	1825.00	100.6	Albian	Logan Canyon (Sable Mb)	Cuttings	Yes
Thebaud C-74	1990.00	103	Albian	Logan Canyon (Cree Mb)	Cuttings	Yes
Thebaud C-74	2200.00	106.5	Albian	Logan Canyon (Cree Mb)	Cuttings	Yes
Thebaud C-74	2205.00	106.6	Albian	Logan Canyon (Cree Mb)	Cuttings	Yes
Thebaud C-74	2390.00	109.7	Albian	Logan Canyon (Cree Mb)	Cuttings	Yes
Thebaud C-74	2560.00	115	Aptian	Logan Canyon (Naskapi Mb)	Cuttings	Yes
Thebaud C-74	2630.00	122.3	Aptian	Logan Canyon (Naskapi Mb)	Cuttings	Yes
Thebaud C-74	2775.00	127.5	Barremian	Mississauga Upper Mb	Cuttings	Yes
Thebaud C-74	2780.00	127.6	Barremian	Mississauga Upper Mb	Cuttings	Yes
Thebaud C-74	3075.00	133.9	Valanginian-Hauterivian	Mississauga Middle Mb	Cuttings	Yes
Thebaud C-74	3615.00	140	Tithonian-Berriasian	Mississauga Middle Mb	Cuttings	Yes
Thebaud C-74	3780.00	146	Tithonian	Mississauga Lower Mb	Cuttings	Yes
Thebaud C-74	4020.00	148.5	Tithonian	Mississauga Lower Mb	Cuttings	Yes
Thebaud C-74	4105.00	149	Tithonian	Mississauga Lower Mb	Cuttings	Yes
Thebaud C-74	4335.00	150	Tithonian	Mississauga Lower Mb	Cuttings	Yes
Thebaud I-93	3080.38	120.1	Hauterivian	Mississauga Middle Mb	Cuttings	Yes

found at quite different depths (Figure 1.5). Examining the same age shales located at different burial depths should provide information about burial effects.

In this thesis the approach is to use <2 μm (oriented) and sidepack (bulk random) XRD mounts to analyze the samples. The <2 μm analysis will help to characterize and identify the clay minerals and the sidepack analysis will help to quantify the minerals that have been identified. With the results of these analyses, this study will investigate the mineral variation with depth, geography and stratigraphy. This study aims to better understand the detrital vs. diagenetic clay minerals and provide insight to the provenance of the clays in the Scotian Basin.

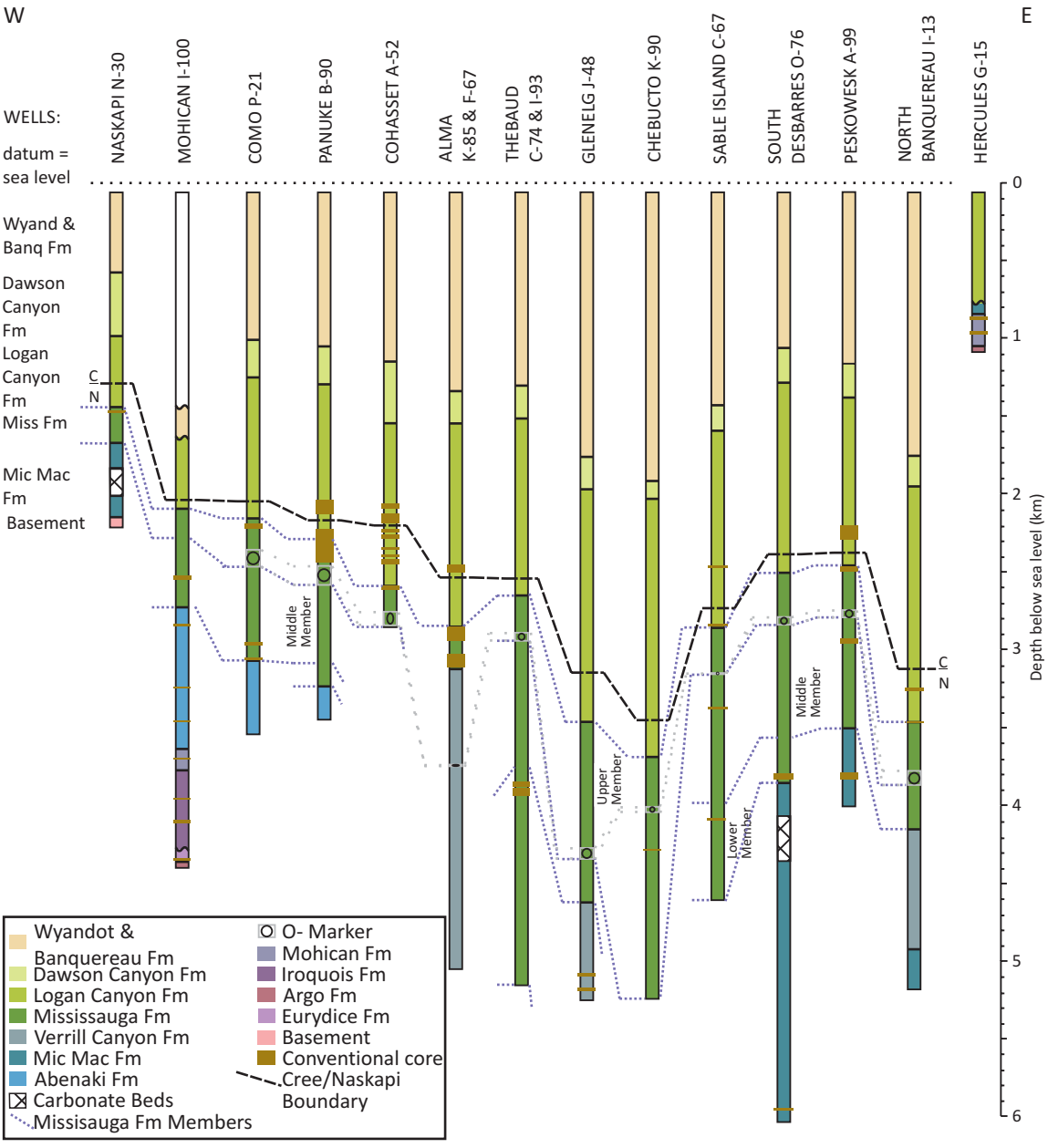

Figure 1.5: Stratigraphy of wells investigated showing the variable burial depths of sediment deposited at similar ages.

CHAPTER 2: GEOLOGICAL SETTING

2.1 GEOLOGICAL SETTING

The Scotian Basin is a 350,000 km^2 area off the eastern coast of Canada that spans from Georges Bank to the central Grand Banks and from the submerged rocks of the coastal plain to the continental rise (Wade & Maclean 1990). This depocenter began forming on a continental passive margin which developed following Late Triassic-Early Jurassic rifting of Pangea between North America and Africa (McIver, 1972; Given, 1977; Wade and MacLean, 1990). During rifting, the Scotian Basin developed a series of horsts and grabens that subsequently localized sub-basins and platforms. Four of these are investigated in this study. From east to west they are: the LaHave Platform, Sable sub-basin, Abenaki Basin and Orpheus Graben (Given, 1977; Wade and MacLean, 1990; OETR, 2011) (Figure 2.1).

2.2 STRATIGRAPHIC NOMENCLATURE

The focus of this study is on the Cretaceous clays in the Scotian Basin (Figure 1.2). The following summary of the lithostratigraphy is based on Wade and MacLean (1990), MacLean and Wade (1993), and OETR, (2011)

The Eurydice Formation is comprised of Late Triassic red sandstones, siltstones and shales. The Argo Formation is an Early-Late Triassic to Early Jurassic series of massive salt beds separated by red shales. It generally overlies the Eurydice Formation, with interpenetrating wedges on the basin margins.

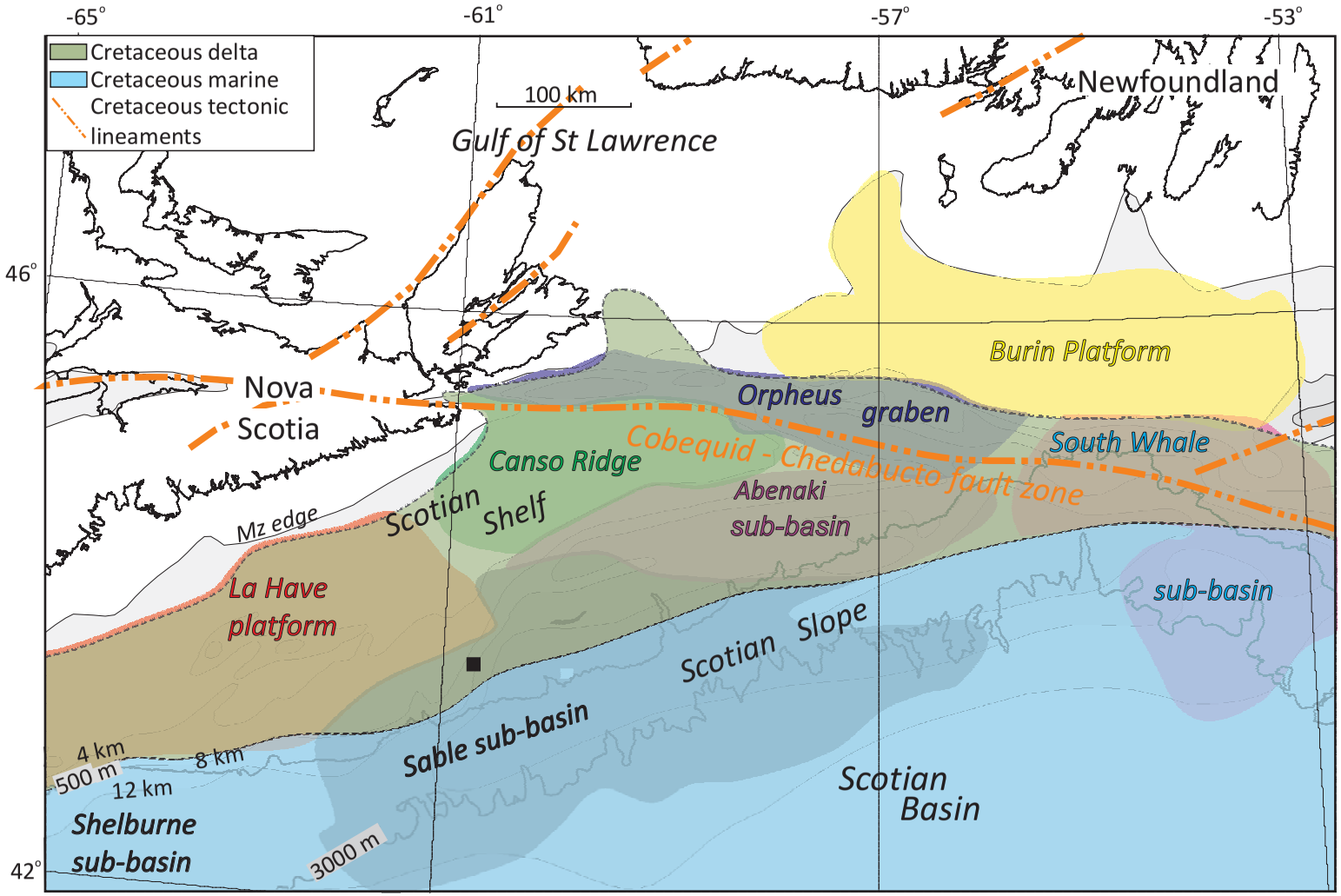

Figure 2.1: Map showing the Scotian Basin, the major Early Cretaceous tectonic lineaments, and basin locations. Modified from Tsikouras et al. (2011).

The Early-Mid Jurassic Iroquois and Mohican Formations overlie the Eurydice Formation and are coeval. The Iroquois Formation is mostly dolostone with an underlying sequence of prograding clastics. The Mohican Formation is a thick clastic sequence of sandstones and shales. The Abenaki Formation overlays the Iroquois and Mohican Formations and is made up of Mid-Late Jurassic carbonates and reef margin sediments.

The Mic Mac Formation, which is contemporaneous with the Abenaki Formation, is a Mid-Late Jurassic clastic fluvio-marine deltaic deposit consisting of interstratified sandstones, shales, limestones and carbonates. Laterally equivalent to the Abenaki and Mic Mac Formations is the Verrill Canyon Formation, a Mid-Late Jurassic to Early Cretaceous deep-water deposit of primarily calcareous shales, and thin beds of limestone, siltstone, and sandstone.

The Late Jurassic – Early Cretaceous Missisauga Formation overlies the Abenaki and Mic Mac Formations, and passes seaward into the Verrill Canyon Formation. It consists of fluvial, deltaic and shelf sediments. It is subdivided into the Lower, Middle, and Upper Members with a distinct seismic marker called the O-marker located in the lower part of the Upper Member. The Kimmeridgian-Berriasian Lower Member is comprised of fine grained sandstones that coarsen upwards, shales and a few thin limestones. The Middle Member is Valanginian-Hauterivian in age and is a thick deposit of sandstone and shale. The Upper Member consists of Hauterivian-Barremian mixed mudstone-sandstone-oolitic limestone beds.

The Aptian-Cenomanian Logan Canyon Formation is divided into four members. The Naskapi Member shale overlies the Missisauga Formation and is overlain by interbedded sandstones and shales of the Cree Member. These are overlain by the Sable Member which is generally shaly with some thin sandstone and siltstone beds. The Marmora Member is a sandstone sequence that overlies the Sable Member. The Shortland Shale Formation is the deeper marine equivalent to the Logan Canyon sandstones.

The Dawson Canyon Formation is an Early Cenomanian to Santonian deposit of marine shales, chalks, and occasional thin limestones. The Wyandot Formation is a Campanian to Maastrichtian chalk with mudstone and occasional thin limestone that overlies the Dawson Canyon Formation. The Campanian-Maastrichtian to Pliocene Banquereau Formation overlies the Wyandot Formation and is predominantly mudstone with lesser sandstones and conglomerate.

2.3 BASIN DEPOSITION, PROVENANCE AND STRUCTURE

During the Early Jurassic, rift basins were depocenters for clastic and carbonate sediments (Figure 2.2). By the Mid Jurassic the Scotian Basin had become a completely marine depositional environment with alluvial plain, deltaic and carbonate deposition. Uplift of the Avalon Terrane on the Grand Banks (Wade & MacLean, 1990) was a product of Early Cretaceous seafloor spreading (Tucholke et al., 2007), which was preceded by Late Jurassic rifting between Iberia and the Grand Banks. This uplift exposed older Mesozoic strata of the Grand Banks which were eroded and deposited in

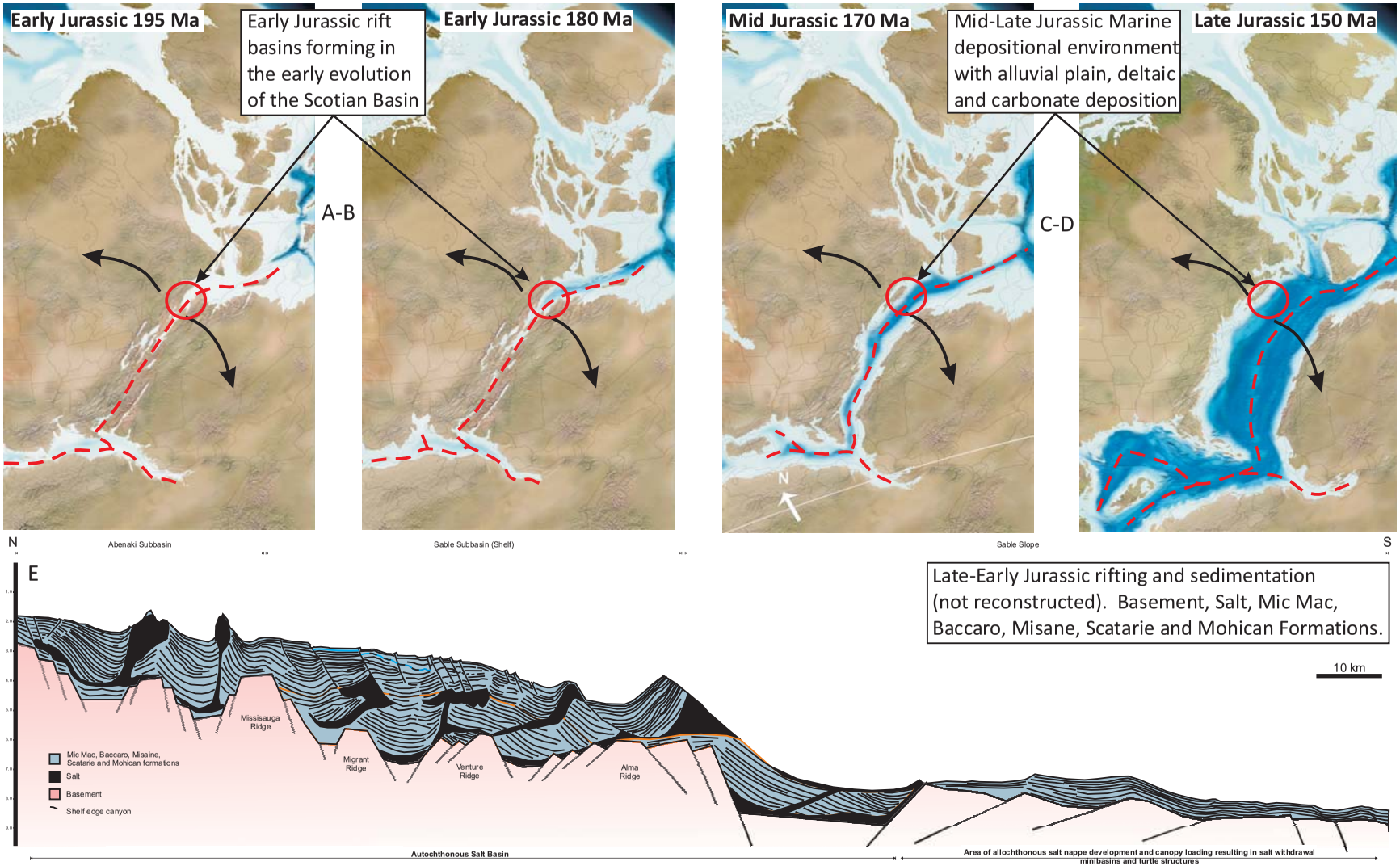

Figure 2.2: Early-Late Jurassic rifting and sedimentation. a-d) Blakey, (2011) Used/modified with permission.
e) K. Kendell 2012, CNSOPB. Used/modified with permission.

the Jeanne d'Arc Basin (Pe-Piper & Piper, 2012). At approximately the same time, there was reactivation of strike-slip faults and crystalline basement uplift (Pe-Piper & Piper, 2004; Reynolds et al., 2009), resulting in mountainous rivers supplying the basin with coarse grained sediment from the Appalachian mountains (Pe-Piper & MacKay, 2006; Cummings et al., 2006; Gobeil et al., 2006). Sediment sources include crystalline basement rocks of the eastern Canadian Shield and the Appalachian orogen and Late Paleozoic fluvial sandstone and shales (Pe-Piper & Piper, 2012). Variation in provenance indicators suggests at least three river systems supplied sediment to the Scotian Basin. At this time the Scotian Basin saw deltaic progradation on the shelf (Figure 2.3) (Wade and MacLean, 1990; MacLean and Wade, 1993; OETR, 2011).

The sediments deposited in the Cretaceous formed mudrocks and sandstones that have experienced diagenesis (Jansa & Noguera-Urrea, 1990). The temperatures at five to six kilometers depth reach as high as 120 to 150°C (Issler, 1984) and the deep reservoirs tend to be overpressured (Mudford, 1990). Salt tectonics, which started around the mid Jurassic, have been a strong influence on the evolution of the Scotian Basin (Ings & Shimeld, 2006).

The Missisauga and Logan Canyon Formations of the Scotian Basin, which were deposited during the Lower Cretaceous as fluvial, deltaic and shelf sediments (Wade & MacLean, 1990), are home to the majority of the oil and gas finds (Wade & MacLean, 1990). They formed mudrock and sandstones that currently lie at 3 to 6 km depth. The Chaswood Formation is the on-shore time equivalent fluvial deposit (Stea & Pullan,

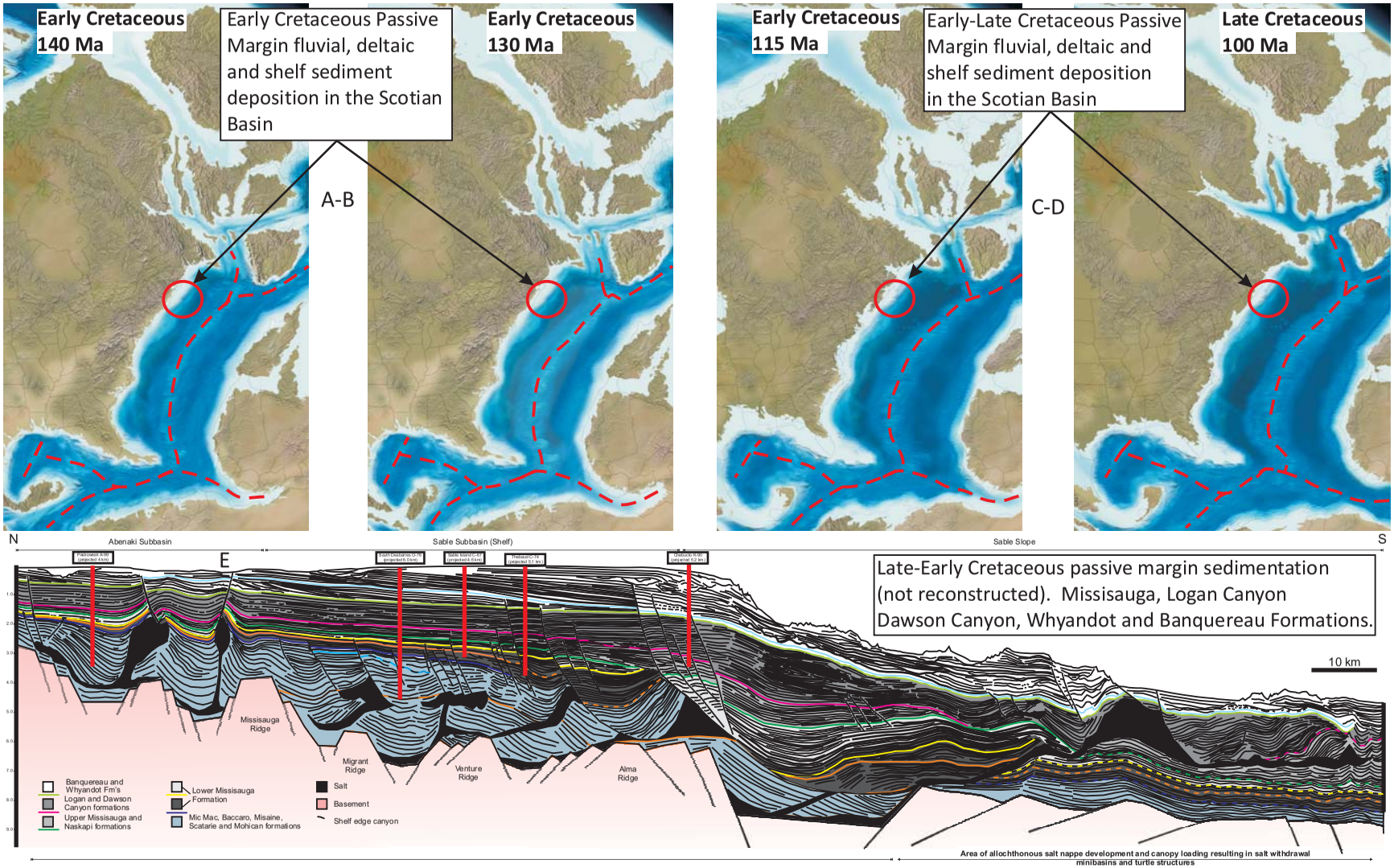

Figure 2.3: Early-Late Cretaceous passive margin sedimentation. a-d) Blakey, (2011) Used/modified with permission.
e) K. Kendell 2012, CNSOPB. Used/modified with permission.

2001) currently outcropping in small areas of Nova Scotia and New Brunswick (Figure 1.4).

Pe-Piper et al. (2008) investigated the variation in major elements and the variation in the mineralogical control of trace-elements to better understand the provenance of the Scotian Basin. Major element PCA (Principal Component Analysis) shows CaO, Na_2O and K_2O behave independently and the loss of CaO and Na_2O during weathering of plagioclase generally occurs together (Pe-Piper et al., 2008). Major element PCA separates western, central and eastern sandstones; however, the dominant influence is high TiO_2 (west) and high K_2O (east) (Pe-Piper et al., 2008). Differences in the detrital minerals in the eastern, central and western Scotian Basin can also be seen in petrologic studies (Pe-Piper et al., 2008).

During the Hauterivian-Aptian, the Banquereau Platform experienced tectonic tilting during reactivation along the Cobequid-Chedabucto Fault. It is postulated that this uplift blocked major river and sediment supply to the Scotian Basin in the Aptian (Piper et al., 2011). During the Aptian small deltas from little rivers transported mostly Meguma Formation sediments into the basin and the large blocked rivers were diverted to the Bay of Fundy. This caused a quiet shale member to be deposited (see Naskapi below) (OETR, 2011; Piper et al., 2011).

Apatite fission track and fluid inclusion data show that during the Cretaceous, the Scotian Basin experienced a regional heating event (Grist et al., 1992; Li et al., 1995; Wierzbicki et al., 2006; Karim et al., 2011, 2012). Studies involving primary fluid inclusions from the lower Cretaceous sandstones of the Mississauga Formation by Karim

et al. (2011), OETR (2011), and Karim et al. (2012) have shown that after an initial rapid and deep burial, some wells were found to be hotter than others. The hotter wells include Thebaud I-93, Glenelg E-58 and N-49, Chebucto K-90, Panuke B-90 and Dauntless D-35, while the cooler wells were found to be Louisbourg J-47, Peskowesk A-99 and several wells in the Venture Field.

Due to abundant supply of ilmenite during the Lower Cretaceous (Pe-Piper et al., 2005), Ti and Fe concentrations in the Scotian Basin are one to two times the global average for sedimentary rocks (Pe-Piper et al., 2008). The high abundance of ilmenite may provide a source of Fe for berthierine. Berthierine most likely altered to chamosite by combining with the Fe from the ilmenite (Gould et al., 2010).

Approximately 20 m thick subaerial basalts are found at the base of the Cree Member of the Logan Canyon Formation in the Orpheus Graben with Jason C-20 and Hercules G-15 also hosting approximately 75 m of pyroclastics underlying tens of meters of the Cree Member (Jansa & Pe-Piper, 1985). This pyroclastic layer is capped by the Top Cree unconformity and it is unknown how much was eroded (Bowman, 2010). Piper at al. (submitted) found Cretaceous zircons in several wells from the Upper Member of the Missisauga Formation and Cree Member of the Logan Canyon Formation. The Cree Member zircons were dated at 105-106 Ma using laser ablation U/Pb dating, and the basaltic lapilli pyroclastic rocks in Hercules G-15 were dated at 103.9 Ma using whole rock K/Ar dating (Bowman, 2010).

2.4 PREVIOUS STUDIES OF SANDSTONE DIAGENESIS

Most of the previous research on diagenesis in the Scotian Basin has been centered on burial diagenesis of sandstones (Jansa & Noguera-Urrea, 1990; Drummond, 1992) with little consideration of interbedded shales. Many of the studies have been on the preservation of porosity by chlorite rims on detrital quartz grains (Drummond, 1992; Gould et al., 2010). The verdine facies (green clay), typically containing minerals such as berthierine (Fe-rich silicate), appears to be an important antecedent to chlorite which forms rims around quartz grains (Pe-Piper & Weir-Murphy, 2008; Gould et al., 2010).

The dispersion of phosphate minerals was investigated by Pe-Piper & Weir-Murphy (2008) as a possible indicator of the early formation of diagenetic berthierine. The most landward portion of the Scotian Basin is the Orpheus Graben. This is where Lower Cretaceous early diagenetic phosphorites and iron silicates are most common (Pe-Piper & Weir-Murphy, 2008), typically found as cements or brownish nodules. It would appear that berthierine and phosphorite in coated grains formed during seafloor diagenesis due to their co-occurrence (Okwese et al., 2011).

Weir-Murphy (2004) found phosphorites were associated with chamosite (Fe-rich chlorite) in the Lower Cretaceous rocks in the Scotian Basin. It was suggested that the precursor of chamosite (berthierine or an Fe-rich clay mineral) and phosphorites precipitated in sandstones under similar conditions (Pe-Piper & Weir-Murphy, 2008). Both minerals were found in sandstones that underlie a transgressive system and most likely formed at a depth where Ferrous Fe is present (Fe-reducing zone) (Pe-Piper & Weir-Murphy, 2008).

Berthierine alters to chamosite rims on detrital framework grains after burial (Aargaard et al., 2000). Thus, berthierine overgrowth altering to chlorite on detrital quartz helped to maintain porosity by preventing quartz overgrowth precipitation in the Venture wells of the Scotian Basin (Gould et al., 2010).

The formation of diagenetic cements such as clay minerals, carbonates and quartz, and their control on reservoir quality was investigated by Karim et al. (2010). This study examined the spatial and temporal distribution of diagenetic cements in relation to lithofacies and stratigraphy, and the diagenetic changes in these cements. Carbonate cements often fill intergranular pores, while Fe-calcite and ankerite form later in the diagenetic sequence. Siderite is formed in two stages, one in early diagenesis and one in late diagenesis (Figure 2.4) (Gould, 2007; Karim et al., 2010).

There has been no previous work on detrital input of clays in the Scotian Basin; however, clay variation in the Chaswood Formation has been studied. Considerable work on clays preserved in coated grains shows early diagenesis of Fe-rich clays now preserved as berthierine or Fe-rich chlorite. Kaolinite cements in sandstones in the Scotian Basin show that some kaolinite was formed during early diagenesis. There is a good understanding of burial diagenesis and clay cements in sandstones, and the thermal conditions of burial diagenesis but no previous work has been done on clays in the Scotian Basin.

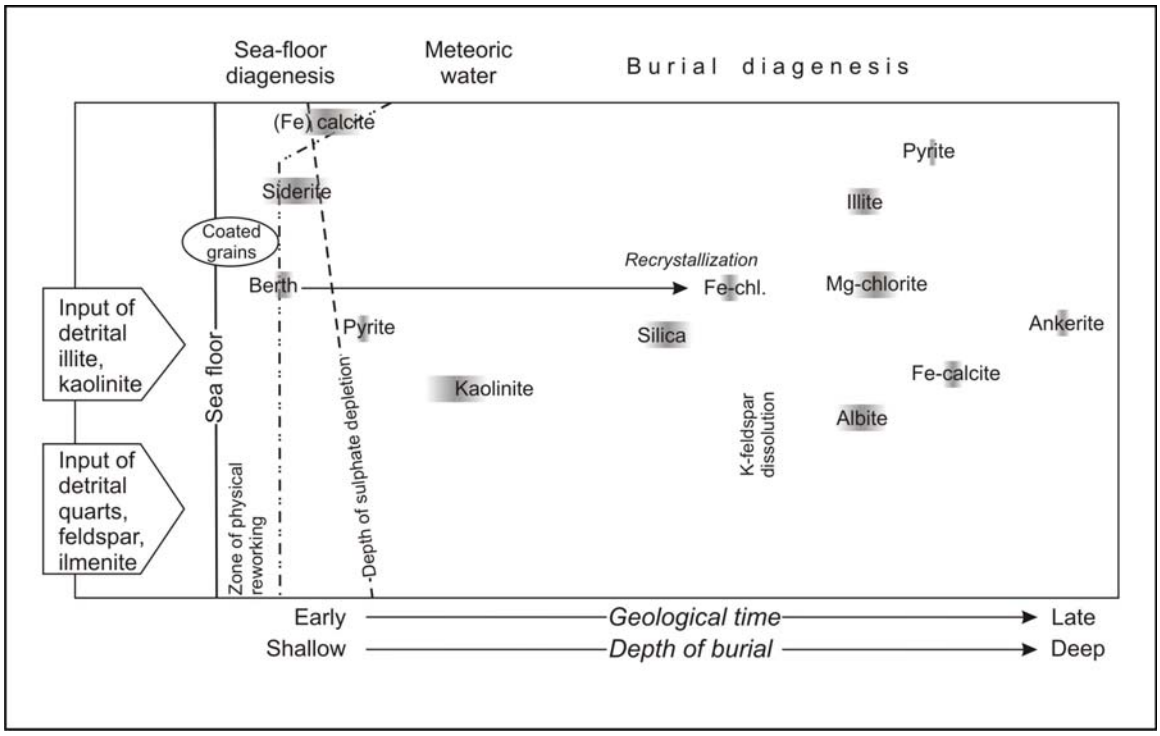

Figure 2.4: Paragenetic sequences of the Scotian Basin (modified from Gould et al. 2010)

CHAPTER 3: METHODS

3.1 SAMPLES AND APPROACH

Most samples collected from the selected wells were obtained from conventional core. Where there are no conventional cores, cuttings were collected. The cores are held at the Geoscience Research Center of the Canadian Nova Scotia Offshore Petroleum Board. The samples were selected on the basis of geographic and stratigraphic basis to ensure the greatest coverage in the basin for investigating the detrital input, early diagenesis and burial diagenesis. The samples included 2 from Alma F-76, 28 from Alma K-85, 10 from Chebucto K-90, 6 from Cohasset A-52, 2 from Como P-21, 7 from Glenelg J-48, 2 from Hercules G-15, 3 from Mohican I-100, 1 from Naskapi N-30, 2 from North Banquereau I-13, 8 from Panuke B-90, 14 from Peskowesk A-99, 5 from Sable Island C-67, 2 from South Desbarres O-76 and 15 from Thebaud C-74 (Table 3.1).

X-ray diffraction is an important tool for identifying and understanding clay minerals. Two different types of analyses were employed in this study: oriented mounts (<2 µm) and the bulk random sidepack mount method of Srodon et al. (2001). The methods used by Gould (2007) for preparing and analyzing <2 µm samples were applied here. The Sidepack analyses were used to quantify the abundance of clay minerals and the <2 µm analyses were used for characterizing particular minerals, with subsequent glycolation, glycerol and heat treatments.

Table 3.1: Wells, well location and depth in the Scotian Basin.

Well Name	Groups	Basin	Subbasin	Lat (NAD83) Surface X	Long (NAD83) Surface Y	Total Drill Depth (m)	True Vertical Depth (m)	Analysis Type	
								Sidepack	<2 Micron
GLENELG J-48	Center	Scotian Basin	Sable Sub-basin	43.627453	-60.106142	5250.00		7	0
CHEBUCTO K-90	Center	Scotian Basin	Sable Sub-basin	43.662494	-59.713539	5239.00		10	3
THEBAUD I-93	Center	Scotian Basin	Sable Sub-basin	43.879108	-60.230058	5166.00		0	1
THEBAUD C-74	Center	Scotian Basin	Sable Sub-basin	43.884886	-60.192469	5150.21		15	4
NORTH BANQUEREAU I-13	East Center	Scotian Basin	Sable Sub-basin	44.209267	58.529569	5202.00		2	1
PESKOWESK A-99	East Center	Scotian Basin	Abenaki Sub-basin	44.470567	-58.977256	4007.00		14	4
HERCULES G-15	North	Scotian Basin	Orpheus Graben	45.572442	-58.786192	1081.10		2	2
SOUTH DESBARRES O-76	North Center	Scotian Basin	Sable Sub-basin	44.098972	-59.932289	6041.00		5	1
SABLE ISLAND C-67	North Center	Scotian Basin	Sable Sub-basin	43.934764	-59.916281	4604.30		0	2
COMO P-21	Northwest Center	Scotian Basin	LaHave Platform	43.846178	-60.804614	3540.00		8	0
COHASSET A-52	Northwest Center	Scotian Basin	LaHave Platform	43.852342	-60.628008	2847.00	2496.00	2	0
PANUKE B-90	Northwest Center	Scotian Basin	LaHave Platform	43.820044	-60.708867	6050.00		6	0
ALMA K-85	Southwest Center	Scotian Basin	Sable Sub-basin	43.579047	-60.716400	3602.00		28	4
ALMA F-67	Southwest Center	Scotian Basin	Sable Sub-basin	43.605211	-60.664950	5054.00		2	0
MOHICAN I-100	West	Scotian Basin	LaHave Platform	42.994253	-62.480211	4393.40		3	0
NASKAPI N-30	West	Scotian Basin	LaHave Platform	43.496261	-62.566139	2205.20		1	1

3.2 WASHING AND SEPARATION OF CUTTINGS

The samples from the selected wells were first washed with warm water in a 63 µm sieve to remove any organic matter and unwanted debris (drill mud, oil, metal fragments from the drill). However, due to the long period since drilling and excess debris, some samples needed to be soaked in soapy water to assist the washing. The samples then were run through a 2 mm sieve prior to separating the shale from other rock types. For the type of XRD analyses used in this study, the required amount of powdered sample is at least 2 g, preferably 3 g. In cases where there was inadequate sample quantity for analysis, the sample was then passed through a 1 mm sieve before separation.

The sieved samples were separated by hand with a binocular microscope with the goal of separating out the shale cuttings. It was not always possible to segregate only the shale component and some samples thus contain more than one lithology such as siltstone and shale. When the samples came from conventional core, sufficient sample from pure shale was available.

3.3 SIDEPACK SAMPLES

The samples were crushed in an agate mortar and pestle until they passed through a 0.4 mm sieve. A McCrone Micronizing Mill was used as the final grinding step to achieve the desired grain size of <20 µm. The mill is a 1/30 HP vibrating mill. The sample is placed in a polypropylene grinding jar, with a capacity of 125 ml and a screw-capped polyethylene grinding lid. The grinding jar accommodates 48 cylindrical

corundum rollers grouped in six layers of eight. They are non-porous, fine-grained, and identical. The sample is placed in the grinding jar, which in turn, is placed into the mill. It oscillates on its axis at 1400 rpm (O'Connor and Chang, 1986).

Zincite (ZnO) was selected as the internal standard, because it is well-crystallized, it has no detectable traces of amorphous substances during XRD analyses and it provides very reproducible diffraction intensities due to its dearth of large crystals (Sroden et al, 2001). Because of this, it has been selected over corundum, which tends to be a more commonly used standard (Srodon et al, 2001). The most advantageous amount of ZnO as a standard is 10% by weight of the sample (Srodon et al, 2001). Therefore, 0.3 grams of ZnO were added to each crushed sample prior to being loaded into the micronizing mill (Table 3.2).

Methanol was used as the most suitable grinding liquid. The use of a grinding liquid provides minimal alteration to the crystal lattice of the sample. Methanol was used as opposed to water because it dries faster. It also prevents swelling of the shale, which has the ability to free individual crystals from the clay (Srodon et al, 2001). Approximately three grams of sample were used. Four milliliters of methanol were added to the sample: any lesser amount of methanol results in Al_2O_3 contamination from the grinding rollers (Srodon et al, 2001). The ground samples were air dried, for approximately seven days each. Once dried, the powder cake was forced through a plastic 0.4 mm screen with a pestle to produce the fine powder which was used for making sidepack mounts.

Table 3.2: Sidepack samples analyzed with corresponding Depth, Formation, sample and weight data.

Well	Depth (m)	Formation	Sample	Sample Wt (g)	Zincite Wt (g)	Zincite Wt %
Alma F-67 (2002)	1190.00	Banquereau Fm	F671190	2.94	0.31	9.74
Alma F-67 (2002)	1750.00	Logan Canyon (Sable Mb)	F671750	3.20	0.30	8.78
Alma K-85 (2006)	2449.40	Logan Canyon (Cree Mb)	K85-2449.40	3.16	0.30	9.50
Alma K-85 (2011)	2449.40	Logan Canyon (Cree Mb)	K85.1.2449.4	3.16	0.30	9.50
Alma K-85 (2006)	2453.85	Logan Canyon (Cree Mb)	K85-2453.85	3.19	0.30	9.50
Alma K-85 (2006)	2455.00	Logan Canyon (Cree Mb)	K85-2455	3.18	0.30	9.46
Alma K-85 (2006)	2456.40	Logan Canyon (Cree Mb)	K85-2456.40	3.17	0.31	9.67
Alma K-85 (2006)	2456.50	Logan Canyon (Cree Mb)	K85-2456.50	3.18	0.30	9.48
Alma K-85 (2006)	2458.15	Logan Canyon (Cree Mb)	K85-2458.15	3.18	0.30	9.44
Alma K-85 (2006)	2460.75	Logan Canyon (Cree Mb)	K85-2460.75	3.18	0.30	9.54
Alma K-85 (2006)	2878.90	Mississauga Upper Mb	K85-2878.98	3.17	0.30	9.58
Alma K-85 (2006)	2880.22	Mississauga Upper Mb	K85-2880.22	3.16	0.30	9.53
Alma K-85 (2006)	2888.26	Mississauga Upper Mb	K85-2888.26	3.15	0.30	9.65
Alma K-85 (2006)	2904.15	Mississauga Upper Mb	K85-2904.15	3.15	0.31	9.69
Alma K-85 (2011)	2904.15	Mississauga Upper Mb	K85.6.2904.15	3.15	0.31	9.69
Alma K-85 (2006)	2906.78	Mississauga Upper Mb	K85-2906.78	3.15	0.30	9.54
Alma K-85 (2006)	2912.04	Mississauga Upper Mb	K85-2912.04	3.15	0.31	9.73
Alma K-85 (2006)	2919.00	Mississauga Upper Mb	K85-2919.0	3.16	0.30	9.58
Alma K-85 (2006)	2919.45	Mississauga Upper Mb	K85-2919.45	3.18	0.31	9.58
Alma K-85 (2006)	2920.30	Mississauga Upper Mb	K85-2920.30	3.16	0.30	9.64
Alma K-85 (2006)	2931.87	Mississauga Upper Mb	K85-2931.87	3.17	0.30	9.51
Alma K-85 (2006)	3038.00	Mississauga Upper Mb	K85-3038	3.17	0.30	9.54
Alma K-85 (2006)	3039.88	Mississauga Upper Mb	K85-3039.88	3.17	0.30	9.46
Alma K-85 (2006)	3044.60	Mississauga Upper Mb	K85-3044.6	3.19	0.30	9.48
Alma K-85 (2006)	3047.90	Mississauga Upper Mb	K85-3047.9	3.19	0.30	9.47
Alma K-85 (2006)	3068.15	Mississauga Upper Mb	K85-3068.15	3.18	0.30	9.53
Alma K-85 (2006)	3071.80	Mississauga Upper Mb	K85-3071.8	3.19	0.31	9.59
Alma K-85 (2006)	3089.05	Mississauga Upper Mb	K85-3089.05	3.19	0.30	9.49
Alma K-85 (2006)	3090.45	Mississauga Upper Mb	K85-3090.45	3.13	0.30	9.74
Alma K-85 (2006)	3093.80	Mississauga Upper Mb	K85-3093.8	3.19	0.30	9.49
Alma K-85 (2006)	3104.10	Verrill Canyon Fm	K85-3104.1	3.16	0.31	9.65
Alma K-85 (2011)	3104.10	Verrill Canyon Fm	K85.11.3104.1	3.16	0.31	9.65
Alma K-85 (2006)	3104.70	Verrill Canyon Fm	K85-3104.7	3.19	0.31	9.64
Chebucto K-90 (2002)	1690.00	Banquereau Fm	K901690	3.20	0.31	9.58
Chebucto K-90 (2002)	2220.00	Logan Canyon (Marmora Mb)	K902220	3.20	0.30	9.00
Chebucto K-90 (2002)	2470.00	Logan Canyon (Marmora Mb)	K902470	3.20	0.31	9.15
Chebucto K-90 (2002)	3780.00	Logan Canyon (Cree Mb)	K903780	3.20	0.30	8.91
Chebucto K-90 (2002)	4370.00	Mississauga Fm	K904370	3.20	0.30	8.94
Chebucto K-90 (2002)	4420.00	Mississauga Fm	K904420	3.20	0.30	8.90
Chebucto K-90 (2002)	4585.00	Mississauga Fm	K904585N	3.20	0.30	9.00
Chebucto K-90 (2002)	4750.00	Mississauga Fm	K904750	3.20	0.31	8.80
Chebucto K-90 (2002)	5120.00	Mississauga Fm	K905120	3.20	0.32	9.67
Chebucto K-90 (2002)	5230.00	Mississauga Fm	K905230	3.20	0.30	8.68
Cohasset A-52 (2011)	2072.90	Logan Canyon (Cree Mb)	A52_2072_9	2.93	0.29	9.90
Cohasset A-52 (2011)	2074.72	Logan Canyon (Cree Mb)	A52_2074_72	3.00	0.30	10.00
Cohasset A-52 (2011)	2123.52	Logan Canyon (Cree Mb)	A52_2123_52	3.00	0.30	10.00
Cohasset A-52 (2011)	2138.22	Logan Canyon (Cree Mb)	A52_2138_22	3.00	0.30	10.00
Cohasset A-52 (2011)	2418.75	Logan Canyon (Naskapi Mb)	A52_2418_75	3.00	0.30	10.00
Cohasset A-52 (2011)	2597.05	Mississauga Upper Mb	A52_2597_05	3.00	0.30	10.00
Como P-21 (2011)	2188.75	Mississauga Upper Mb	P21_2188_75	3.00	0.30	10.00
Como P-21 (2011)	3065.72	Mississauga Middle Mb	P21_3065_72	3.00	0.30	10.00
Glenelg J-48 (2002)	1405.00	Banquereau Fm	J481405	2.51	0.30	11.19
Glenelg J-48 (2002)	3250.00	Logan Canyon (Naskapi Mb)	J483250	3.10	0.31	9.43
Glenelg J-48 (2002)	3645.00	Mississauga Upper Mb	J483645	3.20	0.30	8.90
Glenelg J-48 (2002)	3860.00	Mississauga Upper Mb	J483860	3.20	0.30	9.87
Glenelg J-48 (2002)	4030.00	Mississauga Upper Mb	J484030	3.20	0.31	8.97
Glenelg J-48 (2002)	4385.00	Mississauga Middle Mb	J484385	3.20	0.30	9.92
Glenelg J-48 (2002)	4740.00	Verrill Canyon Fm	J484740	3.20	0.31	9.07

Hercules G-15 (2006)	371.86	Logan Canyon (Marmora Mb)	G15.1220	3.17	0.30	9.49
Hercules G-15 (2006)	646.18	Logan Canyon (Cree Mb/Pyro)	G15-2120	3.17	0.30	9.52
Mohican I-100 (2011)	2533.24	Mississauga Middle Mb	I100_2533_24	3.00	0.30	10.00
Mohican I-100 (2011)	2539.94	Mississauga Middle Mb	I100_2539_94	3.00	0.30	10.00
Mohican I-100 (2011)	2541.23	Mississauga Middle Mb	I100_2541_23	3.00	0.30	10.00
Naskapi N-30 (2011)	1469.10	Mississauga Upper Mb	N30_1469_1	3.00	0.30	10.00
North Banquereau I-13 (2011)	3248.80	Logan Canyon (Naskapi Mb)	I13_3248_8	3.00	0.30	10.00
North Banquereau I-13 (2011)	3249.65	Logan Canyon (Naskapi Mb)	I13_3249_65	3.00	0.30	10.00
Panuke B-90 (2011)	2097.27	Logan Canyon (Cree Mb)	B90_2097_27	3.00	0.30	10.00
Panuke B-90 (2011)	2235.37	Logan Canyon (Naskapi Mb)	B90_2235_37	3.00	0.30	10.00
Panuke B-90 (2011)	2241.57	Logan Canyon (Naskapi Mb)	B90_2241_57	3.00	0.30	10.00
Panuke B-90 (2011)	2245.78	Logan Canyon (Naskapi Mb)	B90_2245_78	3.00	0.30	10.00
Panuke B-90 (2011)	2247.20	Logan Canyon (Naskapi Mb)	B90_2247_2	3.00	0.30	10.00
Panuke B-90 (2011)	2255.49	Logan Canyon (Naskapi Mb)	B90_2255_49	3.00	0.30	10.00
Panuke B-90 (2011)	2256.56	Logan Canyon (Naskapi Mb)	B90_2256_56	3.00	0.30	10.00
Panuke B-90 (2011)	2278.21	Logan Canyon (Naskapi Mb)	B90_2278_21	3.00	0.30	10.00
Peskowesk A-99 (2006)	2209.25	Logan Canyon (Cree Mb)	A99-2209.25spk	3.17	0.30	9.48
Peskowesk A-99 (2011)	2209.25	Logan Canyon (Cree Mb)	A99.01.2209.25	3.17	0.30	9.48
Peskowesk A-99 (2006)	2213.57	Logan Canyon (Cree Mb)	A99-2213.57spk	3.18	0.30	9.44
Peskowesk A-99 (2006)	2215.78	Logan Canyon (Cree Mb)	A99-2215.78spk	3.17	0.30	9.49
Peskowesk A-99 (2006)	2219.03	Logan Canyon (Cree Mb)	A99-2219.03spk	3.14	0.30	9.61
Peskowesk A-99 (2006)	2221.69	Logan Canyon (Cree Mb)	A99-2221.69spk	3.18	0.30	9.52
Peskowesk A-99 (2006)	2228.42	Logan Canyon (Cree Mb)	A99-2228.42spk	3.13	0.30	9.73
Peskowesk A-99 (2006)	2479.35	Mississauga Upper Mb	A99-2479.35spk	3.15	0.30	9.66
Peskowesk A-99 (2006)	2488.85	Mississauga Upper Mb	A99-2488.85spk	3.17	0.30	9.58
Peskowesk A-99 (2006)	2492.62	Mississauga Upper Mb	A99.2492.62spk	3.18	0.30	9.45
Peskowesk A-99 (2006)	2927.36	Mississauga Middle Mb	A99.2927.36spk	3.15	0.30	9.58
Peskowesk A-99 (2011)	2927.36	Mississauga Middle Mb	A99.10.2927.36	3.15	0.30	9.58
Peskowesk A-99 (2006)	2940.90	Mississauga Middle Mb	A99-2940.90spk	3.17	0.30	9.60
Peskowesk A-99 (2006)	2947.43	Mississauga Middle Mb	A99.2947.43spk	3.14	0.30	9.59
Peskowesk A-99 (2006)	3806.51	Mic Mac Fm	A99-3806.51spk	3.18	0.30	9.48
Peskowesk A-99 (2006)	3812.64	Mic Mac Fm	A99.3812.64spk	3.19	0.30	9.50
Peskowesk A-99 (2011)	3812.64	Mic Mac Fm	A99.14.3812.64	3.19	0.30	9.50
Sable Island C-67 (2011)	2474.18	Logan Canyon (Cree Mb)	C67_2474_18	3.00	0.30	10.00
Sable Island C-67 (2011)	2830.45	Logan Canyon (Naskapi Mb)	C67_2830_45	3.00	0.30	10.00
Sable Island C-67 (2011)	2835.42	Logan Canyon (Naskapi Mb)	C67_2835_42	3.00	0.30	10.00
Sable Island C-67 (2011)	3373.45	Mississauga Middle Mb	C67_3373_45	3.00	0.30	10.00
Sable Island C-67 (2011)	4089.87	Mississauga Lower Mb	C67_4089_87	3.00	0.30	10.00
Thebaud C-74 (2002)	1825.00	Logan Canyon (Sable Mb)	C741825	3.20	0.31	9.31
Thebaud C-74 (2011)	1825.00	Logan Canyon (Sable Mb)	1825.1825LC	3.20	0.31	9.31
Thebaud C-74 (2002)	1990.00	Logan Canyon (Cree Mb)	C741990	3.20	0.30	8.93
Thebaud C-74 (2002)	2200.00	Logan Canyon (Cree Mb)	C742200	3.20	0.31	9.23
Thebaud C-74 (2002)	2205.00	Logan Canyon (Cree Mb)	C742205	3.20	0.30	8.75
Thebaud C-74 (2002)	2390.00	Logan Canyon (Cree Mb)	C742390	3.20	0.30	8.77
Thebaud C-74 (2002)	2560.00	Logan Canyon (Naskapi Mb)	C742560	3.20	0.30	8.86
Thebaud C-74 (2011)	2560.00	Logan Canyon (Naskapi Mb)	2560.2560.LC	3.20	0.30	8.86
Thebaud C-74 (2002)	2630.00	Logan Canyon (Naskapi Mb)	C742360	3.20	0.32	9.27
Thebaud C-74 (2002)	2775.00	Mississauga Upper Mb	C742775	3.20	0.30	9.10
Thebaud C-74 (2002)	2780.00	Mississauga Upper Mb	C742780	3.20	0.30	8.67
Thebaud C-74 (2002)	3075.00	Mississauga Middle Mb	C743075	3.20	0.31	9.14
Thebaud C-74 (2002)	3615.00	Mississauga Middle Mb	C743615	3.20	0.31	9.10
Thebaud C-74 (2002)	3780.00	Mississauga Lower Mb	C743780	3.20	0.31	8.94
Thebaud C-74 (2002)	4020.00	Mississauga Lower Mb	C744020	3.20	0.30	8.69
Thebaud C-74 (2002)	4105.00	Mississauga Lower Mb	C744105	3.20	0.30	8.60
Thebaud C-74 (2002)	4335.00	Mississauga Lower Mb	C744335	3.20	0.30	8.95
Thebaud C-74 (2011)	4335.00	Mississauga Lower Mb	4335.4335ML.Mb	3.20	0.30	8.95

Figure 3.1: McCrone Micronizing Mill.

Random sidepack mounts were used to avoid the platy clay crystals from aligning and becoming oriented. To create this type of mount, one side of a typical XRD plastic sample holder had to be cut out. A frosted glass slide was placed over the top of the XRD slide and it was held on its side with the cut hole facing up. Using a spatula, the fine powdered sample was carefully poured into the slide while occasionally giving the slide a firm tap on a counter top to ensure all voids were eliminated.

3.4 <2 µm SAMPLES

Initially, samples from Alma K-85 (4), Peskowesk A-99 (4) and Thebaud C-74 (4) were selected for comparison with the sidepacks. At a later date, samples were selected from Chebucto K-90 (3), Hercules G-15 (2), Naskapi N-30 (1), North Banquereau I-13 (1), Sable Island C-67 (1), South Desbarres O-76 (2) and Thebaud I-93 (1). They were from the same sample as the sidepacks (except South Desbarres O-76), therefore, they were cleaned and crushed as mentioned in the sidepack section. The powder was passed through a 63 µm sieve and the portions of the sample that could not pass through were further crushed using a mortar and pestle until all of the powder passed through the sieve.

The powders were then placed in 1000 mL graduated cylinders with spigots at 20 cm below the 1000 ml mark (Figure 3.2). One percent sodium hexametaphosphate (purified Calgon electrolyte solution) was added to the suspension; the cylinder was shaken for one minute, and then allowed to settle for 16 hours.

At 16 hours the sediment that settled on the inner lip of the spigot was removed using a cotton swab and the suspension (consisting of the <2 µm sediment) was tapped off into a 500 ml centrifuge bottle (Gould 2007) (Figure 3.3). Due to some small sample quantities, several samples needed to be re-suspended to acquire as much of the <2 µm fraction as possible. One ml of 0.5N $CaCl_2$ solution was added to flocculate the sediment and replace the Calgon. The samples were then placed in a centrifuge for 90 minutes at

Figure 3.2: <2 micron samples in 1000ml graduated cylinders with spigots at 20cm below the 1000ml mark.

Figure 3.3: <2 micron samples in 1000ml graduated cylinders and centrifuge bottles after being tapped off.

3250 rpm, after which the supernatant was decanted. The suspension and centrifuge steps were repeated as many times as was needed to get at least 0.4 g of sample.

Samples were placed in aluminum drying dishes in a 60°C oven to drive off any moisture. The sample was then re-suspended in a 500 ml graduated cylinder and shaken. Twenty mL was drawn off with a pipette and placed in the drying dishes and the rest of the suspension was placed back in the centrifuge bottles. The dishes were left overnight in a 60°C oven to remove all water and a net sample weight was calculated. The dried sample was returned to suspension with the rest of the sample in the 500 ml centrifuge bottle.

Using the net sample weight, a 5% standard of talc was added to the first set (Alma K-85, Peskowesk A-99 and Thebaud C-74) (Table 3.3). Five percent zincite was added to the second set of samples (Chebucto K-90, Hercules G-15, Naskapi N-30, North Banquereau I-13, Sable Island C-67, South Desbarres O-76 and Thebaud I-93) (Table 3.4) due to concern that the talc peak may mask other minerals of interest. Another 1 mL of 0.5N $CaCl_2$ solution was added and the solution was centrifuged and decanted again. The sediment was transferred to 50 ml conical tubes, centrifuged and decanted.

To fit into the XRD slide holder, two sets of slides were prepared by cutting 1”x3” regular glass slides and 1”x2” high temperature slides into 1” squares. The high temperature slides are thicker than the regular glass slides. Thus there is significant peak height loss between the air-dried and glycolated analyses when compared with the heated analyses (Figure 3.4). Absolute peak heights cannot be properly compared; however, relative peak heights can be compared. The slides were then frosted (by

Table 3.3: 1st set of <2 µm samples using talc as standard.

Well	Depth	Formation	Sample	Sample Weight	Talc Weight	Talc Wt%
	(m)			(g)	(g)	
Thebaud C-74 (2011)	1825.00	Logan Canyon (Sable Mb)	C74-1825	1.075	0.054	5.0
Thebaud C-74 (2011)	2560.00	Logan Canyon (Naskapi Mb)	C74-2560	1.075	0.054	5.0
Thebaud C-74 (2011)	3780.00	Mississauga Lower Mb	C74-3780	0.400	0.020	5.0
Thebaud C-74 (2011)	4335.00	Mississauga Lower Mb	C74-4335	0.600	0.030	5.0
Peskowesk A-99 (2011)	2209.25	Logan Canyon (Cree Mb)	A99-2209.25	2.475	0.124	5.0
Peskowesk A-99 (2011)	2479.35	Mississauga Upper Mb	A99-2479.35	2.325	0.116	5.0
Peskowesk A-99 (2011)	2927.36	Mississauga Middle Mb	A99-2927.36	1.875	0.094	5.0
Peskowesk A-99 (2011)	3812.64	Mic Mac Fm	A99-3812.64	1.100	0.055	5.0
Alma K-85 (2011)	2449.40	Logan Canyon (Cree Mb)	K85-2449.4	1.375	0.069	5.0
Alma K-85 (2011)	2904.15	Mississauga Upper Mb	K85-2904.15	0.425	0.021	4.9
Alma K-85 (2011)	3038.88	Mississauga Upper Mb	K85-3039.88	1.025	0.051	5.0
Alma K-85 (2011)	3104.10	Verrill Canyon Fm	K85-3104.1	0.700	0.035	5.0

Table 3.4: 2st set of <2 µm samples using zincite as standard.

Well	Depth	Formation	Sample	Sample Weight	Zincite Weight	Zincite Wt %
	(m)			(g)	(g)	PEAK
Chebucto K-90 (2012)	2220.00	Logan Canyon (Marmora Mb)	K90_2220	1.075	0.054	5.0
Chebucto K-90 (2012)	4585.00	Mississauga Fm	K90_4585	0.500	0.025	5.0
Chebucto K-90 (2012)	5120.00	Mississauga Fm	K90_5120	0.500	0.025	5.0
Hercules G-15 (2012)	371.86	LC (Marmora Mb)	N/A	N/A	N/A	N/A
Hercules G-15 (2012)	646.18	LC (Cree Mb)	G-15_646.18	1.075	0.054	5.0
Naskapi N-30 (2012)	1469.10	Miss Upper Mb	N30_1469_1	0.600	0.030	5.0
North Banquereau I-13 (2012)	3248.80	Logan Canyon (Naskapi Mb)	I13_3248_8	1.200	0.060	5.0
Sable Island C-67 (2012)	3373.45	Mississauga Middle Mb	C67_3373_45	0.825	0.041	5.0
South Desbarres O-76 (2012)	3815.10	Mississauga Lower Mb	O-76 3815.10	1.325	0.066	5.0
South Desbarres O-76 (2012)	5956.80	Mic Mac Fm	O-76 5956.80	1.375	0.069	5.0
Thebaud I-93 (2012)	3080.38	Mississauga Middle Mb	I93_3080.38	1.075	0.054	5.0

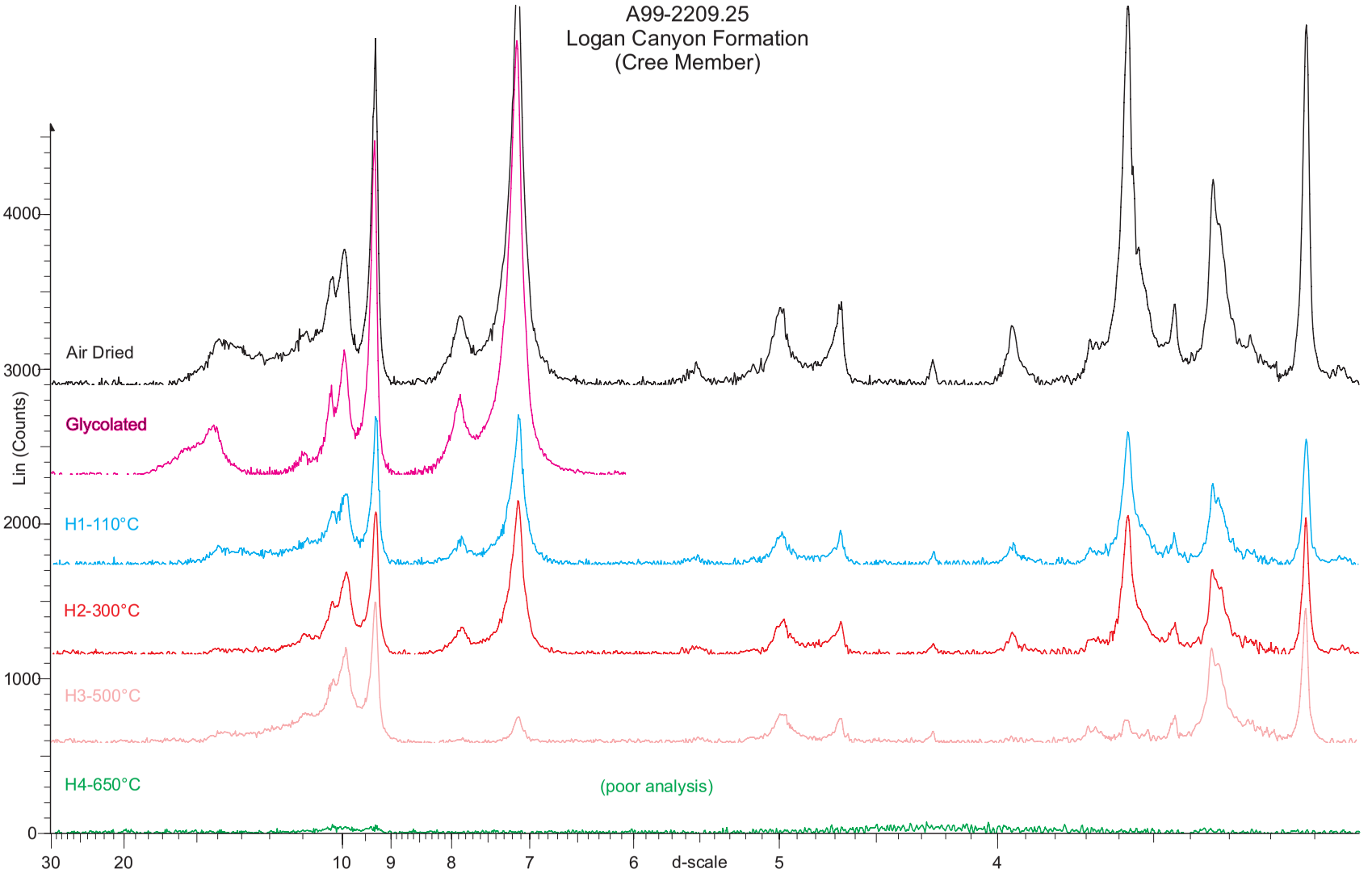

Figure 3.4: X-ray diffraction of Peskowesk A-99 2209.25 m. Scans showing loss of peak height between the air-dried and glycolated analyses when compared with the heat treated analyses.

mildly grinding one side), which provides a superior adhesive surface for the smooth clays. The slides are then thoroughly washed and dried. Using a sonic bath, the sample was stirred well to make a paste. Placing a dollop of clay paste on the slide, a small piece of flexible plastic was used to smear the clay, forming a smooth and even surface. This was left to dry prior to analysis.

3.5 X-RAY DIFFRACTION ANALYSIS

3.5.1 X-RAY DIFFRACTION SETTINGS

The samples were analyzed with a Siemens Kristaloflex diffractometer (XRD) (Co Kα radiation). The diffractometer program (EVA) was used to analyze the X-ray diffractograms.

For the sidepack samples, two ranges of scans were produced. The first range (Range 1) is similar to that for oriented samples. It runs from 5.0° - 69.5° 2θ at a scanning rate (step size) of 0.02° 2θ. Each step was held for five seconds. When the XRD reached 69.5°, the second range (060 reflections) (Range 2) started. It runs from 69.5° - 77.0° 2θ with a step size of 0.010° 2θ. The 060 reflections aid in the quantification of clay minerals which are well resolved and insensitive to structural defects. Each step was held for five seconds. The raw data was then processed and mineral peak areas were picked using the EVA program. For peak pick details see Appendix 3.

After being air dried, the <2 μm samples on the regular glass slides were run with a scanning range of 2°- 52° 2θ, and a step size of 0.02° 2θ , with a 5.0 second count per

step. After this they were placed in a desiccator with ethylene glycol and then analyzed with a scanning range of 2°- 17° 2θ, and a step size of 0.02° 2θ , with a 5.0 second count per step. After being left out for one week this process was repeated using glycerol for four of the samples.

The samples on the high temperature slides were heated to 110°C, 300°C, 500°C and 650°C and were run with a scanning range of 2°- 52° 2θ, and a step size of 0.02° 2θ , with a 5.0 second count per step after each heating. Focus was placed on the peaks between a d-spacing of 30-3 Å.

Picking procedures involved Kα2 stripping, x-axis offset to correctly align the quartz and standard peaks, automatic background removal, followed by measurement of peak areas. In the case of overlapping peaks, the XRD program EVA assigned the trough between the two peaks as the 2θ limit of the peak, with the assumption that the area of the peak outside the 2θ limit was balanced by the area of the peak of interest inside the 2θ limit.

3.5.2 ILLITE CRYSTALLINITY

The Kubler Index (KI) has been used to determine the crystallinity of illite. It is the measure of the full width at half height of the illite-smectite peak at 10 Å (Jaboyedoff et al., 2001). Dues to the abundance of mixed layer clays overlapping the low 2θ side of the illite peak in this study, the half width (right half) at half height was measured. Analysis of illite crystallinity is typically used as a measurement of metamorphism with lower KI values indicating higher crystallinity, therefore, increasing

metamorphic grade (Jaboyedoff et al., 2001). Various studies have correlated this tendency (lower values of KI indicating increasing metamorphic grade) with altering metamorphic mineral assemblages and organic maturity indicators (Kubler, 1964, 1984; Jaboyedoff & Thelin, 1996; Merriman & Frey, 1999). Abid and Hesse (2007) found that the Kubler Index is useful for understanding the provenance and thermal conditions of the source rock, but not for reconstructing the thermal history of the basin that they were investigating. The crystallinity of illite and its relationship to metamorphic grade could help understand the deeper samples and samples that have experienced diagenesis.

Warr and Rice (1994) recognized the fact that a standardized methodology for preparing and analyzing clay minerals formed in the anchizonal/low grade metamorphic zone with an X-ray diffractometer had not been created. This is a problem because XRD results cannot be properly recreated and compared. They found that calibrating equipment with a set of interlaboratory rock chip standards would help solve this problem. This study also provides a crystallinity index standard (CSI) to aid in replication of analyses. The results of this study were tested with regards to metamorphosed rock samples by Leoni (2001). The samples used were from well-defined metamorphic facies characterized by known metamorphic P-T conditions. This helps determine the suitability of the Crystallinity Index Standard (CIS) scale as a potential indicator of metamorphic grade. Leoni (2001) found that the Warr and Rice (1994) Illite Crystallinity (CI) scale can be considered a good progression of the standardization of IC data.

3.6 GEOCHEMISTRY

Published and unpublished whole-rock geochemical analyses of the clay samples were provided by Georgia Pe-Piper. Some are reported in Pe-Piper et al. (2008). Analyses were made by Activation Laboratories Ltd. according to their Code 4Lithoresearch and Code 4B1 packages, which combine lithium metaborate/tetraborate fusion ICP analysis for major elements with ICP-MS analysis for trace elements, using international rock standards (Activation Laboratories Ltd. 2006). Raw geochemical data is available in a data report (Pe-Piper et al. 2007).

3.7 CONCERNS ABOUT VARIABILITY AND ERRORS

Throughout this research, several potential issues with the variability in error using X-ray diffraction analyses on powdered shale samples were identified.

- **Variation with creating the mounts.**

Consistency of the grain size is one of the more important areas for variability. When analyzing clay, rock, or anything in between, attempting to achieve an overall similar grain size in the sample can prove difficult.

Clays are typically much easier to achieve consistency; however, when using a mortar and pestle, the length of the grind, combined with the liquid lubricant used, will be determined by the amount of pressure the individual applies.

Rocks (shale) can prove much more difficult, and that difficulty increases with increasing amounts of harder minerals, such as quartz. Similar to clays, the length of the grind and the liquid lubricant used will be determined by the amount of pressure

applied to the grind. It will also depend on how hard the hardest mineral in the rock is and the abundance of this mineral.

The first step in resolving this issue was to ensure that only shale samples were selected for crushing. The McCrone Micronizing Mill resolved the issue of grain size consistency for the sidepack analyses (Figure 3.1). The <2 μm samples were crushed in a mortar and pestle for short durations and then passed through a 63 μm sieve.

In clay samples crystal orientation can also be an issue. Due to the platy nature of clay crystal structures they tend to align creating a preferred orientation. This is not a problem for oriented mounts such as, <2 μm mounts, but does not allow for quantitative analysis. Using the sidepack method is a good technique for randomly orienting the clay crystals.

Adding an internal standard (10% by weight of ZnO was used here) to the sample is a good way to get true values for the peak intensities; however, normalization of the peaks will need to be performed (sample/standard).

Slide coverage is another potential issue. If the slide is not fully and evenly covered by the sample, then the XRD results may not be accurate. Mixing methanol with the sample and using a pipette to transfer the mixture onto the slide will help ensure even coverage.

While the sample is drying, curling and cracking can also occur. Water will also cause swelling in clay samples which can affect the analysis. Using methanol as opposed to water and drying the samples in an oven at 60°C can help limit the effect of these issues.

- **Variation in the peak picking.**

Measuring peak intensity is quite variable between different users and to a small degree is as much a product of personal interpretation as it is actual mineral content. This is not to say that for example, quartz will be identified in place of calcite. The user should be aware that a large peak can potentially be two overlapping peaks, which is often the case. Some examples of this are: >=13 Å Chlorite and >=15 Å Smectite, 7.16-7.20 Å Kaolinite and Mg Chlorite, and 3.57 Å Kaolinite and 3.55 Å Fe Chlorite. Each of these peaks has a peak intensity of seven to ten which produces large peaks causing potential overlap. There are numerous examples of this and the individual picking the peaks should be aware of this and have a general knowledge of the sample and the potential minerals it may contain.

Running Short Scans around the 3.57 Å Kaolinite and 3.55 Å Fe Chlorite peaks can help to better identify them. Glycolation, glycerol and heat treatments can help to resolve most other peak overlaps.

The diffractogram also shows background peaks (or noise) as well as mineral peaks. These background peaks are continuous throughout the diffractogram and are typically quite small. These background peaks will also provide potential variability between individual interpretations. In some cases it can be challenging to determine where the actual mineral peak begins and ends and where the background peaks begin and end.

The first step in resolving this issue is to mentally picture an unbroken arch or rounded triangle over the peak. Following an unbroken decent from the peak to the

lowest point before the diffractogram starts to climb again is another way to help with this problem. This can also aid in determining if there is only one mineral peak or multiple overlapping peaks. The most important factor in accurately picking peaks is to be consistent. Pick a method that works and do not change part way through analysis.

One example of the latter not working in this study is the 10.1 Å illite-muscovite peak because it is overlapped on the right side by mixed layer clays. This causes the measurement of the area of the illite-muscovite peak in the quantitative analysis from the bulk random sidepack scans to be inaccurate. To compensate for this, instead of measuring from the lowest point on either side of the peak the measurement was from the center of the peak to the lowest point on the left side. This number was then doubled to provide a full peak area.

- **Variation in the XRD over time.**

As the equipment ages there could be potential issues with reproducibility. The X-ray tube (the type used here is Co Kα) will also age with use and over time the peaks will become less intense. The detector will also wear out over time. The best way to avoid this issue is to maintain the equipment and upgrade when needed.

CHAPTER 4: RESULTS

4.1 <2 MICRON SAMPLES

Samples from ten wells were investigated using <2 micron separation and XRD analyses of oriented mounts. These wells are: Alma K-85, Chebucto K-90, Hercules G-15, Naskapi N-30, North Banquereau I-13, Peskowesk A-99, Sable Island C-67, South Desbarres O-76, Thebaud C-74 and Thebaud I-93 (Table 4.1) (Figure 4.1).

Sidepack analyses were not made from two samples from South Desbarres O-76 and Thebaud I-93. The other 23 samples were selected to compare with sidepack XRD analyses that were performed on the same samples.

Alma K-85, Peskowesk A-99 and Thebaud C-74 had two sets of samples made and prepared in several different ways prior to analysis (Table 3.3). Talc was the standard used for both sets. The first set was air dried, after which, one sample from Peskowesk A-99 was treated with glycerol. The second set was treated with ethylene glycol, and then heated to 110°C, 300°C, 500°C, and 650°C prior to each run in the XRD.

It should be noted that several samples were damaged during heating before reaching the highest temperatures. Samples A-99 2209.25, K-85 2449.4 and K-85 2904.15 therefore showed no peaks at 650°C. Samples A-99 2479.35 and A-99 2927.36 showed no peaks at 500°C or 650°C.

Samples from the wells Chebucto K-90, Hercules G-15, Naskapi N-30, North Banquereau I-13, Sable Island C-67, South Desbarres O-76, and Thebaud I-93 were all analyzed three times (Table 3.4). Zincite was used as the standard for this set. The samples were air-dried and analyzed, after which, they were treated with glycol and

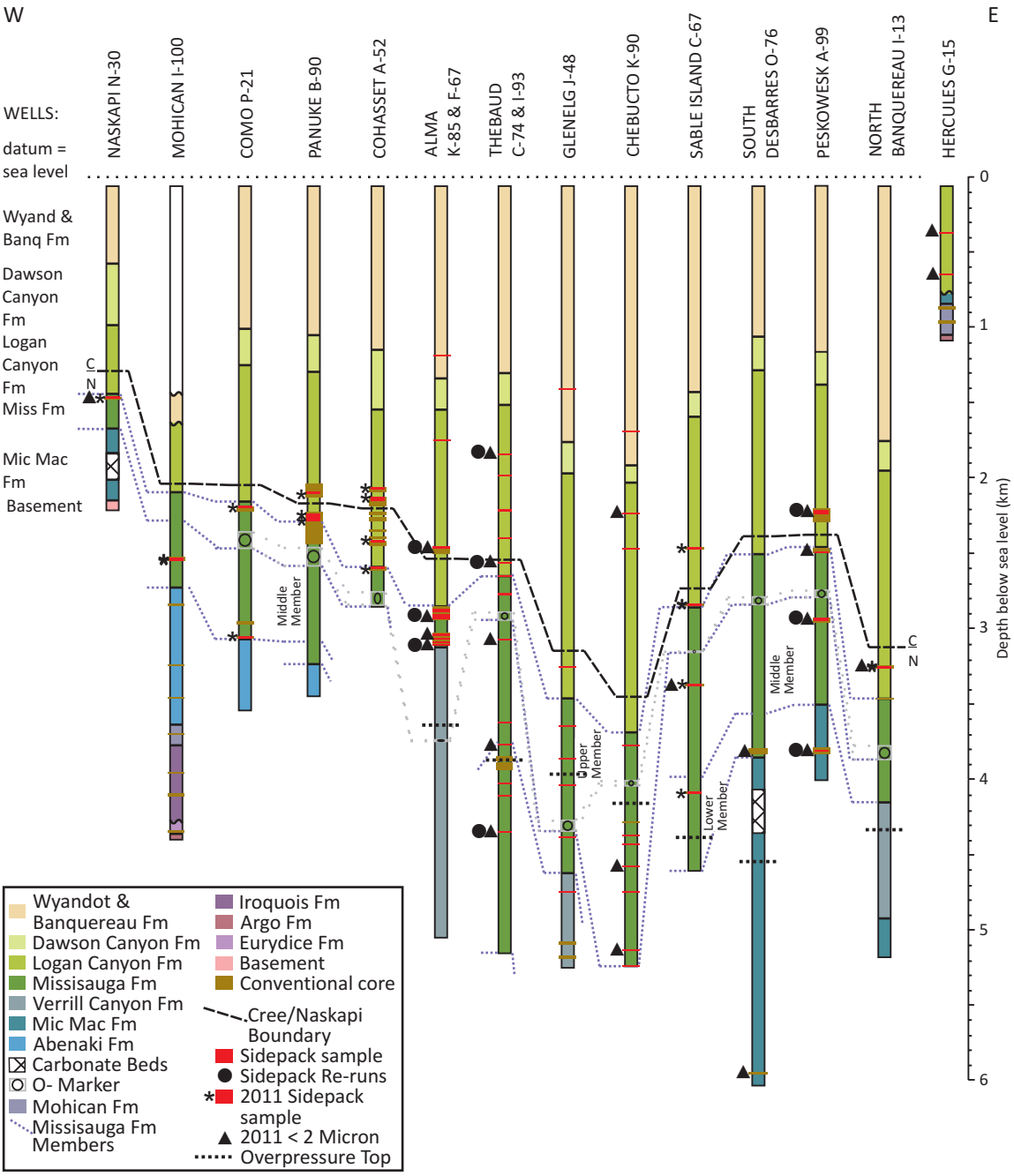

Figure 4.1: Stratigraphy of wells investigated with depths of bulk random sidepack and oriented <2 micron samples.

Table 4.1: <2 Micron samples analyzed with corresponding Depth and Formation data.

Well	Depth (m)	Formation	Weight (g)
ALMA K-85	2449.4	Logan Canyon (Cree Mb)	10.080
ALMA K-85	2904.15	Mississauga Upper Mb	5.060
ALMA K-85	3039.88	Mississauga Upper Mb	10.820
ALMA K-85	3104.1	Verrill Canyon Fm	7.220
CHEBUCTO K-90	2220	Logan Canyon (Marmora Mb)	4.572
CHEBUCTO K-90	4585	Mississauga Fm	5.991
CHEBUCTO K-90	5120	Mississauga Fm	5.701
HERCULES G-15	371.86	Logan Canyon (Marmora Mb)	N/A
HERCULES G-15	646.18	Logan Canyon (Cree Mb/Pyro)	8.628
NASKAPI N-30	1469	Mississauga Upper Mb	9.833
NORTH BANQUEREAU I-13	3248.8	Logan Canyon (Naskapi Mb)	8.661
PESKOWESK A-99	2209.25	Logan Canyon (Cree Mb)	10.380
PESKOWESK A-99	2479.35	Mississauga Upper Mb	8.740
PESKOWESK A-99	2927.36	Mississauga Middle Mb	8.370
PESKOWESK A-99	3812.64	Mic Mac Fm	9.900
SABLE ISLAND C-67	3373.45	Mississauga Middle Mb	8.645
SOUTH DESBARRES O-76	3815.1	Mississauga Lower Mb	9.709
SOUTH DESBARRES O-76	5956.8	Mic Mac Fm	8.805
THEBAULD C-74	1825	Logan Canyon (Sable Mb)	5.010
THEBAULD C-74	2560	Logan Canyon (Naskapi Mb)	6.200
THEBAULD C-74	3780	Mississauga Lower Mb	5.970
THEBAULD C-74	4335	Mississauga Lower Mb	4.260
THEBAULD I-93	3080.38 - 3080.48	Mississauga Middle Mb	8.091

analyzed, and lastly, Hercules G-15, Chebucto K-90 and Naskapi N-30 each had one sample treated with glycerol prior to the third analysis.

Samples treated with glycol and glycerol, when compared with air-dried runs, will show disappearance of some peaks and expansion of other peaks if smectite or other expandable clays are present in the samples. In this study, the XRD program EVA was used to automatically remove background. Removing the background makes identification and isolation of the peaks easier; however, the background removal procedure may also remove parts of overlapping peaks. Due to this fact, when comparing the glycol treated analysis versus the air dried analysis, there is a large apparent loss of peaks between 14.0 Å and 10.0 Å (Figure 4.2) that is consistent across all samples and appears to result from overlapping peaks that are separated by glycolation.

Minerals Present:

The minerals identified and the peak "d-spacing" can be found in Table 4.2, <2 µm sample peak heights can be found in table 4.3 and the XRD scans can be found in Appendix 1. Mineral description of the two standards used are as follows.

Talc (standard added):

Talc is recognized at d-spacings of 9.31 Å (001), 4.67 Å (002), and 3.11 Å (003) (Brindley & Brown, 1980; Moore & Reynolds, 1997; Anthony et al., 2001) (Figure 4.2). At 300°C and 500°C the peak height increases slightly before decreasing in height at 650°C. No shift is seen. Peak 002 stays relatively the same height through all of the heating stages. No shift is seen. The 003 peak shows no collapse with the heat

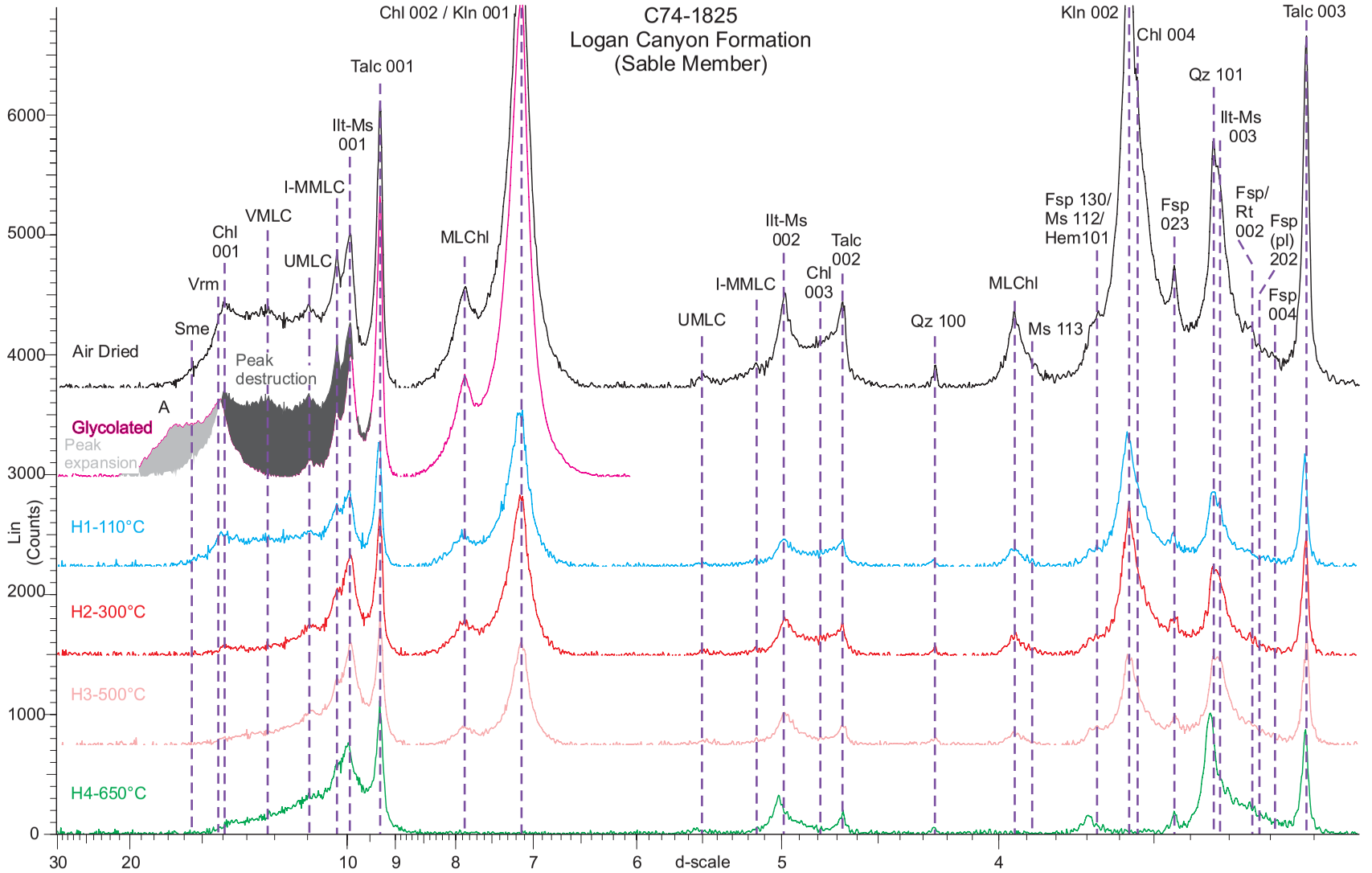

Figure 4.2: Thebaud C-74 1825.25 m <2µm oriented scan showing minerals identified in air-dried, glycolated and heat treatment analyses overlain. Also seen is the apparent loss of peaks from 14.0 Å to 10.0 Å when comparing air-dried and heated analyses.

Table 4.2: <2 µm minerals Identified in Scotian Basin samples.

d-spacing (Å)					Mineral
14.0-20.0					Smectite (Sme)
13.6-14.3 (001)	7.12-7.16 (002)	4.78 (003)	3.54 (004)		Chlorite (Chl)
7.86	3.94				Mixed layer chlorite (MLChl)
11	5.5				Unspecified mixed layer clays (UMLC)
14-14.6					Vermiculite (Vrm)
12.26					Vermiculite/mixed layer clays (VMLC)
10.26	5.15				Illite / Montmorillonite mixed layer (I-MMLC)
10.1 (001)	5.02-5.05 (002)	3.32 (003)			Illite-Muscovite (Ilt-Ms)
9.31 (001) (std)	4.67 (002)	3.11 (003)			Talc
7.12-7.16 (001)	3.57 (002)				Kaolinite (Kln)
12-12.7 (101)	7.5 (130)	3.3 (080)			Sepiolite (Sep)
4.26 (100)	3.34 (101)				Quartz (Qt)
3.69 (101)					Hematite (Hem)
3.68 (130)	3.43 (023)	3.25 (002)	3.22 (202)	3.18 (004)	Feldspar (Fsp)
3.25 (110)					Rutile (Rt)
3.035 (104)					Calcite (Cal)
3.00 (104)					Mg-calcite (Mg-Cal)

(Brindley & Brown, 1980; Moore & Reynolds, 1997; Anthony et al., 2001; Piper et al., 2009)

Table 4.3: <2µm mineral peak heights for each sample analyzed.

	No	6	9	10	23	2	11	12	1	4	13
	Well	Alma K-85	Alma K-85	Alma K-85	Alma K-85	Cheb K-90	Cheb K-90	Cheb K-90	Herc G-15	Herc G-15	Nask N-30
	depth	2449.4	2904.15	3039.88	3104.1	2220	4585	5120	371.86	646.18	1469
	Formation	Logan Canyon	Missisauga	Missisauga	Verrill Canyon	Logan Canyon	Missisauga	Missisauga	Logan Canyon	Logan Canyon	Missisauga
	Member	Cree				Marmora			Marmora	Cree	Upper
Minerals	**Age (Ma)**	110	127.4	133.1	135.8	99.8	130.3	130.9	99.6	99.65	128
smectite	14.00-20.00	160	175	111		570			674	1946	
chlorite (001)	13.6-14.3	331	361	300	299	438	194	229	236		
mixed Layer Clays (001)	11	213	625	452	431	493	340	250	111	487	
vermiculite/mixed layer clays (VMLC) (001)	12.26	444	952	889	744	667	660	619	229	149	
illite/ montmorillonite mixed layer (001)	10.26	700	1376	1153	980	785	882	716	445	236	
illite (001)	10.01	829	1459	1188	994	1209	1035	924	847	281	229
talc (001) (std)	9.31	1292	1883	1786	1244						
mixed layer chlorite (001)	7.86	390	410	396	347	966	403	382	834	304	924
kaolinite (001)/ chlorite (002)	7.14	1885	1779	1883	1543	4119	1855	1682	3702	1173	4614
mixed Layer Clays (002)	5.50	86	132	139	100	174	90	118	146	172	
illite/ montmorillonite mixed layer (001)	5.15	140	229	222	146	181	146	139	146		
illite (002)	4.98	489	751	528	403	924	417	507	750	177	138
chlorite (003)	4.78	281	306	313	167	542	229	355	424	154	310
talc (002)	4.67	471	530	479	340						
quartz (001)	4.26	145	229	174	195	417	340	445	521	199	1980
mixed layer chlorite (002)	3.94	326	264	285	188	549	208	167	535	149	689
muscovite 001	3.89	163	167	125	132	306	125	132	222	113	
feldspar (001)/ hematite/muscovite	3.68	295	480	368	292	702	458	466	785	213	2100
kaolinite (002)	3.57	1690	1529	1556	1188	3091	1209	945	3355	770	3667
chlorite (004)	3.54	1119	1049	830	695	1709	722	813	1209	743	
feldspar (002)	3.43	476	625	521	327	465	167	285	431	254	
quartz (002)	3.34	1319	1953	1424	1350	2612	2014	2641	3202	1083	10621
illite (003)	3.32	1214	1661	1160	938	1327	952	945	1445	399	910
feldspar /rutile (001)	3.24	376	660	479	368	486	257	236	313	245	
plagioclase (001)	3.22	285	438	299	243	299	236	174	118	353	
feldspar (003)	3.18	213	292	264	202	250	167	153	118	313	
talc (003)	3.11	1514	1946	1814	1147	201	222	200	299	127	202
calcite (001)	3.04										
Mg-calcite (001)	3.00										
Zincite (std)	2.47					1334	1835	1620	2084	1024	1285

8	5	14	15	21	19	22	17	3	7	16	18	20
NB I-13	Pesk A-99	Pesk A-99	Pesk A-99	Pesk A-99	SD O-76	SD O-76	SI C-67	Theb C-74	Theb C-74	Theb I-93	Theb C-74	Theb C-74
3248.8	2209.25	2479.35	2927.36	3812.64	3815.1	5956.8	3373.45	1825	2560	3080.43	3780	4335
Logan Canyon	Logan Canyon	Missisauga	Missisauga	Mic Mac	Missisauga	Mic Mac	Missisauga	Logan Canyon	Logan Canyon	Missisauga	Missisauga	Missisauga
Naskapi	Cree	Upper	Middle		Lower		Middle	Sable	Naskapi	Middle	Lower	Lower
117	109.4	125.2	134.6	158.3			142.6	100.6	115	120.1	149	160.8
	181	181	208					465	215	292		
278	299	403	254	118	341	424	320	716	424	382	215	146
466	200	264	493	257	452	1342	535	688	306	806	300	250
994	345	535	910	466	911	2572	1091	702	542	1417	695	570
1214	703	1106	1410	667	1237	3024	1209	1153	980	1577	959	994
1523	875	1307	1535	535	1237	2913	1397	1292	1077	1903	993	1049
	2175	2274	2286	1612				2397	2459		1243	1084
897	449	591	514	195	424	487	459	848	827	535	361	445
3817	2666	2948	2494	771	1877	2322	1883	3947	3724	2500	1903	2127
167	145	104	139	97	125	341	160	118	97	201	97	90
160	131	188	236	153	243	487	222	208	188	333	181	167
827	503	654	695	445	813	1710	813	792	500	1125	535	473
410	154	382	375	153	480	605	431	396	299	445	201	222
	535	737	646	347	257	243	195	716	660	188	431	341
243	160	216	292	146	306	507	208	188	160	83	188	104
508	381	403	292	118	222	264	250	646	521	313	195	327
264	122	195	195	70	174	292	153	292	292	160	174	153
521	290	466	417	174	431	869	438	639	431	410	313	320
2899	2466	2580	1911	611	1154	1557	1306	3724	3231	1959	1306	1842
1446	889	1363	1258	368	1008	1467	1001	2599	1772	972	1035	931
327	521	841	653	389	361	549	334	1014	841	410	347	403
1905	1324	2010	2029	973	2377	4595	2147	2071	1591	1813	1605	1334
1488	1043	1697	1542	639	1314	3212	1515	1855	1174	1889	966	1112
466	322	515	591	243	425	1084	514	514	410	715	403	424
313	195	257	417	222	271	730	285	368	278	354	264	299
236	145	209	278	153	195	521	250	299	195	292	229	160
209	2326	2747	2230	1320	195	348	195	2925	2508	236	1299	1202
	122									167		
				542								
1321					1203	1565	1126			1029		

treatment. The 003 peak shifts slightly to the left at 110°C and gradually moves back to its original location between 300°C, 500°C, and 650°C (Figure 4.2 & 4.7).

Zincite (Znc) (standard added):

Zincite is recognized at d-spacings of 2.81 Å, 2.60 Å, and 2.47 Å (Brindley & Brown, 1980; Moore & Reynolds, 1997; Anthony et al., 2001).

Smectite (Sme):

Varied amounts of smectite were identified through comparing the expansions of the air-dried versus glycolated samples between 6.0-30.0 Å (d-spacing) (Bradley, 1945; Moore & Reynolds, 1997). In air-dried samples, there is a broad peak at 13 Å to 14 Å (Figure 4.3). With glycerol treatment the peak intensifies, sharpens and shifts to approximately 14 Å to 15 Å (Figure 4.3). With glycolation the peak intensifies and sharpens further and shifts to approximately 16 Å to 18 Å (Figure 4.3). In the samples in which smectite is found, there is a significant loss of peak height from 110°C to 300°C which appears to shift into the 10.1 Å illite-muscovite peak area (Figure 4.2). Smectite distribution in the wells studied is summarized in Figure 4.4. The peak height of smectite generally decreases with depth in all wells except Peskowesk A-99 and Alma K-85, where there is a very small increase seen.

Chlorite (Chl):

Chlorite is identified in the samples at d-spacings of 13.6-14.3 Å (001), 7.12-7.16 Å (002) (where it overlaps with kaolinite), 4.78 Å (003) (not seen in sidepacks), and 3.54 Å (004) (Brindley & Brown, 1980; Moore & Reynolds, 1997; Anthony et al., 2001).

There are a few issues with chlorite identification through XRD including:

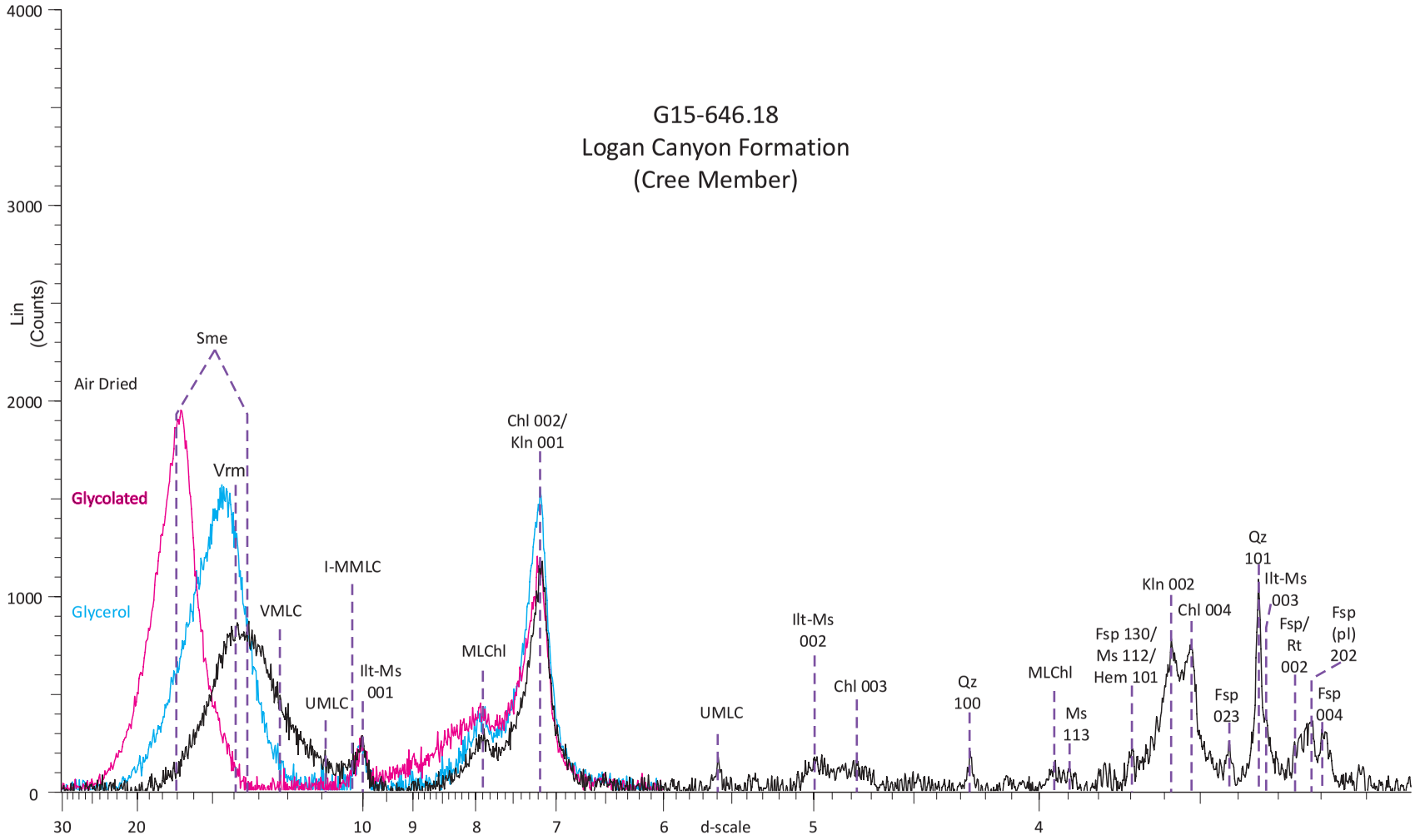

Figure 4.3: X-ray diffraction of Hercules G15 646.18 <2µm oriented sample. Scans showing smectite identification with air-dried, glycolated and glycerol analyses overlain.

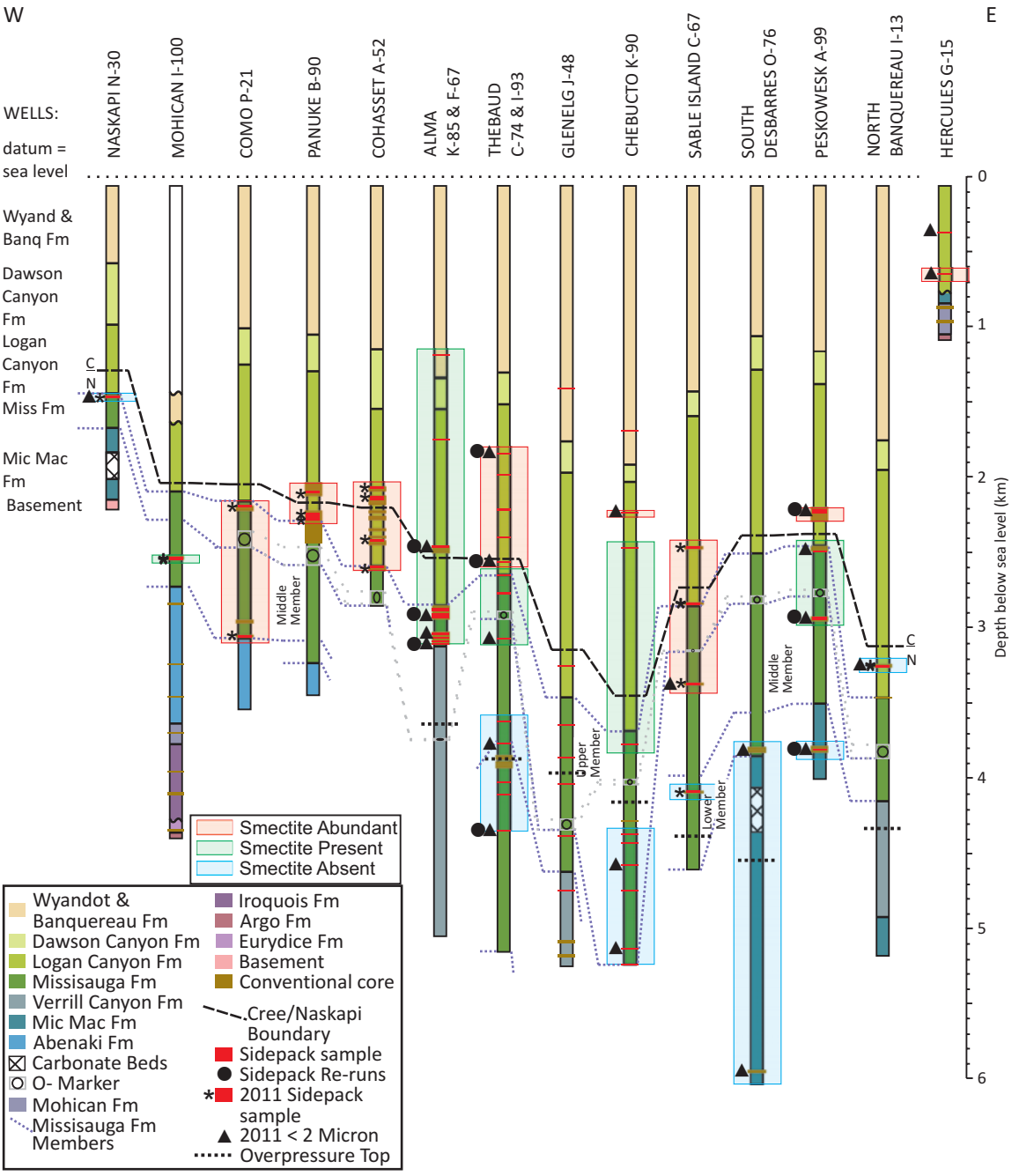

Figure 4.4: Stratigraphy of wells investigated with depths of bulk random sidepack and oriented <2 micron samples, showing smectite abundance with depth.

a) Chlorite and kaolinite completely or partially overlap at the 7.12 Å and 3.54 Å (chlorite) and 7.16 Å, 3.57 Å (kaolinite) peaks, which makes identification and quantification difficult. If the crystallites are sufficiently thick there will be partial to full resolution between the 3.54 Å chlorite and 3.57 Å kaolinite peaks (Moore & Reynolds, 1997). The samples analyzed here have a clear 001 chlorite peak and the 3.54 Å (004 chlorite) and 3.57 Å (002 kaolinite) peaks are partially overlapping but are separated enough to discriminate (Figure 4.5).

b) The high-Fe chlorites have weak, odd-ordered reflections (001, 003 etc.) that can cause the 001 chlorite peak to be obscured or undistinguishable from both the background and/or other minerals (Moore & Reynolds, 1997). One resolution to this is to heat the sample to 550°C for 1 hour. This will cause dehydroxylation of the hydroxide sheet and will cause the 001 peak to increase and shift to the right while greatly weakening the other chlorite peaks (Moore & Reynolds, 1997). At this temperature the peak of kaolinite disappears (basically becoming amorphous) which reveals the chlorite peaks that overlap the kaolinite peaks (Moore & Reynolds, 1997).

In most samples, a small but noticeable decrease in peak height is seen in all chlorite peaks with each increase in temperature (300°C, and 500°C). At 500°C there is a minor shift of the 001 peak to the right. At 650°C, all chlorite peaks are destroyed except the 001 peak which has increases in size and experienced an even greater shift to the right (compared to the 500°C shift) (Figure 4.2 & 4.6). There is no noticeable overall connection between depth and peak height.

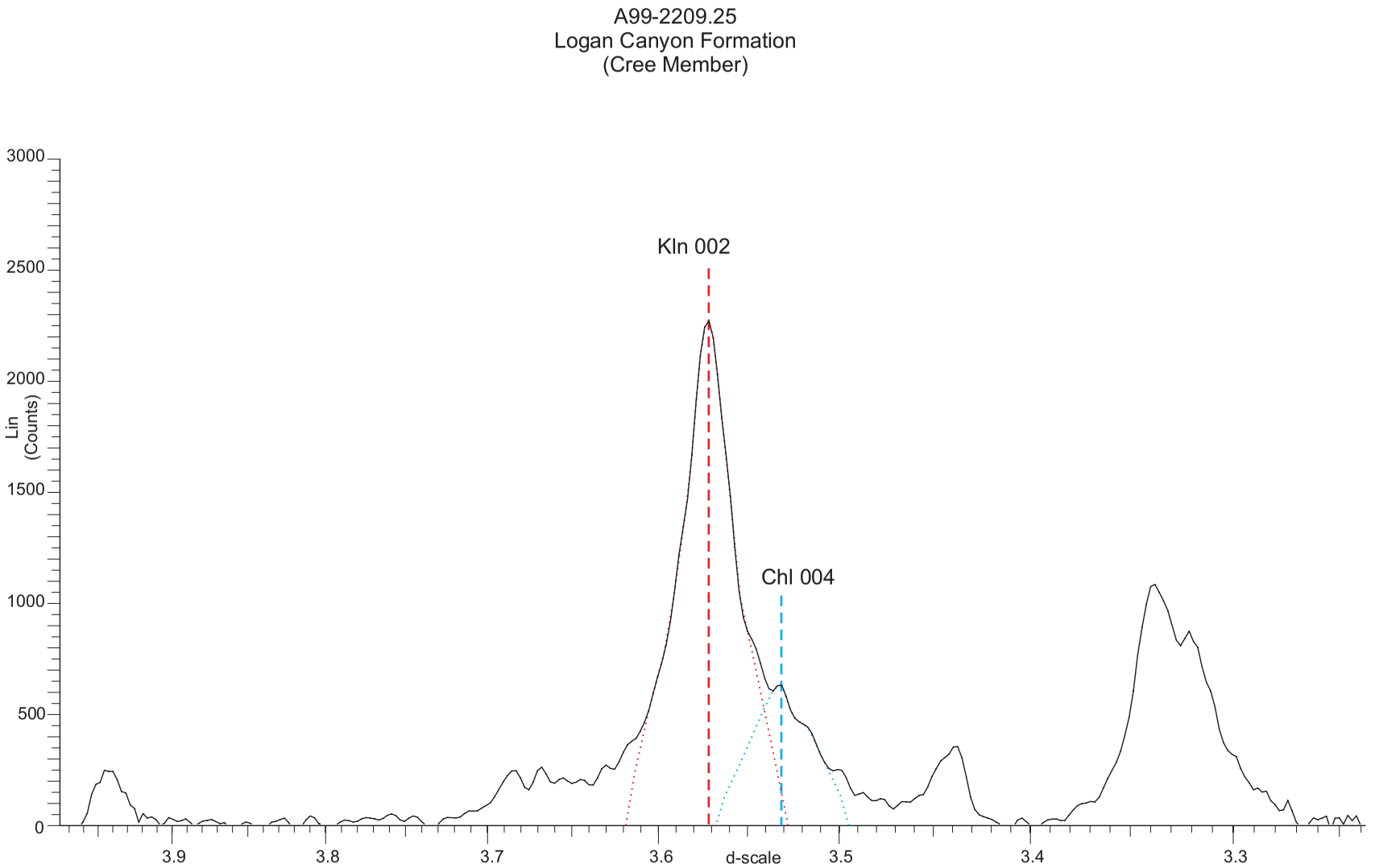

Figure 4.5: X-ray diffraction of the oriented <2µm sample Peskowesk A-99 2209.25 m. Slow scan showing separation of the Kaolinte 002 and Chlorite 004 peaks.

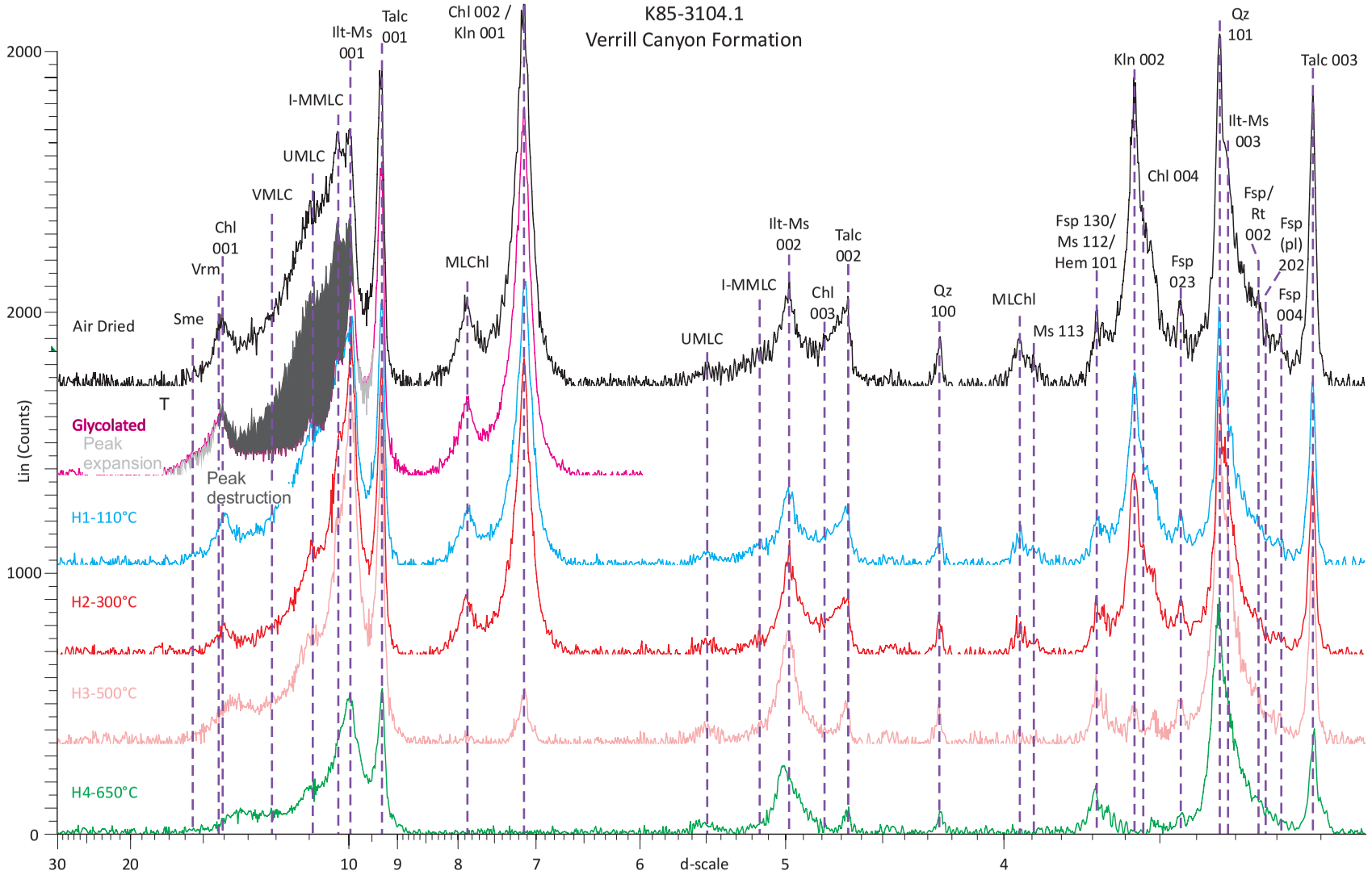

Figure 4.6: X-ray diffraction of Alma K-85 3104.1 m <2 µm oriented scan showing air-dried, glycolated and heat treatment analyses overlain with minerals identified.

Determining the chlorite 001/chlorite 004 peak height ratio will distinguish Fe-chlorite (lower numbers) versus Mg-chlorite (higher numbers). Based on a chlorite 001/chlorite 004 ratio of the sidepack samples, Mg-chlorite is abundant in the Peskowesk A-99 and Thebaud C-74 samples in the Logan Canyon Formation and Fe-chlorite is abundant in the Alma K-85, Como P-21 and Sable Island C-67 samples from Logan Canyon and the Glenelg J-48, Chebucto K-90, and Thebaud C-74 samples in the Missisauga Formation (Figure 4.7) (see Figure 1.4 for possible river locations).

Mixed Layer Chlorite (MLChl):

Mixed layer chlorite is identified in the samples at d-spacings of 7.86 Å and 3.94 Å. The mixed layer chlorites show very minor decrease in peak height at 300°C. Samples from Alma K-85 and Peskowesk A-99 show an almost complete to complete destruction of both peaks at 500°C. Thebaud C-74 samples only show a minor decrease at 500°C and total destruction at 650°C (Figure 4.2 & 4.7). There is no noticeable overall connection between depth in wells and abundance.

Unspecified Mixed layer clay (UMLC):

Unspecified mixed layer clays are present in the samples at d-spacings of 11.0 Å and 5.5 Å (Brindley & Brown, 1980). There is a slight increase in peak height at 300°C, and again at 500°C. There is a peak height increase and slight shift to the left at 650°C. All of these trends are more noticeable at the 5.5 Å peak, likely due to the overlap of other mineral peaks obscuring the reaction of the 11.0 Å peak (Figure 4.2 & 4.7). The 11.0 Å peak has a significant collapse when glycolated, but nevertheless a small peak remains.

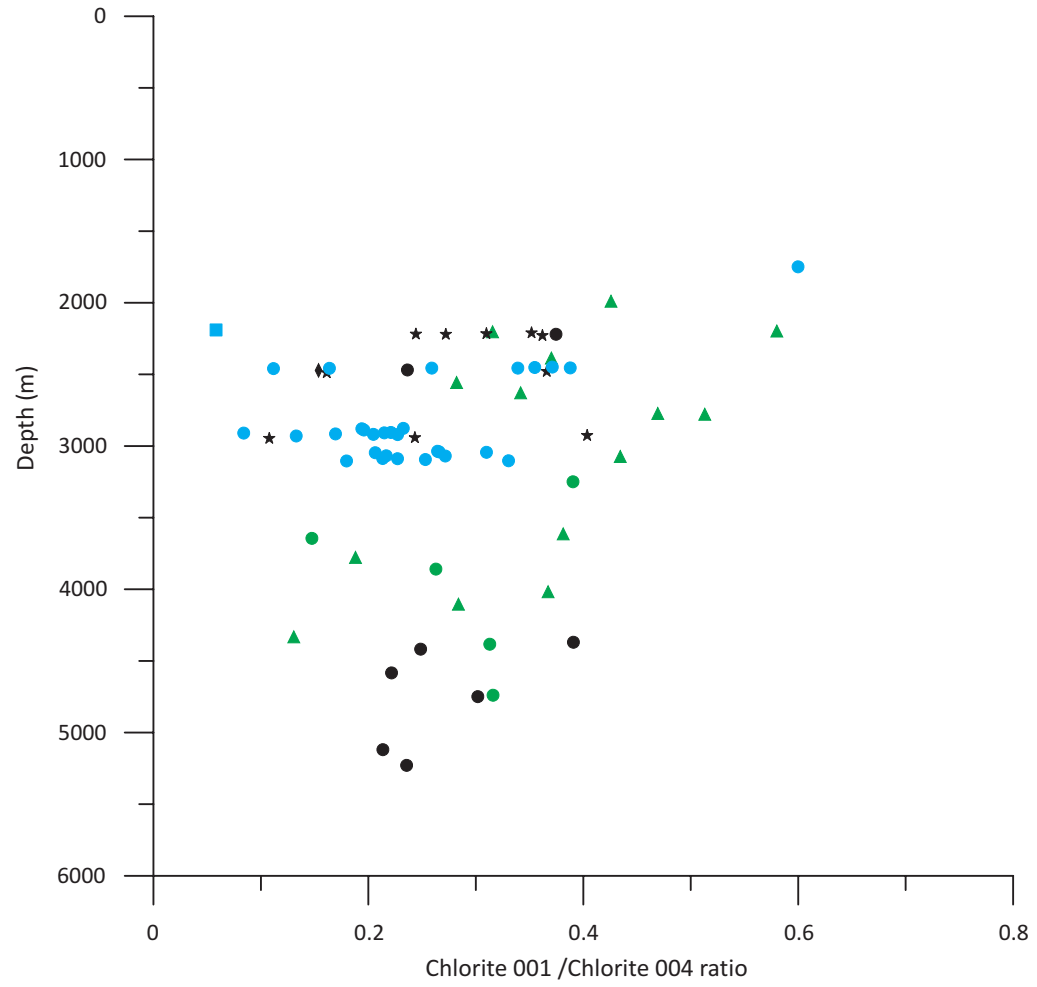

Figure 4.7: Bulk random sidepack samples normalized to the standard showing chlorite 001/chlorite 004 ratio vs Depth. Colour code based on likely provenance from Pe-Piper & Piper (2012).

Vermiculite (Vrm) and Vermiculite-Mixed Layer Clay (VMLC):

Vermiculite is identified in the samples at d-spacings of 14.6-14.0 Å, and vermiculite-mixed layer clay is identified at 12.26 Å (Brindley & Brown, 1980; Piper et al., 2009). The vermiculite peak is hard to distinguish due to overlap of smectite and chlorite in the <2 μm samples. There is a minor decrease in peak height in the both peaks by 300°C followed by a slight increase in each peak by 500°C. Both peaks have a minor decrease in height at 650°C. The vermiculite peak shows a slight expansion when glycolated and the vermiculite mixed layer peak shows a significant collapse when glycolated and may shift left, but is unclear due to smectite (Figure 4.2 & 4.7).

Illite/montmorillonite mixed layer (I-MMLC):

I-MMLC is identified in the samples at d-spacings of 10.26 Å̊ (001) and 5.15 Å̊ (002) (Brindley & Brown, 1980). These peaks were recognized as a mixed layer based on peak locations and peak destruction and probable shift to the left (the large apparent loss of peaks due to the automatic background removal makes the shift uncertain) during glycol treatment (which identified the smectite). There is a minor increase in peak height at 300°C. There is little change in the peaks at 500°C and a minor increase in peak height again at 650°C. There is no shift in the peak positions with heating (Figure 4.2 & 4.7).

Illite-Muscovite (Ilt-Ms):

Illite (1M hydromuscovite, Brindley & Brown, 1980) is identified in the samples at d-spacings of 10.1 Å (illite-muscovite) (001), 5.02-5.05 Å (illite-muscovite) (002), and

3.32 Å (illite-muscovite) (003) (Carroll, 1970; Brindley & Brown, 1980; Moore & Reynolds, 1997).

There is a gradual increase in peak heights at 300°C and 500°C. At 650°C there is significant peak destruction in all peaks and a noticeable shift to the left in the 002 peak. The shift is not noticeable in the other two peaks. The 001 peak loses height after glycolation (Figure 4.2 & 4.7). The loss of peak height could be a consequence of the automatic background removal performed by the EVA program. It could also suggest that there is smectite overlapping the peak. The 113 peak shows a gradual decrease in peak height between 110°C and 300°C. The peak is destroyed by 500°C (Figure 4.8). The 112 peak slightly increases in height after 110°C and by 600°C there is a small shift to the left. Due to the potential overlap of hematite and feldspar and the fact that the 113 peak is destroyed by 500°C, it is assumed that this peak is not the muscovite peak.

Kaolinite (Kln):

Kaolinite is identified in the samples at d-spacings of 7.12-7.16 Å (001) (where it overlaps with chlorite), and 3.57 Å (002) (where it can be separated from chlorite with a slow scan) (Brindley & Brown, 1980; Moore & Reynolds, 1997; Anthony et al., 2001). Kaolinite peak height shows minor destruction at 300°C followed by a more drastic reduction in height at 500°C and it is completely destroyed by 650°C. There is no change with glycolation and no shift is seen with heat treatment (Figure 4.7 & 4.8). A slow scan was used to confirm that both chlorite and kaolinite were present in samples from Alma K-85, Peskowesk A-99 and Thebaud C-74 (Figure 4.5).

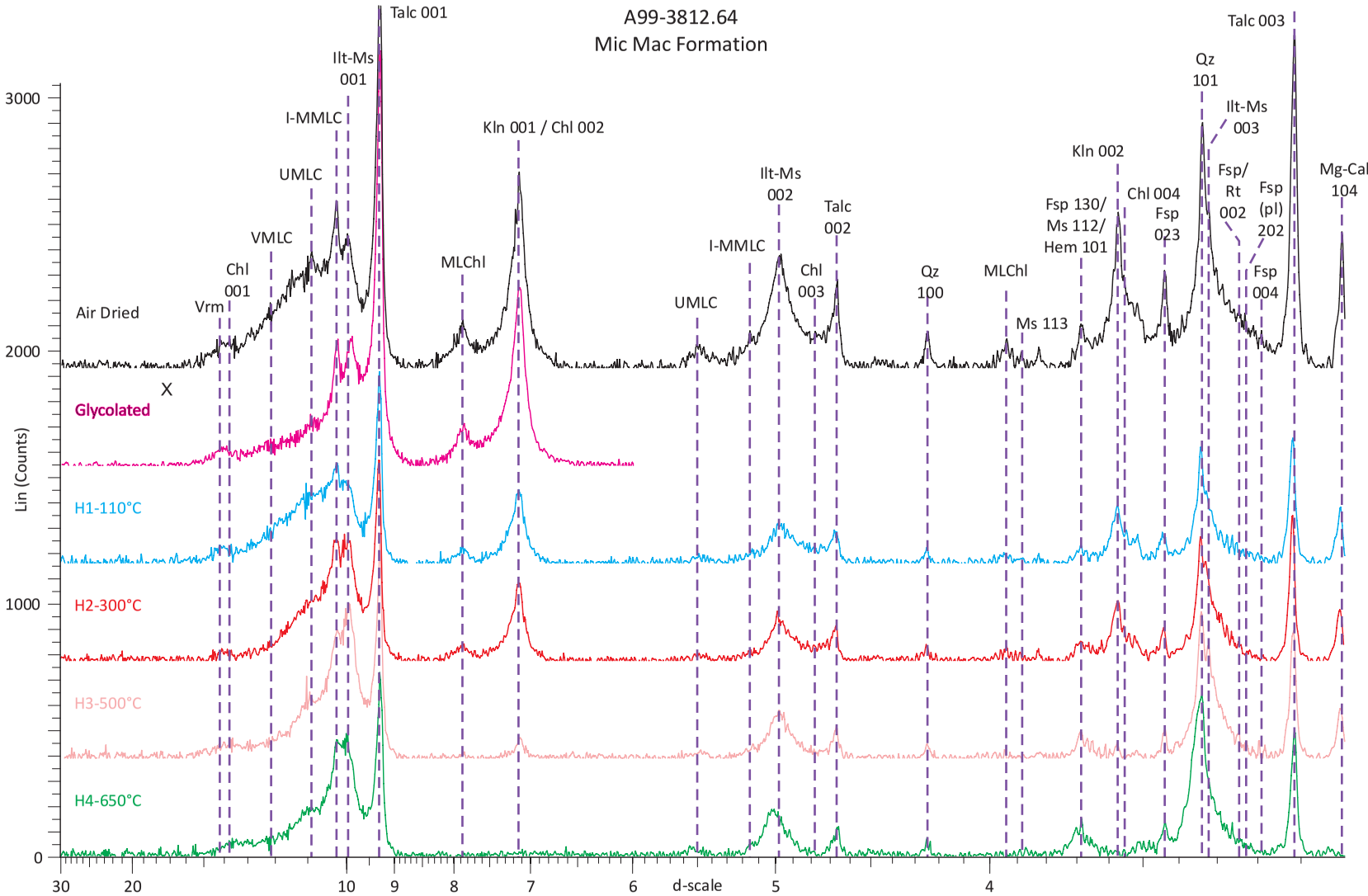

Figure 4.8: X-ray diffraction of Peskowesk A-99 3812.64 m <2µm oriented scan showing minerals identified in air-dried, glycolated and heat treatment analyses overlain with minerals identified.

Sepiolite (Sep):

Sepiolite is characterized by d-spacings of 12.7-12 Å (101), 7.5 Å (130), and 3.3 Å (080) (Carroll, 1970; Brindley & Brown, 1980; Moore & Reynolds, 1997). All of these peaks overlap with mixed layer clays and its presence can neither be confirmed or denied.

Quartz (Qz):

Quartz is identified in the samples at d-spacings of 4.26 Å (100) and 3.34 Å (101) (Brindley & Brown, 1980; Moore & Reynolds, 1997; Anthony et al., 2001). Peak height remains constant on heating. All samples show a minor shift to the right starting at 110°C in some samples and 300°C in others. The peaks slightly broaden to the left with higher temperature. This shift is even more pronounced by 650°C (Figure 4.7 & 4.8).

Hematite (Hem):

Hematite is thought to only be found in the Naskapi N-30 1469.10m sample. It is identified in the samples at d-spacings of 3.69 Å (101) (Brindley & Brown, 1980; Moore & Reynolds, 1997; Anthony et al., 2001). The 3.69 Å is overlapped by the 3.68 Å feldspar and/or the 3.68 Å muscovite peaks. Therefore, it is possible that hematite may be in other samples but it is masked by the 3.68 Å feldspar and 3.68 Å muscovite peak. Feldspar is not found in Naskapi but it is in all other samples. The sample from Naskapi N-30 1469.10m was not heat treated (Figure 4.9). Hematite is thus not confidently identified in the samples.

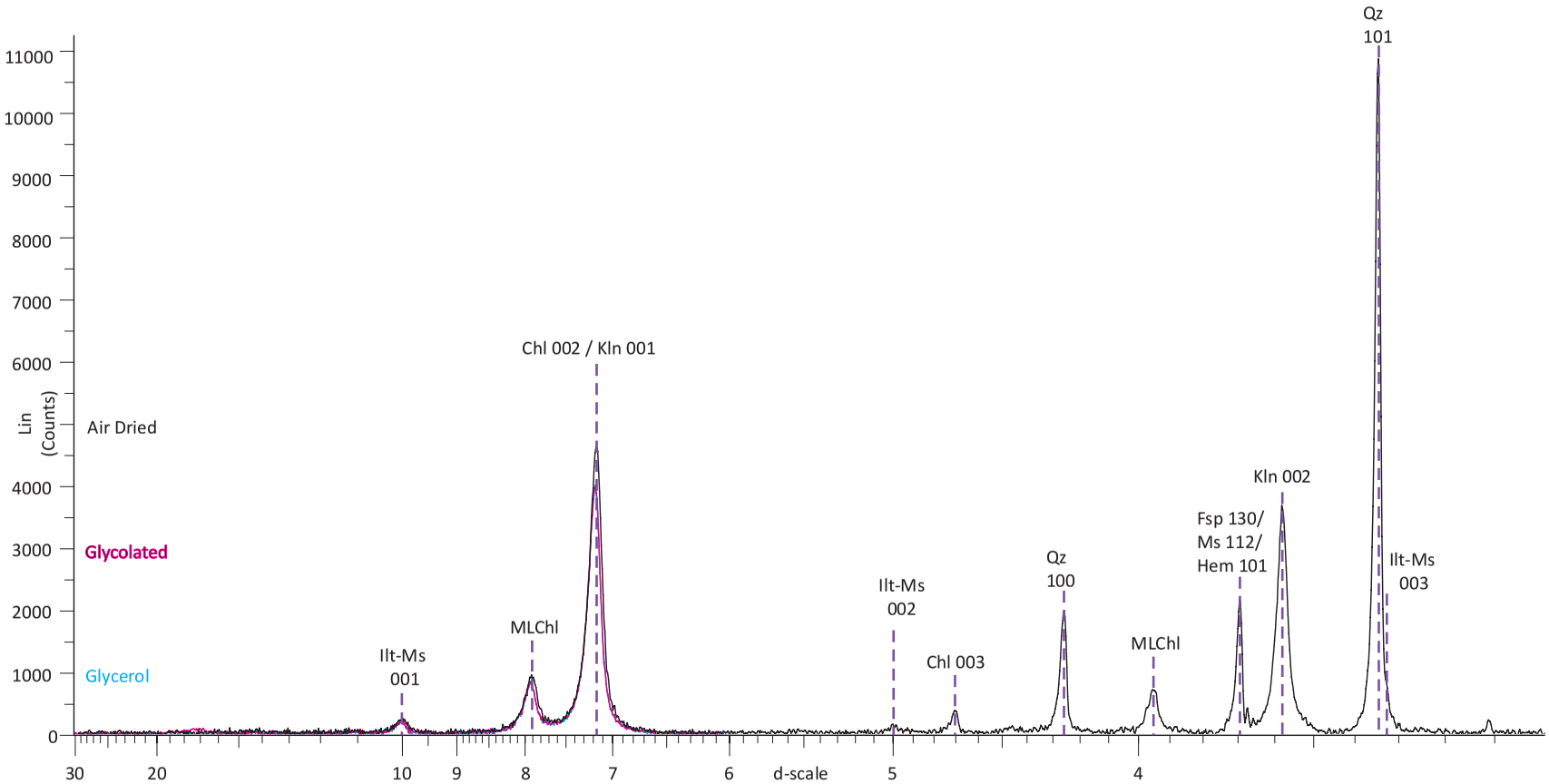

Figure 4.9: X-ray diffraction of Naskapi N-30 1469.10 m <2 µm oriented scan showing air-dried, glycolated and glycerol treatment analyses overlain with minerals identified.

Feldspar (Fsp):

Feldspar may be present in the samples at d-spacing of 3.68 Å (130), 3.43 Å (023), 3.31 Å (220) (masked by quartz), 3.25 Å (002) (possibly feldspar or rutile), 3.22 Å (202) (plagioclase) and 3.18 Å (004) (Brindley & Brown, 1980; Moore & Reynolds, 1997; Anthony et al., 2001). The 3.68 Å peak may mask a hematite peak of 3.69 Å and a muscovite peak of 3.66 Å. The 3.25 Å peak could overlap rutile. All peaks remain relatively stable until 500°C and 650°C. At these temperatures it appears that the peaks increase in height, but this is most likely the result of the destruction of the surrounding kaolinite peaks. Finding two to four sharp peaks in the 3.30-3.18 Å range is a good indicator of the presence of feldspar (Brindley & Brown, 1980). Due to the lack of any peaks in the 6.5-6.4 Å and 4.22-4.03 Å range in the <2 µm samples, there is a lower confidence in identifying these peaks as feldspar (Figure 4.7 & 4.8).

Rutile (Rt):

Rutile may be present in the samples at d-spacing of 3.25 Å (110) (Brindley & Brown, 1980; Moore & Reynolds, 1997; Anthony et al., 2001). The caution here is that this peak may also be feldspar which has the same peak location. The same peak is found in the sidepack mounts, however no other rutile peak is found. This peak remains constant with higher temperatures (Figure 4.7 & 4.8). Therefore, rutile is not identified with confidence.

Calcite (Cal):

Calcite is identified in the samples at d-spacing of 3.035 Å for pure calcite (104) and 3.00 Å (104) (Mg-calcite) (Brindley & Brown, 1980; Moore & Reynolds, 1997;

Anthony et al., 2001). There is a continuum of the 3.035 Å calcite peak shifting to smaller d-spacings with Mg substitution so that Mg-calcite has a d-spacing of 3.00 Å. The 3.035 Å peak shifts to the left at 300°C and the 3.00 Å peak shifts to the right at 300°C. Both peaks are completely destroyed at 500°C (Figure 4.8 & 4.10).

4.2 ILLITE CRYSTALLINITY

Estimates of illite crystallinity were made using the <2 μm samples. With the large amount of mixed layer clays overlapping the 10 Å illite peak on the low 2θ (left) side, it is impossible to get a clear individual peak. The published methods of Jaboyedoff et al. (2001) and Leoni (2001) cannot be applied due to this overlap. Therefore, to estimate a relative illite crystallinity the overall peak was estimated by assuming the high 2θ (right) side was good due to the lack of overlapping on this side. The peak half width at half height was measured on the high 2θ side.

The four samples from Thebaud C-74 were each measured four times to investigate reproducibility of this method (Table 4.4). An average standard deviation of 0.029° 2θ was found. The average values of illite crystallinity between 0-2000 m, 2000-3000 m and 3000-6000 m are 0.193° 2θ, 0.277° 2θ and 0.218° 2θ, respectively. The two maximum peak widths of 0.38° 2θ and 0.34° 2θ were found in the Alma K-85, 2904.15 m (Missisauga Formation) sample and in the Peskowesk A-99, 2479.35 m (Missisauga Formation: Upper Member) sample, respectively. The two minimum peak widths of 0.14° 2θ and 0.16° 2θ were found in the Hercules G-15, 646.18 m (Logan Canyon: Cree

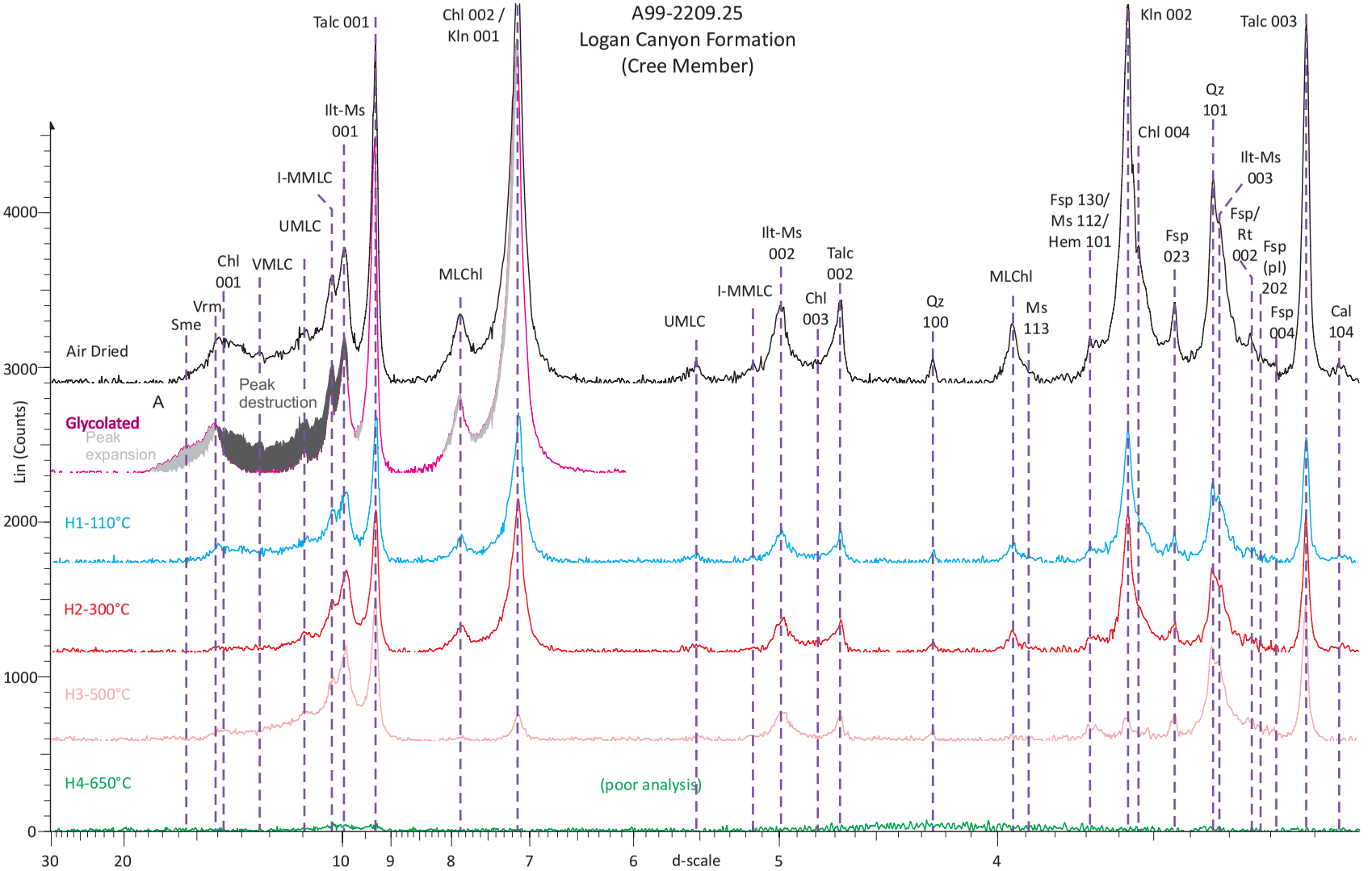

Figure 4.10: X-ray diffraction of Peskowesk A-99 2209.25 m <2µm oriented scan showing minerals identified in air-dried, glycolated and heat treatment analyses overlain with minerals identified.

Table 4.4: <2μm illite crystallinity.

Well	Depth (m)	Formation	Age	location	Illite Height (Counts)	Illite 1/2 Height (Counts)	illite width right (°2θ)	illite peak location (°2θ)	illite half Width @ half height (by hand)-degrees	illite Full Width @ half height (by hand)-degrees
ALMA K-85	2449.4	LC (Cree Mb)	Albian	Southwest Center	825	412.5	10.48	10.32	0.160	0.320
ALMA K-85	2904.15	Miss Upper Mb	Barremian	Southwest Center	1451	725.5	10.46	10.27	0.190	0.380
ALMA K-85	3039.88	Miss Upper Mb	Barremian	Southwest Center	1168	584	10.44	10.29	0.150	0.300
ALMA K-85	3104.1	VC Fm	Hauterivian	Southwest Center	983	491.5	10.42	10.27	0.150	0.300
CHEBUCTO K-90	2220	LC (Marmora Mb)	Ceno-Albian	Center	1206	603	10.34	10.26	0.080	0.160
CHEBUCTO K-90	4585	Miss Fm	Haut-Barre	Center	1035	517.5	10.33	10.26	0.070	0.140
CHEBUCTO K-90	5120	Miss Fm	Haut-Barre	Center	897	448.5	10.34	10.28	0.060	0.120
HERCULES G-15	371.86	LC (Marmora Mb)	Ceno-Albian	North	855	427.5	10.35	10.27	0.080	0.160
HERCULES G-15	646.18	LC (Cree Mb/Pyro)	Albian	North	275	137.5	10.3	10.23	0.070	0.140
NASKAPI N-30	1469	Miss Upper Mb	Barremian	West	224	112	N/A	N/A	N/A	N/A
NORTH BANQUEREAU I-13	3248.8	LC (Naskapi Mb)	Aptian	East Center	1499	749.5	10.37	10.24	0.130	0.260
PESKOWESK A-99	2209.25	LC (Cree Mb)	Albian	East Center	876	438	10.43	10.29	0.140	0.280
PESKOWESK A-99	2479.35	Miss Upper Mb	Haut-Barre	East Center	1306	653	10.47	10.3	0.170	0.340
PESKOWESK A-99	2927.36	Miss Middle Mb	Valanginian	East Center	1524	762	10.45	10.32	0.130	0.260
PESKOWESK A-99	3812.64	Mic Mac Fm	Tithonian	East Center	527	263.5	N/A	N/A	N/A	N/A
SABLE ISLAND C-67	3373.45	Miss Middle Mb	Valanginian	North Center	1364	682	10.33	10.26	0.070	0.140
SOUTH DESBARRES O-76	3815.1	Miss Lower Mb	Kimm to Tith	North Center	1229	614.5	10.36	10.28	0.080	0.160
SOUTH DESBARRES O-76	5956.8	Mic Mac Fm	Kimmeridgian	North Center	2911	1455.5	10.37	10.28	0.090	0.180
THEBAULD C-74	1825	LC (Sable Mb)	Albian	Center	1280	640	10.46	10.32	0.140	0.280
Error Check	1825				1280	640	10.46	10.32	0.140	0.280
Error Check	1825				1280	640	10.45	10.32	0.130	0.260
Error Check	1825				1280	640	10.44	10.32	0.120	0.240
THEBAULD C-74	2560	LC (Naskapi Mb)	Albian	Center	1075	537.5	10.4	10.3	0.100	0.200
Error Check	2560				1075	537.5	10.45	10.3	0.150	0.300
Error Check	2560				1075	537.5	10.45	10.3	0.150	0.300
Error Check	2560				1075	537.5	10.46	10.3	0.160	0.320
THEBAULD I-93	3080.38	Miss Middle Mb	Valanginian	Center	1904	952	10.34	10.23	0.110	0.220
THEBAULD C-74	3780	Miss Lower Mb	Tithonian	Center	984	492	10.45	10.29	0.160	0.320
Error Check	3780				984	492	10.46	10.28	0.180	0.360
Error Check	3780				984	492	10.47	10.28	0.190	0.380
Error Check	3780				984	492	10.47	10.28	0.190	0.380
THEBAULD C-74	4335	Miss Lower Mb	Tithonian	Center	1003	501.5	10.39	10.26	0.130	0.260
Error Check	4335				1003	501.5	10.38	10.26	0.120	0.240
Error Check	4335				1003	501.5	10.39	10.26	0.130	0.260
Error Check	4335				1003	501.5	10.4	10.26	0.140	0.280

Error Check			
Style	average	Standard deviation	average of standard deviation
small	0.133	0.010	
ruler small			
large			0.015
small	0.140	0.027	
ruler small			
large			
small	0.180	0.014	
ruler small			
large			
small	0.130	0.008	
ruler small			
large			

Member [pyroclastic interval]) sample, and the Hercules G-15, 371.86 m (Logan Canyon: Marmora Member) sample respectively.

4.3 SIDEPACK SAMPLES

The fourteen wells investigated using bulk sidepack XRD analyses are: Alma K-85, Chebucto K-90, Cohasset A-52, Como P-21, Glenelg J-48, Hercules G-15, Mohican I-100, Naskapi N-30, North Banquereau I-13, Panuke B-90, Peskowesk A-99, Sable Island C-67, and Thebaud C-74 (Table 3.2). Alma F-67, Cohasset A-52, Como P-21, Mohican I-100, and Panuke B-90 did not have <2 µm analysis performed on the samples. All of the raw areas of the picked peaks were normalized to zincite (the standard used) to aid in quantifying the results. The X-ray diffractograms scans of the sidepack sample can be found in Appendix 2.

Minerals Present:

It was not possible to match all the peaks from the <2 µm samples and the sidepack samples. This is primarily due to two effects: 1) <2 µm separation concentrates smaller minerals, particularly clay minerals. This can be seen in the kaolinite and chlorite and mixed layer clay peaks of the >2 µm samples in contrast to the prominent quartz peak in the sidepack samples; 2) <2 µm samples are oriented, which enhances the basal (001, 002 etc.) reflections. The sidepack samples use a random mount in which all the (hkl) diffractions are equally likely. Overlaps of the <2 µm XRD scans and the sidepack XRD scans can be seen in Figures 4.11 through 4.14. Confidence in mineral identification in the sidepack samples came from comparison with the <2 µm

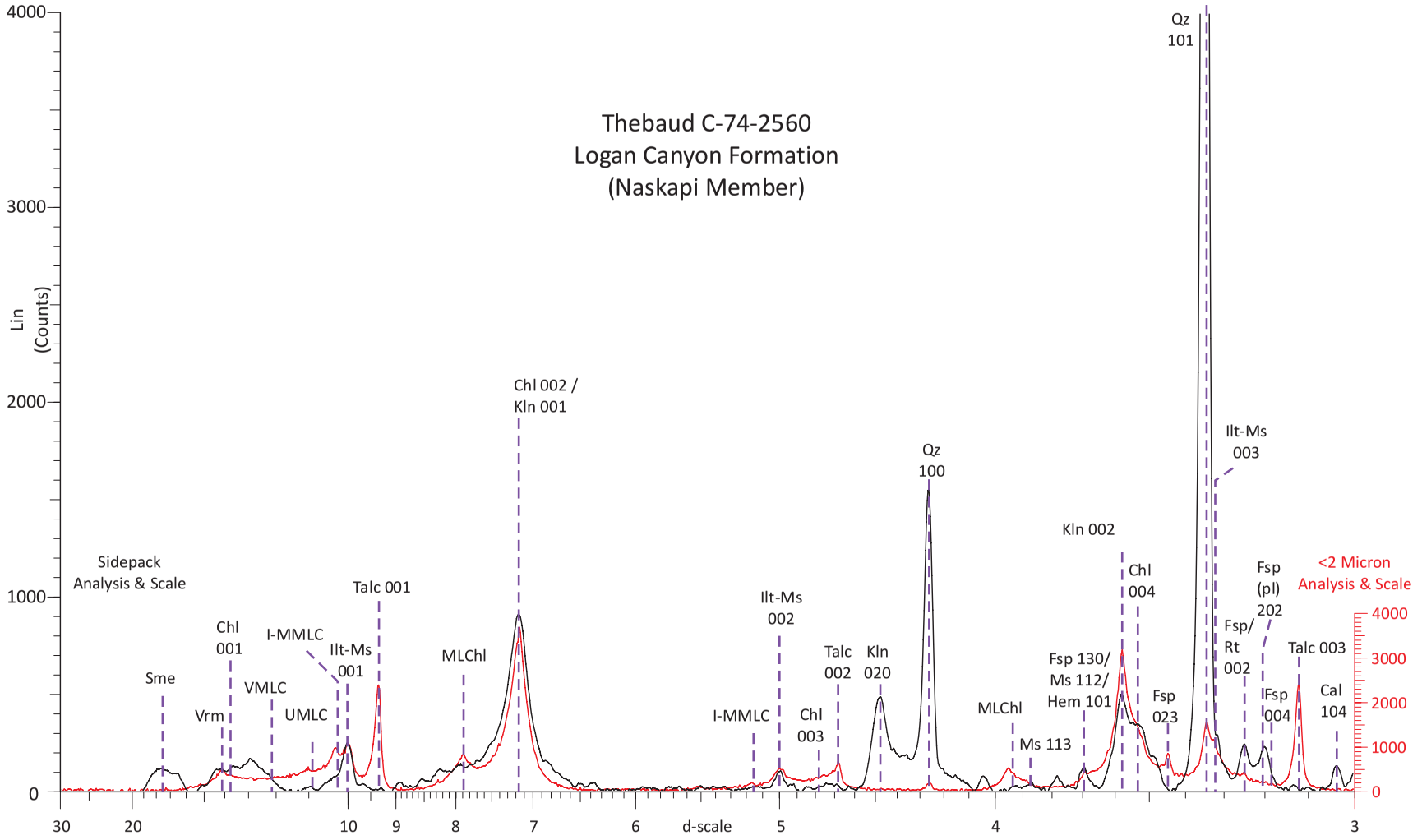

Figure 4.11: X-ray diffraction of Thebaud C-74 2560 m. Scans showing bulk random sidepack and <2 Micron oriented analyses.

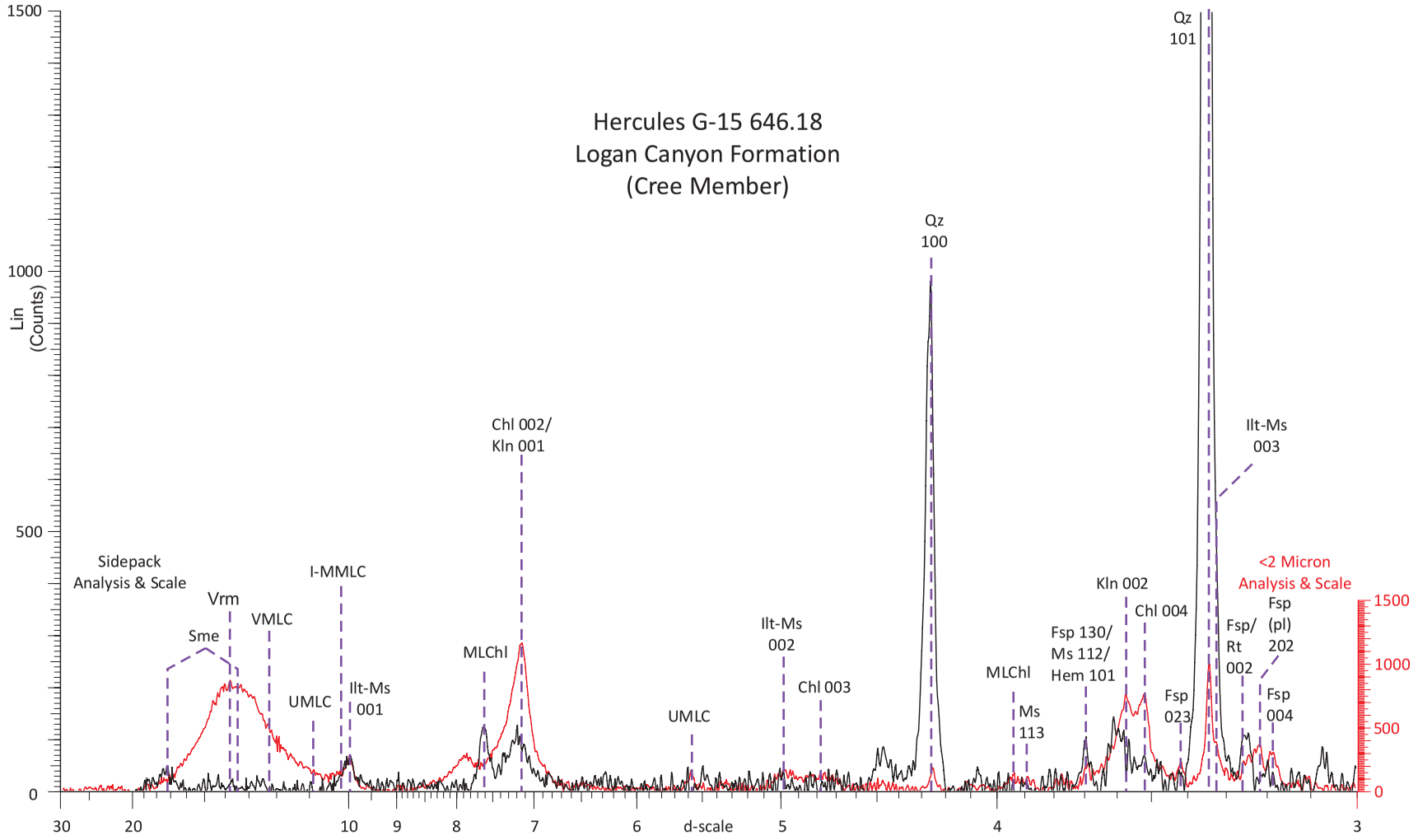

Figure 4.12: X-ray diffraction of Hercules G-15 646.18 m. Scans showing bulk random sidepack and <2 Micron oriented analyses.

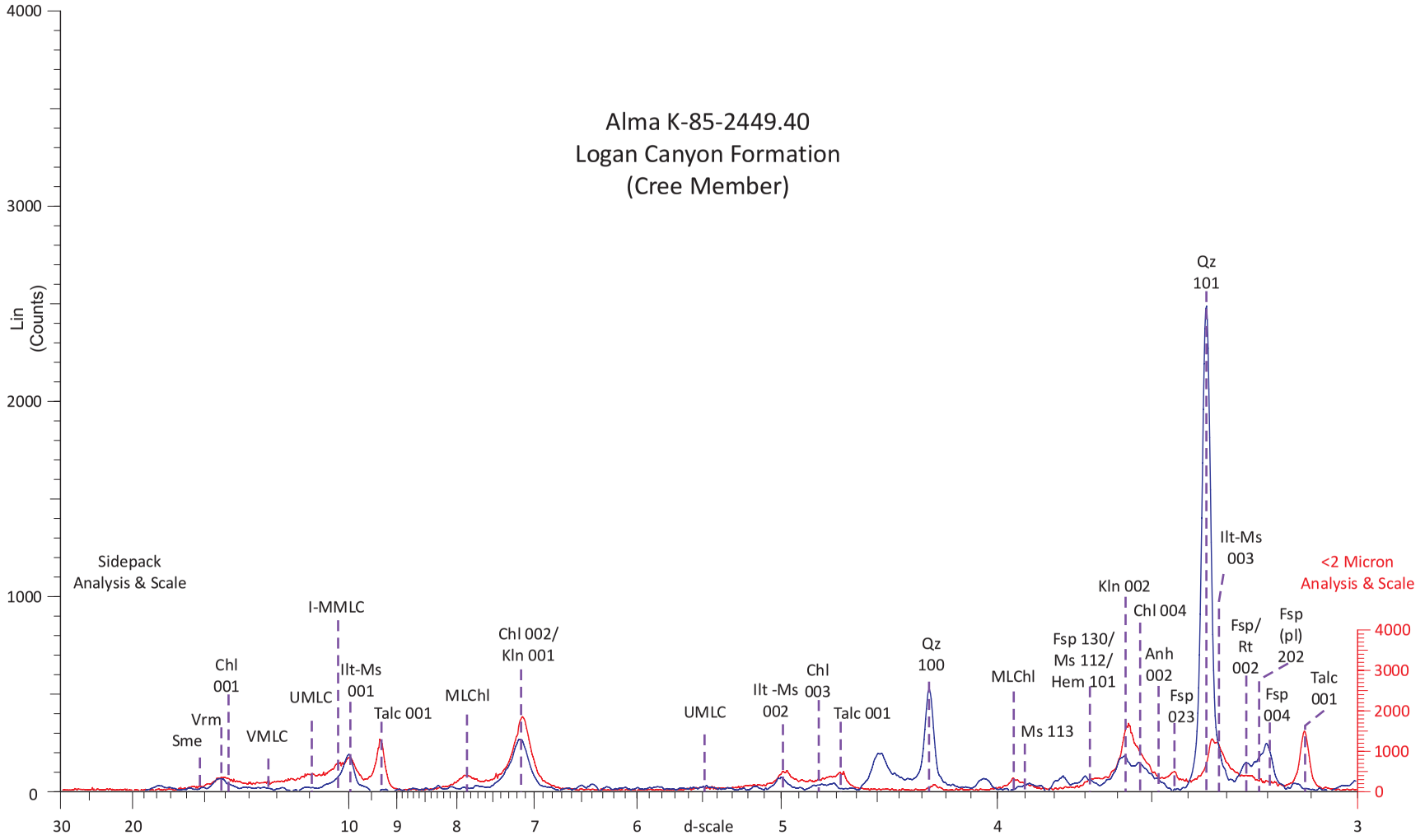

Figure 4.13: X-ray diffraction of Alma K-85 2449.40 m. Scans showing bulk random sidepack and <2 Micron oriented analyses.

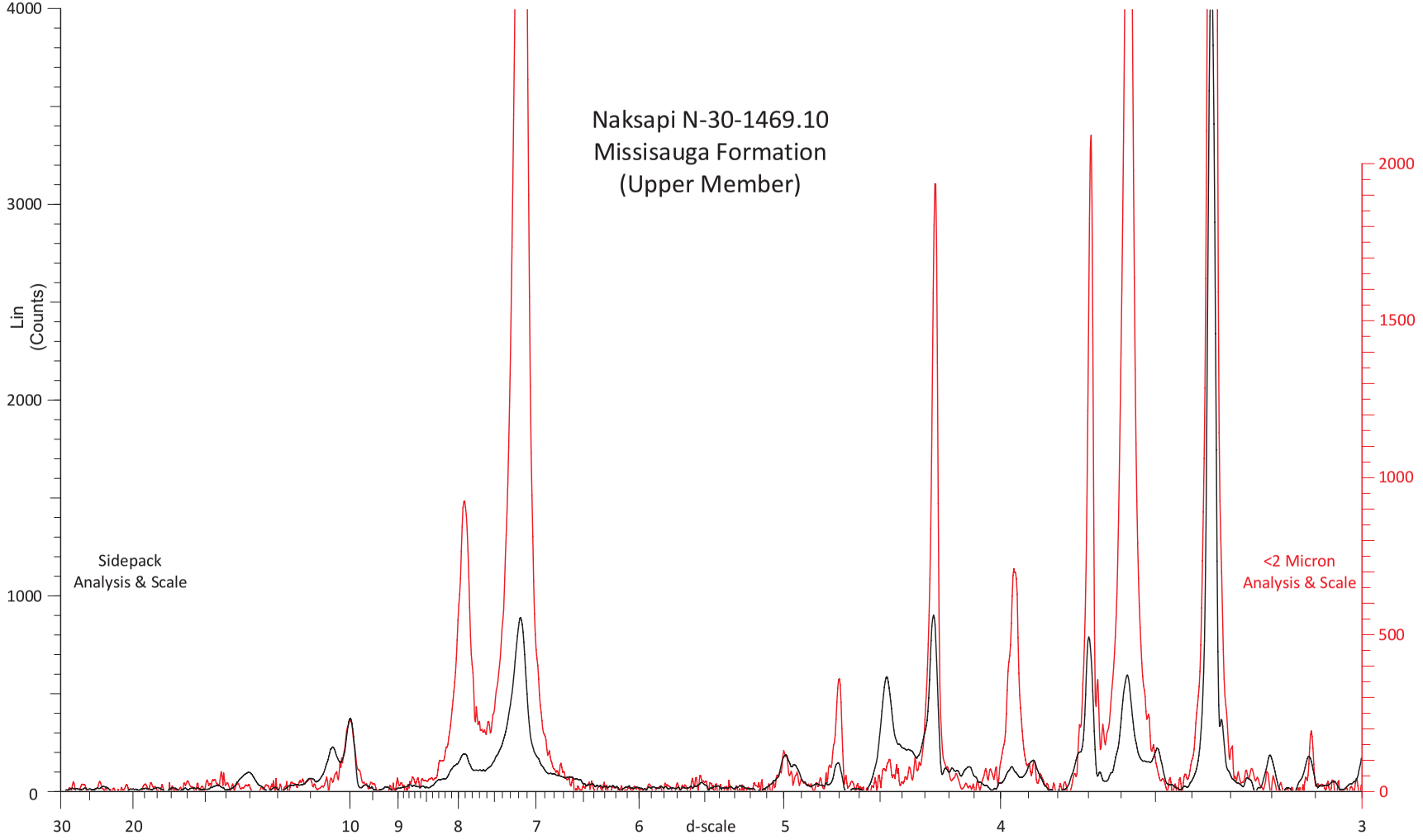

Figure 4.14: X-ray diffraction of Naskapi N-30 1469.10 m. Scans showing bulk random sidepack and <2 Micron oriented analyses.

samples. Minerals that are seen in both the <2 μm and sidepack samples are confidently identified. All of the sidepack mineral peaks and their "d-spacing" can be found in Table 4.5.

Smectite (Sme):

There are several types of smectite recognized in the sidepack samples that were identified through their d-spacings: 17.6 Å, 2.99 Å, 1.5 Å (060) (montmorillonite), and 1.489-1.50 Å (060) (montmorillonite or beidellite), 10.26 Å (illite and montmorillonite mixed layer); 17.0 Å, 1.54 Å (060) (saponite); 15.4 Å (hectorite) and 1.53 Å (060) (hectorite or saponite) (Brindley & Brown, 1980; Moore & Reynolds, 1997; Anthony et al., 2001). Smectite minerals were found in trace to abundant amounts in all wells. Smectite is confidently identified by comparing the sidepack samples with the < 2 μm samples.

Montmorillonite is identified in the sidepack samples at 1.50 Å (060) and hectorite is identified in the sidepack samples at 1.53 Å (060) (Figure 4.15). According to Moore & Reynolds (1997) montmorillonite is di-octahedral and hectorite is tri-octahedral. Both of these are found throughout the studied samples. However, montmorillonite is slightly more abundant than hectorite. Without detailed chemical analysis it is hard to be completely certain about the proportions of di-octahedral vs. tri-octahedral smectite minerals because within particular members of the smectite group, significant variation of properties can be seen even though the different species vary due to the source of layer charge and structure (Moore & Reynolds, 1997).

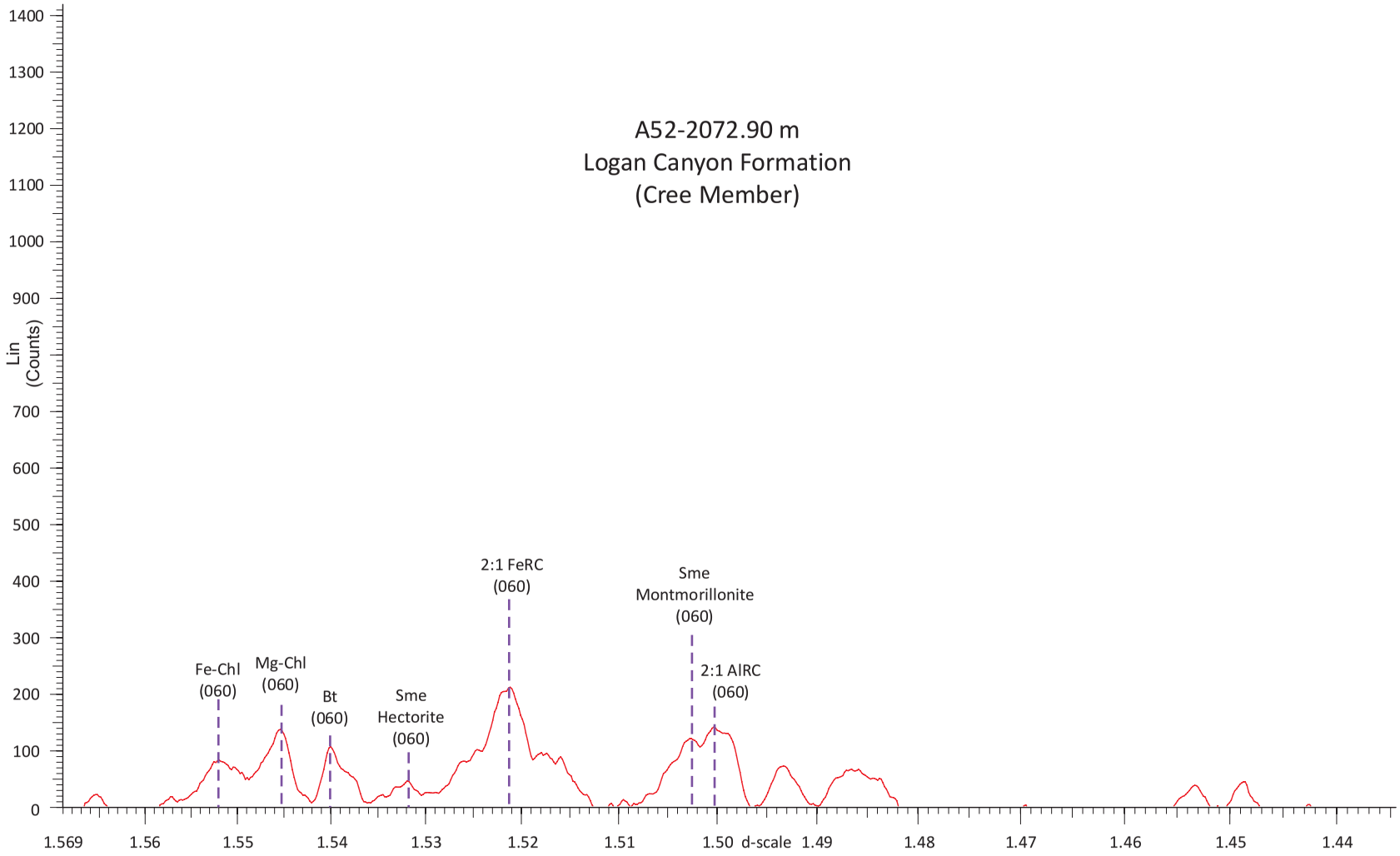

Figure 4.15: X-ray diffraction of Cohasset A-52 2072.90 m bulk random scans showing the minerals identified in the 060 range of the scan.

Table 4.5: Sidepack minerals identified in Scotian Basin samples.

d-spacing (Å)					Mineral
17.6	17	15.4	10.26	2.99	Smectite (Sme)
1.54 (060)	1.53 (060)	1.5 (060)	1.489-1.50 (060)		Smectite (continued)
13.6-14.3 (001)	7.12-7.16 (002)	3.54 (004)	1.55-1.56 (060)	1.538-1.549 (060)	Chlorite (Chl)
7.86	3.94				Mixed layer chlorite (MLChl)
11	5.5				Unspecified mixed layer clays (UMLC)
14-14.6					Vermiculite (Vrm)
12.26					Vermiculite/mixed layer clays (VMLC)
10.26					Illite / Montmorillonite mixed layer (I-MMLC)
10.1 (001)	5.02-5.05 (002)	3.89 (113)	3.66 (112)	3.32 (003)	Illite-Muscovite (Ilt-Ms)
7.12-7.16 (001)	3.57 (002)	2.56 (201)	1.489 (060)		Kaolinite (Kln)
7.5 (130)	1.54-1.55 (060)				Sepiolite (Sep)
4.26 (100)	3.34 (101)				Quartz (Qt)
3.69 (101)					Hematite (Hem)
3.68 (130)	3.31 (220)	3.25 (002)	3.22 (202)	3.18 (004)	Feldspar (Fsp)
3.25 (110)					Rutile (Rt)
3.035 (104)					Calcite (Cal)
3.00 (104)					Mg-calcite (Mg-Cal)
1.51-1.53 (060)					2:1 Fe-rich clays
1.499-1.505 (060)					2:1 Al-rich clays

(Brindley & Brown, 1980; Moore & Reynolds, 1997; Anthony et al., 2001; Piper et al., 2009)

Chlorite (Chl):

Chlorite is identified throughout the samples in various forms. The chlorite d-spacings are: 13.6-14.3 Å, 7.12-7.16 Å (Chl overlapped with Kln), 3.54 Å, and 1.55-1.56 Å (Fe-Chl), and 1.538-1.549 Å (Mg-Chl) (Brindley & Brown, 1980; Moore & Reynolds, 1997; Anthony et al., 2001). Figures 4.6, 4.16, and 4.17 show that Fe-chlorite is very abundant throughout all wells and that Mg-chlorite is not nearly as abundant and it is mostly found in samples taken from depths of 2-3.2 km. Mg-chlorite is not found in any samples from the Chebucto K-90 well. Chlorite is confidently identified by comparing the sidepack samples with the < 2 μm samples (Figures 4.11, 4.15, & 4.18).

Mixed Layer Chlorite (MLChl):

Mixed layer chlorite is identified in the samples at d-spacings of 7.86 Å and 3.94 Å. Mixed layer chlorite is found to be moderate to abundant throughout the wells and is not appear to have any correlation between quantity and depth (Figures 4.13 & 4.18). MLChl is confidently identified through correlation with the <2 μm samples.

Unspecified Mixed Layer Clays (UMLC):

Unspecified mixed layer clays are present in the samples at d-spacings of 11.0 Å, and 5.5 Å (Brindley & Brown, 1980). These peaks are found in low to abundant amounts in most wells (Figures 4.13 & 4.18). Unspecified mixed layer clay locations are confidently identified through correlation with the <2 μm samples.

Vermiculite (Vrm) and Vermiculite-Mixed Layer Clay (VMLC):

Vermiculite is identified in the samples at d-spacings of 14.6-14.0 Å, and vermiculite-mixed layer clay is identified at 12.26 Å (Brindley & Brown, 1980; Piper et

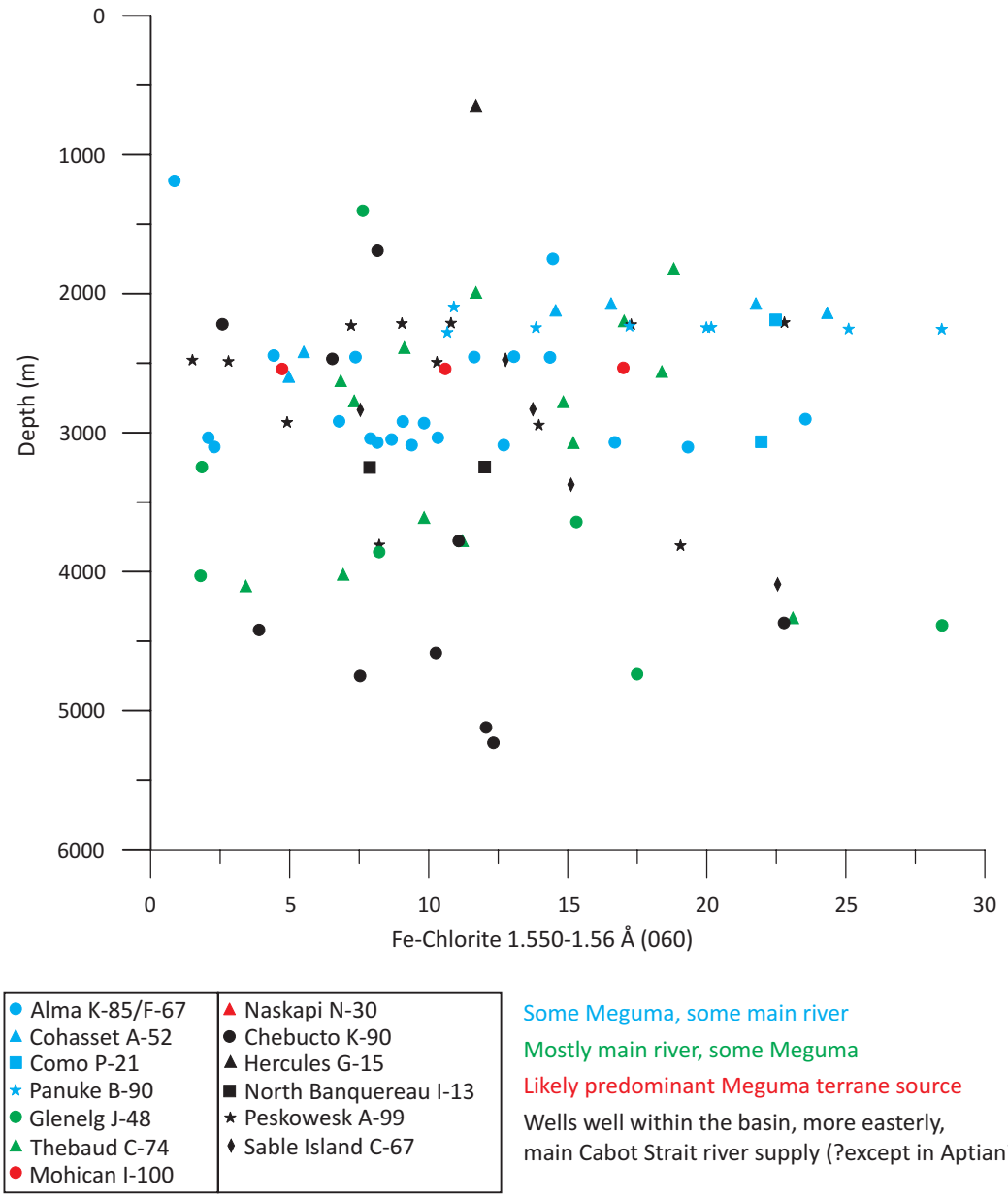

Figure 4.16: Bulk random samples normalized to the standard showing Fe-Chlorite 1.550-1.560 Å (060) vs Depth. Colour code based on likely provenance from Pe-Piper & Piper (2012).

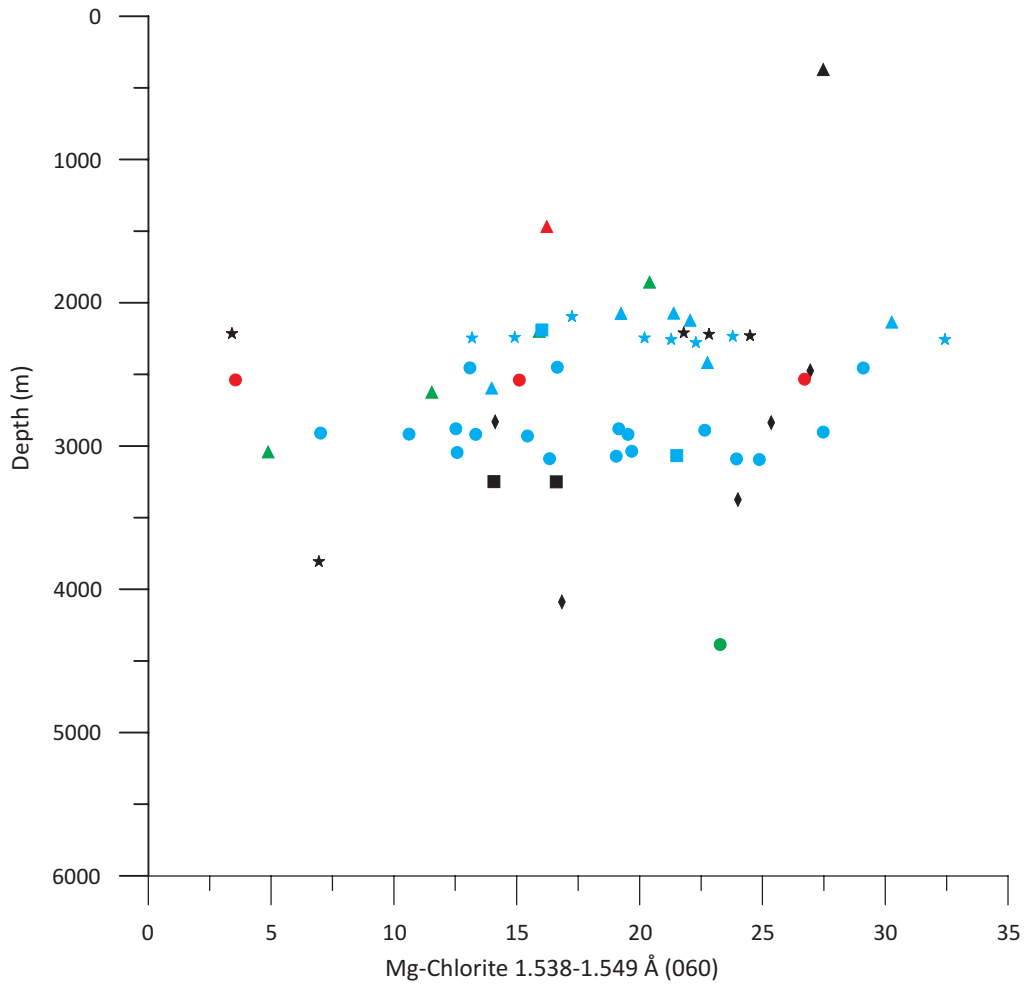

Figure 4.17: Bulk random samples normalized to the standard showing Mg-Chlorite 1.538-1.549 Å (060) vs Depth. Colour code based on likely provenance from Pe-Piper & Piper (2012).

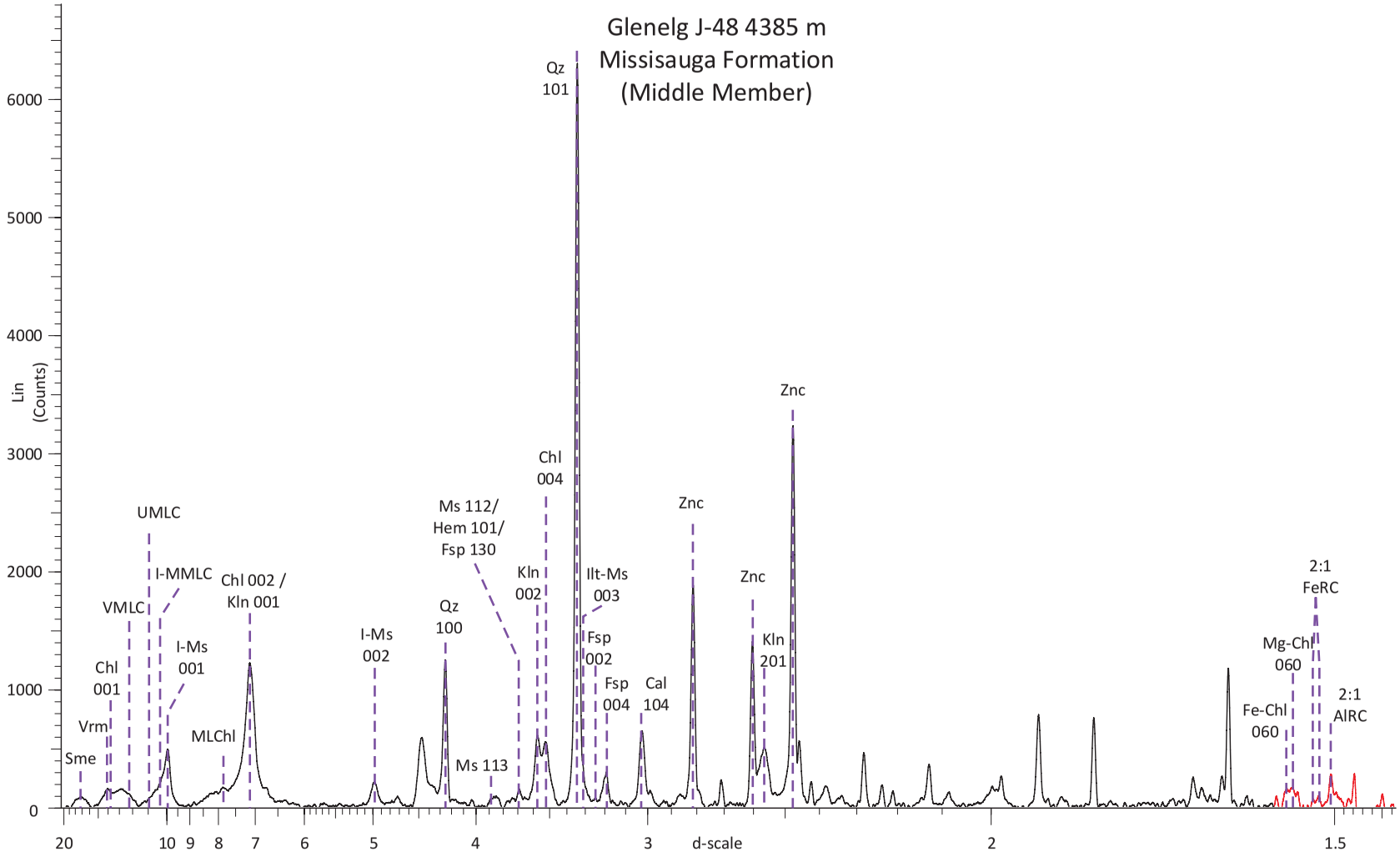

Figure 4.18: X-ray diffraction of Glenelg J-48 4385 m bulk random scans showing key clays found in sidepack analyses.

al., 2009) (Figures 4.13 & 4.18). Vermiculite is moderate to abundant in all wells except North Banquereau I-13, Naskapi N-30 and Cohasset A-52. Vermiculite is most abundant in the Thebaud C-74 and Chebucto K-90 wells (Figure 4.19). Vermiculite-mixed layer clay is most abundant in the samples from the Chebucto K-90 well and is only found in low amounts in the samples from Alma K-85, Hercules G-15, North Banquereau I-13, Peskowesk A-99 and Sable Island C-67 (Figure 4.20). Vermiculite and vermiculite-mixed layer clays are confidently identified through correlation with the <2 µm samples.

Illite/montmorillonite mixed layer (I-MMLC):

I-MMLC is identified in the samples at d-spacings of 10.26 Å (001) (Brindley & Brown, 1980). I-MMLC is found in low to abundant amounts in all wells (Figures 4.13 & 4.18). I-MMLC is confidently identified through correlation with the <2 µm samples.

Illite-Muscovite (Ilt-Ms):

Illite (1M hydromuscovite, Brindley & Brown, 1980) is identified in the samples at d-spacings of 10.1 Å (illite-muscovite) (001), 5.02-5.05 Å (illite-muscovite) (002), and 3.32 Å (illite-muscovite) (003) (Carroll, 1970; Brindley & Brown, 1980; Moore & Reynolds, 1997). The 3.32 Å peak is partially overlapped by a large 3.34 Å quartz peak in the <2 µm analyses but is still visible; however, it is completely overlapped in the bulk random sidepack analyses. There are also two muscovite peaks at 3.89 Å (113), 3.66 Å (112) (interferes with hematite and feldspar). Muscovite polytypes can be identified in random mounts with the 112 peak (Carroll, 1970). Illite is found in moderate to abundant amounts throughout all samples (Figures 4.13 & 4.18). Ilt-Ms is confidently identified through correlation with the <2 µm samples.

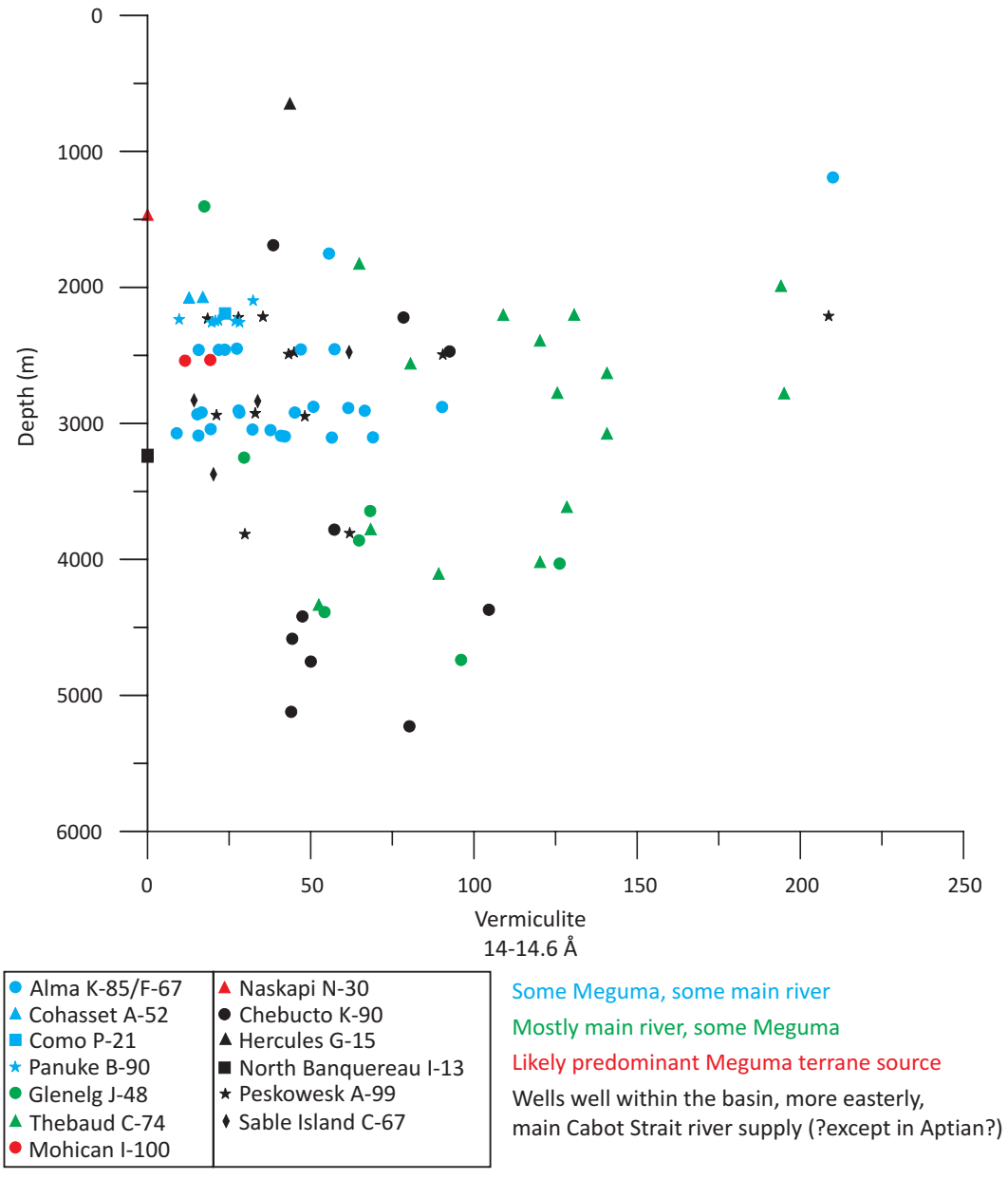

Figure 4.19: Bulk random sidepack samples normalized to the standard showing vermiculite 14-14.6 Å vs Depth. Colour code based on likely provenance from Pe-Piper & Piper (2012).

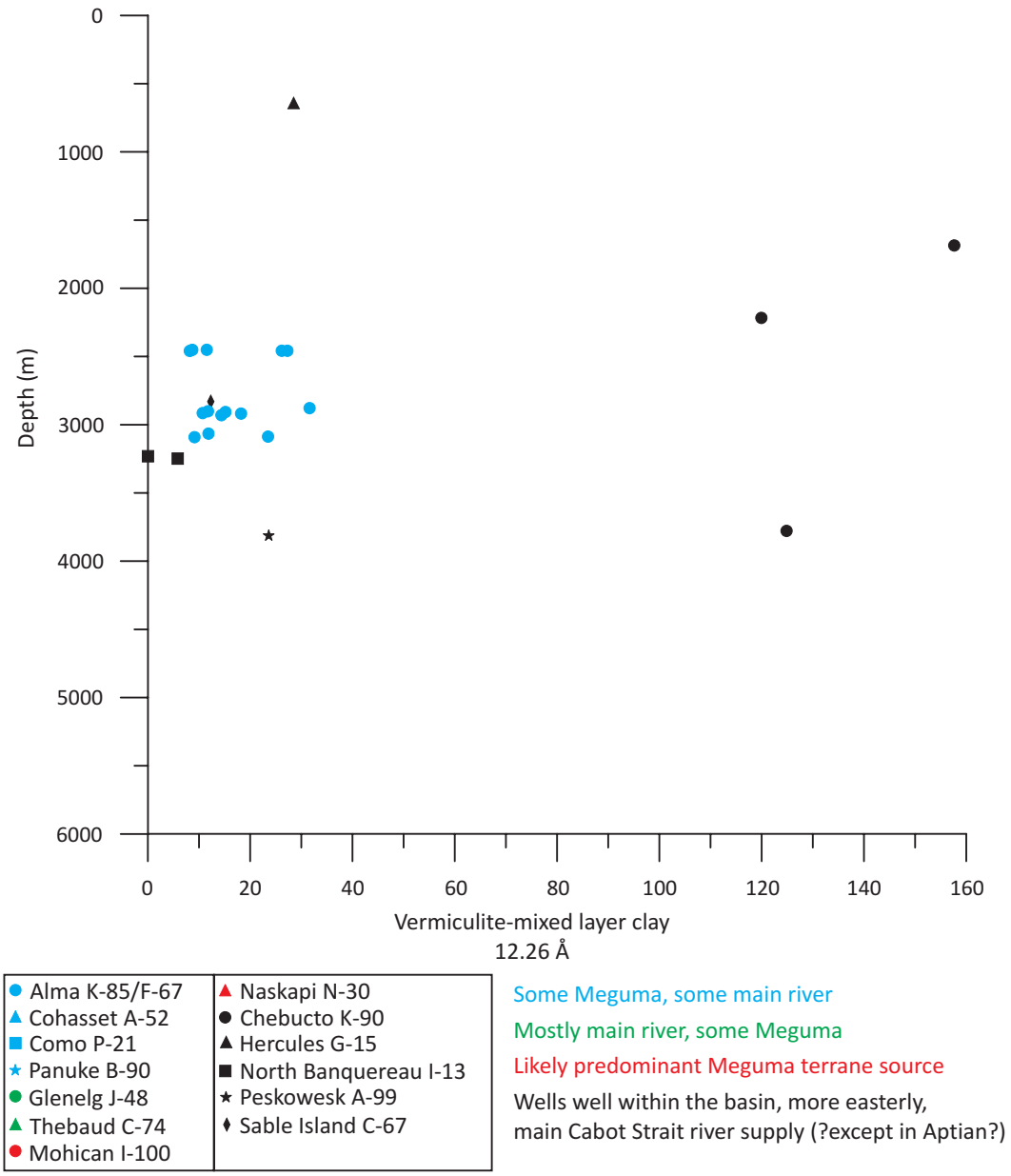

Figure 4.20: Bulk random sidepack samples normalized to the standard showing vermiculite 14-14.6 Å vs Depth. Colour code based on likely provenance from Pe-Piper & Piper (2012).

2:1 Al-rich Clays (2:1 AlRC):

2:1 Al-rich clays (includes Smectite + illite-smectite + illite+ Al-rich mica + dioctahedral vermiculite) are identified in the samples at d-spacings of 1.449-1.505 Å (060) (Brindley & Brown, 1980; Moore & Reynolds, 1997; Srodon et al., 2001) (Figures 4.15 & 4.18). 2:1 Al-rich clays are found in trace to moderate amounts in all wells. The 2:1 Al-rich clays are confidently identified by the peak locations in the 060 range.

2:1 Fe-rich Clays (2:1 FeRC):

2:1 Fe-rich clays (includes nontronite + glauconite + Fe-rich illite + celadonite) are identified in the samples at d-spacings of 1.510-1.530 Å (060) (Brindley & Brown, 1980; Moore & Reynolds, 1997; Srodon et al., 2001) (Figures 4.15 & 4.18). 2:1 Fe-rich clays are found in trace to moderate amounts in all wells; however, in Alma K-85 it is stratigraphically sporadic. The 2:1 Fe-rich clays are confidently identified by the peak locations in the 060 range.

Kaolinite (Kln):

Kaolinite is identified in the samples at d-spacings of 7.12-7.16 Å (001) (where it overlaps with chlorite), 3.57 Å (002) (where it can be separated from chlorite with a slow scan), 2.56Å (002), and 1.489Å (060) (Brindley & Brown, 1980; Moore & Reynolds, 1997; Anthony et al., 2001). Kaolinite is found in every sample, and in most samples is abundant (Figures 4.15 & 4.18). Kaolinite is confidently identified through correlation with the <2 μm samples.

Sepiolite:

Sepiolite is identified at d-spacings of 7.5 Å (130), and 1.54-1.55 Å (060) (Brindley & Brown, 1980; Moore & Reynolds, 1997). It was not confidently confirmed in the <2 µm samples due to the various mixed layer clays that overlap the sepiolite peaks and there may be similar problems in the sidepack samples. It is found ranging from trace to abundant amounts in Cohasset A-52, Como P-21, Mohican I-100, North Banquereau I-13, Panuke B-90 and Sable Island C-67. All the samples that do show these peaks are from the Cree and Naskapi Members of the Logan Canyon Formation which were deposited during a time of volcanism on the Orpheus Graben (the importance of this will be discussed later) and from the Middle and Upper Missisauga Formation. It should also be noted that when the amounts of sepiolite are compared with the amounts of Nb and Ta present in whole rock analyses of the same samples, there is no correlation. Sepiolite can not be confirmed or denied as being in these samples.

Quartz (Qz):

Quartz is identified in the samples at d-spacings of 4.26 Å (100), 3.34 Å (101), and 1.541 Å (060) (Brindley & Brown, 1980; Moore & Reynolds, 1997; Anthony et al., 2001). Quartz is abundant in every sample (Figure 4.13); however, it appears to be most abundant in the samples A-99 2209.25, A-99 2492.62, C-74 1990, G-15 371.86, K-85 3104.1, K-85 3104.7, and C-74 2780. Quartz is confidently identified through correlation with the <2 µm samples.

Hematite (Hem):

Hematite is possibly present in the samples at a d-spacing of 3.69 Å (101) (Brindley & Brown, 1980; Moore & Reynolds, 1997; Anthony et al., 2001). As mentioned in the <2 µm section, the 3.69 Å peak is overlapped by the 3.68 Å feldspar and/or the 3.68 Å muscovite peaks. Therefore, it is possible that hematite may be in most of the samples but it is masked by the 3.68 Å feldspar and 3.68 Å muscovite peak (Figure 4.13). Hematite is not confidently identified in the samples.

Feldspar (Fsp):

Feldspar is identified in the samples at d-spacings of 3.68 Å, 3.43 Å (diluted by quartz), 3.31 Å (Kfs), 3.25 Å (Kfs), 3.22 Å (Pl/Kfs), 3.20 Å (Pl), and 3.18 Å (Pl) (Brindley & Brown, 1980; Moore & Reynolds, 1997; Anthony et al., 2001). The 3.68 Å peak interferes with potential peaks of hematite and muscovite. The 3.25 Å peak could overlap rutile and the 3.43 Å peak partially overlaps with quartz. The potential feldspar peaks are found in moderate to abundant amounts in all samples. As mentioned in the <2 µm section, the peaks that have been identified as possibly feldspar are good indicators of the presence of feldspar, but without peaks in the ranges 6.5-6.4 Å and 4.22-4.03 Å (both in the sidepack and <2 µm samples), there is a lower confidence in identifying these peaks as feldspar (Figures 4.4 & 4.13).

Calcite (Cal):

Calcite is identified in the samples at d-spacings of 3.035 Å for pure calcite (104) and 3.00 Å (104) (Mg-calcite) (Brindley & Brown, 1980; Moore & Reynolds, 1997; Anthony et al., 2001). Calcite is not seen in samples from Cohasset A-52 and Como P-21. In the rest of the wells it appears sporadically in some samples and in low to very

abundant amounts (Figures 4.8, 4.10, & 4.18). Calcite is confidently identified through correlation with the <2 µm samples.

Anhydrite (Anh):

Anhydrite may be present in the samples at a d-spacing of 3.49 Å (002) (Brindley & Brown, 1980; Anthony et al., 2001). It is not found in Hercules G-15 or Chebucto K-90. For the rest of the wells it ranges from moderate to abundant in amount (Figures 4.13, & 4.14). It is difficult to distinguish in the <2 µm and sidepack samples due to overlapping of kaolinite, chlorite, K-feldspar and quartz. Since anhydrite is not confirmed in the <2 µm samples with heat treatment, it is not confidently identified.

4.4 COMPARISON OF <2 µm AND SIDEPACK DATA

There is an overall lack of variability in the <2 µm samples (Figure 4.21). There is slightly more variability in the sidepack samples, however, they are still quite similar (Figure 4.22). Two samples stand out more than others; Hercules G-15 646.18m (Figure 4.3 compared to Figure 4.21) from the Cree Member of the Logan Canyon Formation and Naskapi N-30 1469.1m (Figure 4.9 compared to Figure 4.21) from the Upper Member of the Missisauga Formation.

The peak area for the sidepack samples was normalized to zincite and the peak heights for the <2 µm samples were normalized to either talc or zincite. The normalized illite 10 Å (Figure 4.23) and kaolinite 3.57 Å (Figure 4.24) peaks for the sidepack samples were plotted against the values for the <2 µm samples, as a test of the similarity of the sidepack and <2 µm samples. A perfect match is not expected because the size range in

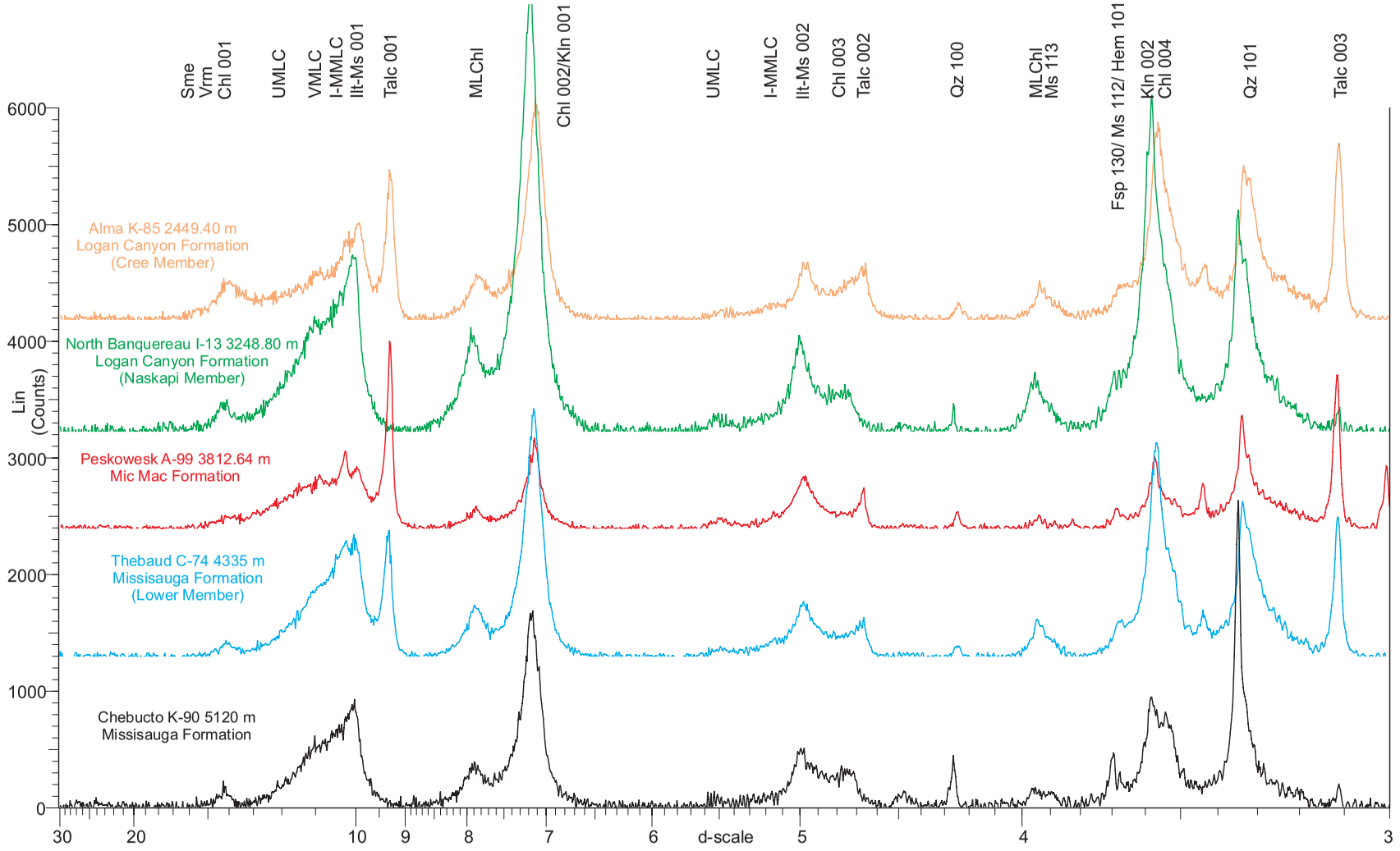

Figure 4.21: X-ray diffraction of K-85 2449.40 m, I-13 3248.80 m, A-99 3812.64 m, C-74 4335 m, K-90 5120 m. <2µm oriented scan showing the similarites between the different depths and different wells. The main difference is the talc standard peaks in K-85, A-99 and C-74.

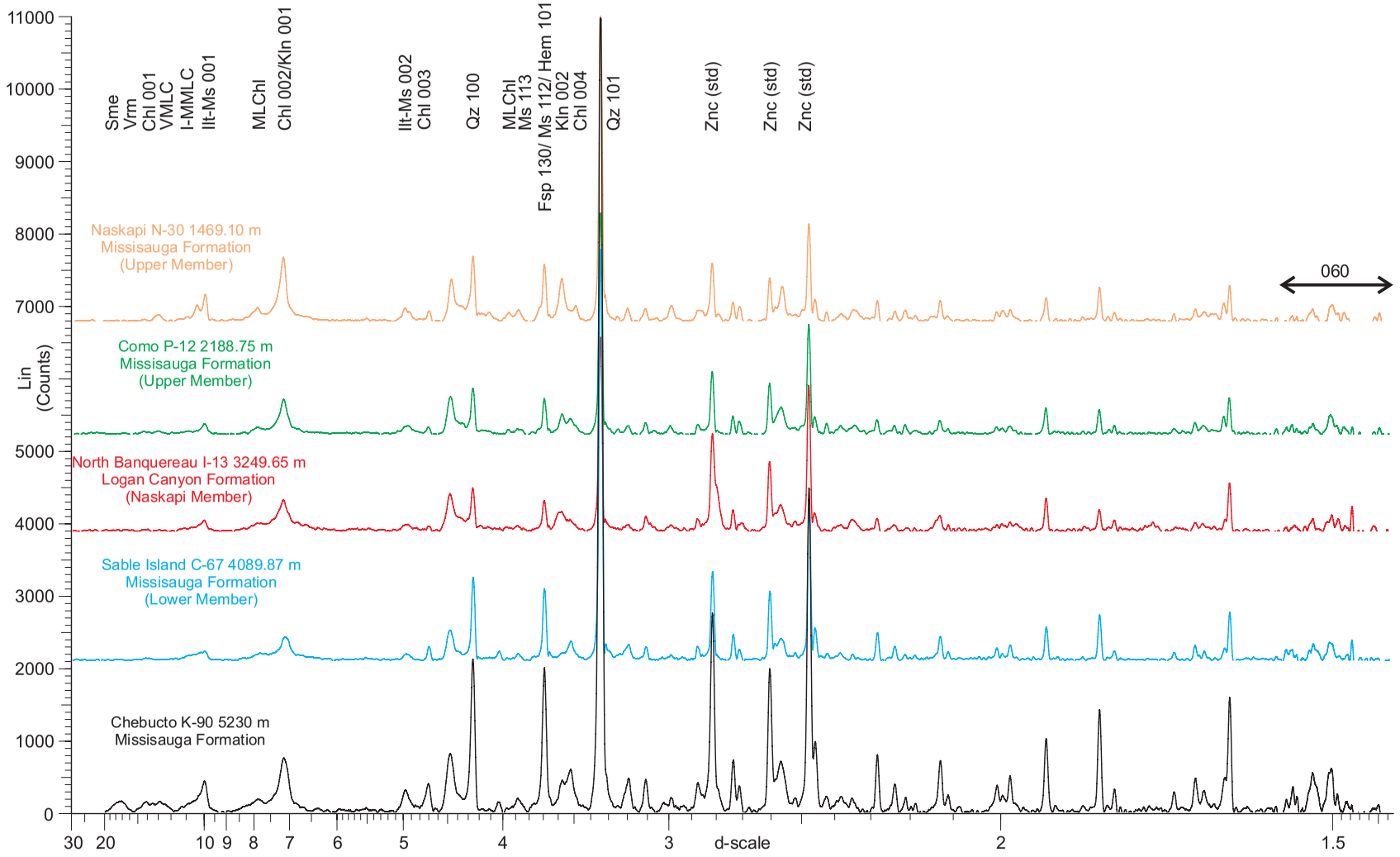

Figure 4.22: X-ray diffraction of N-30 1469.10 m, P-21 2188.75 m, I-13 3249.65 m, C-67 4089.875 m, K-90 5230 m. Bulk random sidepack analysis (including the 060 range) showing the variability or lack thereof between the different depths and different wells.

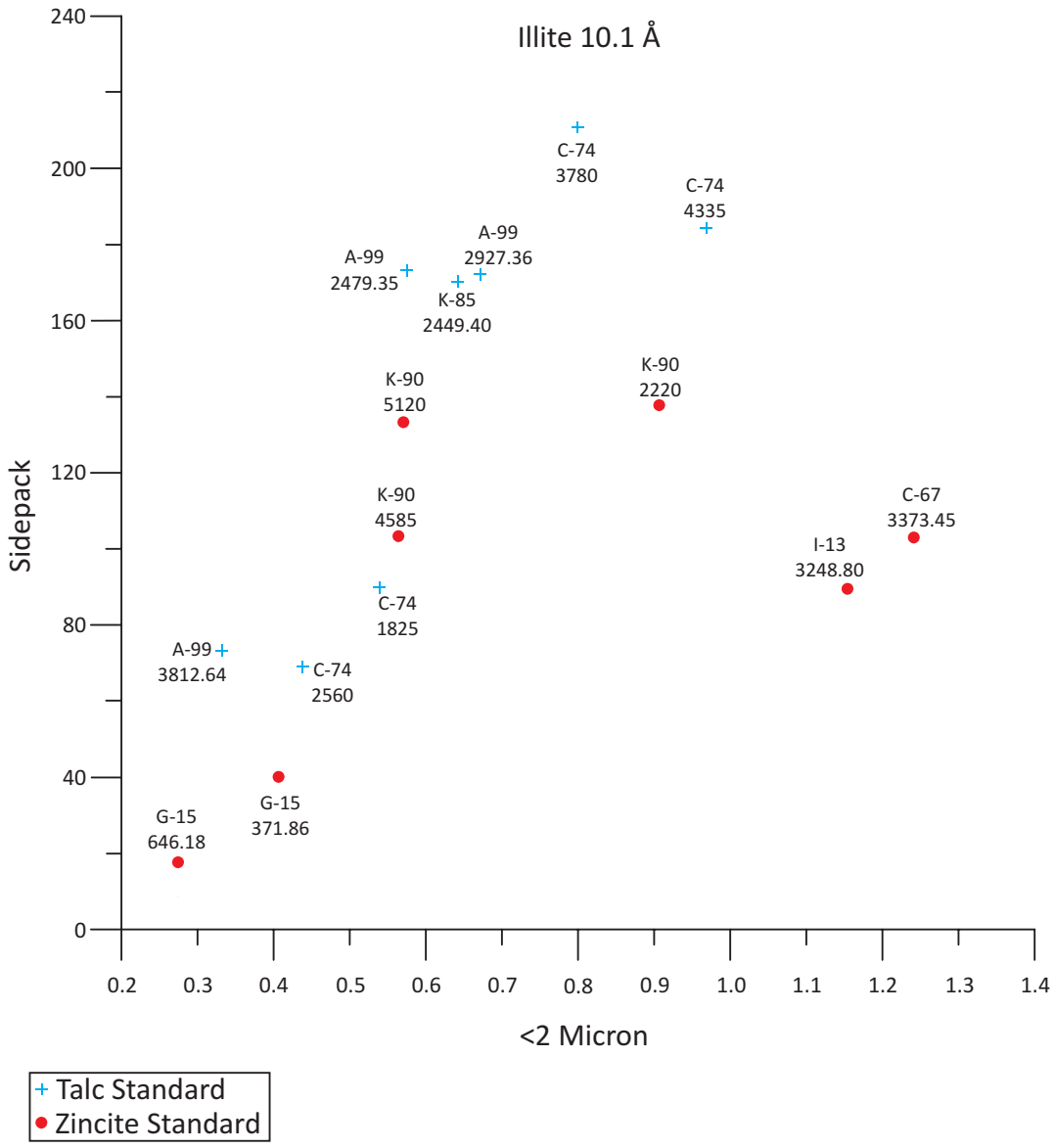

Figure 4.23: Illite 10.1 Å bulk random sidepack samples vs oriented <2µm samples normalized to talc (for <2µm samples) and zincite (for sidepack samples) showing an overall good set of peaks.

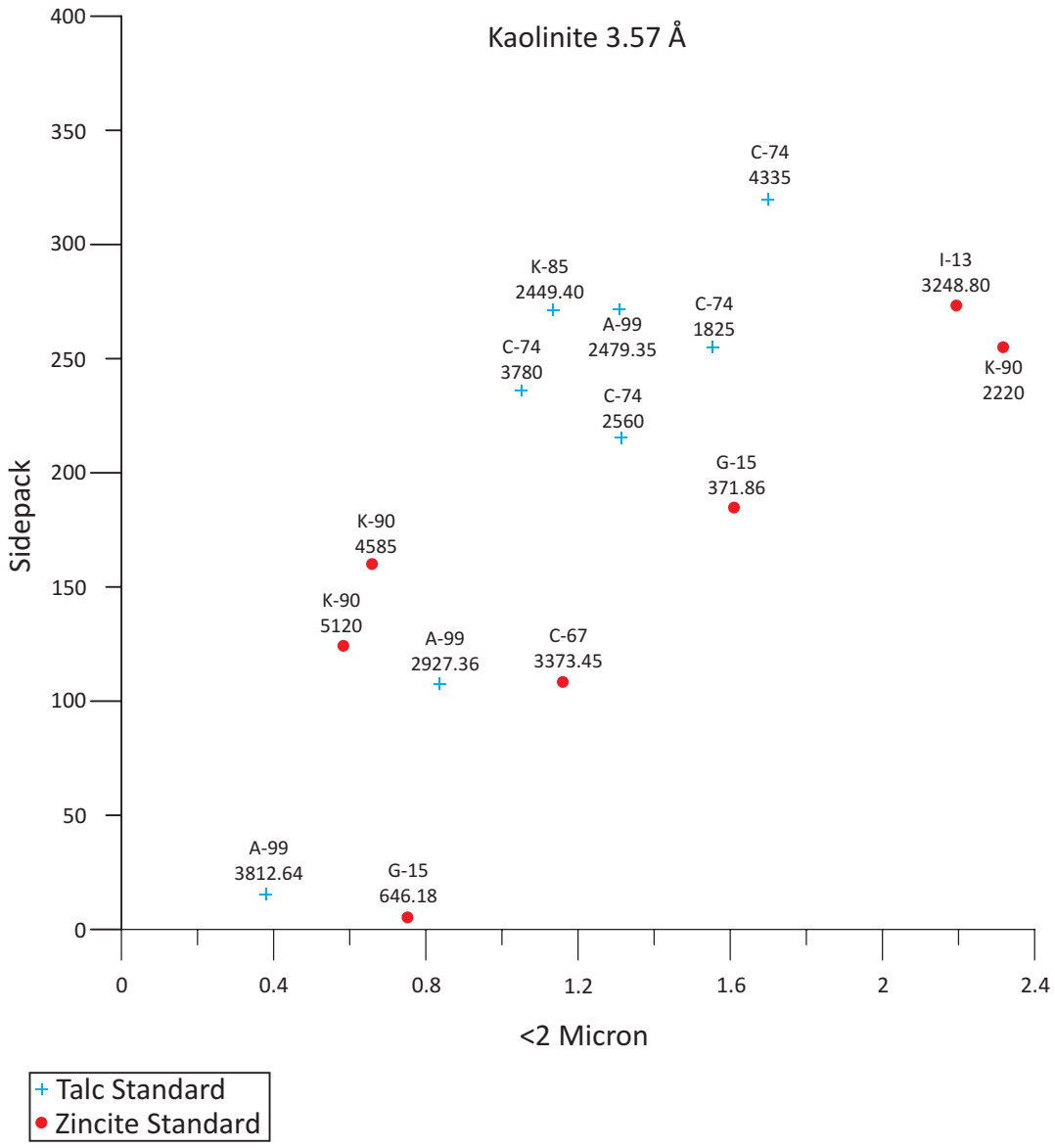

Figure 4.24: Kaolinite 3.57 Å bulk random sidepack samples vs oriented <2µm samples normalized to talc (for <2µm samples) and zincite (for sidepack samples) showing an overall good set of peaks.

the two sample types is different. These plots helped to investigate the concern about the validity of the illite peak picks due to the quantity of mixed layer clays that overlap in the peak areas of illite. In most samples, the correlation is good. Whole rock geochemistry from the samples show that high and low levels of K correspond with samples with high and low quantities of illite and detrital feldspar (Table 4.6).

Sample Hercules G-15 646.18 stands out due to the large amount of smectite present and low amount of other key minerals including illite, kaolinite chlorite, quartz, etc (Figure 4.3). This sample is from a pyroclastic layer found in the Cree Member of the Logan Canyon Formation on the Orpheus Graben. It is also quite silty compared with the other samples.

The <2 μm oriented sample Naskapi N-30 1469.1 is considerably different than the other samples. Neither glycol, nor glycerol solvation had any effect on the XRD analysis (Figure 4.9). The three most prominent peaks are: the 3.34 Å quartz peak, the 7.12-7.16 Å kaolinite peak, and the 3.66 Å muscovite-3.68 Å feldspar-3.69 Å hematite peak.

4.5 MINERAL ABUNDANCE WITH DEPTH

After confirming the validity of the sidepack samples by comparing them with the <2 μm samples, mineral abundance was investigated using the sidepack samples because they have been analyzed quantitatively. No smectite is seen below 3.7 km as seen in Figure 4.4, which distinguishes samples in which smectite is either absent, present (in small amounts) or abundant. The chlorite in the sidepack samples at the

Table 4.6: Whole-rock geochemistry results with Kaolinite, illite, K-feldspar, Chlorite, and Mg/Fe-Chlorite peak areas normalized to zincite (Thebaud I-93 and South Desbarres O-76 are peak heights from <2µm samples).

Project	Depth	Formation	Age (Ma)	Kaolinite	Illite	K-feldspar	Chlorite	Fe-Chlorite	Mg-Chlorite (060)	SiO2	TiO2	Al2O3	Fe2O3T	MnO	MgO	CaO	Na2O	K2O	P2O5	LOI	Total	Nb	Ta
				3.57 Å	10.1 Å	3.31 Å	14.5-13.7 Å	3.54 Å	1.538 - 1.549 Å														
Alma K-85	2449.40	LC (Cree Mb)	110	271.58	170.25		73.56	197.95	16.65	60.79	1.59	19.82	9.03	0.05	2.39	1.08	1.52	3.23	0.45	12.59	99.45	36.00	2.70
Alma K-85	2453.85	LC (Cree Mb)	110.2	196.32	200.62		74.16	208.97		58.77	1.44	19.92	11.64	0.06	2.16	1.27	1.22	3.14	0.34	13.71	99.03	32.00	2.40
Alma K-85	2455.00	LC (Cree Mb)	110.4	203.57	224.31		82.40	212.43	29.10	62.29	1.52	20.16	8.56	0.05	1.89	0.83	1.25	3.18	0.23	12.49	99.69	34.00	2.40
Alma K-85	2456.40	LC (Cree Mb)	110.6	165.63	79.05		51.98	153.16	13.08	60.79	1.46	21.41	8.33	0.03	2.03	0.92	1.28	3.47	0.23	12.18	99.15	31.00	2.20
Alma K-85	2456.50	LC (Cree Mb)	110.8	173.58	98.42		38.30	147.74		60.70	1.45	21.90	7.79	0.03	2.07	0.97	1.29	3.51	0.23	12.64	98.53	31.00	2.30
Alma K-85	2458.15	LC (Cree Mb)	111	199.12	56.93		31.21	190.52		60.94	1.44	21.03	8.92	0.03	1.96	1.04	1.23	3.13	0.22	12.79	99.52	34.00	2.40
Alma K-85	2460.75	LC (Cree Mb)	111.2	226.62	160.39		18.37	164.35		60.96	1.46	20.89	9.05	0.05	2.11	1.04	1.21	3.06	0.11	12.93	100.00	35.00	2.50
Alma K-85	2878.90	Miss Upper Mb	125	440.17	311.75		59.57	256.16	12.52	64.47	1.36	21.84	5.81	0.07	1.43	0.62	1.06	3.13	0.18	9.89	98.77	27.00	2.10
Alma K-85	2880.22	Miss Upper Mb	125.25	532.88	379.20		47.29	243.58	19.15	66.34	1.34	21.43	4.83	0.04	1.30	0.42	1.02	3.13	0.12	9.54	100.33	28.00	2.20
Alma K-85	2888.26	Miss Upper Mb	125.5	451.60	395.08		78.68	400.96	22.66	65.78	1.35	21.66	4.88	0.04	1.34	0.41	1.09	3.27	0.13	8.95	98.61	25.00	2.20
Alma K-85	2904.15	Miss Upper Mb	125.75	347.73	366.96		73.54	332.47		62.16	1.35	23.17	6.28	0.03	1.87	0.30	1.07	3.60	0.13	9.60	100.43	28.00	2.10
Alma K-85	2906.78	Miss Upper Mb	126	243.50	312.00		48.64	226.45	27.52	67.09	1.24	20.20	5.09	0.02	1.60	0.30	1.06	3.29	0.08	7.78	100.28	25.00	1.80
Alma K-85	2912.04	Miss Upper Mb	126.25	360.45	85.56		9.97	118.68	7.00	59.26	1.25	23.13	8.55	0.07	1.24	0.65	3.23	2.39	0.19	9.98	99.19	92.00	7.00
Alma K-85	2919.00	Miss Upper Mb	126.5	290.81	220.61		60.34	294.72	10.60	60.77	1.46	21.60	9.36	0.08	1.81	0.69	1.13	2.94	0.14	11.39	99.89	38.00	2.60
Alma K-85	2919.45	Miss Upper Mb	126.5	302.02	281.12		63.49	279.20	13.33	60.27	1.35	22.36	8.84	0.07	1.88	0.84	1.11	3.10	0.14	10.85	98.92	35.00	2.50
Alma K-85	2920.30	Miss Upper Mb	126.6	449.85	281.04		56.82	334.41	19.52	60.33	1.35	23.55	7.92	0.03	1.73	0.42	1.21	3.28	0.15	10.53	98.93	35.00	2.80
Alma K-85	2931.87	Miss Upper Mb	126.75	301.68	350.31		35.22	264.66	15.44	61.96	1.23	23.37	6.97	0.02	1.68	0.36	1.04	3.32	0.01	9.48	99.56	28.00	2.00
Alma K-85	3038.00	Miss Upper Mb	127.5	391.50	249.24		71.30	269.68	19.69	63.55	1.66	21.79	6.60	0.06	1.64	0.44	1.12	2.98	0.12	10.99	99.94	38.00	2.80
Alma K-85	3039.28	Miss Upper Mb	127.75	316.37	305.66		79.74	299.78		62.83	1.62	21.48	7.32	0.05	1.73	0.40	1.14	3.21	0.19	10.51	98.76	31.00	2.30
Alma K-85	3044.60	Miss Upper Mb	128	286.73	396.54		75.95	244.74	12.57	61.20	1.41	24.43	6.09	0.03	1.78	0.33	1.08	3.50	0.11	10.34	99.50	31.00	2.20
Alma K-85	3047.90	Miss Upper Mb	128.2	255.36	414.79		58.37	282.30		64.30	1.31	21.92	5.77	0.06	1.72	0.33	0.99	3.50	0.06	9.34	100.08	29.00	2.00
Alma K-85	3068.15	Miss Upper Mb	128.4	237.98	247.36		45.73	210.89		64.23	1.29	21.63	6.18	0.06	1.72	0.40	1.08	3.27	0.09	9.77	99.32	27.00	2.00
Alma K-85	3071.80	Miss Upper Mb	128.6	266.47	376.32		69.99	257.45	19.04	63.90	1.58	21.73	6.20	0.04	1.72	0.30	1.11	3.34	0.03	9.70	99.77	31.00	2.30
Alma K-85	3089.05	Miss Upper Mb	128.8	265.91	329.25		64.31	301.52	16.34	61.88	1.49	21.77	7.88	0.07	1.80	0.47	1.12	3.28	0.19	11.23	98.87	32.00	2.40
Alma K-85	3090.45	Miss Upper Mb	129	250.23	266.35		50.56	222.29	23.94	64.03	1.51	20.49	7.36	0.07	1.81	0.47	1.16	2.98	0.09	10.22	99.83	38.00	2.80
Alma K-85	3093.80	Miss Upper Mb	129.1	264.30	294.07		62.14	245.52	24.88	63.45	1.50	21.14	7.12	0.07	1.77	0.52	1.17	3.07	0.14	10.48	100.16	36.00	2.50
Alma K-85	3104.10	VC Fm	130	393.36	603.99		62.38	346.86		66.33	1.38	20.04	6.10	0.04	1.57	0.41	1.08	2.87	0.15	8.95	99.59	29.00	2.30
Alma K-85	3104.70	VC Fm	130	302.04	414.61		71.24	215.52		65.43	1.39	20.49	6.41	0.04	1.58	0.41	1.12	2.98	0.11	9.08	99.57	32.00	2.30
Chebucto K-90	1690.00	banq Fm	58.6	8.15	66.67			21.06		75.17	0.54	11.09	4.27	0.01	1.47	3.80	0.29	3.17	0.13	10.93	99.89	8.70	0.63
Chebucto K-90	2220.00	LC (Marmora Mb)	99.8	254.99	137.80		75.48	201.25		65.51	1.09	19.19	7.39	0.04	1.37	1.54	0.50	3.20	0.11	9.21	99.91	16.40	1.23
Chebucto K-90	2470.00	LC (Marmora Mb)	100	503.22	194.04		71.25	301.32		64.21	0.99	17.59	6.22	0.06	1.35	5.95	0.43	3.02	0.14	11.15	99.39	16.90	1.19
Chebucto K-90	3780.00	LC (Cree Mb)	126.5	473.57	36.12		95.49			29.81	0.32	5.15	5.44	0.17	1.20	55.74	0.55	1.45	0.11	30.98	96.60	4.90	0.40
Chebucto K-90	4370.00	Miss Fm	130.2	190.61	201.14		94.09	240.58		61.45	1.21	18.77	10.57	0.09	1.61	3.29	0.69	2.85	0.16	10.92	95.32	22.77	1.79
Chebucto K-90	4420.00	Miss Fm	130.25	159.50	145.09		40.19	161.53		60.28	1.41	19.18	8.55	0.07	1.73	4.10	0.84	3.33	0.20	11.55	96.68	36.60	2.79
Chebucto K-90	4585.00	Miss Fm	130.3	160.09	103.39		37.50	169.09		60.41	1.37	19.20	9.59	0.08	1.74	3.50	0.86	3.21	0.24	11.35	95.55	34.00	2.70
Chebucto K-90	4750.00	Miss Fm	130.4	171.14	103.38		52.82	174.77		62.00	1.49	20.12	8.20	0.06	1.62	2.14	0.82	3.10	0.18	11.08	98.62	40.20	2.78
Chebucto K-90	5120.00	Miss Fm	130.9	124.20	133.17		43.19	202.01		63.59	1.35	19.74	8.85	0.06	1.70	1.36	0.79	2.99	0.17	9.16	96.66	26.77	2.01
Chebucto K-90	5230.00	Miss Fm	131	115.66	89.65		48.21	204.50		64.93	1.26	17.49	9.44	0.08	1.63	2.13	0.83	2.67	0.16	9.28	97.43	24.34	1.79
Cohasset A-52	2072.90	LC (Cree Mb)	109	247.72	73.18	57.24		123.88	21.38	62.85	1.38	23.67	6.54	0.06	1.47	0.31	0.79	2.83	0.08	8.84	99.99	28.10	1.71
Cohasset A-52	2074.72	LC (Cree Mb)	109	255.04	57.01	64.99		128.17	19.25	59.23	1.41	25.97	7.79	0.05	1.59	0.28	0.84	2.73	0.06	10.38	98.51	28.00	1.77
Cohasset A-52	2123.52	LC (Cree Mb)	110	204.08	63.68	69.86		173.66	22.06	60.34	1.50	23.84	8.04	0.05	1.76	0.28	0.94	3.12	0.08	10.45	98.45	33.00	1.98
Cohasset A-52	2138.22	LC (Cree Mb)	111	140.39	49.77	80.02		228.96	30.26	58.97	1.63	21.43	10.65	0.05	1.96	0.60	1.00	3.39	0.29	11.41	98.40	35.50	2.23

Cohasset A-52	2418.75	LC (Naskapi Mb)	119	194.84	46.73	91.66		215.82	22.76	59.54	1.72	20.03	10.61	0.04	2.14	0.94	1.19	3.44	0.31	15.45	97.98	41.30	2.49
Cohasset A-52	2597.05	Miss Upper Mb	125	311.98	97.92	84.62		161.25	13.98	61.42	1.19	24.50	6.95	0.03	1.67	0.15	0.69	3.28	0.08	8.49	100.10	22.10	1.35
Como P-21	2188.75	Miss Upper Mb	125.5	281.43	111.38	77.64	13.03	223.32	16.01	58.09	1.36	26.27	8.35	0.02	1.60	0.14	0.75	3.31	0.07	11.98	99.53	32.10	1.96
Como P-21	3065.72	Miss Middle Mb	149	29.22	168.04	127.79		144.07	21.51	62.85	1.46	20.89	6.64	0.02	1.80	0.21	0.67	5.31	0.13	8.96	98.56	40.30	2.43
Naskapi N-30	1469.00	Miss Upper Mb	128	755.78	268.25	171.42		95.78	16.22	94.69	0.85	2.70	0.83	0.01	0.08	0.13	0.26	0.21	0.02	1.43	100.06	10.00	1.20
North Banquereau I-13	3248.80	LC (Naskapi Mb)	117	273.30	89.33	55.73		157.31	16.60	59.35	1.23	24.11	9.10	0.09	1.68	0.33	0.67	3.32	0.08	10.07	99.89	23.40	1.49
North Banquereau I-13	3249.65	LC (Naskapi Mb)	117	307.15	79.76	62.73		67.09	14.06	55.42	1.14	24.70	11.04	0.11	1.76	1.14	0.65	3.42	0.58	10.38	99.80	22.20	1.37
Panuke B-90	2097.27	LC (Cree Mb)	110.5	155.90	111.71	111.04		156.57	17.24	56.96	1.46	23.42	9.56	0.06	2.60	1.04	1.09	3.52	0.26	16.41	100.20	40.00	2.25
Panuke B-90	2235.37	LC (Naskapi Mb)	118.5	102.81	58.38	75.84		151.18	23.80	66.01	1.39	18.29	7.56	0.07	1.62	0.79	1.04	3.00	0.21	8.63	98.70	33.10	2.06
Panuke B-90	2241.57	LC (Naskapi Mb)	119.1	141.64	159.77			179.98	14.92	66.14	1.24	19.47	6.19	0.04	1.91	0.29	1.03	3.55	0.10	7.44	99.61	26.30	1.54
Panuke B-90	2245.78	LC (Naskapi Mb)	119.5	152.99	123.43			193.67	20.20	63.67	1.19	21.05	6.54	0.05	2.06	0.33	1.03	3.95	0.08	8.98	100.10	24.80	1.45
Panuke B-90	2247.20	LC (Naskapi Mb)	119.7	172.70	195.58	107.18		172.74	13.18	57.97	1.09	24.88	8.15	0.03	2.19	0.25	0.91	4.43	0.06	9.81	99.08	22.80	1.36
Panuke B-90	2255.49	LC (Naskapi Mb)	120.5	184.40	108.66	84.40		187.21	21.29	61.54	1.18	21.21	8.51	0.13	2.29	0.49	0.92	3.56	0.13	9.36	100.30	25.30	1.50
Panuke B-90	2256.56	LC (Naskapi Mb)	120.6	128.93	92.11	82.92		164.65	32.43	62.01	1.19	20.33	9.14	0.15	2.18	0.56	0.92	3.32	0.14	8.87	100.60	24.80	1.46
Panuke B-90	2278.21	LC (Naskapi Mb)	122.8	312.60	113.39	73.52		230.90	22.29	60.21	1.18	25.77	6.61	0.04	1.77	0.17	0.72	3.40	0.08	11.33	98.33	24.10	1.44
Peskowesk A-99	2209.25	LC (Cree Mb)	109.4	909.83	443.19		141.34	401.52	21.79	53.94	1.67	21.59	15.33	0.11	1.82	0.47	1.13	3.62	0.27	17.74	100.13	32.00	2.40
Peskowesk A-99	2213.57	LC (Cree Mb)	109.4	247.52	168.49			261.40		54.68	1.75	21.17	13.49	0.17	2.29	1.27	1.22	3.50	0.42	16.75	99.60	40.00	2.70
Peskowesk A-99	2215.78	LC (Cree Mb)	109.4	254.66	133.37		69.46	224.16	3.41	56.99	1.71	22.19	10.50	0.07	2.19	1.14	1.34	3.50	0.33	16.53	98.87	38.00	2.20
Peskowesk A-99	2219.03	LC (Cree Mb)	109.5	248.64	157.63		60.51	247.41	22.83	59.17	1.73	21.76	9.31	0.09	2.16	0.88	1.27	3.28	0.31	14.97	99.17	36.00	1.90
Peskowesk A-99	2221.69	LC (Cree Mb)	109.6	267.93	150.02		62.63	229.98		57.99	1.62	22.85	9.47	0.11	2.08	1.05	1.16	3.26	0.37	14.38	98.82	37.00	1.90
Peskowesk A-99	2479.35	Miss Upper Mb	125.2	271.38	173.12		50.46	137.78		60.03	1.36	25.36	7.06	0.04	1.77	0.21	0.92	3.10	0.10	10.97	99.87	32.00	1.80
Peskowesk A-99	2488.85	Miss Upper Mb	125.4	203.08	126.19		29.41	182.29		60.53	1.52	24.54	6.91	0.06	1.72	0.45	0.99	3.05	0.19	11.45	100.00	37.00	2.10
Peskowesk A-99	2492.62	Miss Upper Mb	125.5	283.59	66.15			190.37		66.59	1.46	18.89	7.60	0.03	1.32	0.36	1.00	2.53	0.19	10.01	99.24	49.00	2.70
Peskowesk A-99	2927.36	Miss Middle Mb	134.6	107.53	172.12		72.70	180.04		66.30	1.14	18.35	7.08	0.02	2.00	0.69	0.98	3.32	0.09	8.65	99.34	42.00	2.70
Peskowesk A-99	2940.90	Miss Middle Mb	135	381.42	588.32		43.16	177.26		57.25	1.54	27.81	5.20	0.03	2.32	0.20	0.84	4.62	0.13	10.64	99.80	37.00	2.40
Peskowesk A-99	2947.43	Miss Middle Mb	135.2	159.55	142.95		23.62	218.78		63.88	1.54	19.94	7.24	0.15	1.86	0.44	1.17	3.54	0.19	11.30	99.35	56.00	3.60
Peskowesk A-99	3812.19	Mic Mac Fm	149	15.40	73.26			20.10		44.52	0.84	13.26	7.78	0.09	2.90	27.51	Fa	2.41	0.11	21.60	97.01	20.90	1.39
Sable Island C-67	2474.18	LC (Cree Mb)	108.6	154.84	66.02	95.95	35.47	230.31	26.95	58.86	1.62	21.36	10.13	0.03	2.18	0.44	1.16	3.87	0.29	15.00	98.75	34.50	2.17
Sable Island C-67	2830.45	LC (Naskapi Mb)	122.8	210.78	215.89	124.96		145.48	14.12	57.50	1.08	24.95	8.67	0.07	1.96	0.25	0.85	4.55	0.06	12.75	100.80	19.90	1.29
Sable Island C-67	2835.42	LC (Naskapi Mb)	123	222.02	90.44	85.02		222.32	25.35	59.01	1.51	22.70	9.69	0.17	1.85	0.61	0.89	3.32	0.26	10.25	100.40	37.00	2.15
Sable Island C-67	3373.45	Miss Middle Mb	142.6	108.37	102.98	90.37		176.11	23.99	63.06	1.44	20.36	7.51	0.05	1.86	0.51	0.98	4.04	0.17	9.14	98.46	49.00	3.08
Sable Island C-67	4089.87	Miss Lower Mb	148.5	60.02	64.37	70.96		195.91	16.83	66.04	1.51	18.61	6.98	0.04	1.49	0.63	0.97	3.47	0.19	6.66	98.32	78.60	5.35
South Desbarres O-76	3815.10	Missisauga		0.959	1.03					56.66	1.26	20.66	12.68	0.19	2.25	1.48	0.62	3.89	0.25	12.27	98.84	47.20	2.36
South Desbarres O-76	5956.80	Mic Mac		0.995	1.86					64.32	1.19	21.80	4.99	0.05	1.40	1.00	1.00	4.03	0.15	8.35	99.62	41.40	2.30
Thebaud C-74	1825	LC (Sable Mb)	100.6	254.98	89.98			108.72	20.53	58.37	1.08	18.51	15.21	0.07	1.50	2.45	0.47	2.07	0.24	11.46	99.33	16.50	1.22
Thebaud C-74	1990	LC (Cree Mb)	103	428.20	149.57		93.74	220.08		64.22	1.22	19.02	9.22	0.05	1.42	1.89	0.50	2.30	0.13	10.95	98.87	19.50	1.44
Thebaud C-74	2200	LC (Cree Mb)	106.5	531.56	188.65		115.43	198.86	15.90	61.73	1.26	18.76	10.47	0.07	1.63	2.69	0.64	2.55	0.16	10.57	99.46	24.80	1.79
Thebaud C-74	2205	LC (Cree Mb)	106.6	485.29	180.29		93.65	296.47		61.84	1.34	19.25	10.63	0.06	1.67	1.73	0.62	2.65	0.19	11.27	98.91	24.40	1.79
Thebaud C-74	2390	LC (Cree Mb)	109.7	448.17	242.81		132.05	356.19		64.08	1.29	17.70	9.90	0.05	1.68	1.84	0.65	2.59	0.19	11.22	99.33	23.80	1.74
Thebaud C-74	2560	LC (Naskapi Mb)	115	215.27	68.93		44.28	156.79		62.14	1.48	21.07	9.05	0.05	1.55	1.23	0.55	2.65	0.19	11.18	98.34	34.40	3.03
Thebaud C-74	2630	LC (Naskapi Mb)	122.3	416.32	153.21		109.94	321.46	11.67	61.95	1.46	21.29	8.70	0.07	1.70	1.16	0.56	2.92	0.16	10.71	99.37	31.80	2.28
Thebaud C-74	2775	Miss Upper Mb	127.5	518.10	305.62		127.29	271.05		64.18	1.30	19.18	8.49	0.06	1.66	1.54	0.66	2.77	0.16	10.04	99.69	24.30	1.72
Thebaud C-74	2780	Miss Upper Mb	127.6	290.85	195.14		98.61	192.06		63.32	1.42	20.57	8.17	0.06	1.65	0.94	0.68	3.02	0.15	10.63	99.13	28.50	2.04
Thebaud C-74	3075	Miss Middle Mb	135	350.66	212.47		122.02	280.70	4.70	61.45	1.38	19.48	11.24	0.05	1.69	1.05	0.57	2.95	0.11	9.90	99.73	30.40	2.18
Thebaud C-74	3615	Miss Middle Mb	140	207.27	225.29		66.52	174.39		62.58	1.42	20.49	8.40	0.06	1.62	0.91	0.66	3.66	0.16	9.39	98.41	47.30	3.50
Thebaud C-74	3780	Miss Lower Mb	146	236.11	210.82		46.13	245.18		70.07	1.18	14.98	7.84	0.11	1.39	0.89	0.79	2.53	0.16	7.35	98.58	42.30	3.05
Thebaud C-74	4020	Miss Lower Mb	148.5	332.77	308.64		76.07	206.99		61.69	1.41	21.40	8.37	0.10	1.59	1.14	0.73	3.32	0.19	9.69	98.56	47.60	3.55

Thebaud C-74	4105	Miss Lower Mb	149	261.27	190.88		65.17	229.44		63.48	1.40	20.72	7.41	0.11	1.48	1.30	0.68	3.21	0.19	10.17	99.58	45.10	3.18
Thebaud C-74	4335	Miss Lower Mb	150	319.71	184.38		32.81	250.98		60.65	1.48	22.97	7.97	0.11	1.58	1.07	0.55	3.24	0.16	10.88	98.67	47.20	2.78
Thebaud I-93	3080.38	Miss Middle Mb	120.1	1.90	1.85					50.31	2.71	27.72	9.82	0.03	2.42	0.23	1.22	5.33	0.18	14.01	99.54	81.80	5.37

14.5-13.7 Å peak, corresponding principally to Mg-chlorite, tends to disappear with depth (Figure 4.25). This can be seen in the Upper Missisauga Formation samples from Thebaud C-74, Glenelg J-48, and Chebucto K-90. The Upper Missisauga is found at greater depths in Chebucto and Glenelg than it is in Thebaud. The sidepack samples also show that with deeper burial, vermiculite is disappearing (Figures 4.19 & 4.26).

Using Thebaud C-74, Glenelg J-48, and Chebucto K-90 example, the 2:1 Al rich clays (Figure 4.27) and 2:1 Fe-rich clays (Figure 4.28) appear to increase in abundance with depth, however, the Fe-rich clays are a little more scattered than the Al-rich clays. Kaolinite begins to decrease with depth at around 3 km (Figure 4.29) based on the 3.57 Å kaolinite peak in the sidepack samples.

There is a large amount of illite in Alma K-85 at around 3 km. Illite is a little peculiar in the sense that it appears as if it mildly increases until approximately 2.5 km, and stabilizes until around 4.4 km and then decreases in quantity (Figure 4.30), which is contrary to the common understanding that illitization of smectite and kaolinite occurs with depth (Kulbicki & Millot, 1961; Cassou et al., 1977).

The Fe-chlorite sidepack peak of 1.550-1.560 Å (060) shows no significant change with burial depth (Figure 4.16). The bulk random sidepack peaks for Mg-chlorite 1.538-1.549 Å (060) show that Mg-chlorite is mostly constrained between 2.0-3.2 km depth (Figure 4.17).

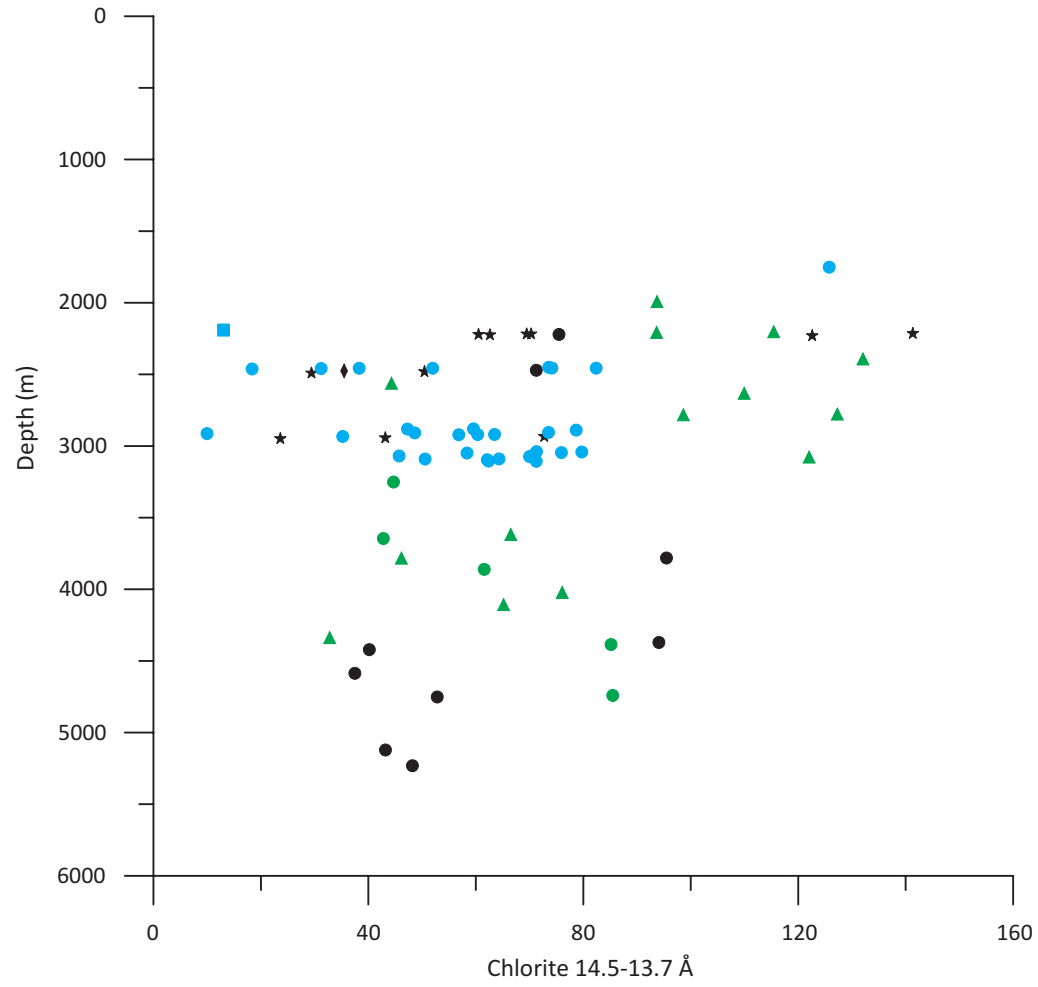

Figure 4.25: Bulk random samples normalized to the standard showing Chlorite 14.5-13.7 Å vs Depth. Colour code based on likely provenance from Pe-Piper & Piper (2012).

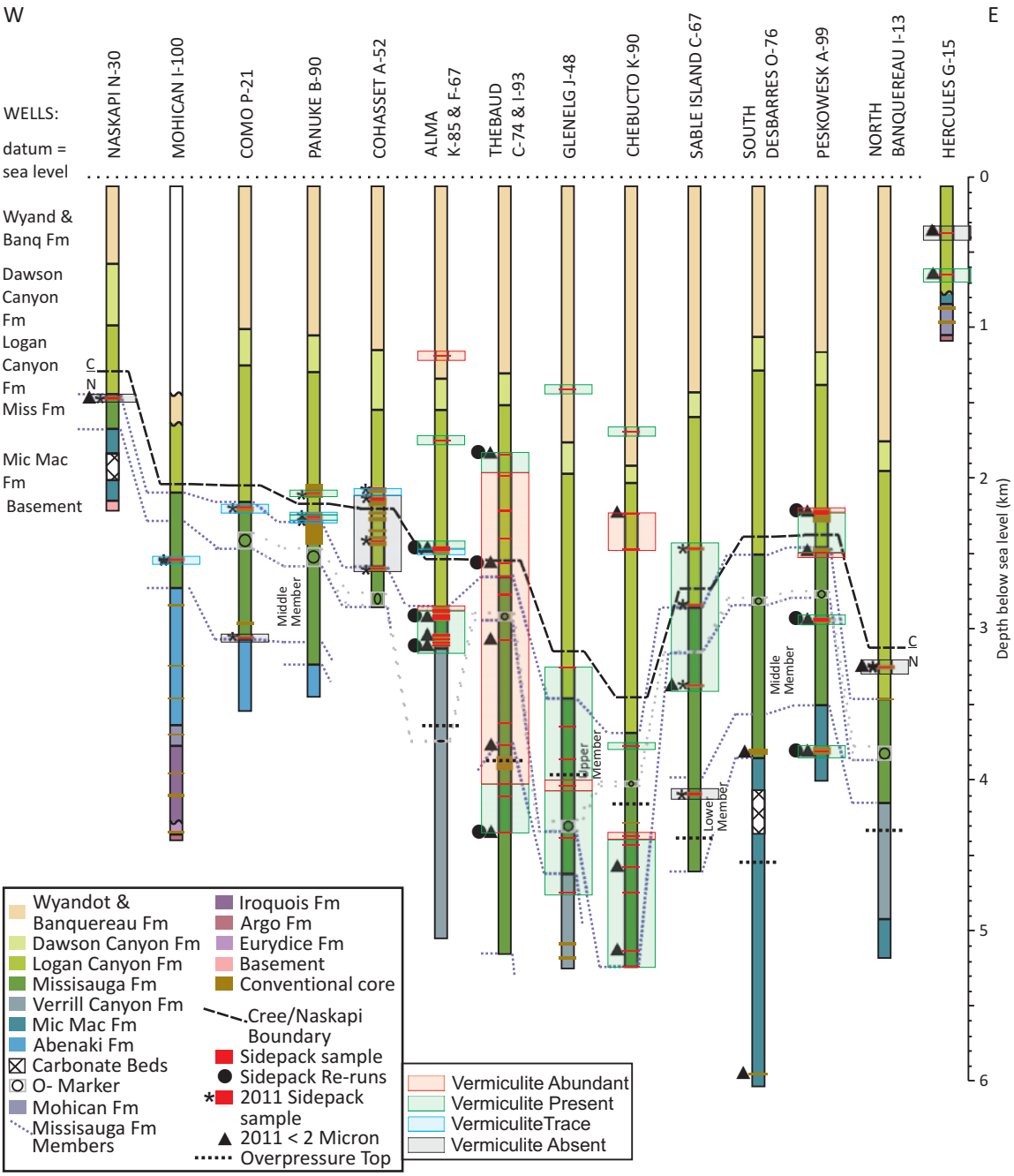

Figure 4.26: Stratigraphy of wells investigated with depths of bulk random sidepack and oriented <2 micron samples, showing vermiculite abundance with depth.

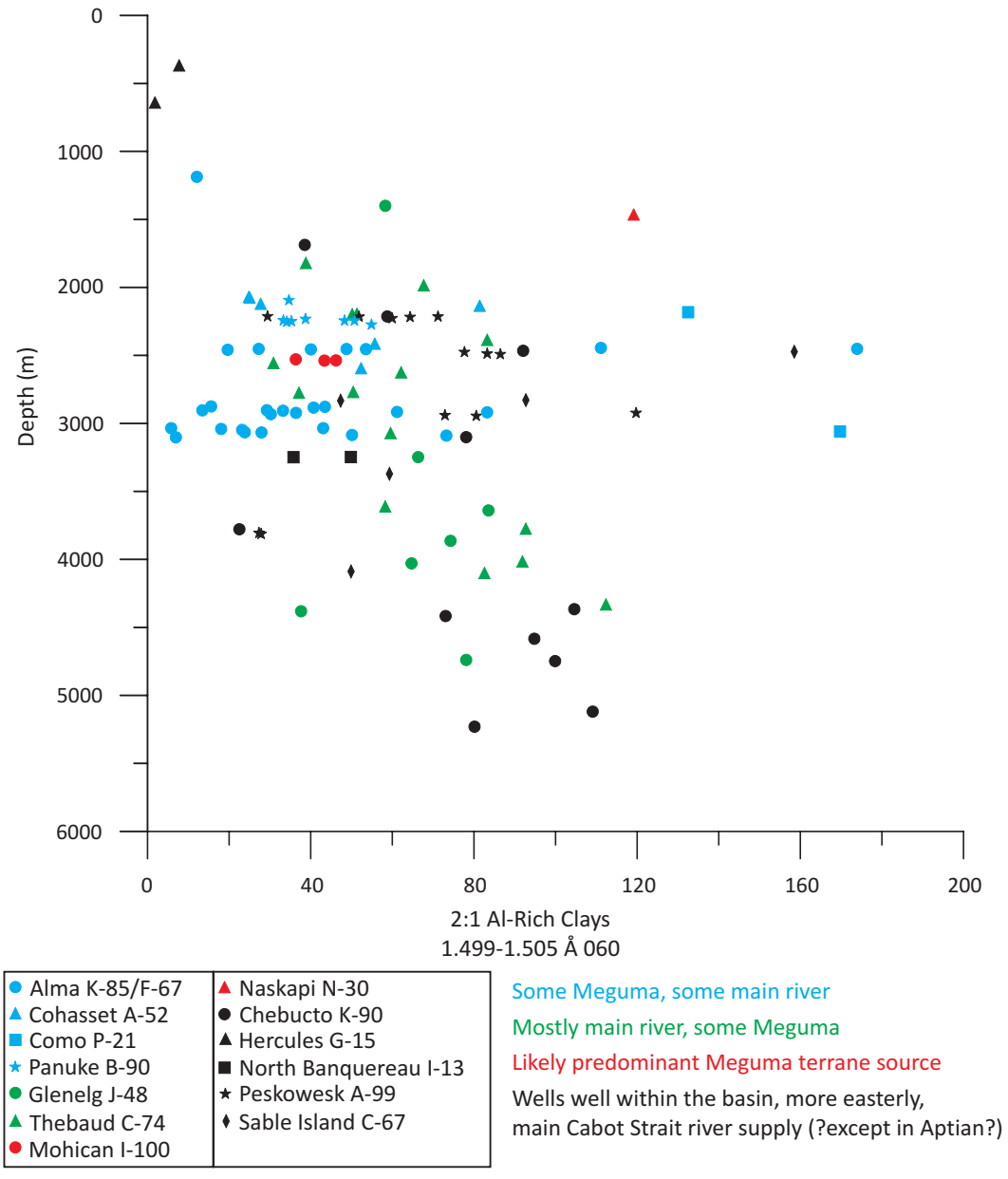

Figure 4.27: Bulk random samples normalized to the standard showing 2:1 Al-rich clays 1.499-1.505 (060) Å vs Depth. Colour code based on likely provenance from Pe-Piper & Piper (2012).

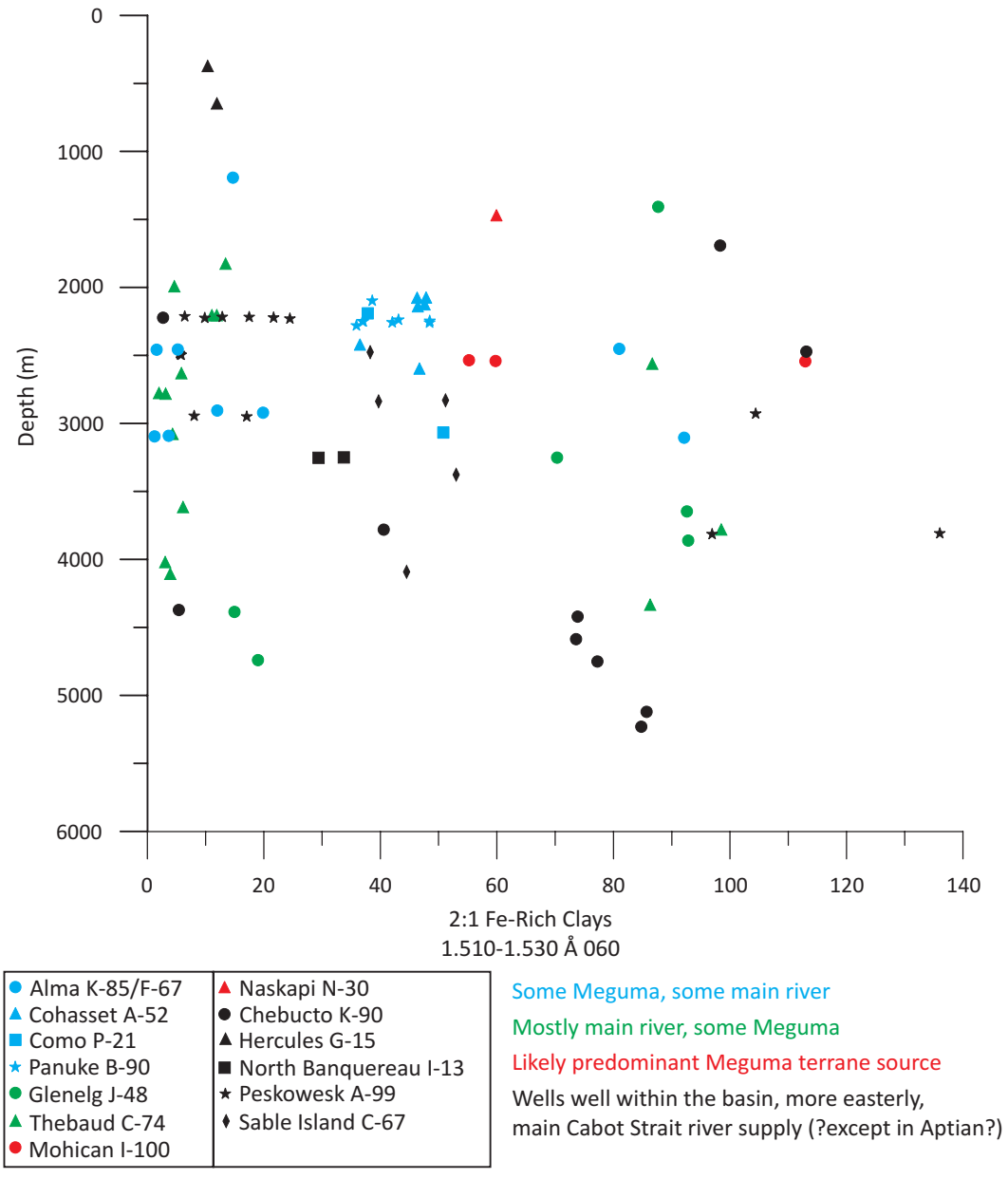

Figure 4.28: Bulk random samples normalized to the standard showing 2:1 Fe-rich clays 1.510-1.530 (060) Å vs Depth. Colour code based on likely provenance from Pe-Piper & Piper (2012).

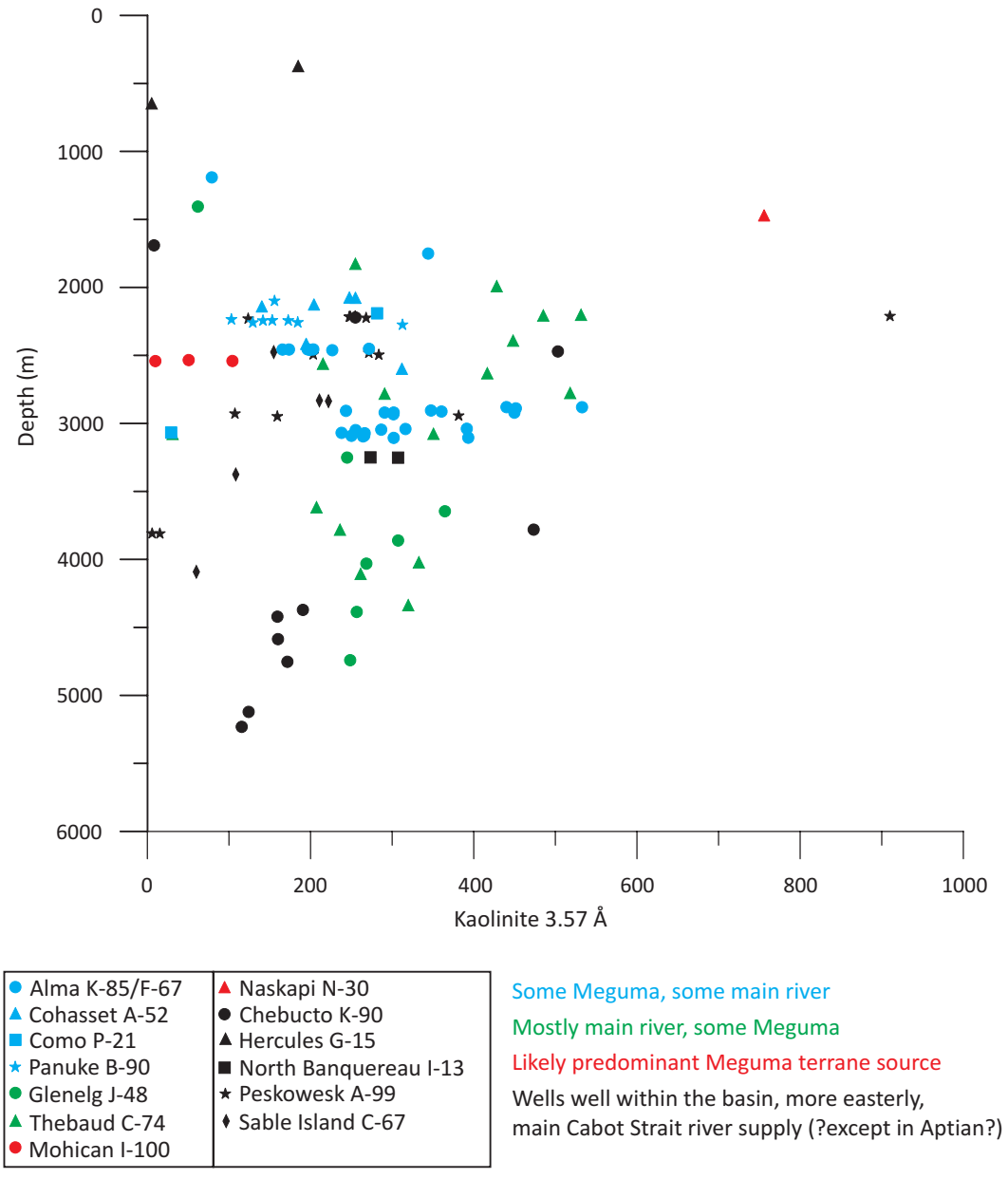

Figure 4.29: Bulk random samples normalized to the standard showing Kaolinite 3.57 Å vs Depth. Colour code based on likely provenance from Pe-Piper & Piper (2012).

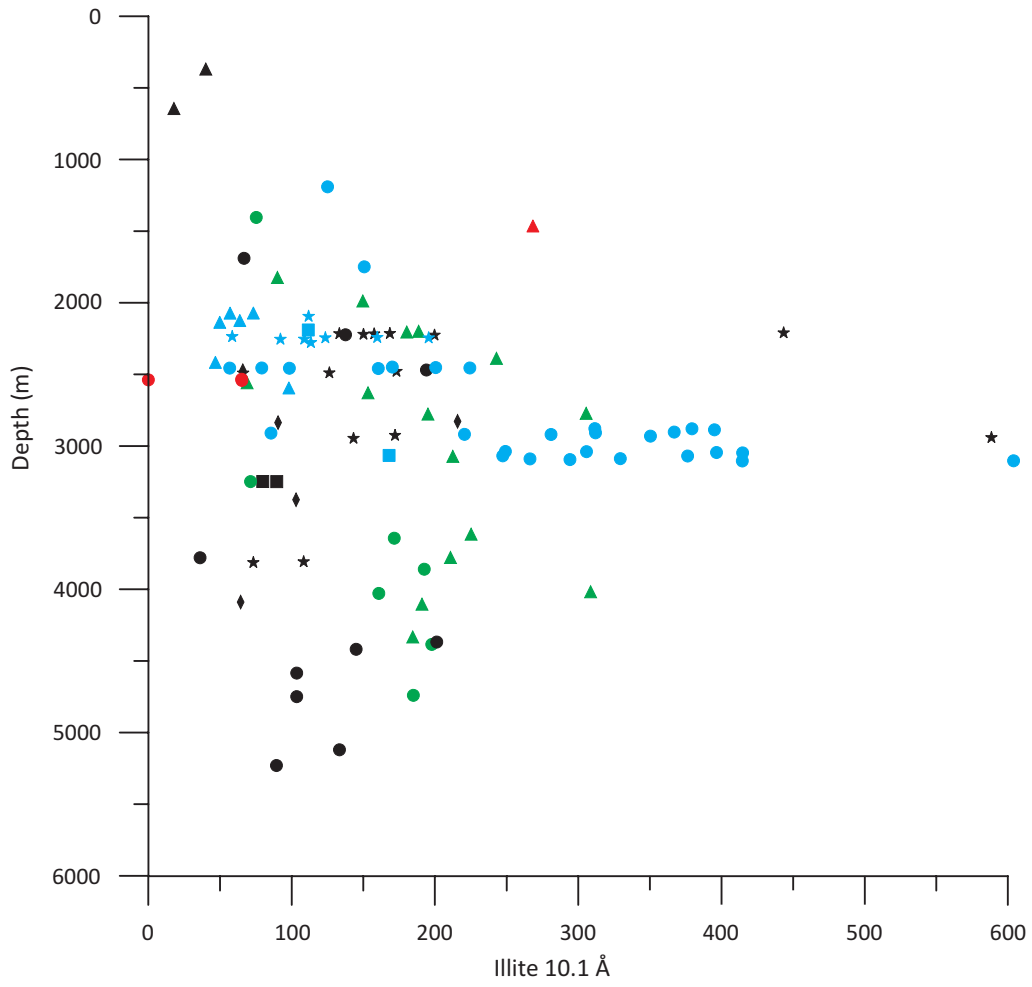

Figure 4.30: Bulk random samples normalized to the standard showing Illite 10.1 Å vs Depth. Colour code based on likely provenance from Pe-Piper & Piper (2012).

CHAPTER 5: DISCUSSION

5.1 X-RAY DIFFRACTOMETER REPRODUCIBILITY OVER TIME

While trying to understand some of the variability in the XRD analyses, it was found that the detector for the XRD was losing resolution and needed to be replaced. Several potential issues came to mind when considering variability and errors with sample preparation and analysis: 1) How reliable is the data from the X-ray diffractometer over time as the detector ages? 2) Variations and errors in creating the different types of mounts for the samples. 3) Variations and errors in picking and identifying the mineral peaks. 4) Problems with overlapping peaks in low 2θ range of bulk random sidepack samples.

Groups of samples analyzed in this thesis were run on the XRD in 2002, 2006, 2008 and 2011 using the same CoKα x-ray tube. The detector in the XRD was replaced around 2000 and again in 2010. Three samples from 2002 and six samples from 2006 were re-run in 2011 after the detector was replaced and peak heights were compared (Figure 5.1). The 2002 and 2006 samples fall in two distinct clusters, however, eight out of nine of the 2011 samples (triangles in Figure 5.1) plotted within the 2006 cluster. This suggests that any variation in peak height was more of an issue with either picking the peaks or sample preparation as opposed to poor analyses due to the detector problems. Use of a standard should minimize problems due to instrument variability.

Due to the platy nature of clay minerals, the orientation of the crystals is an important factor when creating the mount. Bulk sidepack mounts are intended to provide a random mount for clay powders that can be used to quantify the analyses,

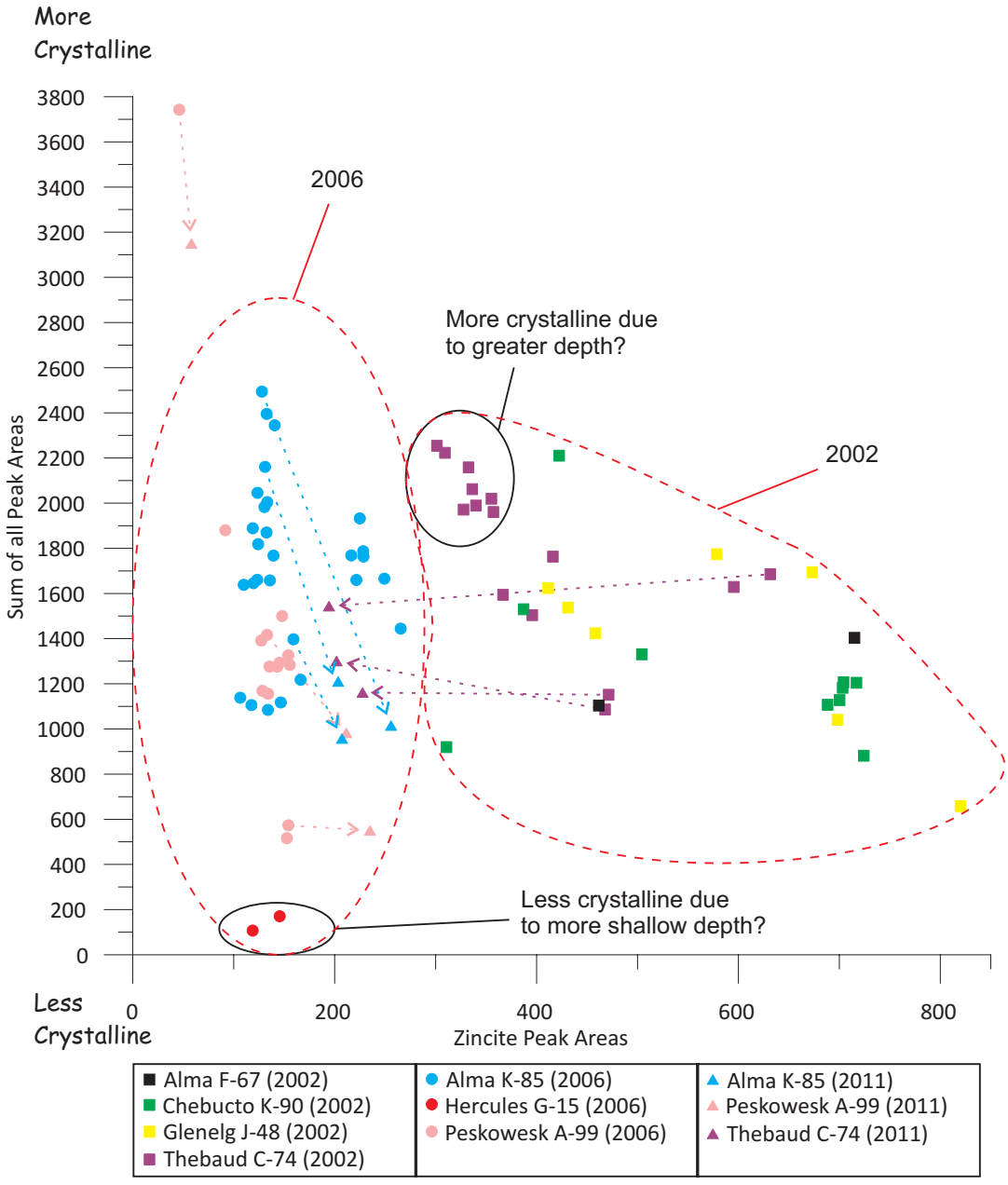

Figure 5.1: The sum of all bulk random sidepack peak areas vs Zincite peak areas (all normalized to zincite). Investigating XRD reproducibility over time. Starting in 2002 with a relatively new detector leading up to 2010 replaced with new detector.

particularly using the 060 diffractions. Less than 2 µm sample mounts are best for creating oriented mounts that concentrate the finest clay particles. This mount is more difficult to quantify but provides the best basal reflections (001, 002, etc.) which aids in mineral identification.

Grain size is an important component to consider when contemplating sample mounting issues. The sample needs to be ground to as uniform a grain size as possible to ensure precision and accuracy of the analyses without grinding the non clay minerals to a clay mineral size. For bulk random sidepack samples <20 µm can be achieved by when grinding with a micronizing mill after the sample has been crushed with a mortar and pestle. Care needs to be taken with the mortar and pestle as grinding too long and too hard will crush non clay minerals as well. For oriented <2 µm samples, crushing the samples with a mortar and pestle will achieve a grain size that will pass through a 63 µm sieve. The <2 µm portion of the sample will then be ready to separate through suspension and centrifuging the sample.

Picking peaks is reproducible between different people but everyone has slight variations in how and what they pick. The picks done by others were all checked and where the variations were found to be the greatest the peaks were re-picked. The major peaks are picked consistantly; however, the minor peaks are more variable. Many mineral peaks partially or fully overlap, which can cause errors in identification and quantification. EVA, the software used to process the diffractograms adjusts for peak overlap by limiting the area to a straight line where the peaks meet and assuming that the canceled out area equals the area measured. Unfortunately this will

occasionally cause over-exaggerated and under-exaggerated values. Identification of the low 2θ peaks with expandable mixed layer clays can be aided by glycol and glycerol treatments. Heat treatment is another step to help identify clay minerals. The sidepack peaks were compared with the <2 μm peaks (Figure 4.23 & 4.24) which demonstrated the correlation was good. Using random sidepack mounts, the scan can be extended to the 060 range (high 2θ) will help clarify the many overlapping peaks in the low 2θ range (Figure 4.15).

5.2 CAUSES OF CLAY MINERAL VARIABILITY

There is less variability in the composition of clays in the Scotian Basin than originally anticipated. However, there are subtle variations present in the abundance of clay minerals. The variability, or lack thereof, in the clay minerals present may result from several factors: 1) Analytical error caused by poor sample preparation, analytical equipment issues, and/or XRD analysis errors. The <2 μm samples have been compared with the sidepack samples and have seen good correlation where expected. 2) Variations in the grain size of sediment will have an impact on clay mineral variability because minerals tend to sort by grain size. This effect will be greatest in the bulk sidepack samples. 3) Variations in source rock, petrology and weathering may have a big impact on the variability of the clay minerals, not only on the detrital minerals but also on the diagenesis that takes place after deposition. 4) Variations in surface and burial diagenesis can alter the clay minerals, potentially masking the source and

environmental conditions at the time of deposition. This could cause the minerals to become more variable or more uniform.

5.3 VARIATIONS DUE TO GRAIN SIZE

Some of the samples investigated in this study were shale and some were mudstone with silt laminae. Silt content can be estimated by the amount of quartz present or by using a quartz/illite ratio. Thus to better understand the silt content of these samples a quartz/illite ratio was investigated (Table 5.1). It is difficult to accurately pick the illite peak because of the overlap of many mixed layer clays in the same region. Comparison of the sidepack samples normalized to the standard against <2 µm samples normalized to the standard shows that the picking of the illite peak is reliable (Figure 4.23).

Quartz in clays is generally considered mostly detrital (Potter, Maynard & Pryor, 1980). Biogenic quartz in diatoms, radiolarians and other taxa has not been reported as significant in the deltaic sediments of the Scotian Basin. There may be authigenic quartz in these samples as such quartz precipitation occurs in sandstones between >80-100° C (Bjorlykke et al., 2008) and may also be present in shales: its effect is assumed to be minor compared to detrital quartz.

Generally, a high quartz content in a sample would suggest it is coarser grained (Mongelli et al., 1996). The age of each analyzed sample has been estimated by interpolating depth between biostratigraphic picks in OETR (2011), using the timescale of Gradstein et al. (2004) (Figure 5.2). Variations in quartz/illite ratio show that there is

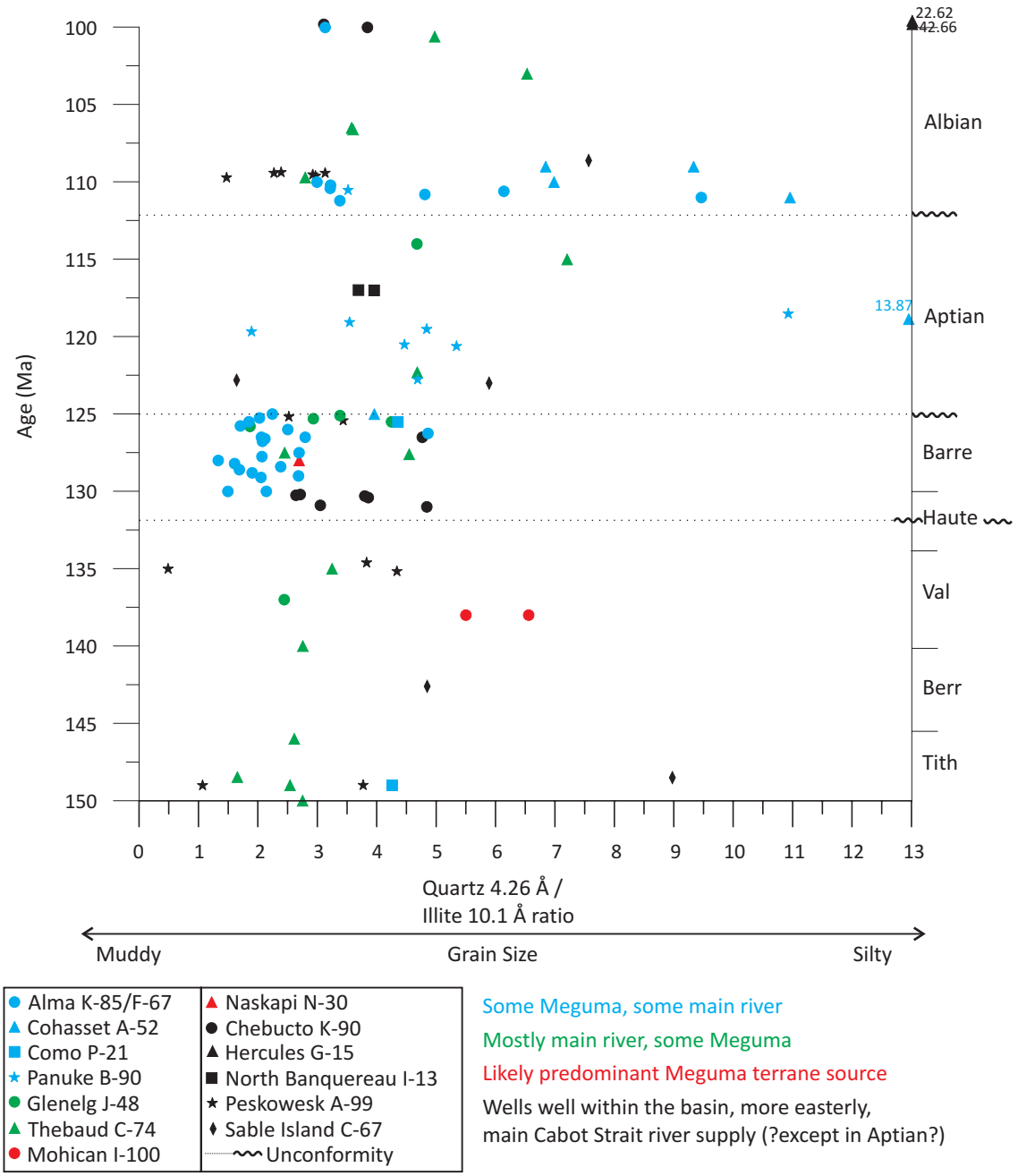

Figure 5.2: Bulk random sidepack samples examined using quartz 4.26 Å over illite 10.1 Å ratio to determine grain size of the clay samples. Colour code based on likely provenance from Pe-Piper & Piper (2012).

Table 5.1: Sidepack sample peak area normalized to zincite standard. Kaolinite/illite and quartz/illite ratios plus Nb and Ta amounts (high values potentially linked to ash content).

Graph #	Geochem	Well	Depth	Formation #	Formation	Age	Age (Ma)	Kaolinite	Kaolinite /Illite	Illite	Quartz /Illite	Quartz	% Quartz	Nb	Ta	Sepiolite	Sepiolite (060)	Colour
	File #		(m)					3.57		10.1		4.26				7.5 Å	1.54 - 1.55 Å	
0.5		Alma F-67	1190.00	1	Banq Fm	CAMPANIAN	72	79.01	0.63	125.09	4.41	551.18	30.38					
1		Alma F-67	1750.00	3	LC (Sable Mb)	ALBIAN	100	344.23	2.29	150.64	3.13	471.52	17.15					
2	14-224	Alma K-85	2449.40	4	LC (Cree Mb)	ALBIAN	110	271.58	1.60	170.25	2.99	509.36	18.73	36.00	2.70			
3	16-57	Alma K-85	2453.85	4	LC (Cree Mb)	ALBIAN	110.2	196.32	0.98	200.62	3.22	646.14	24.31	32.00	2.40			
4	16-58	Alma K-85	2455.00	4	LC (Cree Mb)	ALBIAN	110.4	203.57	0.91	224.31	3.22	721.43	27.26	34.00	2.40			
5	16-59	Alma K-85	2456.40	4	LC (Cree Mb)	ALBIAN	110.6	165.63	2.10	79.05	6.14	485.02	27.40	31.00	2.20			
6	14-225	Alma K-85	2456.50	4	LC (Cree Mb)	ALBIAN	110.8	173.58	1.76	98.42	4.81	473.23	24.71	31.00	2.30			
7	16-60	Alma K-85	2458.15	4	LC (Cree Mb)	ALBIAN	111	199.12	3.50	56.93	9.46	538.43	27.56	34.00	2.40			
8	16-61	Alma K-85	2460.75	4	LC (Cree Mb)	ALBIAN	111.2	226.62	1.41	160.39	3.38	541.61	28.10	35.00	2.50			
9	14-226	Alma K-85	2878.98	6	Miss Upper Mb	Barremian-Aptian	125	440.17	1.41	311.75	2.24	698.94	22.53	27.00	2.10			
10	14-227	Alma K-85	2880.22	6	Miss Upper Mb	Barremian	125.25	532.88	1.41	379.20	2.03	768.06	19.91	28.00	2.20			
11	14-228	Alma K-85	2888.26	6	Miss Upper Mb	Barremian	125.5	451.60	1.14	395.08	1.85	730.39	19.15	25.00	2.20			
12	14-229	Alma K-85	2904.15	6	Miss Upper Mb	Barremian	125.75	347.73	0.95	366.96	1.70	623.37	18.22	28.00	2.10			
13	14-230	Alma K-85	2906.78	6	Miss Upper Mb	Barremian	126	243.50	0.78	312.00	2.50	780.74	26.34	25.00	1.80			
14	14-231	Alma K-85	2912.04	6	Miss Upper Mb	Barremian	126.25	360.45	4.21	85.56	4.86	415.70	16.14	92.00	7.00			
15	16-62	Alma K-85	2919.00	6	Miss Upper Mb	Barremian	126.5	290.81	1.32	220.61	2.80	616.81	23.98	38.00	2.60			
16	16-63	Alma K-85	2919.45	6	Miss Upper Mb	Barremian	126.5	302.02	1.07	281.12	2.06	578.79	20.77	35.00	2.50			
17	14-232	Alma K-85	2920.30	6	Miss Upper Mb	Barremian	126.6	449.85	1.60	281.04	2.12	595.02	18.56	35.00	2.80			
18	16-64	Alma K-85	2931.87	6	Miss Upper Mb	Barremian	126.75	301.68	0.86	350.31	2.07	725.43	23.78	28.00	2.00			
19	16-65	Alma K-85	3038.00	6	Miss Upper Mb	Barremian	127.5	391.50	1.57	249.24	2.69	670.58	22.07	38.00	2.80			
20	14-233	Alma K-85	3039.88	6	Miss Upper Mb	Barremian	127.75	316.37	1.04	305.66	2.07	631.70	23.17	31.00	2.30			
21	16-66	Alma K-85	3044.60	6	Miss Upper Mb	Barremian	128	286.73	0.72	396.54	1.33	528.01	18.19	31.00	2.20			
22	16-67	Alma K-85	3047.90	6	Miss Upper Mb	Barremian	128.2	255.36	0.62	414.79	1.60	665.53	22.08	29.00	2.00			
23	16-68	Alma K-85	3068.15	6	Miss Upper Mb	Barremian	128.4	237.98	0.96	247.36	2.38	589.57	24.98	27.00	2.00			
24	16-69	Alma K-85	3071.80	6	Miss Upper Mb	Barremian	128.6	266.47	0.71	376.32	1.69	635.52	22.93	31.00	2.30			
25	16-70	Alma K-85	3089.05	6	Miss Upper Mb	Barremian	128.8	265.91	0.81	329.25	1.90	626.05	23.11	32.00	2.40			
26	16-71	Alma K-85	3090.45	6	Miss Upper Mb	Hauterivian-Barremian	129	250.23	0.94	266.35	2.68	714.62	26.21	38.00	2.80			
27	16-72	Alma K-85	3093.80	6	Miss Upper Mb	Hauterivian-Barremian	129.1	264.30	0.90	294.07	2.05	602.98	22.67	36.00	2.50			
28	14-234	Alma K-85	3104.10	11	VC Fm	Hauterivian	130	393.36	0.65	603.99	1.50	903.49	22.47	29.00	2.30			
29	16-73	Alma K-85	3104.70	11	VC Fm	Hauterivian	130	302.04	0.73	414.61	2.14	887.82	26.37	32.00	2.30			
29.50	21-339	Chebucto K-90	1690.00	1	Banq Fm	THANETIAN-SELANDIAN	58.6	8.15	0.12	66.67	8.99	599.58	35.47	8.70	0.63			
30	21-340	Chebucto K-90	2220.00	2	LC (Marmora Mb)	CENOMANIAN-ALBIAN	99.8	254.99	1.85	137.80	3.11	428.28	18.04	16.40	1.23			
31	21-341	Chebucto K-90	2470.00	2	LC (Marmora Mb)	ALBIAN	100	503.22	2.59	194.04	3.84	745.36	17.84	16.90	1.19			
31.50	21-342	Chebucto K-90	3780.00	4	LC (Cree Mb)	BARREMIAN	126.5	473.57	13.11	36.12	4.76	172.09	10.65	38.10	3.13			
32	21-344	Chebucto K-90	4370.00	6	Miss Fm	BARREMIAN-HAUTERIVIAN	130.2	190.61	0.95	201.14	2.71	545.22	22.15	22.77	1.79			
33	21-345	Chebucto K-90	4420.00	6	Miss Fm	BARREMIAN-HAUTERIVIAN	130.25	159.50	1.10	145.09	2.64	382.91	23.16	36.60	2.79			
34	21-346	Chebucto K-90	4585.00	6	Miss Fm	BARREMIAN-HAUTERIVIAN	130.3	160.09	1.55	103.39	3.80	392.59	19.60	34.00	2.70			
35	21-347	Chebucto K-90	4750.00	6	Miss Fm	BARREMIAN-HAUTERIVIAN	130.4	171.14	1.66	103.38	3.86	398.77	17.21	40.20	2.78			
36	21-348	Chebucto K-90	5120.00	6	Miss Fm	BARREMIAN-HAUTERIVIAN	130.9	124.20	0.93	133.17	3.05	406.01	17.67	26.77	2.01			
37	21-349	Chebucto K-90	5230.00	6	Miss Fm	HAUTERIVIAN	131	115.66	1.29	89.65	4.84	433.88	21.14	24.34	1.79			
38	21-581	Cohasset A-52	2072.90	4	LC (Cree Mb)	ALBIAN	109	247.72	3.39	73.18	6.84	500.44	15.21	28.10	1.71	49.69		Grey
39	21-582	Cohasset A-52	2074.72	4	LC (Cree Mb)	ALBIAN	109	255.04	4.47	57.01	9.33	531.76	15.76	28.00	1.77	134.74		Grey
40	21-583	Cohasset A-52	2123.52	4	LC (Cree Mb)	ALBIAN	110	204.08	3.20	63.68	6.98	444.41	16.20	33.00	1.98	39.12		Dark-Grey
41	21-585	Cohasset A-52	2138.22	4	LC (Cree Mb)	ALBIAN	111	140.39	2.82	49.77	10.95	544.91	15.44	35.50	2.23	103.97		Brown
42	21-590	Cohasset A-52	2418.75	4	LC (Naskapi Mb)	APTIAN	119	194.84	4.17	46.73	13.87	648.32	18.81	41.30	2.49			Brown
43	21-592	Cohasset A-52	2597.05	7	Miss Upper Mb	APTIAN-BARREMIAN	125	311.98	3.19	97.92	3.96	387.45	12.73	22.10	1.35			Light Grey
44	21-594	Como P-21	2188.75	7	Miss Upper Mb	APTIAN-BARREMIAN	125.5	281.43	2.53	111.38	4.35	484.80	13.32	32.10	1.96	42.65	14.58	Mid-Grey

45	21-597	Como P-21	3065.72	8	Miss Middle Mb	TITHONIAN	149	29.22	0.17	168.04	4.26	715.56	19.51	40.30	2.43	20.21	8.48	Grey
45.50		Glenelg J-48	1405.00	1	Banq Fm	LUTETIAN	44.8	61.95	0.82	75.29	4.00	301.09	21.53					
46		Glenelg J-48	3250.00	5	LC (Naskapi Mb)	APTIAN	114	244.79	3.44	71.16	4.67	332.59	17.05					
47		Glenelg J-48	3645.00	7	Miss Upper Mb	APTIAN	125.1	364.73	2.12	171.65	3.38	580.11	18.05					
48		Glenelg J-48	3860.00	7	Miss Upper Mb	APTIAN	125.3	307.36	1.60	192.50	2.93	564.21	17.55					
49		Glenelg J-48	4030.00	7	Miss Upper Mb	APTIAN-BARREMIAN	125.5	268.52	1.67	160.67	4.25	682.35	25.84					
50		Glenelg J-48	4385.00	8	Miss Middle Mb	APTIAN-BARREMIAN	125.8	256.65	1.30	197.68	1.86	368.60	14.55					
51		Glenelg J-48	4740.00	11	VC Fm	VALANGINIAN	137	248.69	1.35	184.71	2.44	450.98	15.53					
52		Hercules G-15	371.86	2	LC	CENOMANIAN-ALBIAN	99.6	184.79	4.60	40.18	22.62	908.94	51.24					
53		Hercules G-15	646.18	4	LC	CENOMANIAN-ALBIAN	99.65	5.26	0.30	17.73	42.66	756.52	36.29					
54		Mohican I-100	2533.24	8	Miss Middle Mb	VALANGINIAN	138	50.68	0.78	65.04	6.55	426.29	15.63			9.37		Grey
55		Mohican I-100	2539.94	8	Miss Middle Mb	VALANGINIAN	138	104.25	1.60	65.19	5.50	358.40	11.55				10.77	Grey
56		Mohican I-100	2541.23	8	Miss Middle Mb	VALANGINIAN	138	9.76	4.50	0.00	50.00	174.65	5.19			17.39		Dark-grey
57	14-422	Naskapi N-30 2011	1469.10	7	Miss Upper Mb	BARREMIAN	128	755.78	2.82	268.25	2.69	721.45	10.93	10.00	1.20			Grey
58	21-604	North Banquereau I-13	3248.80	5	LC (Naskapi Mb)	APTIAN	117	273.30	3.06	89.33	3.68	328.94	13.41	23.40	1.49	13.77	4.37	Grey-red
59	21-605	North Banquereau I-13	3249.65	5	LC (Naskapi Mb)	APTIAN	117	307.15	3.85	79.76	3.95	315.31	12.31	22.20	1.37	92.68	3.15	Red
60	21-541	Panuke B-90	2097.27	4	LC (Cree Mb)	ALBIAN	110.5	155.90	1.40	111.71	3.51	392.61	13.54	40.00	2.25	45.95		Brown
61	21-543	Panuke B-90	2235.37	5	LC (Naskapi Mb)	APTIAN	118.5	102.81	1.76	58.38	10.92	637.56	20.37	33.10	2.06	43.35		Brown-Grey
62	21-545	Panuke B-90	2241.57	5	LC (Naskapi Mb)	APTIAN	119.1	141.64	0.89	159.77	3.54	565.79	16.57	26.30	1.54	65.98	14.20	Green
63	21-546	Panuke B-90	2245.78	5	LC (Naskapi Mb)	APTIAN	119.5	152.99	1.24	123.43	4.83	596.71	16.39	24.80	1.45	77.57		Green
64	21-547	Panuke B-90	2247.20	5	LC (Naskapi Mb)	APTIAN	119.7	172.70	0.88	195.58	1.89	369.75	10.91	22.80	1.36		7.44	Red-Brown
65	21-548	Panuke B-90	2255.49	5	LC (Naskapi Mb)	APTIAN	120.5	184.40	1.70	108.66	4.46	484.81	14.24	25.30	1.50	113.20		Light-Grey
66	21-549	Panuke B-90	2256.56	5	LC (Naskapi Mb)	APTIAN	120.6	128.93	1.40	92.11	5.34	491.75	15.69	24.80	1.46	86.00		Red-Brown
67	21-552	Panuke B-90	2278.21	5	LC (Naskapi Mb)	APTIAN	122.8	312.60	2.76	113.39	4.68	531.14	13.69	24.10	1.44			Grey-Green
68	14-535	Peskowesk A-99	2209.25	4	LC (Cree Mb)	ALBIAN	109.4	909.83	2.05	443.19	2.39	1058.50	16.43	32.00	2.40			
69	14-536	Peskowesk A-99	2213.57	4	LC (Cree Mb)	ALBIAN	109.4	247.52	1.47	168.49	2.27	382.43	17.48	40.00	2.70			
70	14-537	Peskowesk A-99	2215.78	4	LC (Cree Mb)	ALBIAN	109.4	254.66	1.91	133.37	3.13	417.00	18.26	38.00	2.20			
71	14-538	Peskowesk A-99	2219.03	4	LC (Cree Mb)	ALBIAN	109.5	248.64	1.58	157.63	2.92	460.51	19.51	36.00	1.90			
72	14-539	Peskowesk A-99	2221.69	4	LC (Cree Mb)	ALBIAN	109.6	267.93	1.79	150.02	2.96	444.38	19.80	37.00	1.90			
73		Peskowesk A-99	2228.42	4	LC (Cree Mb)	ALBIAN	109.7	123.32	0.62	199.70	1.47	293.25	13.00					
74	14-541	Peskowesk A-99	2479.35	7	Miss Upper Mb	APTIAN-BARREMIAN	125.2	271.38	1.57	173.12	2.52	435.82	20.01	32.00	1.80			
75	14-542	Peskowesk A-99	2488.85	7	Miss Upper Mb	APTIAN-BARREMIAN	125.4	203.08	1.61	126.19	3.43	433.16	22.02	37.00	2.10			
76	14-543	Peskowesk A-99	2492.62	7	Miss Upper Mb	APTIAN-BARREMIAN	125.5	283.59	4.29	66.15	15.64	1034.25	35.33	49.00	2.70			
77	14-544	Peskowesk A-99	2927.36	8	Miss Middle Mb	HAUTERIVIAN	134.6	107.53	0.62	172.12	3.83	658.78	24.53	42.00	2.70			
78	14-545	Peskowesk A-99	2940.90	8	Miss Middle Mb	HAUTERIVIAN	135	381.42	0.65	588.32	0.48	284.92	12.07	37.00	2.40			
79	14-546	Peskowesk A-99	2947.43	8	Miss Middle Mb	HAUTERIVIAN	135.2	159.55	1.12	142.95	4.33	619.64	26.87	56.00	3.60			
79.25		Peskowesk A-99	3806.51	10	Mic Mac Fm	TITHONIAN	149	5.91	0.05	108.30	1.07	116.06	4.16					
79.75	21-266	Peskowesk A-99	3812.64	10	Mic Mac Fm	TITHONIAN	149	15.40	0.21	73.26	3.77	276.21	6.07	20.90	1.39			
80	21-599	Sable Island C-67	2474.18	4	LC (Cree Mb)	ALBIAN	108.6	154.84	2.35	66.02	7.56	499.17	11.49	34.50	2.17	134.28	16.32	Light-black
81	21-600	Sable Island C-67	2830.45	5	LC (Naskapi Mb)	APTIAN	122.8	210.78	0.98	215.89	1.64	354.09	10.98	19.90	1.29	43.86	9.76	Red
82	21-601	Sable Island C-67	2835.42	5	LC (Naskapi Mb)	APTIAN	123	222.02	2.45	90.44	5.88	531.60	15.05	37.00	2.15	111.98		Brown-Grey
82.25	21-602	Sable Island C-67	3373.45	8	Miss Middle Mb	BERRIASIAN	142.6	108.37	1.05	102.98	4.84	498.89	14.63	49.00	3.08	38.74		
82.75	21-603	Sable Island C-67	4089.87	9	Miss Lower Mb	BAJOCIAN	148.5	60.02	0.93	64.37	8.97	577.33	19.76	78.60	5.35	27.57	11.56	
83	21-350	Thebaud C-74	1825.00	3	LC (Sable Mb)	ALBIAN	100.6	254.98	2.83	89.98	4.97	447.34	19.35	16.50	1.22			
84	21-351	Thebaud C-74	1990.00	4	LC (Cree Mb)	ALBIAN	103	428.20	2.86	149.57	6.53	976.23	24.82	19.50	1.44			
85	21-352	Thebaud C-74	2200.00	4	LC (Cree Mb)	ALBIAN	106.5	531.56	2.82	188.65	3.57	674.23	18.38	24.80	1.79			
86	21-353	Thebaud C-74	2205.00	4	LC (Cree Mb)	ALBIAN	106.6	485.29	2.69	180.29	3.60	648.52	16.46	24.40	1.79			
87	21-354	Thebaud C-74	2390.00	4	LC (Cree Mb)	ALBIAN	109.7	448.17	1.85	242.81	2.80	678.72	17.25	23.80	1.74			
88	21-355	Thebaud C-74	2560.00	5	LC (Naskapi Mb)	ALBIAN	115	215.27	3.12	68.93	7.20	496.28	22.61	34.40	3.03			
89	21-356	Thebaud C-74	2630.00	5	LC (Naskapi Mb)	ALBIAN	122.3	416.32	2.72	153.21	4.68	716.96	20.24	31.80	2.28			
90	21-357	Thebaud C-74	2775.00	7	Miss Upper Mb	BARREMIAN	127.5	518.10	1.70	305.62	2.45	748.04	17.90	24.30	1.72			
91	21-358	Thebaud C-74	2780.00	7	Miss Upper Mb	BARREMIAN	127.6	290.85	1.49	195.14	4.54	886.60	26.61	28.50	2.04			

92	21-359	Thebaud C-74	3075.00	8	Miss Middle Mb	VALANGINIAN-HAUTERIVIAN	135	350.66	1.65	212.47	3.25	689.85	20.42	30.40	2.18			
93	21-360	Thebaud C-74	3615.00	8	Miss Middle Mb	TITHONIAN-BERRIASIAN	140	207.27	0.92	225.29	2.75	620.48	23.22	47.30	3.50			
94	21-361	Thebaud C-74	3780.00	9	Miss Lower Mb	TITHONIAN	146	236.11	1.12	210.82	2.61	550.47	18.61	42.30	3.05			
95	21-362	Thebaud C-74	4020.00	9	Miss Lower Mb	TITHONIAN	148.5	332.77	1.08	308.64	1.66	512.96	18.47	47.60	3.55			
96	21-363	Thebaud C-74	4105.00	9	Miss Lower Mb	TITHONIAN	149	261.27	1.37	190.88	2.54	484.64	20.37	45.10	3.18			Dark-grey
97	21-364	Thebaud C-74	4335.00	9	Miss Lower Mb	TITHONIAN	150	319.71	1.73	184.38	2.75	507.03	14.87	47.20	2.78			Grey-red

a trend of coarsening of the samples starting at the Mid Hauterivian unconformity through to the Early Aptian, then declining through until the Aptian-Albian boundary (top of Naskapi Member), where it rapidly coarsens. Through the Early Cretaceous there were several main rivers flowing into the Scotian Basin that brought sediment from the Canadian Shield in Labrador, and the Appalachian orogen in New Brunswick, Nova Scotia and Newfoundland (Pe-Piper & Piper, 2012) (Figure 5.3). The Naskapi shale member onlaps onto a regional unconformity on the Banquereau Platform and Orpheus Graben and is found to thin out towards the Orpheus Graben (Piper et al., 2011). Regional seismic reflection profiles show Barremian tectonic uplift and tilting of the Banquereau Platform (Piper et al., 2011). Therefore, it has been proposed that starting in the Late Hauterivian through the Aptian, there was tectonism and tilting of the Scotian Shelf along the Cobequid-Chedabucto fault, which, in the Aptian, cut off the major river supply from the Appalachian terranes and diverted it to the Bay of Fundy (Piper et al., 2011) (Figure 5.4). Direct river flow was re-established in the Cree Member (Albian), hence the quartz abundance, in a general manner, is related to proximal fluvial supply.

Bulk random sidepack analysis of the 060 peak of Mg-chlorite (1.538-1.549 Å) shows a high overall abundance (Figure 5.5), with a similar stratigraphic variation to the quartz/illite ratio (Figure 5.2). Kaolinite also shows a similar stratigraphic distribution (Figure 5.6). Vermiculite, illite, 2:1 Al-rich clays, and 2:1 Fe-rich clays (Figures 5.7, 5.8, 5.9, & 5.10) also show a gradual increase through the Lower Cretaceous, low values in the Aptian and higher values again in the Albian. Fe-chlorite, in contrast, shows no

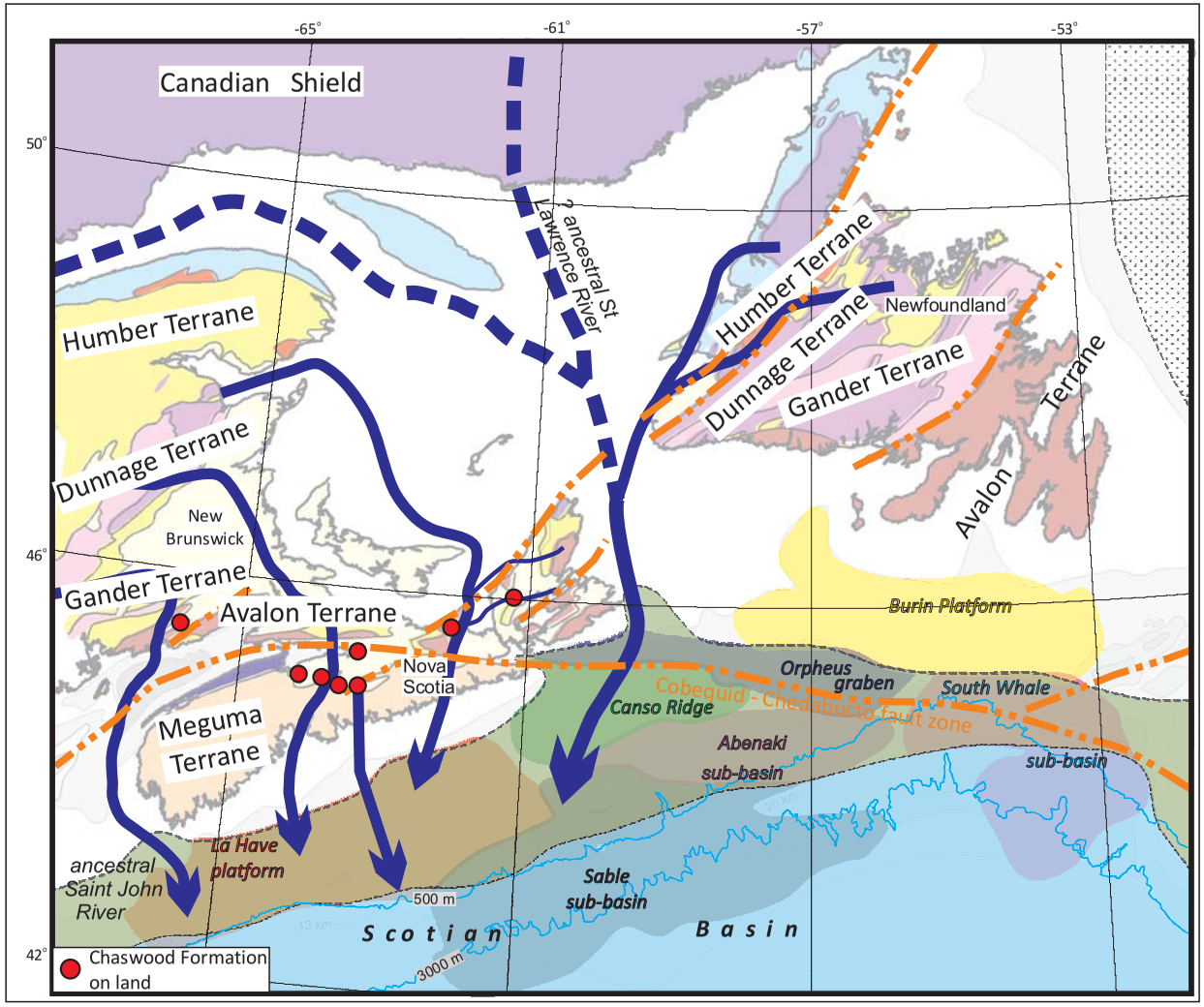

Figure 5.3: Map showing Paleo-rivers, basin locations in the Scotian Basin and sediment sources: The Canadian Shield and Appalachian orogen lying north of the Scotian Basin. Also showing the Lower Cretaceous Chaswood Formation onshore. Modified from Tsikouras et al. (2011).

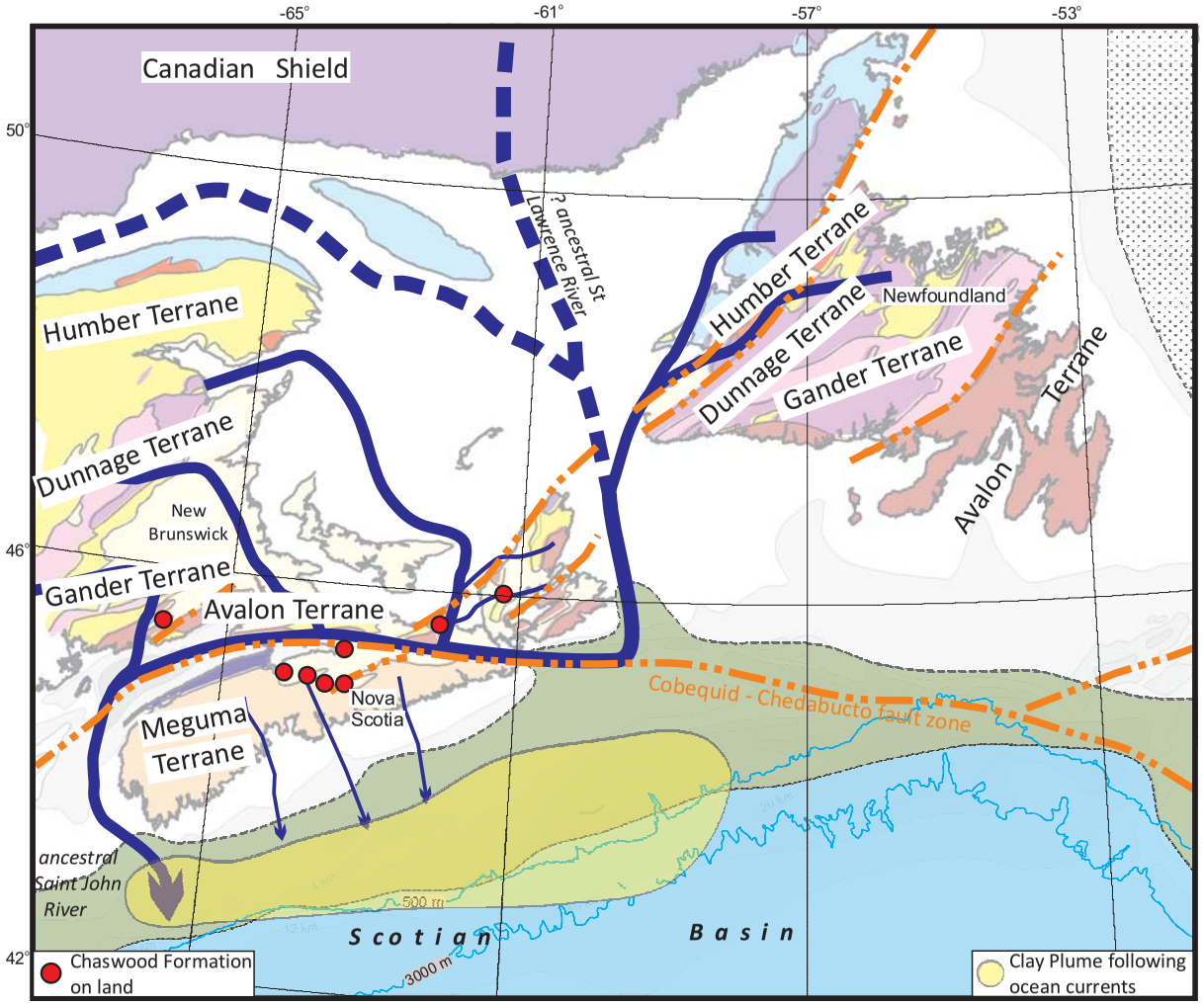

Figure 5.4: Map showing reconstructed Paleo-rivers post Scotian Shelf tilting. Re-distribution of rivers altered sediment supply during the Late Hauterivian-Early Albian. During this time the primary source of sediment was the Meguma terrane. Clay Plume follows ocean currents. Modified from Tsikouras et al. (2011) based on concepts in Piper et al. (2011)

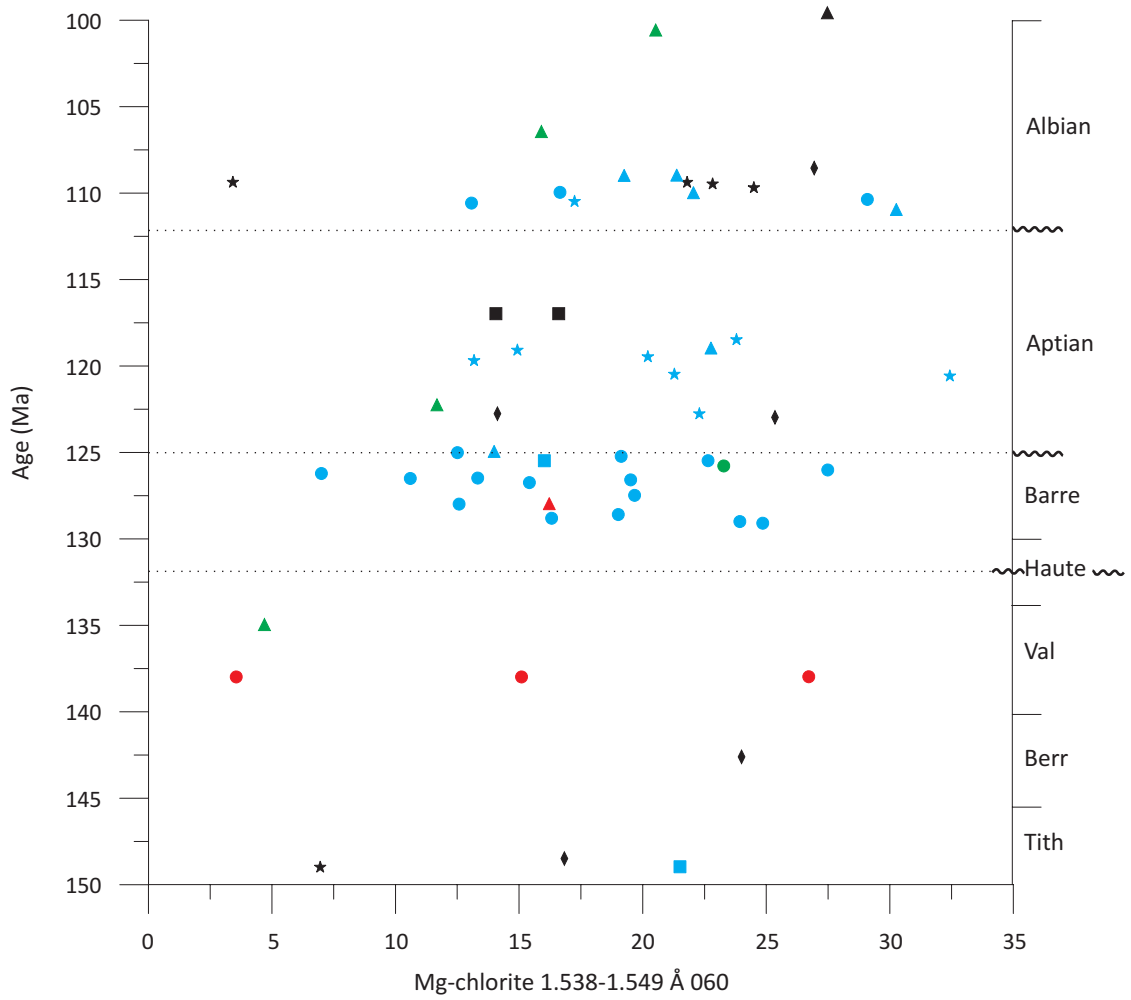

● Alma K-85/F-67	▲ Naskapi N-30
▲ Cohasset A-52	● Chebucto K-90
■ Como P-21	▲ Hercules G-15
★ Panuke B-90	■ North Banquereau I-13
● Glenelg J-48	★ Peskowesk A-99
▲ Thebaud C-74	♦ Sable Island C-67
● Mohican I-100	~~~ Unconformity

Some Meguma, some main river

Mostly main river, some Meguma

Likely predominant Meguma terrane source

Wells well within the basin, more easterly, main Cabot Strait river supply (?except in Aptian?)

Figure 5.5: Bulk random samples normalized to the standard showing Mg-chlorite 1.538-1.549 Å (060) vs Age. Colour code based on likely provenance from Pe-Piper & Piper (2012).

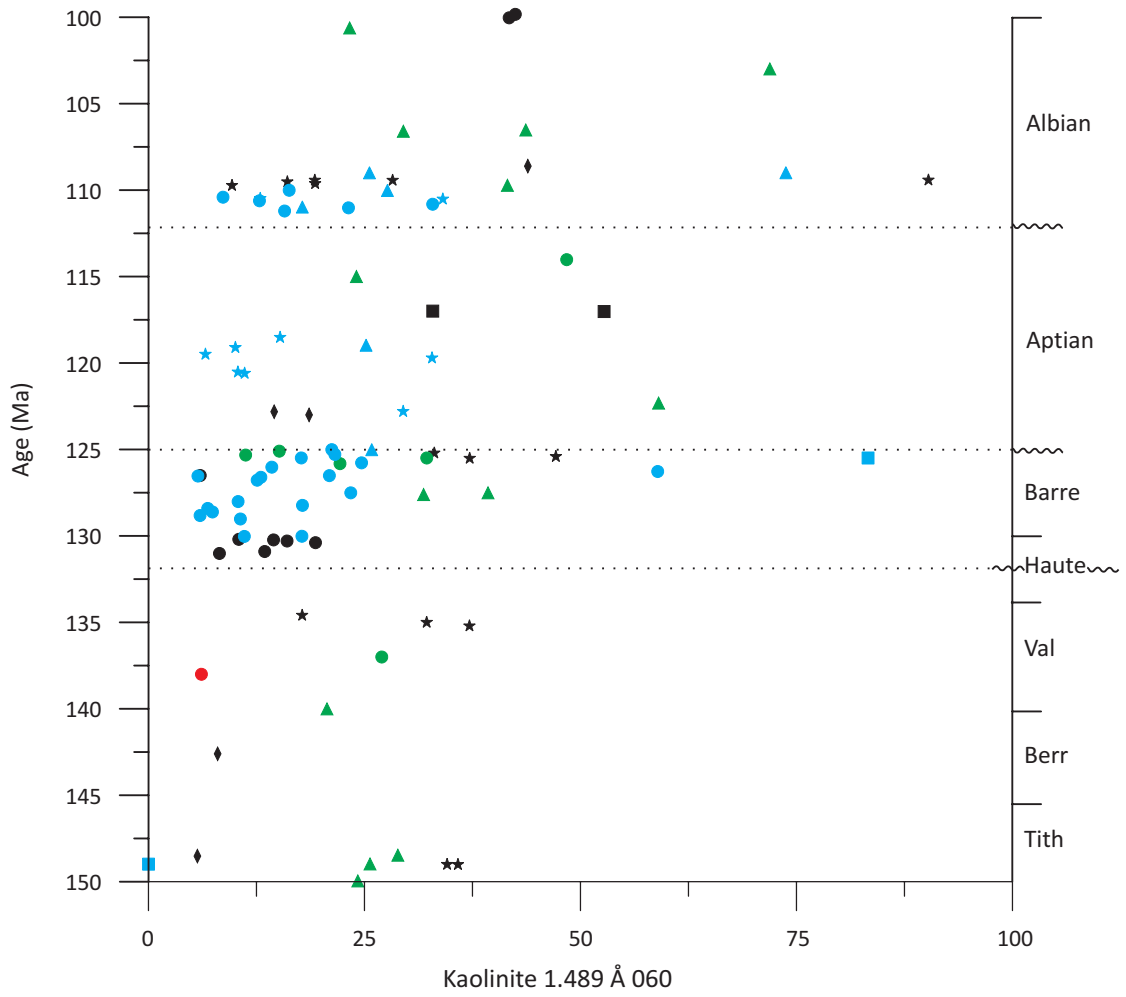

Alma K-85/F-67	Naskapi N-30
Cohasset A-52	Chebucto K-90
Como P-21	Hercules G-15
Panuke B-90	North Banquereau I-13
Glenelg J-48	Peskowesk A-99
Thebaud C-74	Sable Island C-67
Mohican I-100	Unconformity

Some Meguma, some main river

Mostly main river, some Meguma

Likely predominant Meguma terrane source

Wells well within the basin, more easterly, main Cabot Strait river supply (?except in Aptian?)

Figure 5.6: Bulk random samples normalized to the standard showing Kaolinite 1.489 Å 060 vs Age. Colour code based on likely provenance from Pe-Piper & Piper (2012).

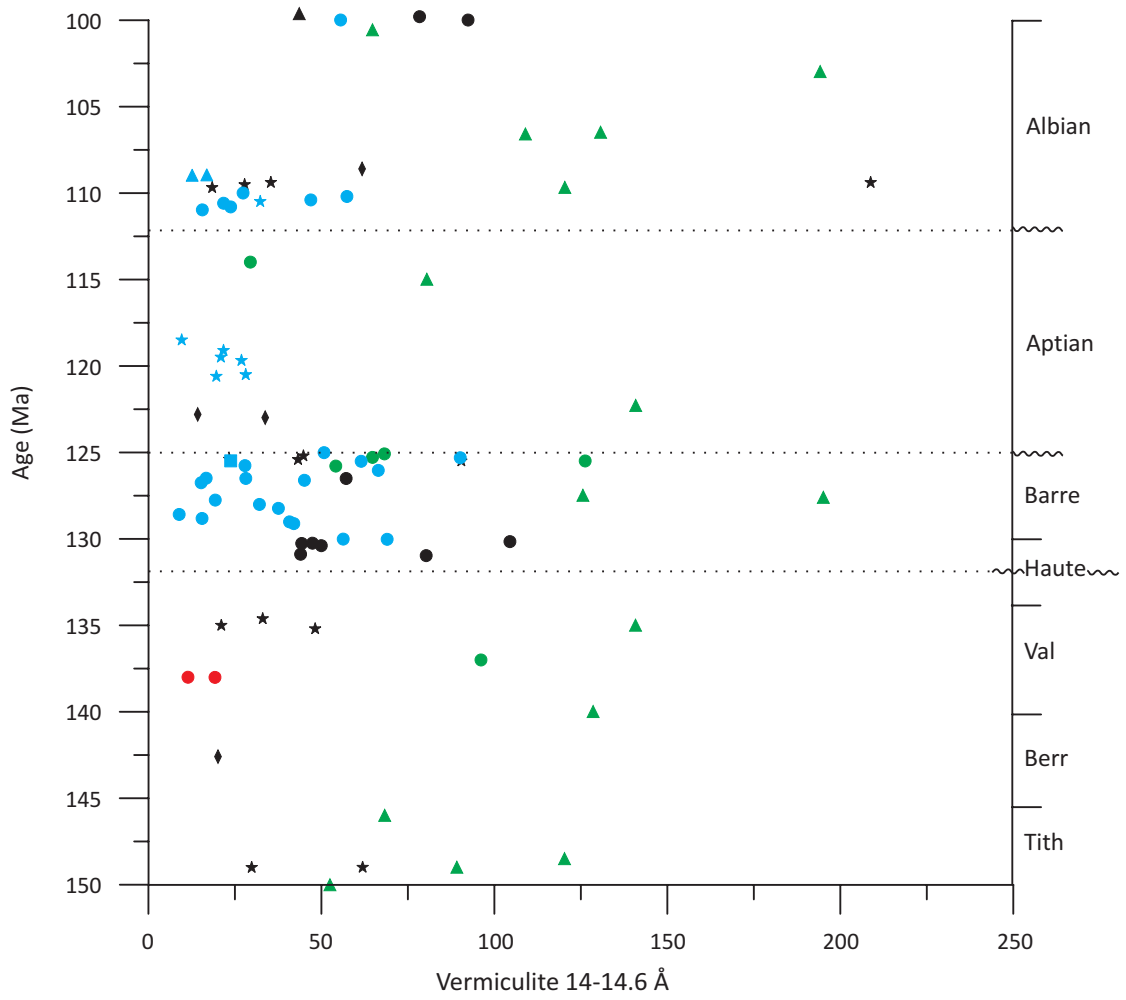

Alma K-85/F-67	Naskapi N-30
Cohasset A-52	Chebucto K-90
Como P-21	Hercules G-15
Panuke B-90	North Banquereau I-13
Glenelg J-48	Peskowesk A-99
Thebaud C-74	Sable Island C-67
Mohican I-100	Unconformity

Some Meguma, some main river

Mostly main river, some Meguma

Likely predominant Meguma terrane source

Wells well within the basin, more easterly, main Cabot Strait river supply (?except in Aptian?)

Figure 5.7: Bulk random samples normalized to the standard showing Vermiculite 14-14.6 Å vs Age. Colour code based on likely provenance from Pe-Piper & Piper (2012).

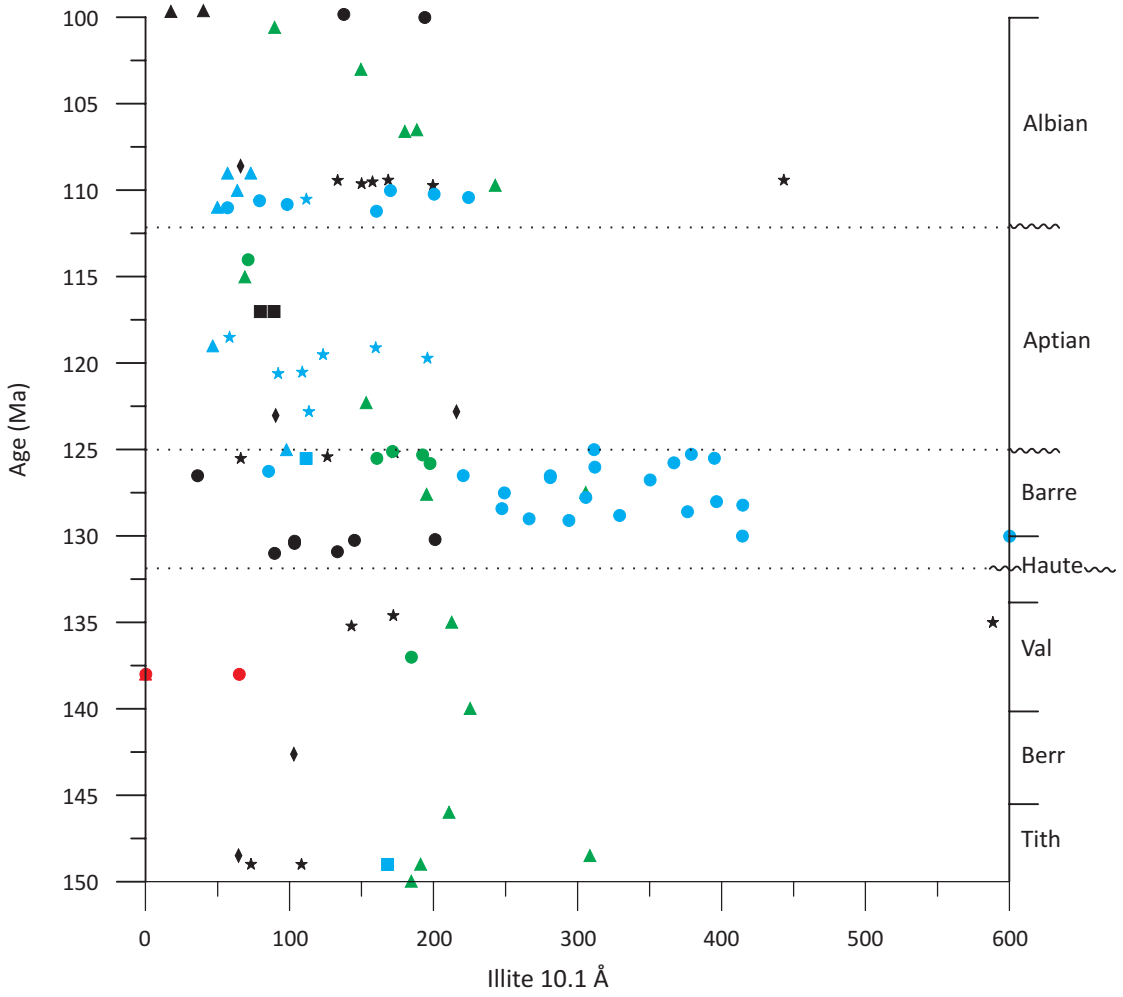

● Alma K-85/F-67	▲ Naskapi N-30
▲ Cohasset A-52	● Chebucto K-90
■ Como P-21	▲ Hercules G-15
★ Panuke B-90	■ North Banquereau I-13
● Glenelg J-48	★ Peskowesk A-99
▲ Thebaud C-74	♦ Sable Island C-67
● Mohican I-100	Unconformity

Some Meguma, some main river

Mostly main river, some Meguma

Likely predominant Meguma terrane source

Wells well within the basin, more easterly, main Cabot Strait river supply (?except in Aptian?)

Figure 5.8: Bulk random samples normalized to the standard showing Illite 10.1 Å vs Age. Colour code based on likely provenance from Pe-Piper & Piper (2012).

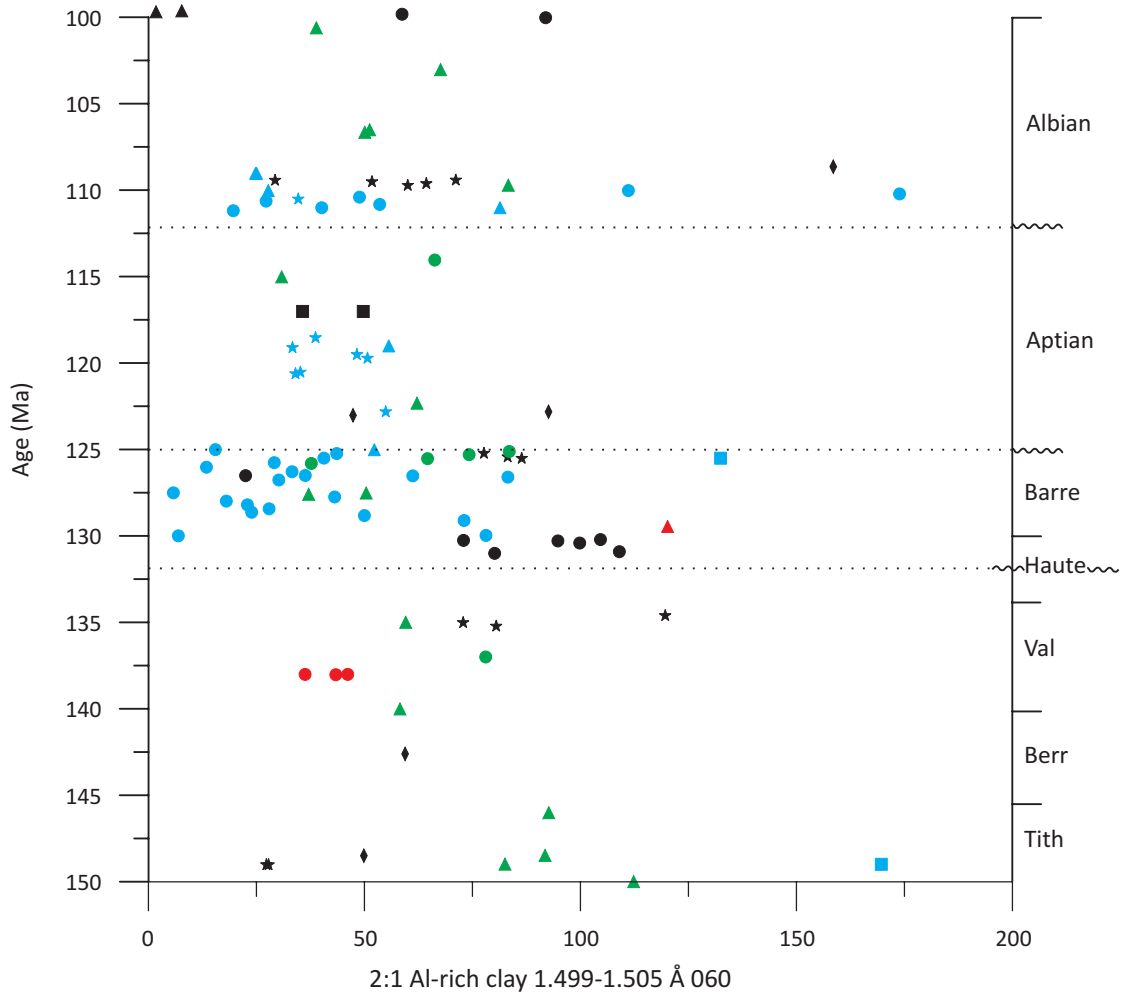

Alma K-85/F-67	Naskapi N-30
Cohasset A-52	Chebucto K-90
Como P-21	Hercules G-15
Panuke B-90	North Banquereau I-13
Glenelg J-48	Peskowesk A-99
Thebaud C-74	Sable Island C-67
Mohican I-100	Unconformity

Some Meguma, some main river

Mostly main river, some Meguma

Likely predominant Meguma terrane source

Wells well within the basin, more easterly, main Cabot Strait river supply (?except in Aptian?)

Figure 5.9: Bulk random samples normalized to the standard showing 2:1 Al-rich clay 1.499-1.505 Å 060 vs Age. Colour code based on likely provenance from Pe-Piper & Piper (2012).

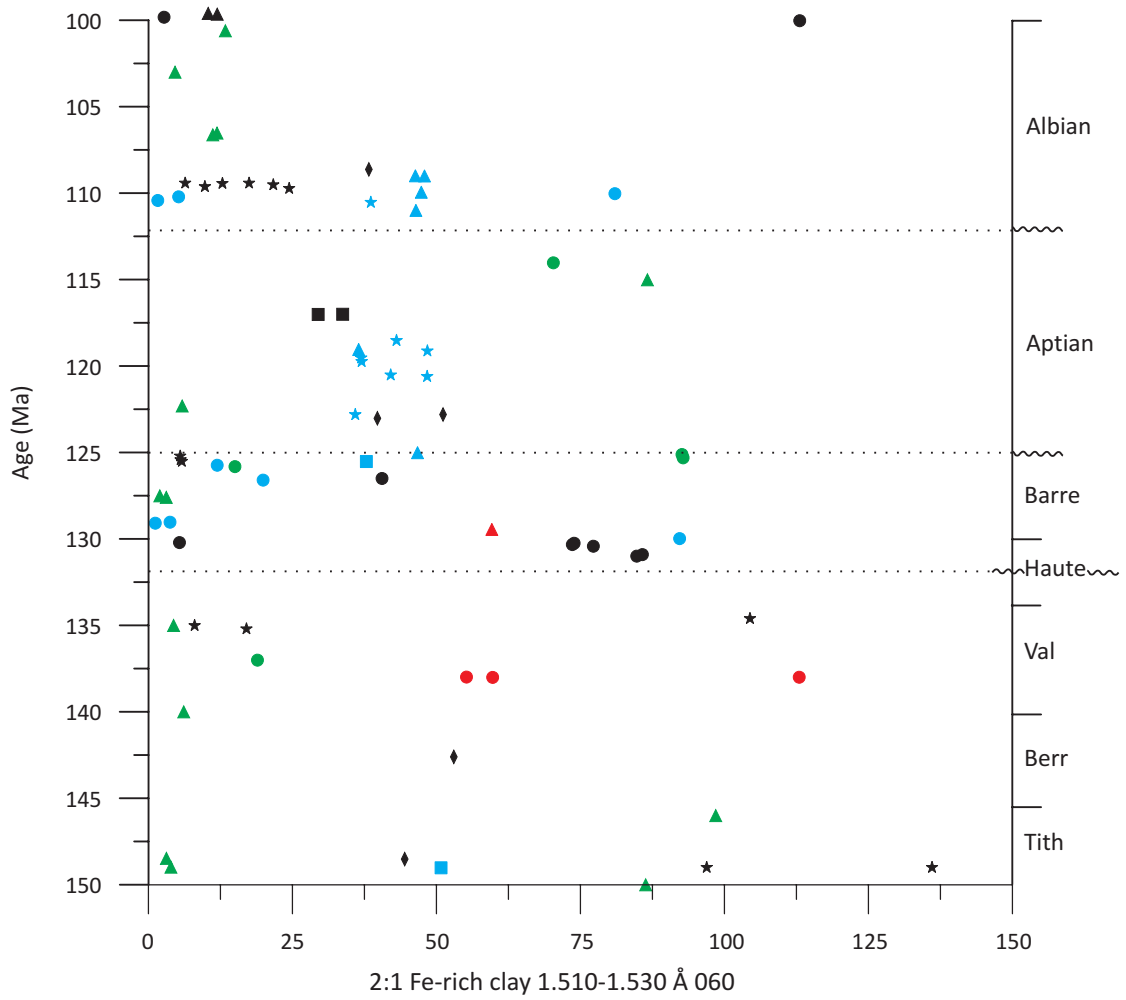

Alma K-85/F-67	Naskapi N-30
Cohasset A-52	Chebucto K-90
Como P-21	Hercules G-15
Panuke B-90	North Banquereau I-13
Glenelg J-48	Peskowesk A-99
Thebaud C-74	Sable Island C-67
Mohican I-100	Unconformity

Some Meguma, some main river

Mostly main river, some Meguma

Likely predominant Meguma terrane source

Wells well within the basin, more easterly, main Cabot Strait river supply (?except in Aptian?)

Figure 5.10: Bulk random samples normalized to the standard showing 2:1 Fe-rich clay 1.510-1.530 Å 060 vs Age. Colour code based on likely provenance from Pe-Piper & Piper (2012).

systematic stratigraphic variation (Figure 5.11). This suggests that vermiculite, illite, 2:1 Al-rich clays and 2:1 Fe-rich clays are predominantly detrital, whereas Fe-chlorite is diagenetic. Diagenetic formation of Fe-rich clay and berthierine are pre-cursors with alter to Fe-chlorite below 2 km (Pe-Piper & Weir-Murphy, 1998; Okwese et al., 2011).

5.4 VARIATIONS WITH DEPTH AND TEMPERATURE

Geothermal conditions and depth of burial are a major control on alteration of clay minerals in sedimentary basins (Merriman, 2005). Diagenesis starts at the seafloor and continues with burial and is influenced by fluxes of fluids originating from compacting clays.

Smectite is not found below 3.7 km (Figure 4.4) based on both <2 µm and sidepack sample analysis. In this study smectite disappears well before the onset of the overpressure zone and has contradicted the suggestion of Wadden (2003) that smectite disappears at the onset of the overpressure zone. However, the findings of Wadden (2003) that smectite decreases down well is confirmed by this study. This study shows that there is no correlation between smectite and overpressure and that depth is a better predictor of smectite abundance. It is well established that smectite alters to illite with burial (Hower et al., 1976; Boles and Franks, 1979; Awwiller, 1993).

Illite abundance based on the 10 Å illite peak in the sidepack samples mildly increases until approximately 2.5 km, and stabilizes until around 4.4 km and then decreases, except for apparently anomalous values around 3 km in Alma K-85 (Figure 4.30). This is contrary to the common understanding that illitization of smectite and

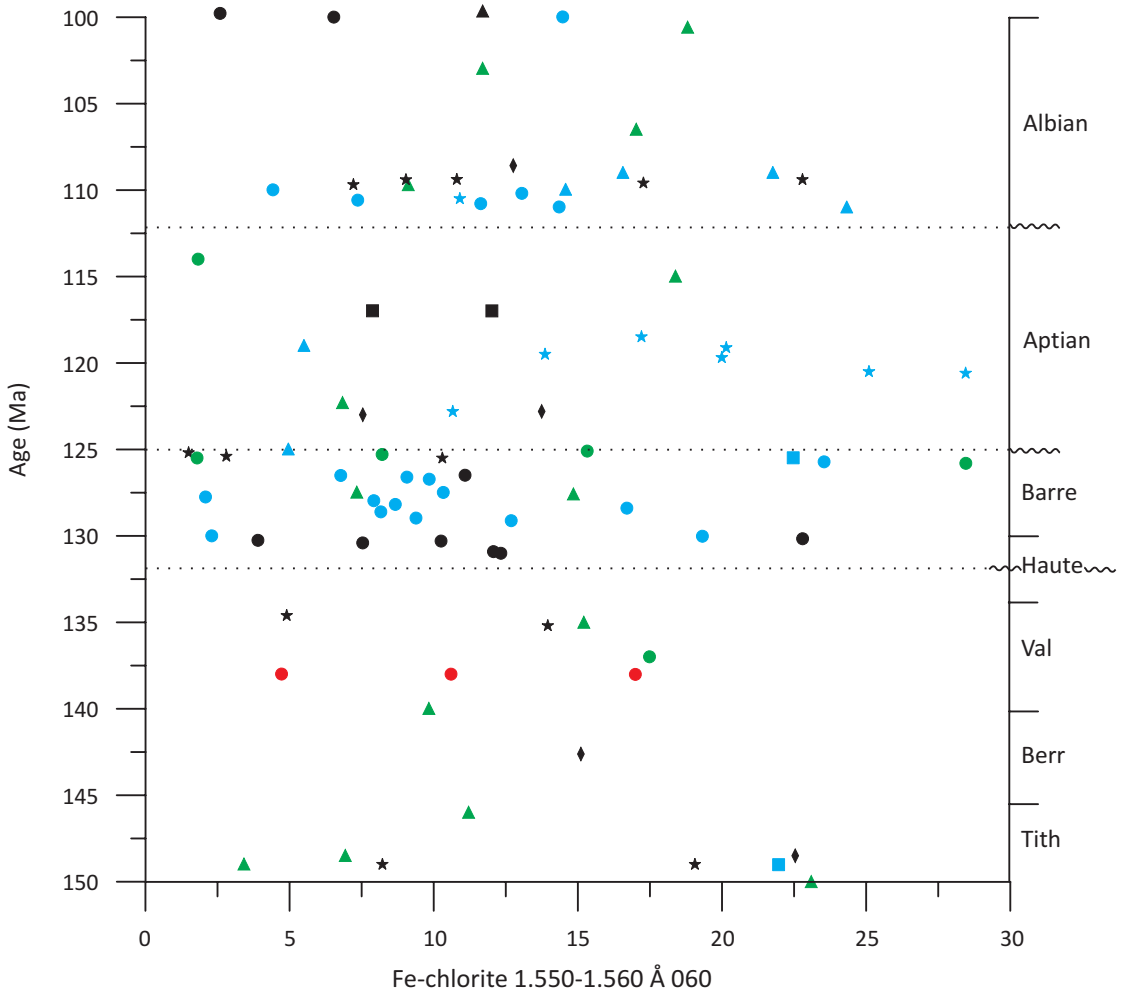

Alma K-85/F-67	Naskapi N-30
Cohasset A-52	Chebucto K-90
Como P-21	Hercules G-15
Panuke B-90	North Banquereau I-13
Glenelg J-48	Peskowesk A-99
Thebaud C-74	Sable Island C-67
Mohican I-100	Unconformity

Some Meguma, some main river

Mostly main river, some Meguma

Likely predominant Meguma terrane source

Wells well within the basin, more easterly, main Cabot Strait river supply (?except in Aptian?)

Figure 5.11: Bulk random samples normalized to the standard showing Fe-chlorite 1.550-1.560 Å 060 vs Age. Colour code based on likely provenance from Pe-Piper & Piper (2012).

kaolinite occurs with depth (Kulbicki & Millot, 1961; Cassou et al., 1977). The apparent anomalous illite values at Alma K-85 are not confirmed by the <2 µm sample analyses, nor the 2:1 Al-rich clays (Figure 4.27), and is probably a result of severe interference with mixed layer clays. Illite diagenesis in the Jeanne d'Arc Basin is enhanced by the passage of deep K-bearing fluids (Abid & Hesse, 2007). The samples from the Scotian Basin that show generally high K also show higher quantities of illite, whereas low K samples correspond to low illite (Table 4.6). However, there are samples with high K that have low quantities of illite. The samples with high K and low illite are typically the samples with still fresh detrital K-feldspar, which may explain the difference.

The chlorite in the bulk random sidepack samples at the 14.5-13.7 Å peak, corresponding principally to Mg-chlorite, tends to disappear with depth (Figure 4.25). The Fe-chlorite sidepack peak of 1.550-1.560 Å (060) shows no significant change with burial depth (Figure 4.16). However, there is a concentration of Fe-chlorite that matches the anomalous illite abundance around 3 km in the Alma K-85 well, which suggests that they may have a similar source. The bulk random sidepack peaks for Mg-chlorite at 1.538-1.549 Å (060) show that abundant Mg-chlorite occurs mostly between 2-3.2 km burial depth (Figure 4.17), principally in the Cree Member of the Logan Canyon Formation and Upper Member of the Missisauga Formation (Figure 5.5).

The Upper Missisauga Formation has been buried deeper in Glenelg J-48 and Chebucto K-90 when compared with Thebaud C-74. Comparison of the quantity of vermiculite in the sidepack samples from each of these wells shows that vermiculite disappears with burial (Figure 4.19). It is well understood that with burial, vermiculite

converts to corrensite and then eventually into chlorite (Potter, Maynard & Pryor, 1980). This appears inconsistent with the decrease of chlorite with depth seen at the 14.5-13.7 Å peak.

Macroscopic vermiculite is tri-octahedral and typically forms from alteration of trioctahedral micas and chlorites and fine grained vermiculite can be either tri-octahedral or di-octahedral (Brindley & Brown, 1980). Di-octahedral vermiculite can be identified with a 060 d-spacing between 1.49 and 1.50 (overlapping with other 2:1 Al-rich clays) and tri-octahedral vermiculite can be identified with a 060 d-spacing between 1.51 and 1.53 Å (Brindley & Brown, 1980). In a few samples, 060 vermiculite peaks were found in the 1.51 to 1.53 Å range, suggesting that the vermiculite found in these samples is tri-octahedral.

The sidepack samples show that the 2:1 Al rich clays (includes Smectite + illite-smectite + illite+ Al-rich mica) (Figure 4.27) and 2:1 Fe-rich clays (includes nontronite + glauconite + Fe-rich illite + celadonite) (Figure 4.28) increase in abundance with depth. The abundance of Fe-rich clays shows considerable scatter.

Based on the 3.57 Å kaolinite peak in the sidepack samples, kaolinite abundance begins to decrease with depth at approximately 3 km (Figure 4.29). Similar observations have been made elsewhere by other authors (Kulbicki & Millot, 1961; Burton et al., 1987). Kaolinite has been found to alter to illite and chlorite with depth (Kulbicki & Millot, 1961; Burton et al., 1987). Kaolinite shows no pattern of decreasing markedly at overpressure zones, which contradicts the suggestion of Wadden (2003). There are only four wells with samples that are below the overpressure zones; Chebucto K-90

(OP=4157 m), Glenelg J-48 (OP=3976 m), South Desbarres O-76 (OP=4546 m), and Thebaud C-74 (OP=3879 m) (Appendix 2).

Understanding if any of the wells have experienced any temperature fluctuation may aid in characterizing the variability of diagenesis throughout the Scotian Basin. Fluid inclusion studies from silica and carbonate cements in the Lower Cretaceous sandstones in the Scotian Basin have shown higher than average homogenization temperatures in Thebaud, Glenelg and Chebucto for the Upper Missisauga Formation (Karim et al., 2011; Karim et al., 2012). These wells are referred to as "hot" wells in this study.

No connection was seen between the abundance of smectite from the sidepack samples and the temperature of the wells (Figure 4.4). Based on the sidepack samples, there is little correlation between illite and temperature (Figure 4.30). The hotter wells (Thebaud, Glenelg and Chebucto) have slightly higher amounts of illite. Other studies have found that temperature has little to do with the diagenesis of illite and smectite and that the evolution of these minerals is based more on time, fluid transfer and burial depth (Claret et al., 2004; Abid & Hesse, 2007).

Based on the 14.5-13.7 Å bulk random sidepack peaks, chlorite (predominantly Mg-chlorite) is found to be more abundant in the "hotter" wells than in the "cooler" wells (Figure 5.12). This is not confirmed by the 1.538 - 1.549 Å Mg-chlorite bulk random sidepack peaks (Figure 5.13) and 3.54 Å Fe-chlorite bulk random sidepack peaks (Figure 5.14), which show that both are abundant between 2-3 km, however Fe-chlorite is more abundant than Mg-chlorite below these depths.

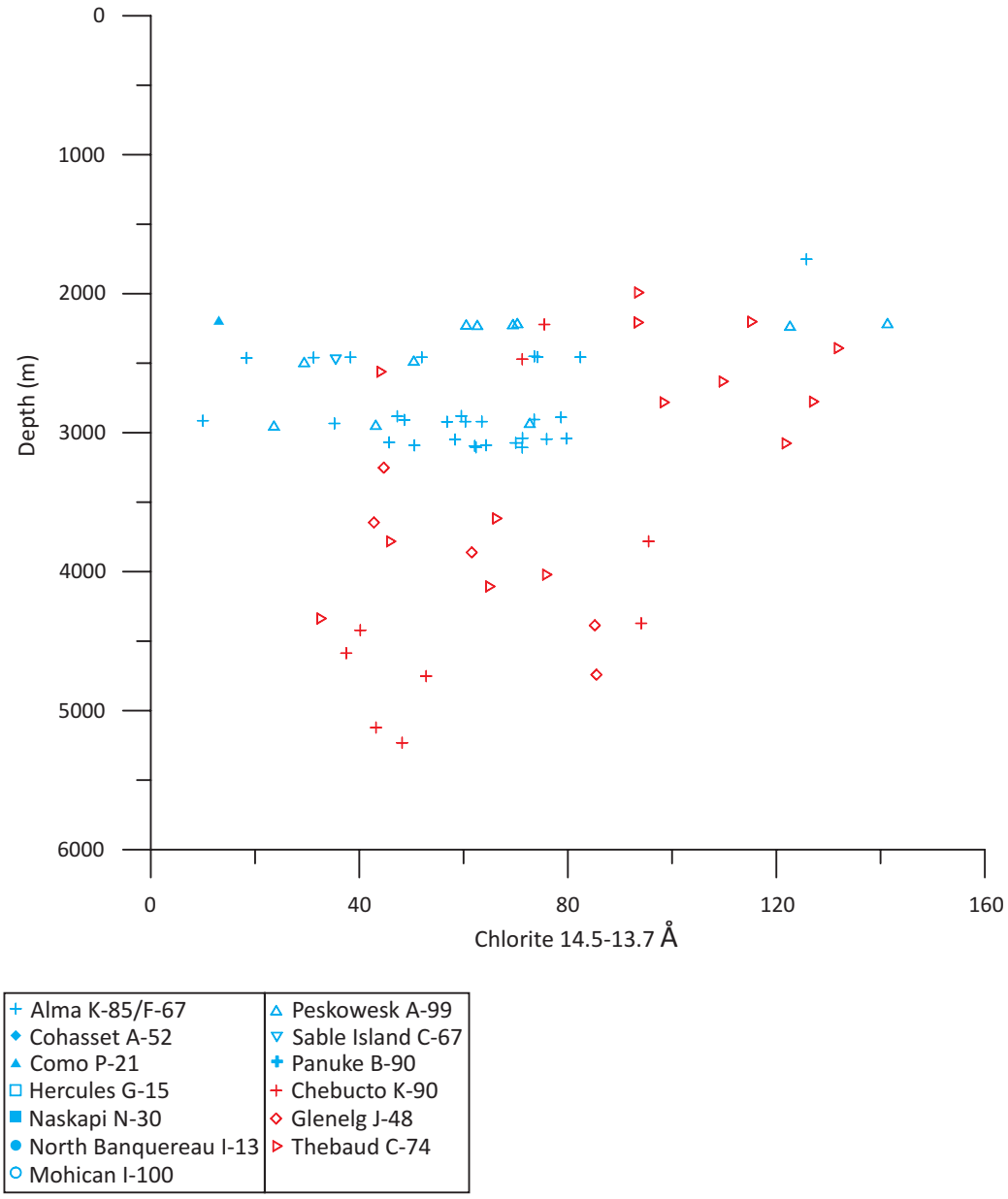

Figure 5.12: Sidepack samples showing Chlorite 14.5-13.7 Å vs Depth. Wells known to be colder in blue, wells known to be hotter in red. (Based on Karim et al. 2011, 2012).

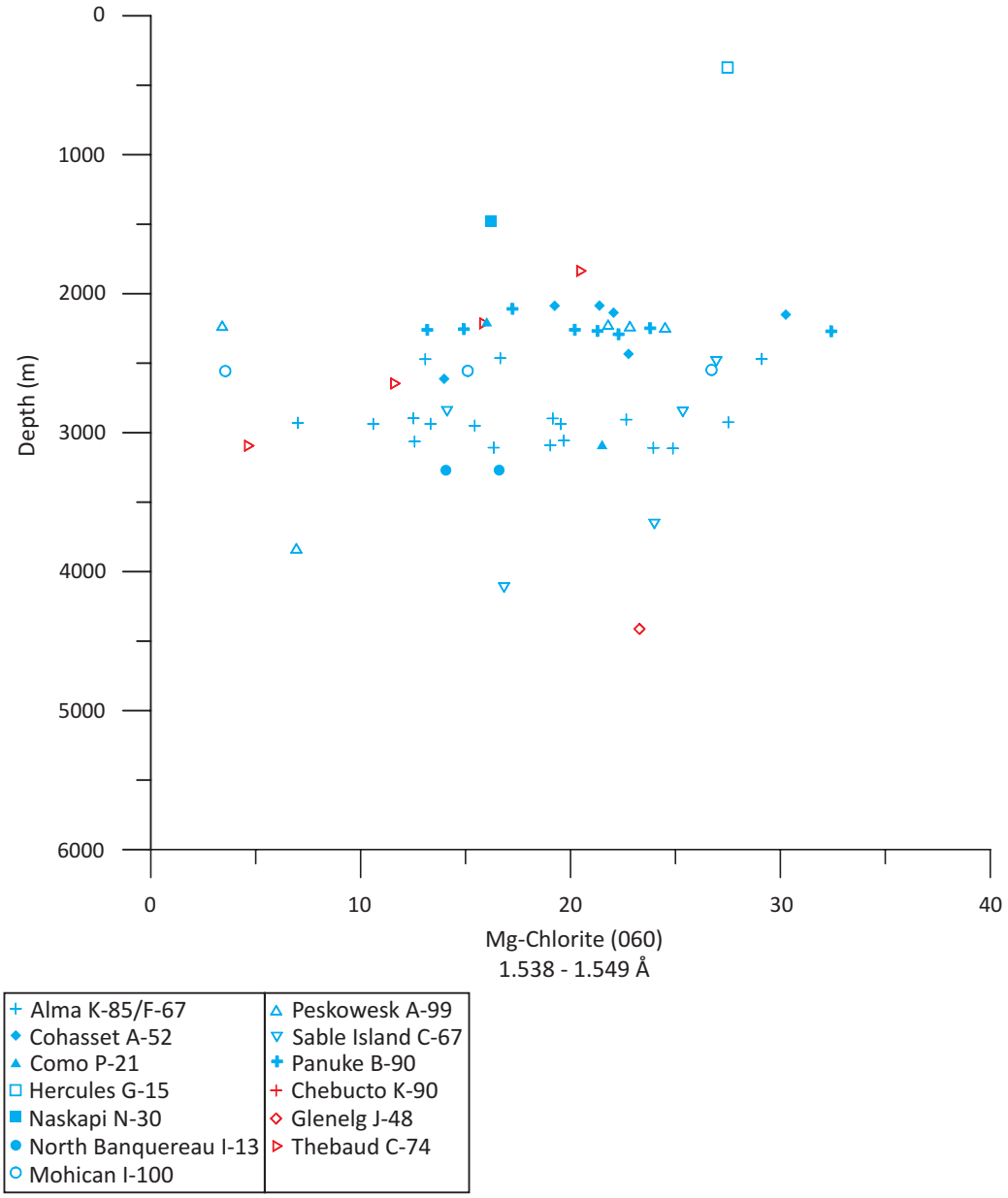

Figure 5.13: Bulk random samples normalized to the standard showing Mg-Chlorite 1.538 - 1.549 Å vs Depth. Wells known to be colder in blue, wells known to be hotter in red. (Based on Karim et al. 2011, 2012).

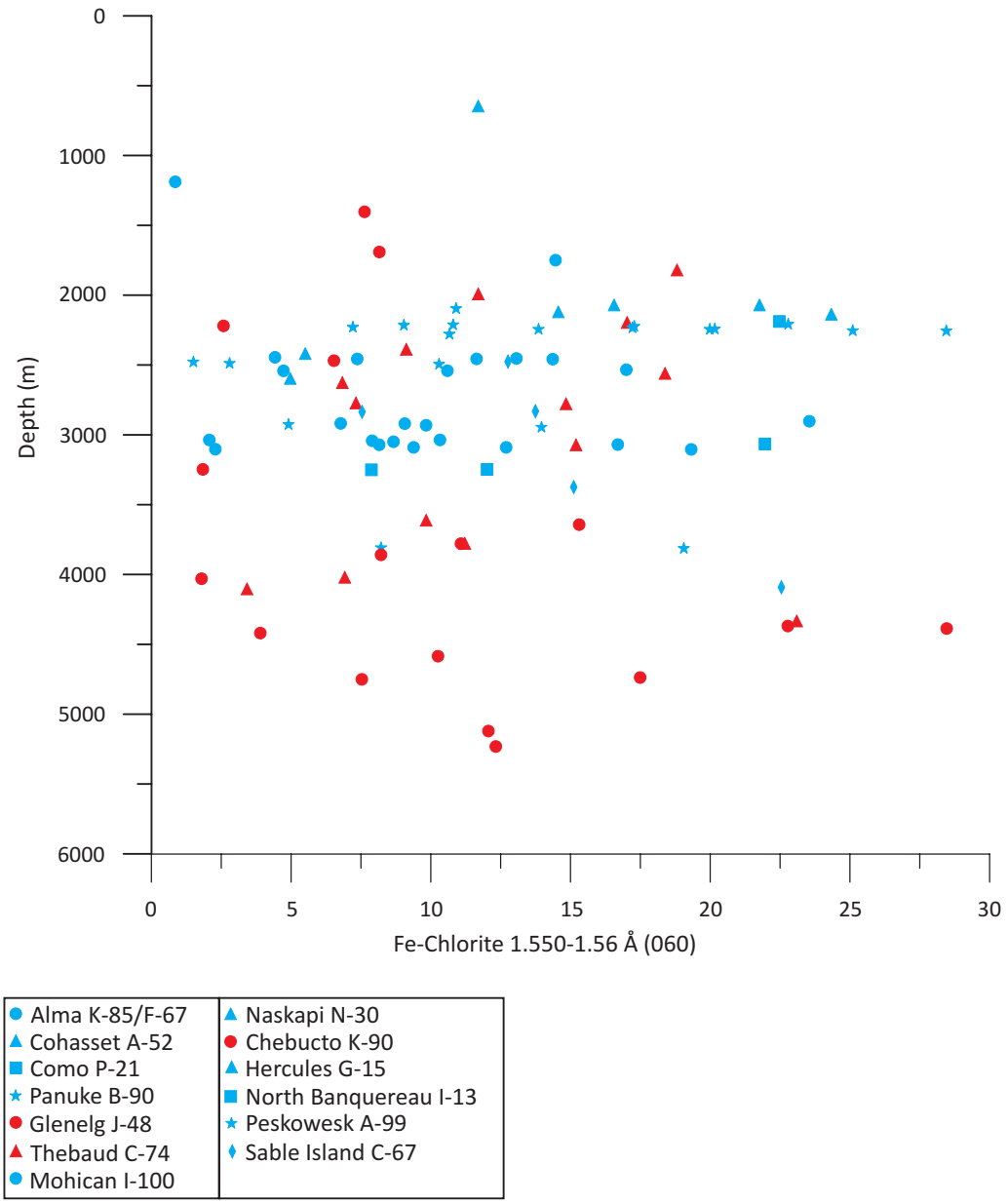

Figure 5.14: Bulk random samples normalized to the standard showing Fe-Chlorite 1.550-1.560 Å (060) vs Depth. Wells known to be colder in blue, wells known to be hotter in red. (Based on Karim et al. 2011, 2012).

Vermiculite is more abundant in hotter wells than it is in colder wells (Figure 5.15). Hydrothermal Fe-vermiculite has been identified in samples from the Red Sea that formed by precipitation from Fe, Si, and Mg-rich supersaturated fluids (Singer & Stoffers, 1981). This may suggest a role for hydrothermal fluids in Thebaud, Glenelg and Chebucto.

Illite crystallinity (Table 4.4) shows that the samples below 4 km are more crystalline, with a Kubler index of ≤0.13. Illite in samples from the Middle Member of the Missisauga Formation is slightly less crystalline than in the samples below 4 km. Illite in samples from the Upper Member of the Missisauga Formation and the Naskapi Member of the Logan Canyon Formation is less crystalline, with a Kubler index of ≥0.15. Illite in samples from the Marmora, Sable and Cree Members of the Logan Canyon is more crystalline, with an average Kubler index of 0.11. Illite has been proven to become more crystalline with burial (Leoni, 2001; Jaboyedoff et al., 2001). A progression of increased crystallinity with depth is what is expected (Figure 1.3). The illite in the samples from the Cree, Sable and Marmora Members of the Logan Canyon Formation may be sourced from a more crystalline basement, which would explain for the lower Kubler index values, plus soils, which would explain the higher Kubler index values.

5.5 VARIATIONS DUE TO ASH AND RELATED VOLCANISM

Volcanic activity in the Scotian Basin has been reported in the Late Jurassic and Early Cretaceous (Bowman 2010). Sandstones contain detrital volcanic clasts and zircons from Cretaceous volcanic rocks (Piper et al., in press). Volcanic ash has been

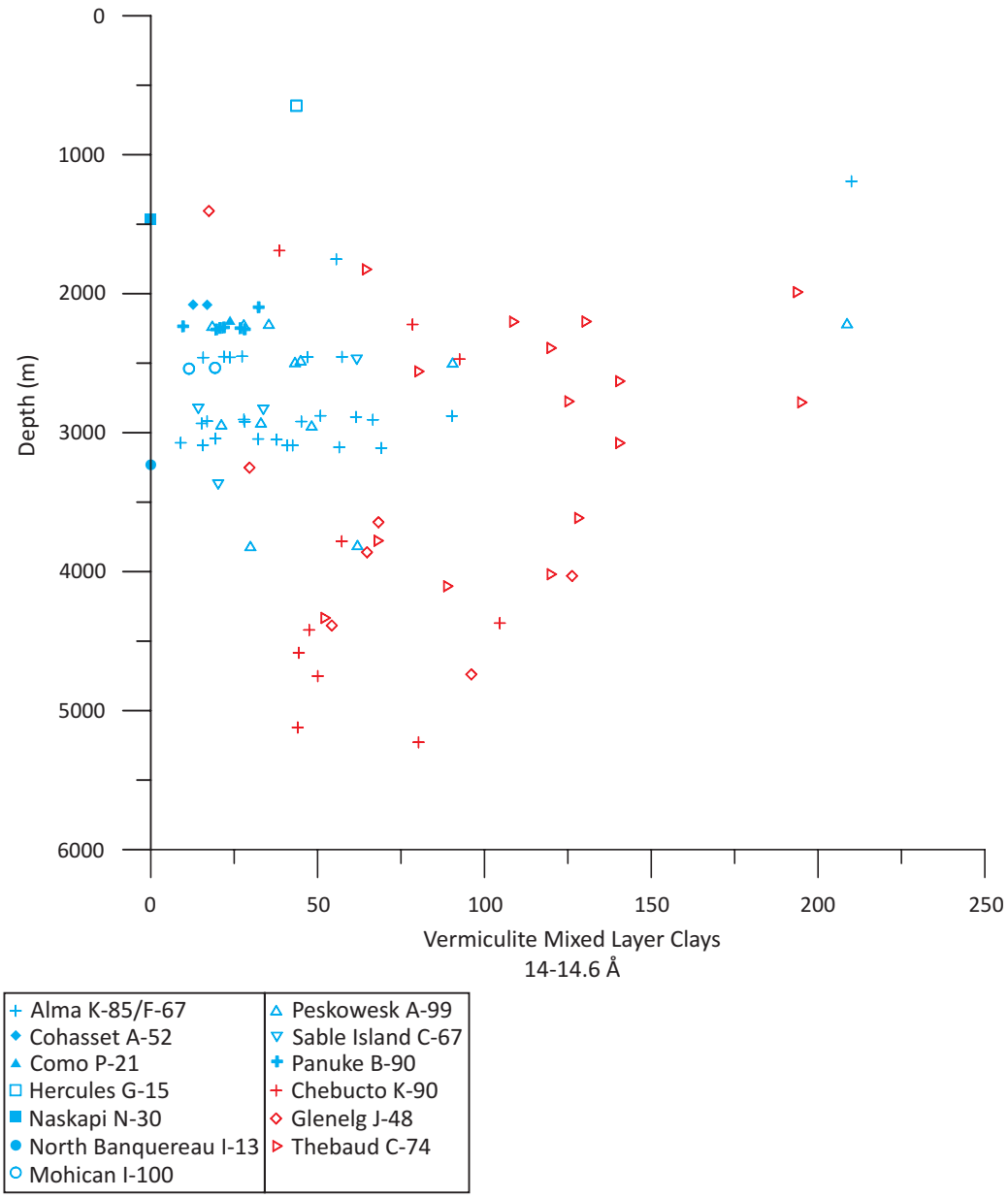

Figure 5.15: Bulk random samples normalized to the standard showing vermiculite 14-14.6 Å vs Depth. Wells known to be colder in blue, wells known to be hotter in red. (Based on Karim et al. 2011, 2012).

identified in the Cretaceous onshore Chaswood Formation in Nova Scotia (Pe-Piper & Piper, 2010). Therefore, there is a need to consider the possible role of volcanic ash in the clays of the Scotian Basin.

Ash is considered an important factor in clay mineral formation because it easily alters to clay minerals (Merriman, 2005). Two percent of the current daily global sediment yield from rivers (estimated at 7.5 km^3/year total [Einsele, 2000]) could possibly be volcanogenic clay, assuming that the majority of the annual ash production altered to clays (Merriman, 2005). The role of submarine volcanism is difficult to approximate, but potentially doubles that amount (Merriman, 2005).

Ash can react differently when deposited in different environments. It can be preserved or it can be altered to kaolinite when ash falls in an acidic watery environment (rich in organics). It typically alters to smectite if it falls in a slightly alkaline watery environment (marine), and it can also alter to zeolite and K-feldspar in highly alkaline wet environments (playa lake) (Moore & Reynolds 1997).

The sample Hercules G-15 646.18 is from a pyroclastic interval at the top of Naskapi Member of the Logan Canyon Formation (Jansa & Pe-Piper, 1985; Bowman, 2010). Based on the <2 µm samples, it has by far the most smectite based on the extreme expansion and destruction in the 20-14 Å peak range when treated with glycol and glycerol (Figure 4.3). The sample Hercules G-15 371.86 is from the Marmora Member of the Logan Canyon Formation and has the next greatest amount of smectite (Appendix 1). Hercules G-15 is only 20-50 km south of Scatarie Ridge, which is known to contain volcanic rocks that are part of a 127 ± 15 Ma series of dykes outcropping on the

sea floor (Delabio et al., 1979; Jansa et al., 1993). The abundance of smectite is probably related to erosion of pyroclastic rocks related to the Scatarie Ridge volcanics, as the abundant ash deposited likely altered to smectite. This large influx of ash increases the difficulty in determining detrital minerals versus diagenetic minerals.

The majority of samples with high levels of smectite occur in the Cree and Naskapi Members of the Logan Canyon Formation and the Upper Member of the Missisauga Formation, which are levels where volcanic rocks have been identified either from wells in Orpheus Graben (Bowman, 2010) or from detrital zircon (Piper et al., in press) (Appendix 1). High concentrations of Nb and Ta have been identified as being characteristic of some volcanic rocks in the Scotian Basin (Pe-Piper et al., 2007; Zhang et al., submitted). Over half of the Scotian Basin samples with high levels of Nb and Ta and shallower than 3.7 km also contain varying amounts of smectite (Figure 4.4, Table 5.1). The samples that have high Nb and Ta but no smectite are mostly below the 3.7 km maximum depth for smectite found in the Scotian Basin. For example, there are five samples in Thebaud C-74 that have high levels of Nb and Ta but no smectite and all but one of the samples are below the 3.7 km maximum depth for smectite, the one outlier is found at 3.6 km. There is, however, no correlation between the amount of smectite and the amount of Nb and Ta, suggesting that direct input of air-fall ash is not the only source of smectite. One quarter of the samples that have sepiolite (not confidently identified) also contain smectite and are found in the Upper and Middle Members of the Missisauga Formation, which could suggest volcanism was occurring at earlier stages than what has been reported to date, as suggested by Zhang et al., (submitted). Nb and

Ta amounts are found to be variable in the samples that also have sepiolite and no correlation is seen.

5.6 VARIATIONS DUE TO CLIMATE

Kaolinite and smectite or smectite-illite mixed layer clay have been proven to be practical tools for reconstructing the paleoclimate in North Western Europe during the Mesozoic (Sladen, 1983; Deconinck & Bernoulli, 1991; Hallam et al., 1991). Since kaolinite is a humid weathering product, low levels of kaolinite may indicate an arid phase and it has been shown that the absence of kaolinite is representative of an arid climate in Northwest Europe in the Triassic (Jeans, 1978). Using kaolinite as a paleoclimate indicator, a shift into an arid phase has been recognized during the Barremian (125-130 Ma) – Aptian (112-125 Ma) in Western Europe (Ruffell & Batten, 1990). These authors found evidence of evaporites, carbonate-rich sediments, red beds, and depletion of kaolinite. Kaolinite forms in soils under humid climatic conditions from where it can be transported to the sea and be deposited; or is can form from diagenesis, after deposition, under the influence of meteoric water.

The variation in the amount of kaolinite through time in the Chaswood Formation (Pe-Piper et al., 2005) compares well with the Ruffell & Batten (1990) findings on the Barremian-Aptian arid phase of Western Europe (Figure 5.16). Since the Chaswood Formation represents the fluvial equivalent of the Scotian Basin deltaic sediments, a similar pattern of kaolinite abundance might be expected in the Missisauga and Logan Canyon Formations.

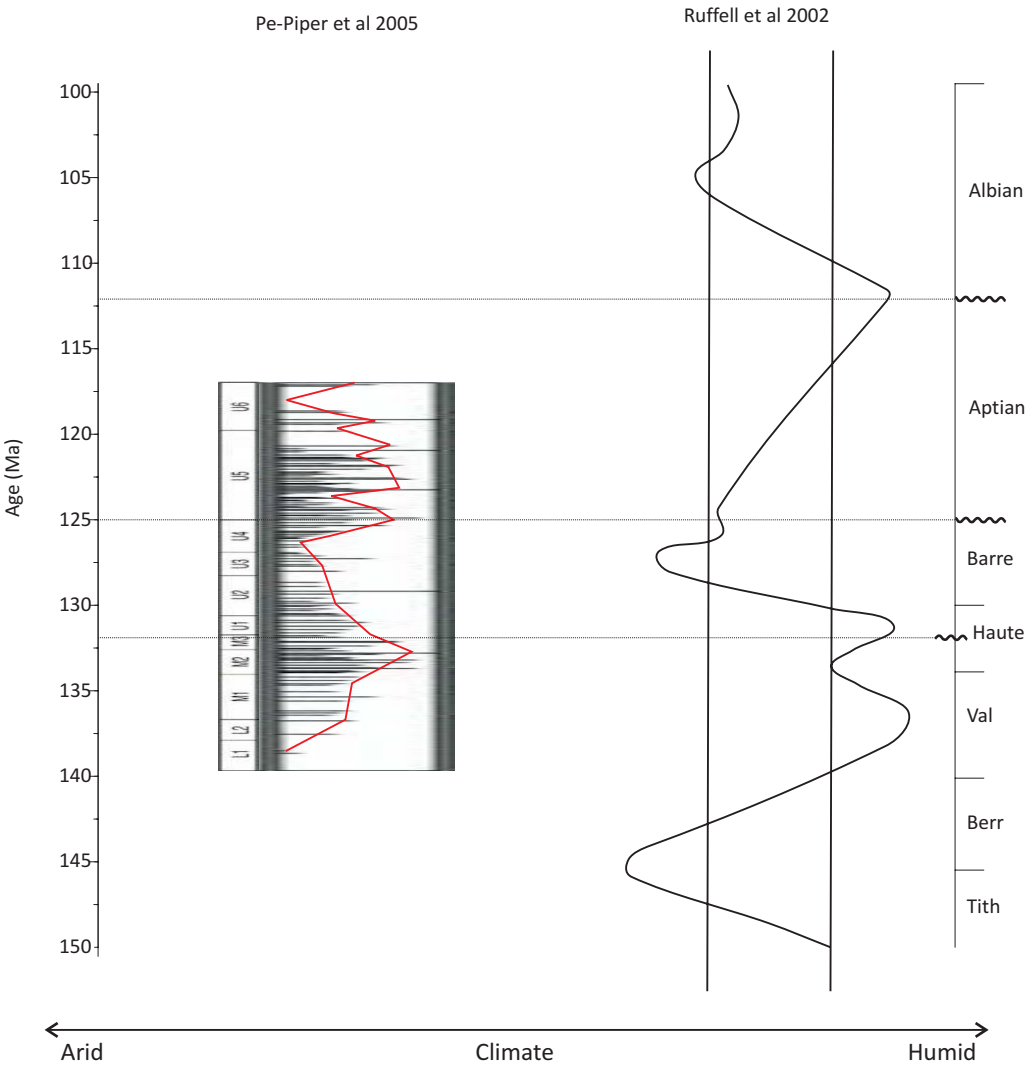

Figure 5.16: Chaswood Formation kaolinite/illite ratio (data from Pe-Piper et al.,2005), compared with western European generalized Kaolinite curve (data from Ruffell et al., 2002).

The main issue with using kaolinite as a climate indicator is determining what is detrital versus what is diagenetic in a specific sedimentaory sequence. Surface to early burial diagenesis will alter feldspars, micas and illite to kaolinite, whereas deeper burial will cause illitization of kaolinite (Kulbicki & Millot, 1961).

There are three processes that influence the amount of kaolinite in these samples. Kaolinite could be detrital and thus reflect climatic conditions (presumably some do)for its source area; it could have formed through early diagenesis (increasing the amount of kaolinite), or it could have been altered to illite through burial diagenesis (decreasing the amount of kaolinite). Diagenetic formation of kaolinite can be evaluated by comparing shale samples with sandstone samples from similar depths. Shale samples from Cohasset A-52, North Banquereau I-13, Panuke B-90, and Sable Island C-67 are within 10 m of sandstone samples that show significant amounts of pore-filling kaolinite (Gould et al., 2011). Early diagenesis is likely in wells like Thebaud C-74, Sable Island C-67, Como P-21, Cohasset A-52 and Panuke B-90 as during the Early Cretaceous these wells would have been on the top of the delta, which would have allowed fresh meteoric water to flush through the sediment, promoting alteration (cf. Okwese et al. 2011). There is a linear trend between kaolinite and illite with increasing scatter as the abundance of each mineral increases; the samples with increased illite show decreased kaolinite and vice versa (Figure 5.17). Some of the samples that increase in kaolinite and decrease in illite are interpreted as having diagenetic kaolinite based on the amount of kaolinite in nearby sandstone samples. It has been found that

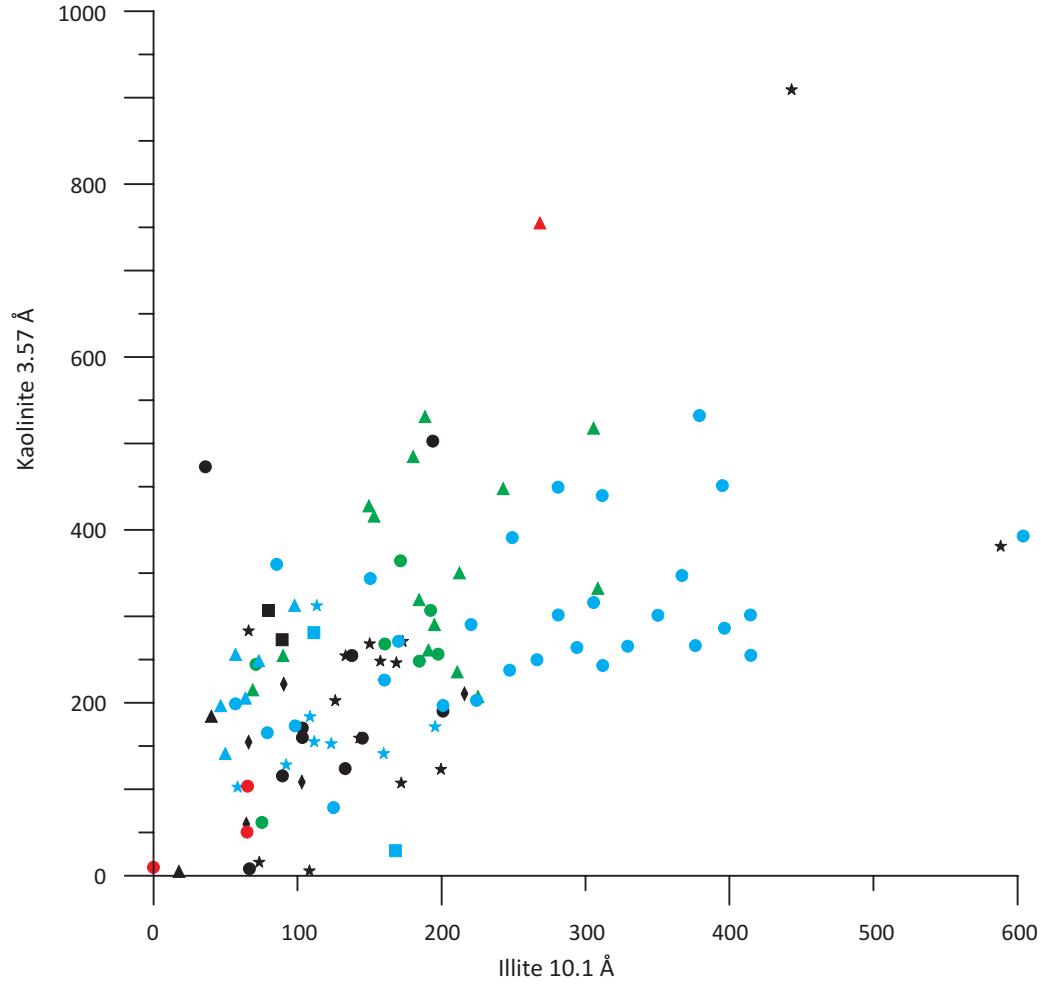

Figure 5.17: Bulk random sidepack samples showing kaolinite 3.75 Å vs illite 10.1 Å. Colour code based on likely provenance from Pe-Piper & Piper (2012).

major diagenetic changes in sandstone beds are mirrored in adjacent shales (Abid & Hesse, 2007; Piper et al., 2009).

K-feldspar dissolution is an important factor in the precipitation of kaolinite in sandstones (Blanche & Whitaker, 1978; Hancock, 1978; Hancock & Taylor, 1978). It is not clear whether a similar process occurs in shales. The K-feldspar peaks (without possible overlap by rutile) are seen in less than half of the wells and of those, very few show a decrease in K-feldspar with an increase in kaolinite (Figure 5.10).

There is no correlation between values of the kaolinite/illite ratio in this study and values of the kaolinite/illite ratio determined for the Chaswood Formation by Pe-Piper et al. (2005) or the results of Ruffell & Batten (1990) (Figure 5.18). There are a few explanations for the variance between the Chaswood Formation data and the Scotian Basin data: 1) It may be because the local climate was different for each source area. 2) The hinterland has experienced episodic uplift that can be seen in the Chaswood Formation unconformities (Hundert et al., 2006) and the mid-Hauterivian, base of Aptian and base of Albian unconformities (Wade & Maclean, 1990; Maclean & Wade, 1993; OETR, 2011). Thus, delivery of weathered soil materials to the basin might be more an indicator of tectonic uplift than climatic change. 3) The diversion to the Bay of Fundy in the Aptian (Piper et al., 2011) of the main rivers that entered the basin at the Cabot Strait may have changed the source area for shale deposition at that time. 4) Diagenesis in the marine basin has further changed the relative abundance of kaolinite. It is thus most likely that this diagenesis is the main cause of variability in the clays in the Scotian Basin.

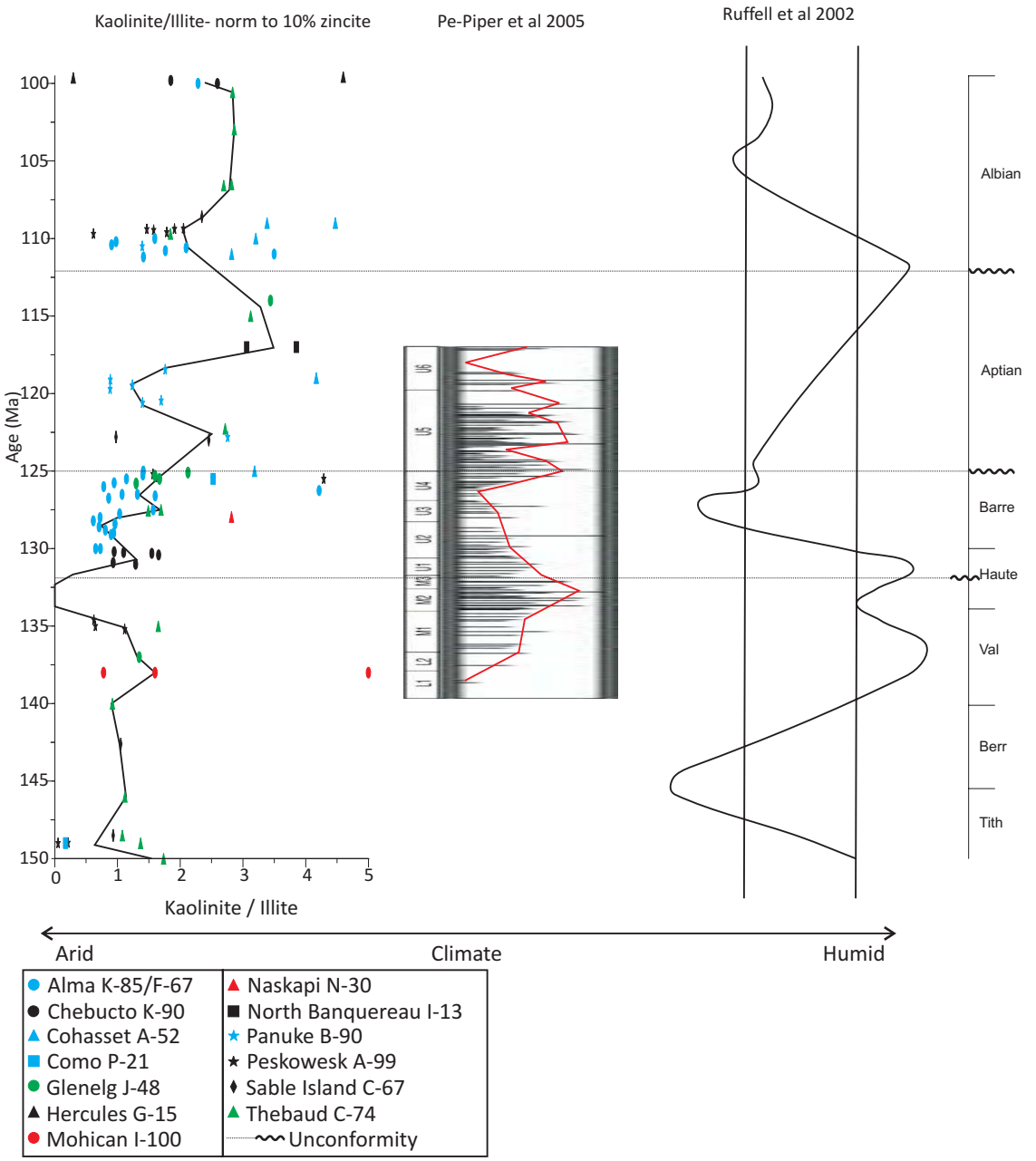

Figure 5.18: Kaolinite/illite ratio from sidepack samples compared with the Chaswood Formation kaolinite/illite ratio (data from Pe-Piper et al.,2005), compared with western European generalized Kaolinite curve (data from Ruffell et al., 2002).

5.7 VARIATIONS IN PROVENANCE

This study has found an overall uniformity in the mineral composition of the clays in the Scotian Basin (Figure 4.21 & Figure 4.22). The most prominent variation is found in two samples; Hercules G-15 646.18m (Figure 4.22 compared to Figure 4.21) from the Cree Member of the Logan Canyon Formation and Naskapi N-30 1469.1m (Figure 4.9 compared to Figure 4.21) from the Upper Member of the Missisauga Formation. This uniformity is thought to be a product of a broadly constant river source (Figure 5.3) as shown by sandstone petrology (Tsikouras et al., 2011) and geochemistry (Pe-Piper et al., 2008). River plumes can get caught in oceanic circulation patterns and spread sediment over many tens of kilometers.

The abundance of smectite can be linked to the Scatarie Ridge volcanics, as the abundant ash deposited (Bowman, 2010) has likely altered to smectite over time. Fe-chlorite is formed during diagenesis (Figure 4.16). However, the abundance of Mg-chlorite in stratigraphic intervals with high detrital input for the Meguma Terrane (Reynolds et al., in press) suggests the Meguma Terrane as a possible source. The chlorite in the Meguma Terrane has been found to be mostly Mg-chlorite (C.E. White pers. comm. to D.J.W. Piper, 2012).

The abundance of illite found in Alma K-85 is thought to be principally an artifact of interference with mixed layer clays. However, those clays and high illite-muscovite may also be due to reactivation of the Cobequid-Chedabucto fault in the Late Baremian-Early Aptian which would have changed the source from mostly Appalachian and Shield Terrane to mostly Meguma Terrane (Reynolds et al., in press). Muscovite is a very

abundant mineral in sandstones of the Scotian Basin (Reynolds et al., 2009). In shale samples, common muscovite is typically found with biotite, which would suggest they are both detrital (Figure 5.19). The samples containing muscovite and biotite together are mostly from wells in the western Scotian Basin with four from the LaHave Platform and two from central Scotian Basin. Comparison of biotite and muscovite abundance (Figure 5.19) with quartz (a proxy for grain size, Figure 5.2) shows that the samples that do contain muscovite and biotite are in the mid range of grain size on average. Radiometric dating shows that almost all muscovite in sandstones is derived from the Meguma Terrane (Reynolds et al., 2009), which could also be a source for biotite. The Meguma Terrane of southern Nova Scotia is therefore probably a contributor of muscovite to shales during the Lower Cretaceous.

The increase in abundance of vermiculite around 2.2 km depth (Figure 4.19) may suggest a probable source of the Meguma Terrane of Nova Scotia as vermiculite is found in well drained soils in humid regions where the source hosts mica schists (Moore & Reynolds, 1997). However, the greater abundance of vermiculite in hotter wells than cooler wells (Figure 5.15) supports a possible hydrothermal origin.

There is an abundance of 2:1 Fe-rich clays throughout the Scotian Basin, stratigraphically and geographically (Figure 4.28). An abundance of detrital ilmenite is a cause of an unusually high quantity of Ti and Fe in the Lower Cretaceous shales of the Scotian Basin due to diagenesis (Pe-Piper et al., 2005). This created favorable conditions for early diagenesis of Fe-chlorite (Okwese et al., 2011) and possibly 2:1 Fe-rich clays.

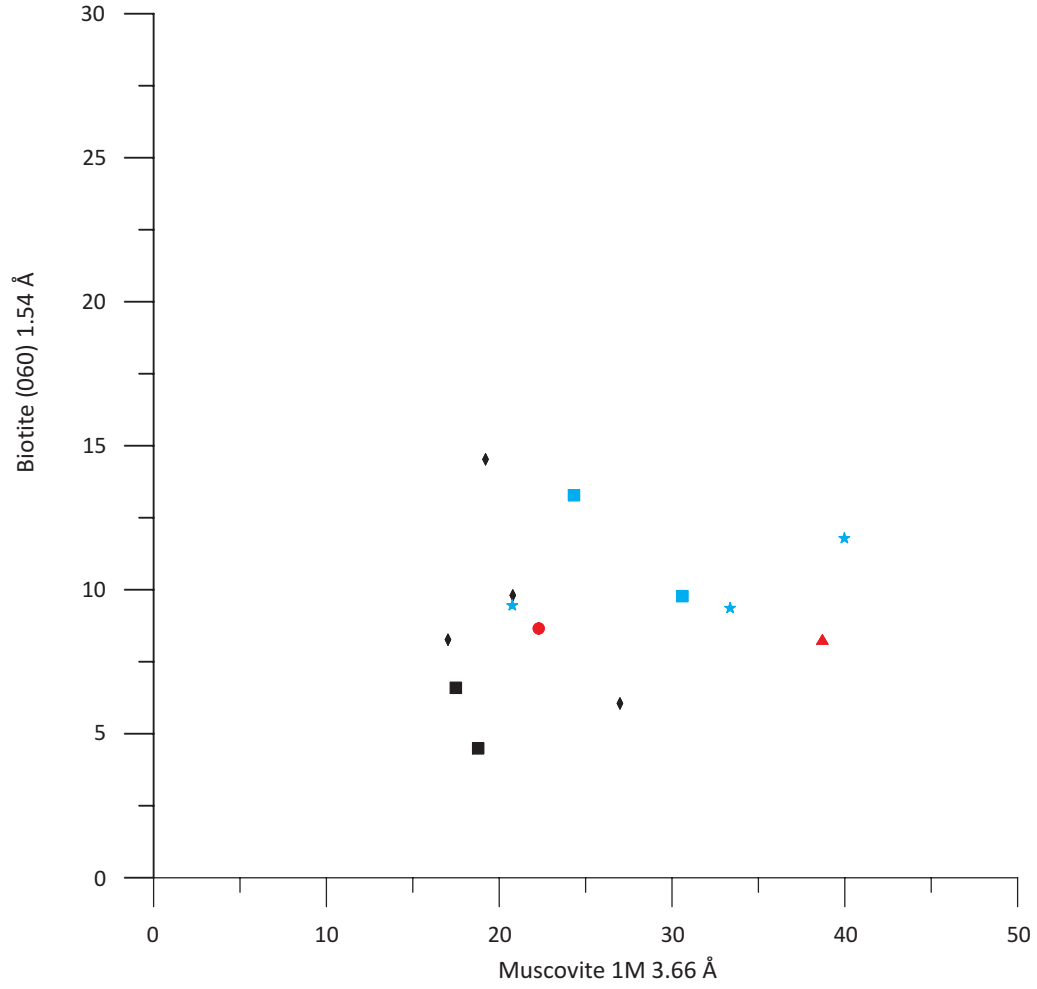

● Alma K-85/F-67	▲ Naskapi N-30
▲ Cohasset A-52	● Chebucto K-90
■ Como P-21	▲ Hercules G-15
★ Panuke B-90	■ North Banquereau I-13
● Glenelg J-48	★ Peskowesk A-99
▲ Thebaud C-74	♦ Sable Island C-67
● Mohican I-100	

Some Meguma, some main river

Mostly main river, some Meguma

Likely predominant Meguma terrane source

Wells well within the basin, more easterly, main Cabot Strait river supply (?except in Aptian?)

Figure 5.19: Bulk random samples normalized to the standard showing Biotite 1.54 Å vs Muscovite 3.66 Å. Colour code based on likely provenance from Pe-Piper & Piper (2012).

CHAPTER 6: CONCLUSIONS

This thesis represents the first detailed study of clay minerals in the Scotian Basin. It has documented the clay minerals present in the Upper Jurassic to Lower Cretaceous shales and interpreted them in terms of detrital input, early diagenesis and burial diagenesis. Understanding clay minerals can lead to a better understanding of paleoclimates, depositional environments, provenance, oil and gas reservoir quality, oil and gas generation and migration and thermal conditions with burial.

6.1 DETRITAL INPUT

The quartz/illite ratio shows a trend of coarsening of the grain size of the samples from the Late Jurassic until the Early Aptian, followed by more fine sediment deposition until the Aptian-Albian boundary (top of Naskapi Member), where it rapidly coarsens again. There is a mild correlation between the quartz/illite ratio and Mg-chlorite and kaolinite abundance and a better correlation between the quartz/illite ratio and vermiculite, illite, 2:1 Al-rich clays, and 2:1 Fe-rich clays suggesting that all are predominantly detrital minerals. There is no correlation between the quartz/illite ratio and Fe-chlorite. This study shows a change in sediment supply during the Aptian. The change in grain size suggests that the main river supply was re-directed. The sediment came from smaller rivers and from a distal source and was most likely carried in a plume with the ocean currents from southern Nova Scotia.

The abundance of Mg-chlorite in the samples at 2-3.2 km depth suggests that the Meguma Terrane was an important source during this time. This is also supported

but the correlation of muscovite and biotite in the samples from wells in the western portion of the Scotian Basin. Muscovite and biotite, when found together, are considered detrital and the majority of muscovite in the sandstones of the Scotian Basin has been identified as sourced from the Meguma Terrane. The abundance of vermiculite in the clays of the Scotian Basin and in the Chaswood Formation suggests that Meguma Terrane or the Appalachian soils were a source as well.

The abundance of smectite in the samples from Hercules G-15 is interpreted to be from altered ash that was sourced from the Scatarie Ridge volcanic center. This study suggests that one source of smectite in the Scotian Basin can be tied to the Scatarie Ridge volcanic rocks, as the abundant ash deposited has likely altered to smectite over time, but it warrants further investigation. Even though Nb and Ta have been identified as being characteristic of volcanic rocks, there was not a very good correlation between Nb and Ta and smectite abundance in the samples. This suggests that either the volcanics that deposited the ash were not rich in Nb and/or Ta, or that ash deposited on land was reworked. This requires further study with more <2 μm samples from the Orpheus Graben and the Scotian Basin. When considering the samples that do contain high levels of Nb and Ta, plus the samples with abundance of smectite and possible sepiolite, they are found throughout the Missisauga Formation and in the Cree and Naskapi Member of the Logan Canyon Formation, which suggests that volcanism in the Scotian Basin has occurred earlier than has been thought so far. However, this requires further study.

The climate shift to an arid phase in the Barremian-Aptian cannot be correlated in the clays of the Scotian Basin. There is not a clear climate signal in the Scotian Basin due to a mix of factors. Primarily, the effects of diagenesis have altered the marine sediment enough to mask any correlation.

6.2 EARLY DIAGENESIS

Ash from the Scatarie ridge volcanic center and possibly earlier volcanism was altered to smectite at the surface and early burial. This can be seen by the relatively shallow depths of the Hercules G-15 samples. The lack of correlation between Nb and Ta and smectite abundance in the samples suggests that air-fall ash was not directly deposited, but the ash was altered and eroded before being re-deposited. Comparison of kaolinite and illite abundance in the bulk random samples, as well as, the abundance of pore filling kaolinite in nearby sandstone samples suggests that kaolinite has precipitated during early diagenesis. Such early diagenetic kaolinite is suspected of masking the climate signature during the Barremian-Aptian arid shift seen in northwestern Europe and potentially in the Chaswood Formation.

The chlorite in the Meguma Terrane consists almost entirely of Mg-chlorite and it can be surmised that Fe-chlorite is mostly (if not completely) diagenetic in the Scotian Basin. The samples in this study show a sharp increase in Fe-chlorite at around 2 km and high levels being sustained until around 3.2 km. This suggests that Fe-rich sediments were being deposited at the time. A similar pattern can be seen in the 2:1 Fe-rich clays, which consist of glauconite and/or celadonite.

6.3 BURIAL DIAGENESIS

Smectite is found to be abundant to moderately abundant in more shallow to medium depths and is not found in samples deeper than 3.7 km. It is widely accepted that smectite converts to illite with burial which is what is found in the Scotian Basin. Vermiculite is also found to become less abundant with depth. When considering the increase in abundance of Al-rich clay and Fe-rich clay this study suggests that vermiculite is partially altering to Al-rich clays and perhaps to Fe-rich clays. There is no visible effect of the higher than average diagenetic temperatures found in the Thebaud, Glenelg and Chebucto wells.

The illite crystallinity determined from the samples in the Scotian Basin has provided some insight into the progression of illite with burial. Below 4 km the illite is more crystalline, which suggests the crystals have experienced anchizonal recrystallization. Samples from the Middle Member of the Missisauga Formation show some recrystallization and some less crystalline illite crystals. Illite from the samples from the Upper Member of the Missisauga Formation and the Naskapi Member of the Logan Canyon are less crystalline which suggests that the illite is detrital from soils. The samples from the Marmora, Sable and Cree Members of the Logan Canyon are more crystalline which suggests that more crystalline basement, potentially from Newfoundland, is the primary source.

REFERENCES

Aagaard, P., Jahren, J.S., Harstad, A.O., Nilsen, O. and Ramm, M., 2000. Formation of grain-coating chlorite in sandstones. Laboratory synthesized vs. natural occurrences. Clay Mineral., v. 35, p. 261–269.

Abid, I., and Hesse, R., 2007. Illitizing fluids as precursors of hydrocarbon migration along transfer and boundary faults of the Jeanne d'Arc Basin offshore Newfoundland, Canada. Marine and Petroleum Geology. v. 24, p. 237-245.

Anthony, J.W., Bideaux, R. A., Bladh, K. W., and Nichols, M. C., 2001. Eds., Handbook of Mineralogy, Mineralogical Society of America, Chantilly, VA 20151-1110, USA. http://www.handbookofmineralogy.org/.

Awwiller, D.N., 1993. Illite smectite formation and potassium mass-transfer during burial diagenesis of mudrocks-a study from the Texas Gulf-coast Paleocene-Eocene. Journal of Sedimentary Petrology. v. 63 (3), p. 501-512.

Bell, J.S., and Campbell, G.R., 1990. Petroleum resources, Chapter 12 in Geology of the Continental Margin of Eastern Canada, M.J. Keen and G.L. Williams (ed); Geological Survey of Canada, Geology of Canada. no. 2, p. 677-720.

Bjorlykke, K., Jahren, J., Mondol, N. H., Marcussen, O., Croize, D., Peltonen, C., and Thyberg, B., 2008. Sediment Compaction and Rock Properties. AAPG International Conference and Exhibition Abstracts.

Blakey, R., (2011), Colorado Plateau Geosystems, Inc, http://cpgeosystems.com/globaltext.html

Blanche, J. B., and Whitaker, J. H. Mc D., 1978. Diagenesis of part of the Brent Sand Formation (Middle Jurassic) of the northern North Sea Basin. Journal of the Geological Society, London. v. 135, p. 73-82.

Boles, J.R., and Franks, S.G., 1979. Clay diagenesis in Wilcox sandstones of southwest Texas. Journal of Sedimentary Petrology. v. 49, p. 55-70.

Bowman, S., 2010. Cretaceous tectonism and volcanism in the eastern Scotian Basin, offshore Nova Scotia. Masters Thesis, Saint Mary's University.

Bradley, W.F., 1945. Molecular associations between montmorillonite and some polyfunctional organic liquids. Journal of American Chemical Society. v. 67, p. 975-981

Brindley, G. W. and G. Brown (1980) Crystal structures of clay minerals and their identification. Mineralogical Society Monograph No. 5. Mineralogical Society, London.

Burton, J.H., Krinsley, D.H., and Pye, K., 1987. Authigenesis of kaolinite and chlorite in Texas Gulf Coast sediments. Clays and Clay Minerals. v. 35, p. 291-296.

Carroll, D., 1970. Clay Minerals: A guide to their X-ray identification: The Geological Society of America. Special Paper 126.

Cassou, A.-M., Connan, J., and Porthault, B., 1977. Relations between maturation of organic matter and geothermal effect, as exemplified in Canadian east coast offshore wells. Bulletin of Canadian Petroleum Geology. v. 25, no. 1, p. 174-194.

Claret, F., Sakharov, B.A., Drits, V.A., Velde, B., Meunier, A., Griffault, L. and Lanson, B., 2004. Clay minerals in the Meuse-Haute Marne underground laboratory (France): Possible influence of organic matter on clay mineral evolution. Clays and Clay Minerals. v. 52, no. 5, p. 515-532.

Connan, J., 1974. Time-temperature relation in oil genesis. American Association of Petroleum Geologists. v. 58, no. 12, p. 2516-2521.

Cummings, D.I., Hart, B.S. and Arnott, R.W.C., 2006. Sedimentology and stratigraphy of a thick, areally extensive fluvial-marine transition, Missisauga Formation, offshore Nova Scotia, and its correlation with shelf margin and slope strata. Bulletin of Canadian Petroleum Geology. v. 54, p. 152–174.

Curtis, C. D., Hughes, C. R., Whiteman, J. A., and Whittle, C.K., 1985. Compositional variation within some sedimentary chlorites and some comments on their origin: Mineralogical Magazine. *v.* 49, p. 375-386.

Deconinck, J.-F., and Bernoulli, D., 1991. Clay mineral assemblages of Mesozoic pelagic and flysch sediments of the Lomabardian basin (Southern Alps): implications for palaeotectonics, palaeoclimate and diagenesis. Geologische Rundschau. v. 80, p. 1-17.

Delabio, R., Lachance, G., Steens, R., and Wanless, R. 1979. Age determinations and geological studies, K-Ar isotopic ages, Report 14. Geological Survey of Canada Paper 79-02, 67p.

Drummond, K.J., 1992. Geology of Venture, a geopressured gas field, offshore Nova Scotia. In: Giant Oil and Gas Fields of the Decade 1978–1988 (Ed. M.T. Halbouty), AAPG Mem. v. 54, p. 55–71.

Einsele, G., 2000. Sedimentary basins: Evolution, facies, and sediment budget. Springer, Berlin. p. 792.

Frost, R.L., and Rintoul, L., 1996. Lattice vibrations of montmorillonite: an FT Raman and X-Ray diffraction study. Applied Clay Science, v. 11, p. 171-183

Given, M.M., 1977. Mesozoic and early Cenozoic geology of offshore Nova Scotia. Bulletin of Canadian Petroleum Geology. v. 25, p. 63-91

Gobeil, J.-P., Pe-Piper, G. and Piper, D.J.W., 2006. The Early Cretaceous Chaswood Formation in the West Indian Road pit, central Nova Scotia. Canadian Journal of Earth Sciences. v. 43, p. 391–403.

Gould, K., 2007. Chlorite diagenesis in reservoir sandstones of the Lower Missisauga Formation, offshore Nova Scotia. Masters Thesis, Saint Mary's University.

Gould, K., Pe-Piper, G., and Piper, D.J.W., 2010. Relationship of diagenetic chlorite rims to depositional facies in Lower Cretaceous reservoir sandstones of the Scotian Basin. Sedimentology. v. 57, p. 587-610.

Gould, K., Karim, A., Piper, D.J.W., and Pe-Piper, G., 2011. Lithofacies and diagenesis of selected conventional core from Jurassic and Early Cretaceous terrigenous clastic rocks, Scotian Basin. Geological Survey of Canada, Open File 6945.

Gradstein, F.M., and Ogg, J.G., 2004. Geological time scale 2004 – why, how, and where next! Lethaia, v. 37, p. 175-181.

Grist, A.M., Reynolds, P.H., and Zentilli, M., 1992. The Scotian Basin offshore Nova Scotia: thermal history and provenance of sandstones from apatite fission track and 40Ar/39Ar data. Canadian Journal of Earth Sciences. v. 29, p. 909-924.

Hallam, A., Grose, J. A., and Ruffell, A. H., 1991. Palaeoclimatic significance of changes in clay mineralogy across the Jurassic-Cretaceous boundary in England and France. Palaeogeography Palaeoclimatology Palaeoecology. v. 81, p. 173-187.

Hancock, N. J., 1978. Diagenetic modelling in the middle Jurassic Brent Sand of the Northern North Sea. European Offshore Petroleum Conference and Exhibition, London, Oct. 1978, p. 275-280.

Hancock, N.J., and Taylor, A. M., 1978. Clay mineral diagenesis and oil migration in the Middle Jurassic Brent Sand Formation. Journal of Geological Society, London. v. 135, p. 69-72.

Hillier, S. and Velde, B., 1991. Octahedral occupancy and the chemical composition of diagenetic (low-temperature) chlorites: Clay Minerals. v. 26, p. 149-168.

Hoffman, J. and Hower, J. (1979) Clay mineral assemblages as low grade metamorphic geothermometers: Application to the thrust faulted disturbed belt of Montana: in *Aspects of Diagenesis,* P. A. Scholle and P. S. Schluger, eds., SEPM Spec. Publ. v. 26, p. 55-79.

Hower, J., Eslinger, E.V., Hower, M.E., and Perry, E.A., 1976. Mechanism of burial metamorphism of argillaceous sediment. Mineralogical and chemical evidence. Geological Society of America Bulletin. v. 87 (5), p. 725-737.

Hundert, T., Piper, D.J.W., and Pe-Piper, G., 2006. Genetic model and exploration guidelines for kaolin beneath unconformities in the Lower Cretaceous Fluvial Chaswood Formation, Nova Scotia. Exploration and Mining Geology. v. 15, p. 9-26.

Ings, S.J. and Shimeld, J.W., 2006. A new conceptual model for the structural evolution of a regional salt detachment on the northeast Scotian margin, offshore eastern Canada. AAPG Bulletin. v. 90, p. 1407–1423.

Issler, D.R., 1984. Calculation of organic maturation levels for offshore eastern Canada – implications for general application of Lopatin's method. Canadian Journal of Earth Sciences. v.21, p. 477–488.

Jaboyedoff, M., and Thelin, P., 1996. New data on the low-grade metamorphism in the Brianconnais domain of the Prealps, western Switzerland. European Journal of Mineralogy. v. 8, p. 577-592.

Jaboyedoff, M., Bussy, F., Kubler, B., and Thelin, P., 2001. Illite "crystallinity" revisited. Clays and Clay Minerals. v. 49, no. 2, p. 156-167.

Jansa, L.F. and Pe-Piper, G., 1985. Early Cretaceous volcanism on the northeastern American margin and implications for plate tectonics. Geological Society of America Bulletin. v. 96, p. 83-91.

Jansa, L.F. and Noguera-Urrea, V.H., 1990. Geology and diagenetic history of overpressured sandstone reservoirs, Venture gas field, offshore Nova-Scotia, Canada. AAPG Bulletin. v. 74, p. 1640–1658.

Jansa, L.F., Pe-Piper, G., and Loncarevic, B.D., 1993. Appalachian basement and its intrusion by Cretaceous dykes, offshore southeast Nova Scotia, Canada. Canadian Journal of Earth Sciences. v. 30, p. 2495-2509.

Jeans, C. V., 1978. The origin of the Triassic clay assemblages of Europe with special reference to the Keuper Marl and Rhaetic of parts of England. Philosophical Transactions of the Royal Society, London. v. 289, p. 549-639.

JunFeng, J., and Browne, P.R.L., 2000. Relationship between illite crystallinity and temperature in active geothermal systems of New Zealand. Clays and Clay Minerals. v. 48, n. 1, p. 139-144.

Karim, A., Pe-Piper, G., and Piper, D.J.W., 2010. Controls on diagenesis of Lower Cretaceous reservoir sandstones in the western Sable Subbasin, offshore Nova Scotia. Sedimentary Geology. v. 224, p. 65-83.

Karim, A., Pe-Piper, G., Piper, D.J.W., and Hanley, J.J., 2011. Thermal and hydrocarbon-charge history and the relationship between diagenesis and reservoir connectivity: Venture field, offshore Nova Scotia, eastern Canada. Canadian Journal of Earth Sciences. v. 48, p. 1293-1306.

Karim, A., Hanley, J.J., Pe-Piper, G., and Piper, D.J.W., 2012. Paleohydrogeological and thermal events recorded by fluid inclusions and stable isotopes of diagenetic minerals in Lower Cretaceous sandstones, offshore Nova Scotia, Canada. The American Association of Petroleum Geologists Bulletin. v. 96, p. 1147-1169

Kendell, K.L., 2012. Canada-Nova Scotia Offshore Petroleum Board Call for Bids NS12-1**.** http://www.cnsopb.ns.ca/call_for_bids_12_1/cnsopb/.

Kleeberg, R., Monecke, T., and Hillier, S., 2008. Preferred orientation of mineral grains in sample mounts for quantitative XRD measurements: How random are powder samples? Clays and Clay Minerals. v. 56, no. 4, p. 404-415.

Kübler, B., 1964. Les argiles, indicateurs de métamorphisme. *Revue de l'Institut Français du Pétrole*. v. 19, p. 1093–1112.

Kübler, B., 1984. Les indicateurs des transformations physiques et chimiques dans la diagenèse, température et calorimétrie. In: *Thermobarométrie et Barométrie Géologiques,* M. Lagache, ed., Société Française de Minéralogie et Cristallographie, Paris. p. 489–596.

Kulbicki, G. and Millot, G., 1961. Diagenesis of Clays in Sedimentary and Petroliferous Series. Clays and Clay Minerals. v. 10, p. 329-330.

Leoni, L., 2001. New standardized illite crystallinity data from low-to very-low grade metamorphic rocks (Northern Apennines, Italy). European Journal of Mineralogy. v. 13, p. 1109-1118.

Li, G., Ravenhurst, C.E., and Zentilli, M., 1995. Implications of apatite fission track analysis for the thermal history of the Scotian Basin, offshore Nova Scotia, Canada. Bulletin of Canadian Petroleum Geology. v. 43, no. 2, p. 127-144

MacLean, B.C., and Wade, J.A., 1993. Seismic Markers and Stratigraphic Picks in the Scotian Basin Wells. East Coast Basin Atlas Series, Geological Survey of Canada, 276p.

McIlroy, D., Worden, R.H., and Needham, S.J., 2003. Faeces, clay minerals and reservoir potential. Journal of the Geological Society, London. v. 160, p. 489-493.

McIver, N., 1972. Mesozoic and Cenozoic stratigraphy of the Nova Scotia Shelf. Canadian Journal of Earth Science. v. 9, p. 54-70.

Merriman, R.J., and Kemp, S.J., 1996. Clay minerals and sedimentary basin maturity. Mineralogical Society Bulletin. v. 111, p. 7-8.

Merriman, R.J., and Frey, M., 1999. Pattern of very low-grade metamorphism in metapelitic rocks. In: Low-Grade Metamorphism, M. Frey and D. Robinson ed., Blackwell Science, Oxford, UK. p. 61-107.

Merriman, R.J., 2005. Clay minerals and sedimentary basin history. European Journal of Mineralogy. v. 17, p. 7-20.

Mongelli, G., Cullers, R.L., and Muelheisen, S., 1996. Geochemistry of Late Cretaceous – Oligocenic shales from the Varicolori Formation, southern Apennines, Italy: implications for mineralogical, grain-size control and provenance. European Journal of Mineralogy. v. 8, p. 733-754.

Moore, D.M., and Reynolds, R.C., 1997. X-ray diffraction and the identification and analysis of clay minerals. (2nd edition) New York: Oxford University Press.

Mudford, B.S., 1990. A one-dimensional, two phase model of overpressure generation in the Venture gas field, offshore Nova Scotia. Bulletin of Canadian Petroleum Geology. v. 38, p. 246–258.

O'Connor, B.H., and Chang, W-J., 1986. The amorphous character and particle size Distributions of powders produced with the Micronizing Mill for quantitative X-ray powder diffractometry. X-ray Spectrometry. v. 15, p. 267-270.

Odin, G. S., 1990, Clay mineral formation at the continent-ocean boundary: The verdine facies: Clay Minerals. v. 25, p. 477–483.

OETR 2011. Atlas: Play Fairway Analysis, Offshore Nova Scotia, Canada. Accessed May 2012 at http://www.novascotiaoffshore.com/analysis#atlas

Okwese, A., Pe-Piper, G., and Piper, D.J.W., 2011. Controls on regional variability in marine pore-water diagenesis below the seafloor in Upper Jurassic-Lower Cretaceous prodeltaic sandstone and shales, Scotian Basin, Eastern Canada. Marine and Petroleum Geology. v. 29, p. 175-191.

Pe-Piper, G. and Piper, D.J.W., 2004. The effects of strike-slip motion along the Cobequid-Chedabucto-SW Grand Banks fault system on the Cretaceous–Tertiary evolution of Atlantic Canada. Canadian Journal of Earth Sciences. v. 41, p. 799–808.

Pe-Piper, G., Dolansky, L., and Piper, D.J.W., 2005. Sedimentary environment and diagenesis of the Lower Cretaceous Chaswood Formation, southeastern Canada: The origin of kaolin-rich mudstones. Sedimentary Geology. v. 178, p. 75-97.

Pe-Piper, G. and MacKay, R.M., 2006. Provenance of Lower Cretaceous sandstones onshore and offshore Nova Scotia from electron microprobe geochronology and chemical variation of detrital monazite. Bulletin of Canadian Petroleum Geology. v. 54, p. 366–379

Pe-Piper, G., Piper, D.J.W., Jansa, L.F., and de Jonge, A., 2007. Early Cretaceous opening of the North Atlantic Ocean: Implications of the petrology and tectonic setting of the Fogo Seamounts off the SW Grand Banks, Newfoundland. Geological Society of America Bulletin. v. 119, p. 712-724.

Pe-Piper, G., Triantaphyllidis, S., Piper, D.J.W., Moulton, B., and Hubley, R.F., 2007. A lithological assessment of the Lower Cretaceous sediments of the Scotian Basin. Geological Survey of Canada, open file 5880.

Pe-Piper, G., and Weir-Murphy, S., 2008. Early diagenesis of inner-shelf phosphorite and iron-silicate minerals, Lower Cretaceous of the Orpheus graben, southeastern Canada: Implications for the origin of chlorite rims. AAPG Bulletin. v. 92, no. 9, p. 1153-1168.

Pe-Piper, G., Triantafyllidis, S., and Piper, D.J.W., 2008. Geochemical identification of clastic sediment provenance from known sources of similar geology: The Cretaceous Scotian Basin, Canada. Journal of Sedimentary Research. v. 78, p. 595-607.

Pe-Piper, G., Tsikouras, B., Piper, D.J.W., and Triantafyllidis, S., 2009. Chemical fingerprinting of detrital minerals in the Upper Jurassic–Lower Cretaceous sandstones, Scotian Basin. Geological Survey of Canada, Open File 6288.

Pe-Piper, G., and Piper, D.J.W., 2010. Volcanic ash in the Lower Cretaceous Chaswood Formation of Nova Scotia: source and implications. Canadian Journal of Earth Sciences. v. 47, p. 1427-1443.

Pe-Piper, G., Piper, D.J.W., LeFort, D., and Ledger-Piercey, S., 2011. Sediment provenance and diagenesis, Lower Cretaceous of the Alma K-85 well, Scotian Shelf. Geological Survey of Canada, Open File 6837.

Pe-Piper, G., and Piper, D.J.W., 2012. Cretaceous re-activation of the passive-margin Scotian Basin. Chapter 13 in Recent Advances in Tectonics of Sedimentary Basins, C. Busby and A. Azor (ed); p. 270-287.

Piper, D.J.W., Pe-Piper, G., Hundert, T., and Venugopal, D.V., 2007. The Lower Cretaceous Chaswood Formation in southern New Brunswick: provenance and tectonics. Canadian Journal of Earth Science. v. 44, p. 665-677.

Piper, D.J.W., Hundert, T., Pe-Piper, G., and Okwese, A.C., 2009. The roles of pedogenesis and diagenesis in clay mineral assemblages: Lower Cretaceous fluvial mudrocks, Nova Scotia, Canada. Sedimentary Geology. v. 213, p. 51-63.

Piper, D.J.W., Bowman, S.J., Pe-Piper, G., and MacRae, R. A., 2011. The ups and downs of Guysborough County – the mid Cretaceous Naskapi Member in the Scotian Basin: eustacy or tectonics? Atlantic Geoscience Society Abstracts, *37th Annual Colloquium & Annual General Meeting. Atlantic Geology, v. 47, p. 37-38.*

Piper, D.J.W., Pe-Piper, G., Tubrett, M., Triantaphyllidis, S., and Strathdee, G., Submitted. Detrital zircon geochronology and polycyclic sediment sources, Cretaceous Scotian Basin, southeastern Canada. Canadian Journal of Earth Sciences.

Potter, P.E., Maynard, J.B., and Pryor, W.A., 1980. Sedimentology of shale. Springer-Verlag, New York.

Reynolds, P.H., Pe-Piper, G., Piper, D.J.W. and Grist, A.M., 2009. Single-grain detrital muscovite ages from Lower Cretaceous sandstones, Scotian basin, and their implications for provenance. Bulletin of Canadian Petroleum Geology. v. 57, p. 25–42.

Reynolds, P.H., Pe-Piper, G., and Piper, D.J.W., Submitted. Detrital muscovite geochronology and the Cretaceous tectonics of the inner Scotian Shelf, southeastern Canada. Canadian Journal of Earth Sciences.

Ruffell, A.H., and Batten, D.J., 1990. The Barremian-Aptian arid phase in Western Europe. Palaeogeography, Palaeoclimatology, Palaeoecology. v.80, p. 197-212.

Ruffell, A.H., McKinley, J.M., and Worden, R.H., 2002. Comparison of clay mineral stratigraphy to other proxy palaeoclimate indicators in the Mesozoic of NW Europe. Philosophical Transactions of the Royal Society. v. 360, p. 675-693.

Shata, S., 2007. Illite crystallinity: Instrumental effect and its relation to crystallite size and lattice distortion. Z. Kristallogr. Suppl. v. 26, p. 11-116.

Shoval, S., and Zlatkin, O., 2009. Climatic changes during the Pliocene as observed from climate-sensitive rocks and clay minerals of the Sedom formation, the Dead Sea Basin. Clay Minerals. v. 44, p. 469–486.

Singer, A., and Stoffers, P., 1981. Hydrothermal vermiculite from the Atlantis II Deep, Red Sea. Clays and Clay Minerals. v. 29, p. 454-458.

Sladen, C.P., 1983. Trends in Early Cretaceous clay mineralogy in NW Europe. Zitteliana. v. 10, p. 251-259.

Srodon, J., Drits, V.A., McCarty, D.K., Hsieh, J.C.C., and Eberl, D.D., 2001. Quantitative X-ray diffraction analysis of clay-bearing rocks from random preparations. Clays and Clay Minerals. v. 49, no. 6, p. 514-528.

Stea, R. and Pullan, S., 2001. Hidden Cretaceous basins in Nova Scotia. Canadian Journal of Earth Sciences. v. 38, p. 1335–1354.

Strathdee, G., 2010. Determining the provenance of the Chaswood Formation using optical microscopy, geochemical analysis and hot-cathode cathodoluminescent microscopy. Honours Thesis, Saint Mary's University.

Triantafyllidis, S., Pe-Piper, G., MacKay, R., Piper, D.J.W., and Strathdee, G., 2010. Monazite as a provenance indicator for the Lower Cretaceous reservoir sandstones, Scotian Basin. Geological Survey of Canada, Open File 6732.

Tsikouras, B., Pe-Piper, G., Piper, D.J.W., and Schaffer, M., 2011. Varietal heavy mineral analysis of sediment provenance, Lower Cretaceous Scotian Basin, eastern Canada. Sedimentary Geology. v. 237, p. 150-165.

Tucholke, B.E., Sawyer, D.S. and Sibuet, J.-C., 2007. Breakup of the Newfoundland–Iberia rift. Geological Society of London Special Publication 282, p. 9–46.

Wadden, J., 2003. Clay mineralogy of the Cretaceous shales of the wells: Alma (F-67), Chebucto (K-90), Glenelg (J-48), and Thebaud (C-74). Honours Thesis, Saint Mary's University.

Wade, J.A., and MacLean, B.C., 1990. The geology of the southeastern margin of Canada, Chapter 5 in Geology of the Continental Margin of Eastern Canada, M.J. Keen and G.L. Williams (ed); Geological Survey of Canada, Geology of Canada. no. 2, p. 167-238.

Walker, G.F., 1956. The mechanism of dehydration of Mg-vermiculite. Clays and Clay Minerals. v. 4, p. 101-115.

Way, D.S., 1973. Terrain analysis: A guide to site selection using aerial photographic interpretation. Dowden, Hutchinson and Ross, Stroudsburg, Pa.

Warr, L.N., and Rice, A.H.N., 1994. lnterlaboratory standardization and calibration of clay mineral crystallinity and crystallite size data. Journal of Metamorphic Geology. v. 12, p. 141-152.

Weir-Murphy, S.L., 2004. The Cretaceous rocks of the Orpheus Graben, offshore Nova Scotia. Masters Thesis, Saint Mary's University.

Wierzbicki, R., Dravis, J., Al-Aasm, I., and Harland, N. 2006. Burial dolomitization and dissolution of upper Jurassic Abenaki platform carbonates, Deep Panuke reservoir, Nova Scotia, Canada. American Association of Petroleum Geology. v. 90, no. 11, p. 1843-1861.

Zhang, Y.Y., Pe-Piper, G., and Piper, D.J.W., Submitted. Tectonism and volcanism in the middle Mesozoic of the Scotian Basin, offshore eastern Canada: success and limitations of bulk geochemistry as a provenance indicator.

APPENDIX 1:
X-RAY DIFFRACTION OF <2 MICRON SAMPLES

K85-2449.4
Logan Canyon Formation
(Cree Member)

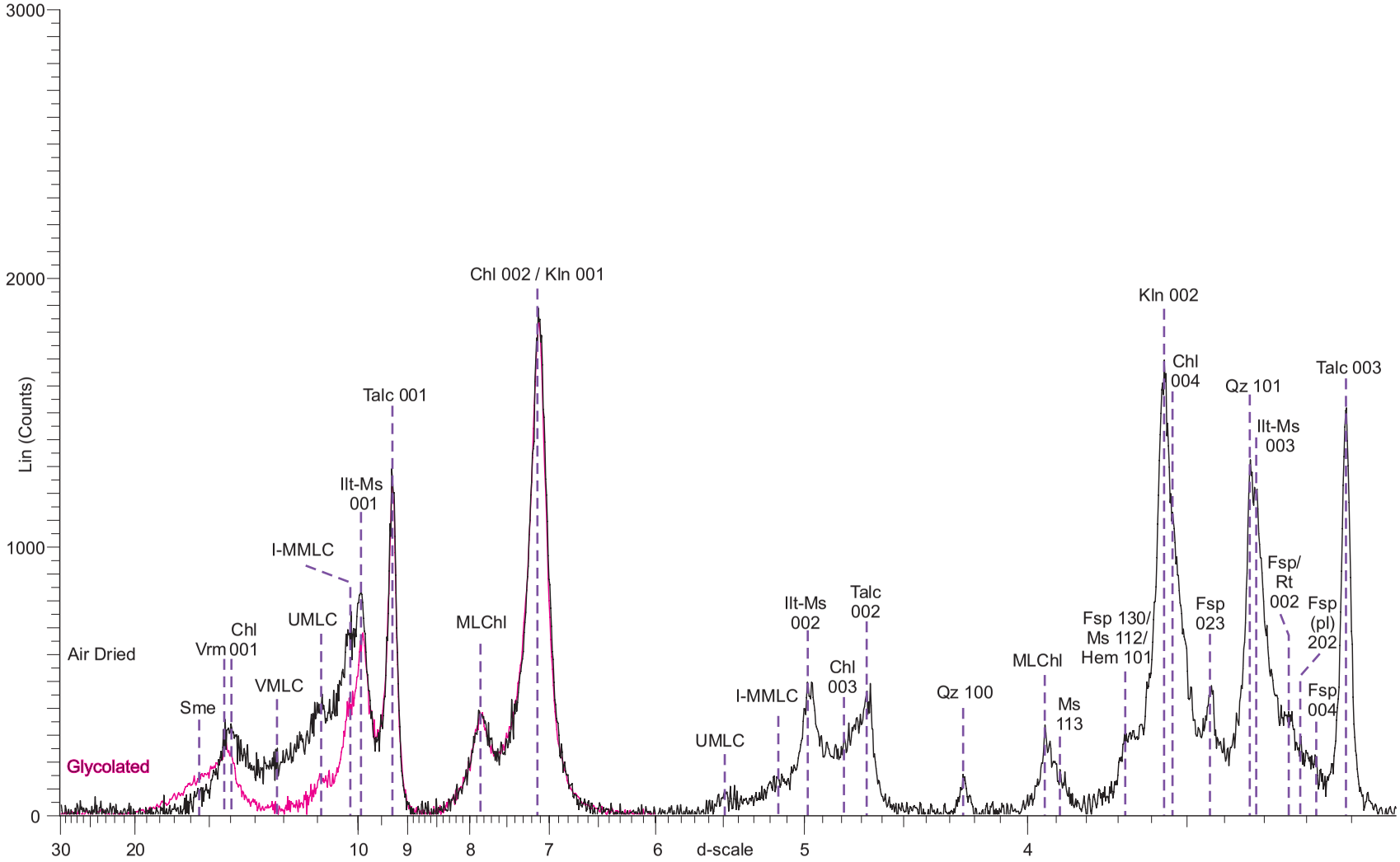

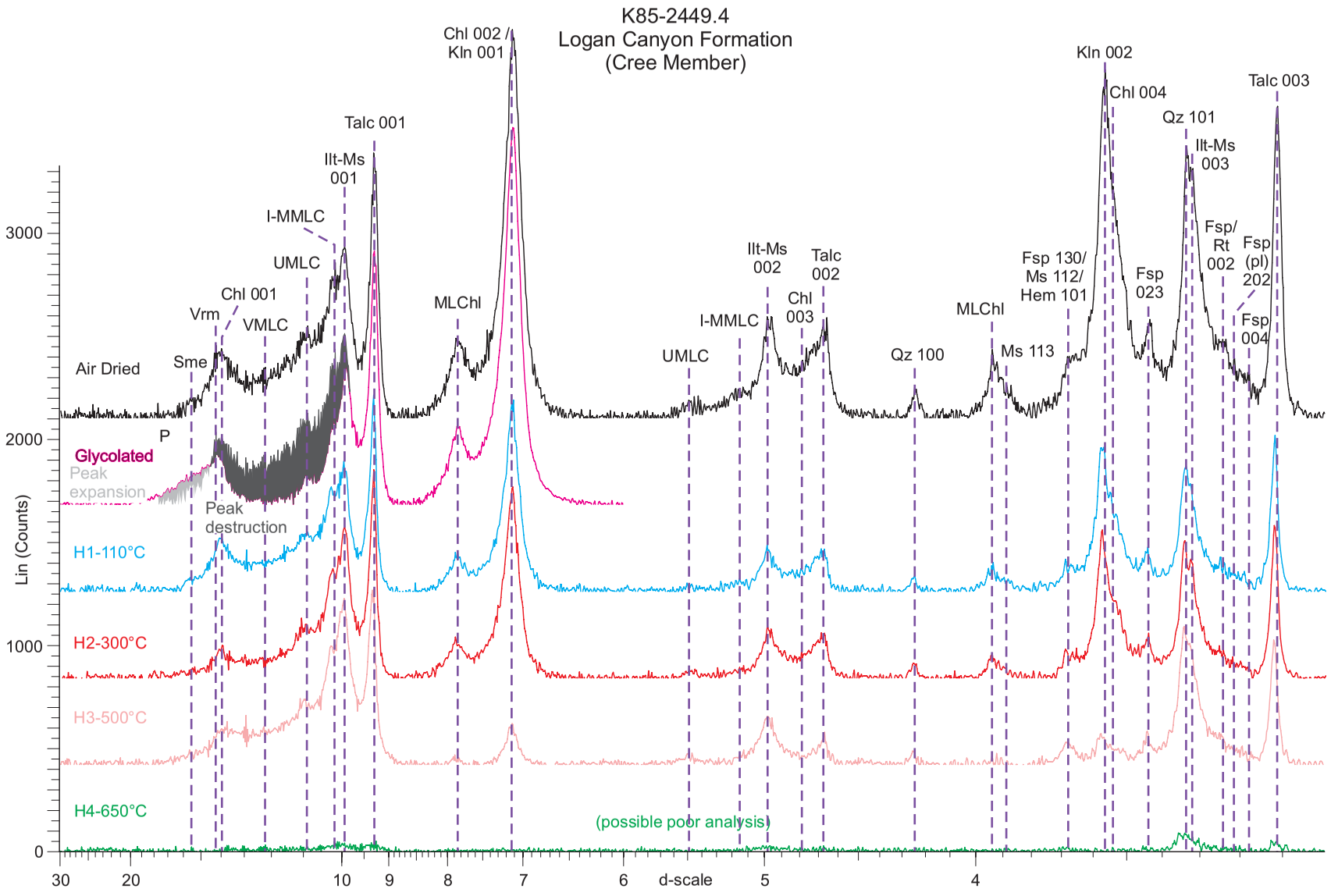
K85-2449.4
Logan Canyon Formation
(Cree Member)
Chl 002 /
Kln 001
Talc 001
Ilt-Ms
001
I-MMLC
UMLC
Chl 001
Vrm
VMLC
Sme
Air Dried
P
MLChl
Ilt-Ms
002
Talc
002
Chl
003
I-MMLC
UMLC
Qz 100
MLChl
Ms 113
Fsp 130/
Ms 112/
Hem 101
Kln 002
Chl 004
Fsp
023
Qz 101
Ilt-Ms
003
Fsp/
Rt
002
Fsp
(pl)
202
Fsp
004
Talc 003
Glycolated
Peak
expansion
Peak
destruction
H1-110°C
H2-300°C
H3-500°C
H4-650°C
(possible poor analysis)
Lin (Counts)
3000
2000
1000
0
30
20
10
9
8
7
6
d-scale
5
4

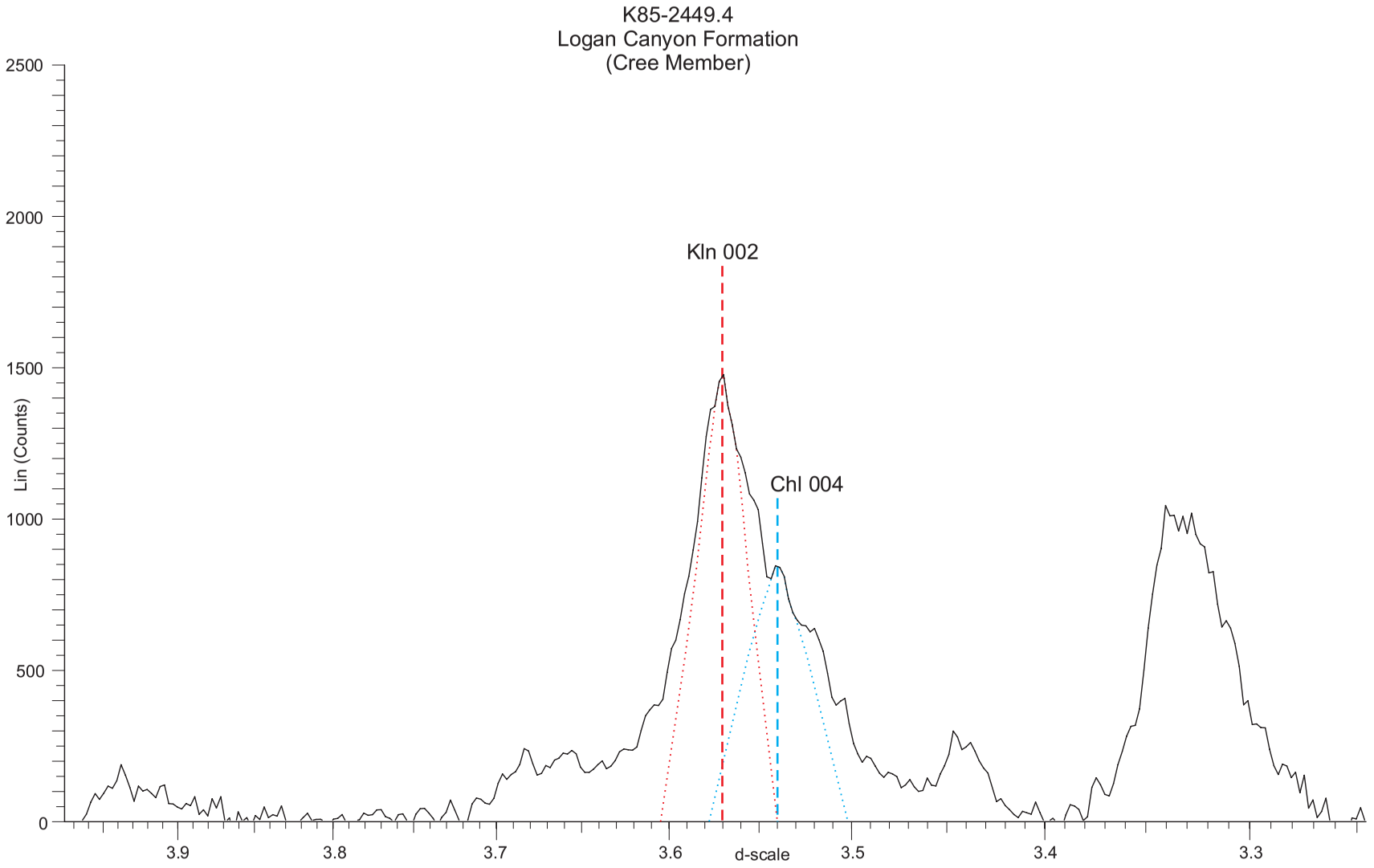
K85-2449.4
Logan Canyon Formation
(Cree Member)
Kln 002
Chl 004
Lin (Counts)
2500
2000
1500
1000
500
0
3.9
3.8
3.7
3.6
d-scale
3.5
3.4
3.3

K85-2904.15
Missisauga Formation

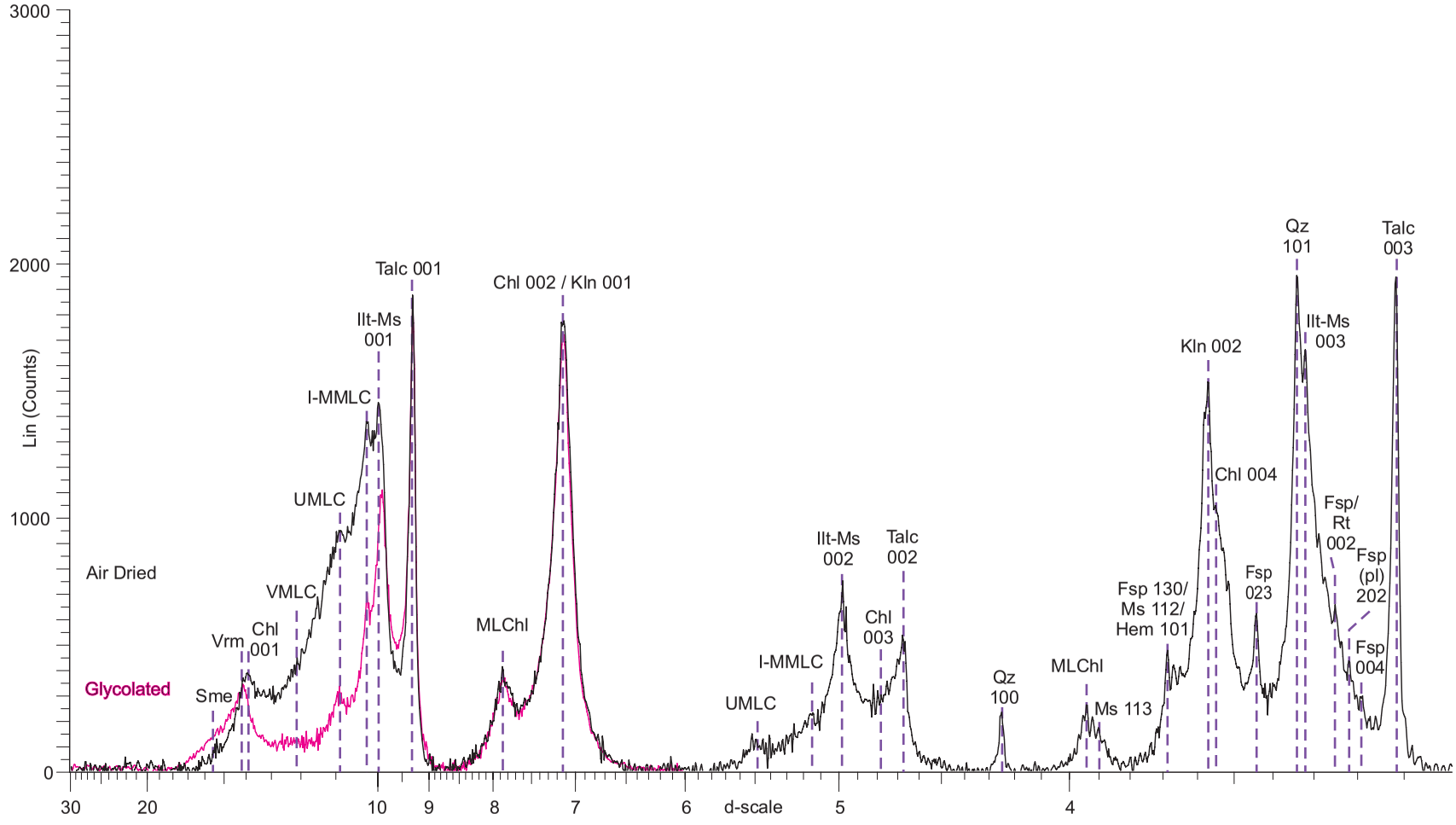

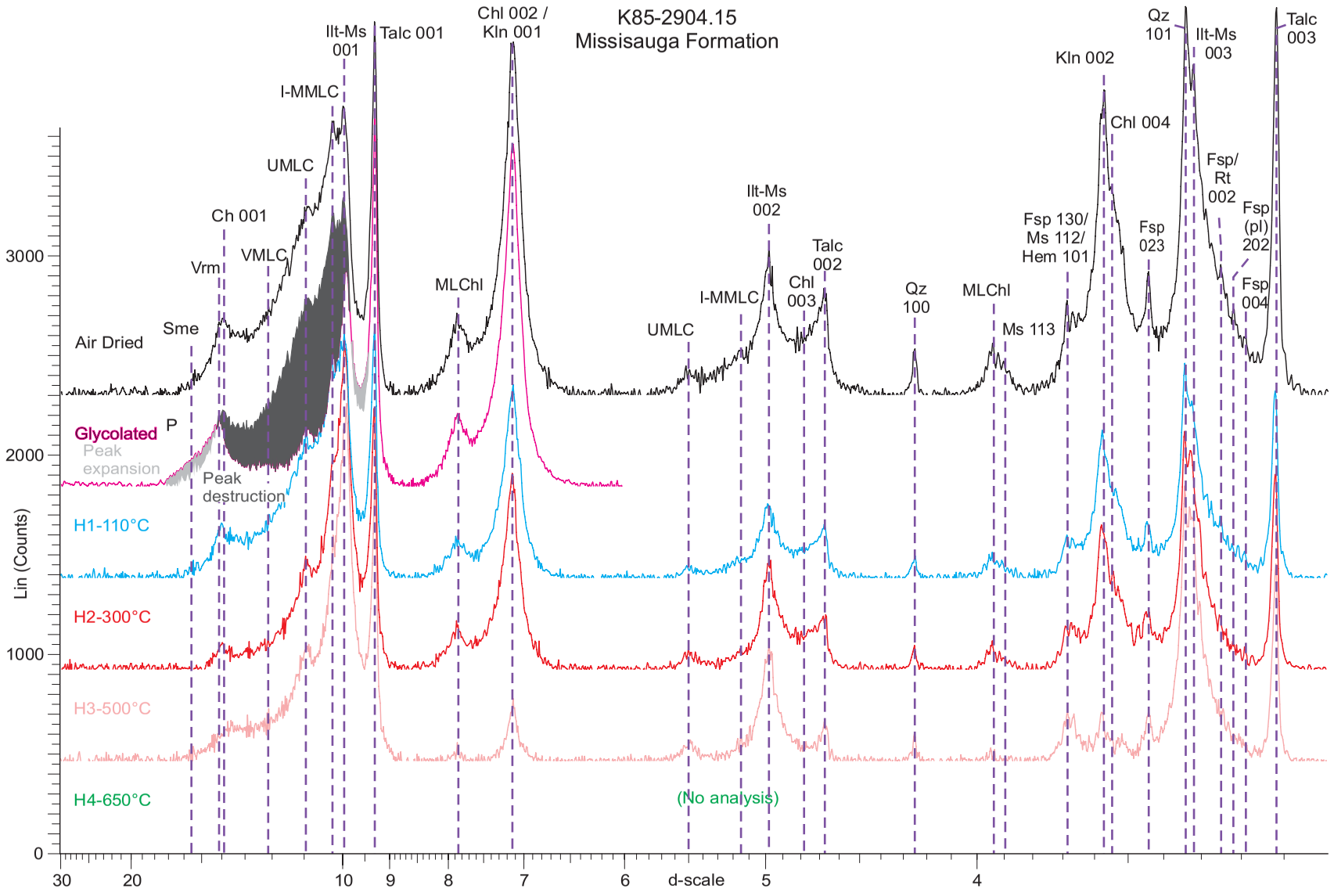
K85-2904.15
Missisauga Formation
Air Dried
Glycolated
Peak expansion
Peak destruction
H1-110°C
H2-300°C
H3-500°C
H4-650°C
(No analysis)
Lin (Counts)
d-scale
Sme
Vrm
Ch 001
VMLC
UMLC
I-MMLC
Ilt-Ms 001
Talc 001
MLChl
Chl 002 / Kln 001
Ilt-Ms 002
Chl 003
Talc 002
Qz 100
Ms 113
Fsp 130/ Ms 112/ Hem 101
Kln 002
Chl 004
Fsp 023
Qz 101
Ilt-Ms 003
Fsp/ Rt 002
Fsp (pl) 202
Fsp 004
Talc 003

K85-2904.15
Missisauga Formation

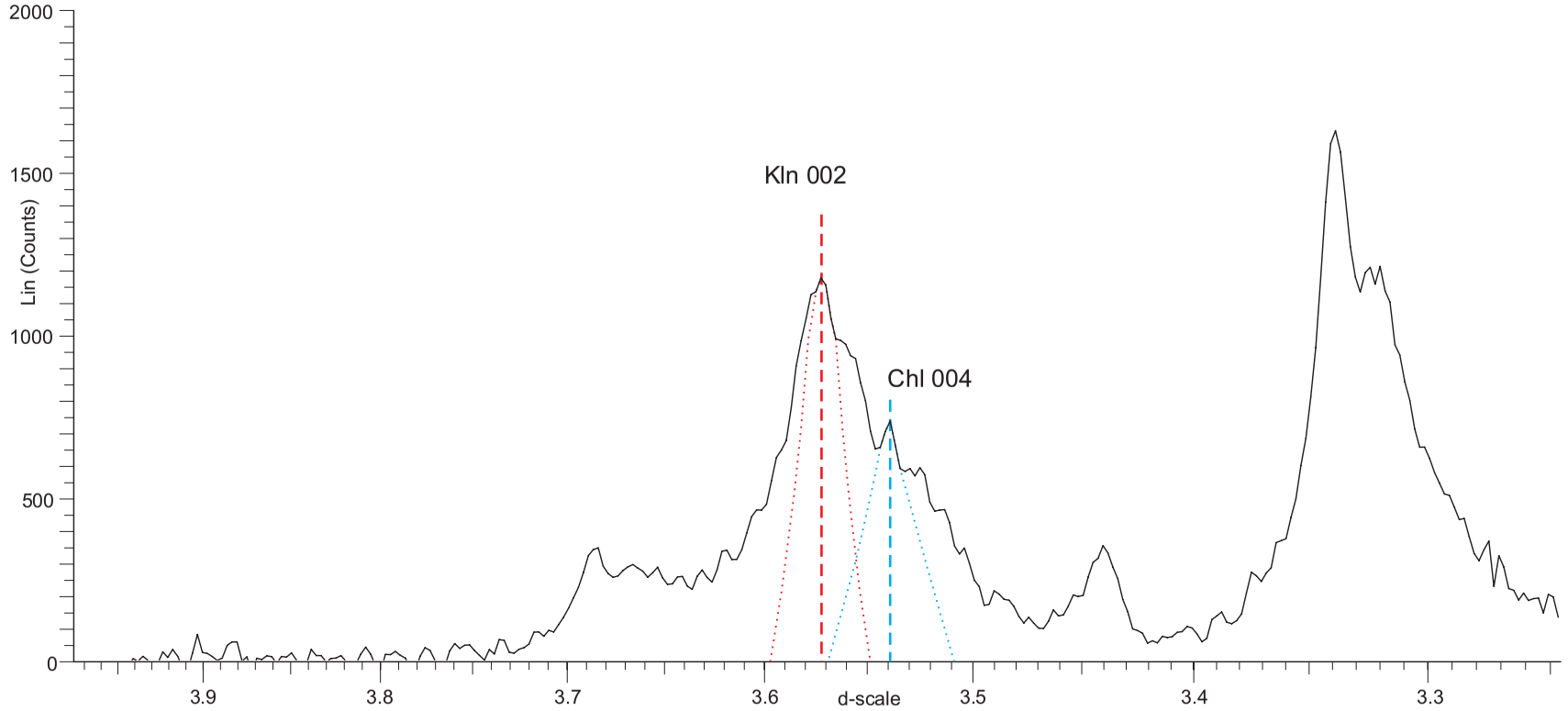

K85-3039.88
Missisauga Formation

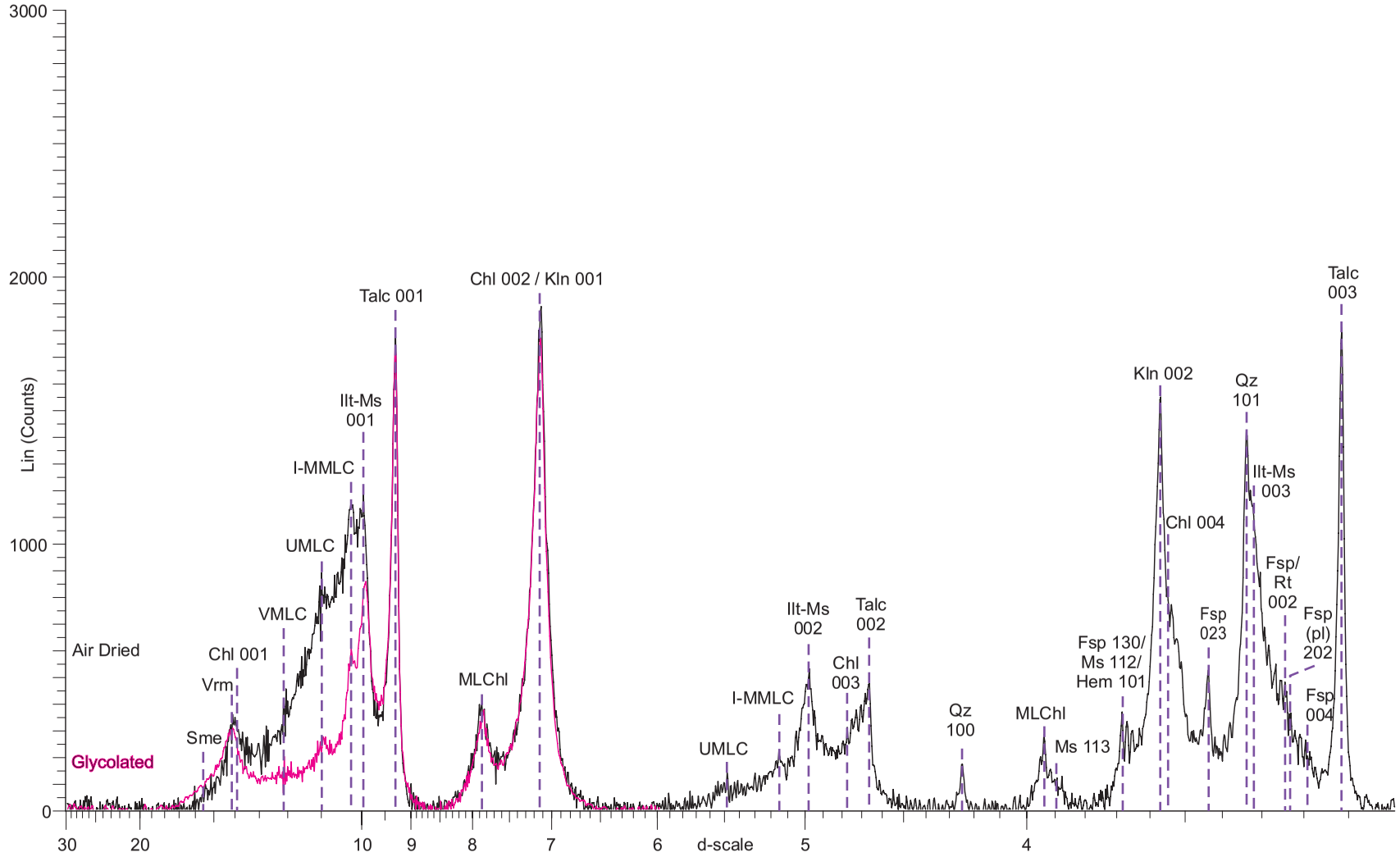

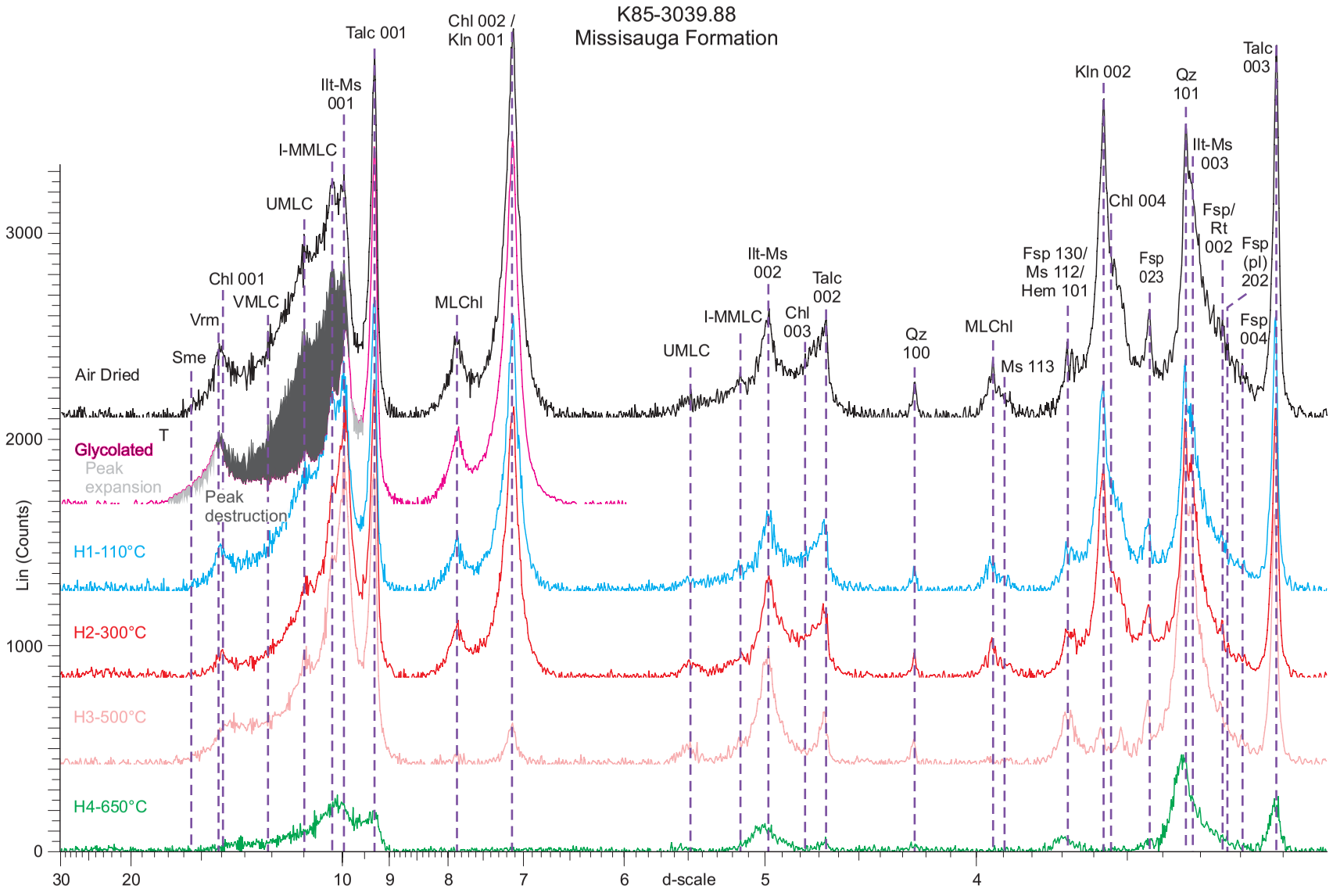
K85-3039.88
Missisauga Formation
Talc 001
Chl 002 /
Kln 001
Ilt-Ms
001
I-MMLC
UMLC
Chl 001
VMLC
Vrm
Sme
MLChl
Air Dried
T
Glycolated
Peak
expansion
Peak
destruction
H1-110°C
H2-300°C
H3-500°C
H4-650°C
Lin (Counts)
3000
2000
1000
0
30
20
10
9
8
7
6
d-scale
5
4
UMLC
I-MMLC
Ilt-Ms
002
Chl
003
Talc
002
Qz
100
MLChl
Ms 113
Fsp 130/
Ms 112/
Hem 101
Kln 002
Chl 004
Fsp
023
Qz
101
Ilt-Ms
003
Fsp/
Rt
002
Fsp
(pl)
202
Fsp
004
Talc
003

K85-3039.88
Missisauga Formation

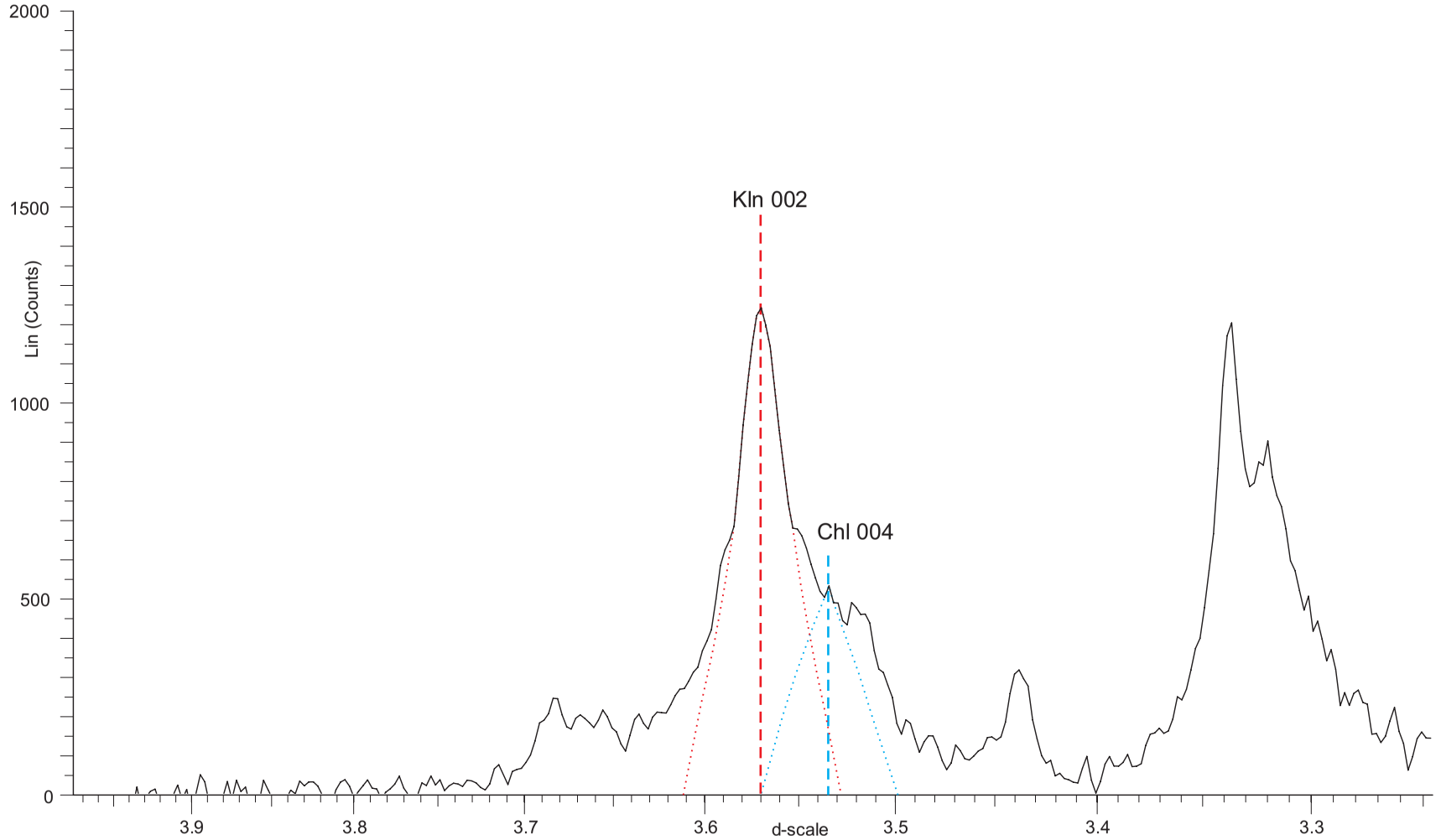

K85-3104.1
Verrill Canyon Formation

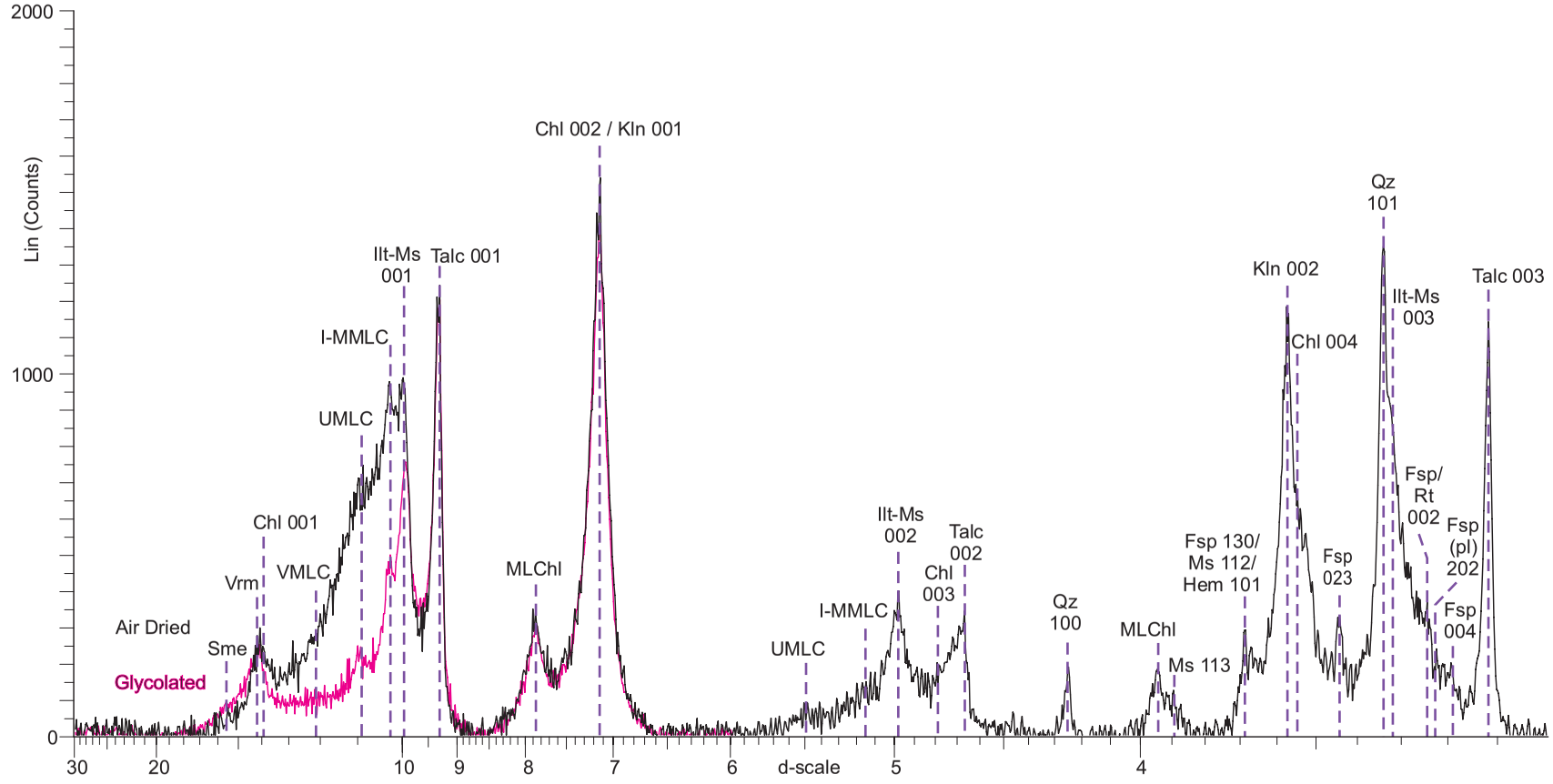

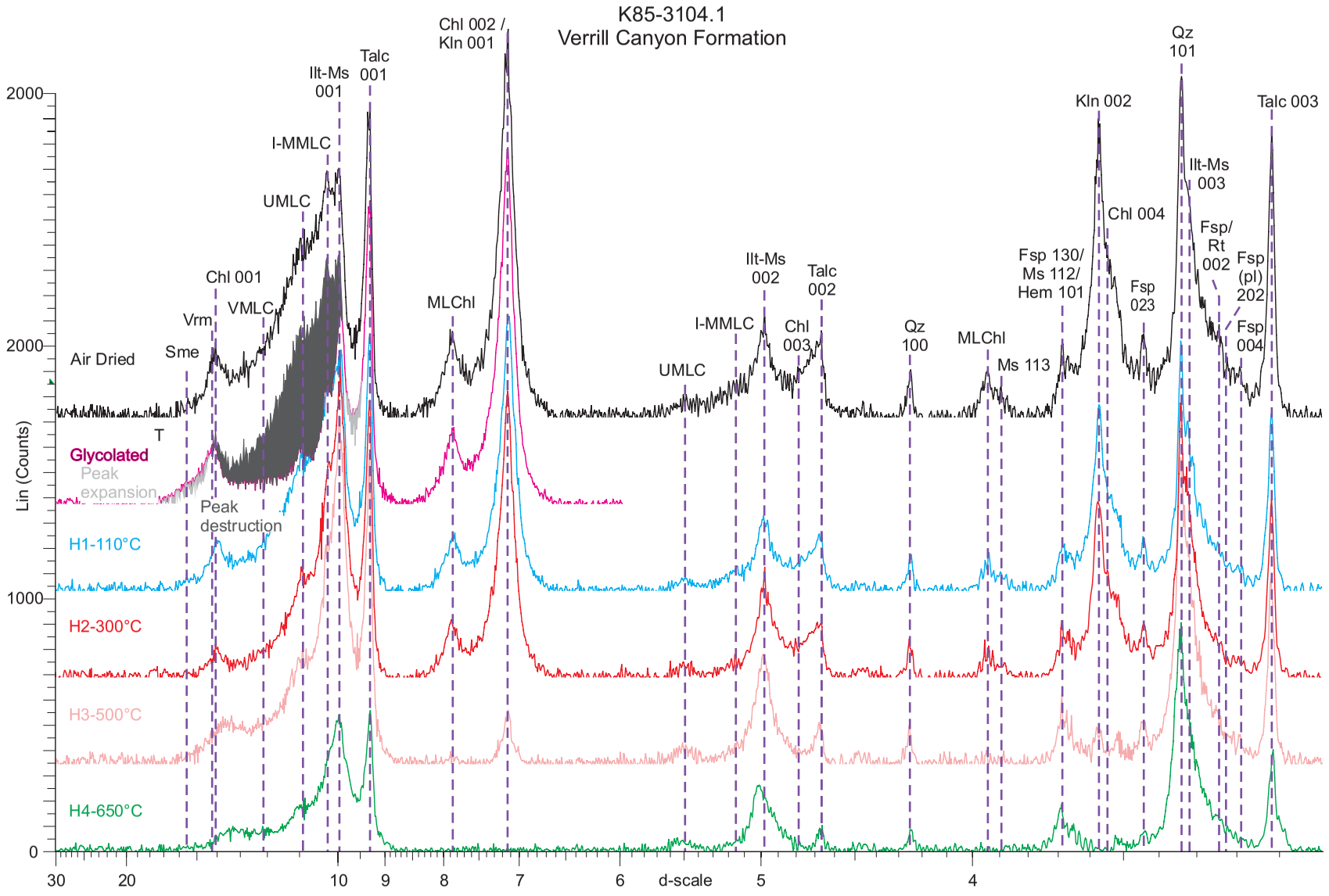
K85-3104.1
Verrill Canyon Formation
Air Dried
Glycolated
Peak expansion
Peak destruction
H1-110°C
H2-300°C
H3-500°C
H4-650°C
T
Sme
Vrm
Chl 001
VMLC
UMLC
I-MMLC
Ilt-Ms 001
Talc 001
Chl 002 / Kln 001
MLChl
UMLC
I-MMLC
Ilt-Ms 002
Chl 003
Talc 002
Qz 100
MLChl
Ms 113
Fsp 130/ Ms 112/ Hem 101
Kln 002
Chl 004
Fsp 023
Qz 101
Ilt-Ms 003
Fsp/ Rt 002
Fsp (pl) 202
Fsp 004
Talc 003
Lin (Counts)
2000
2000
1000
0
30
20
10
9
8
7
6
d-scale
5
4

K85-3104.1
Verrill Canyon Formation

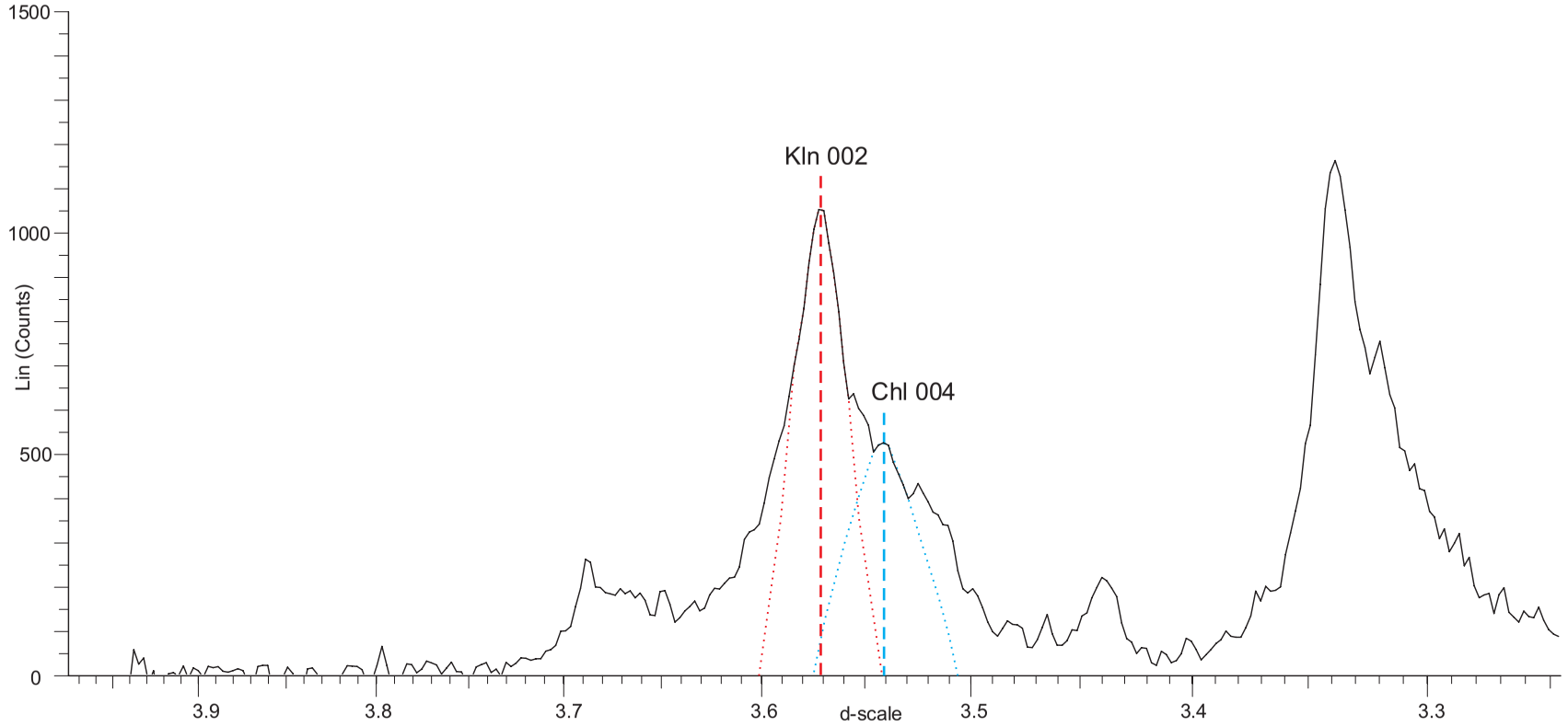

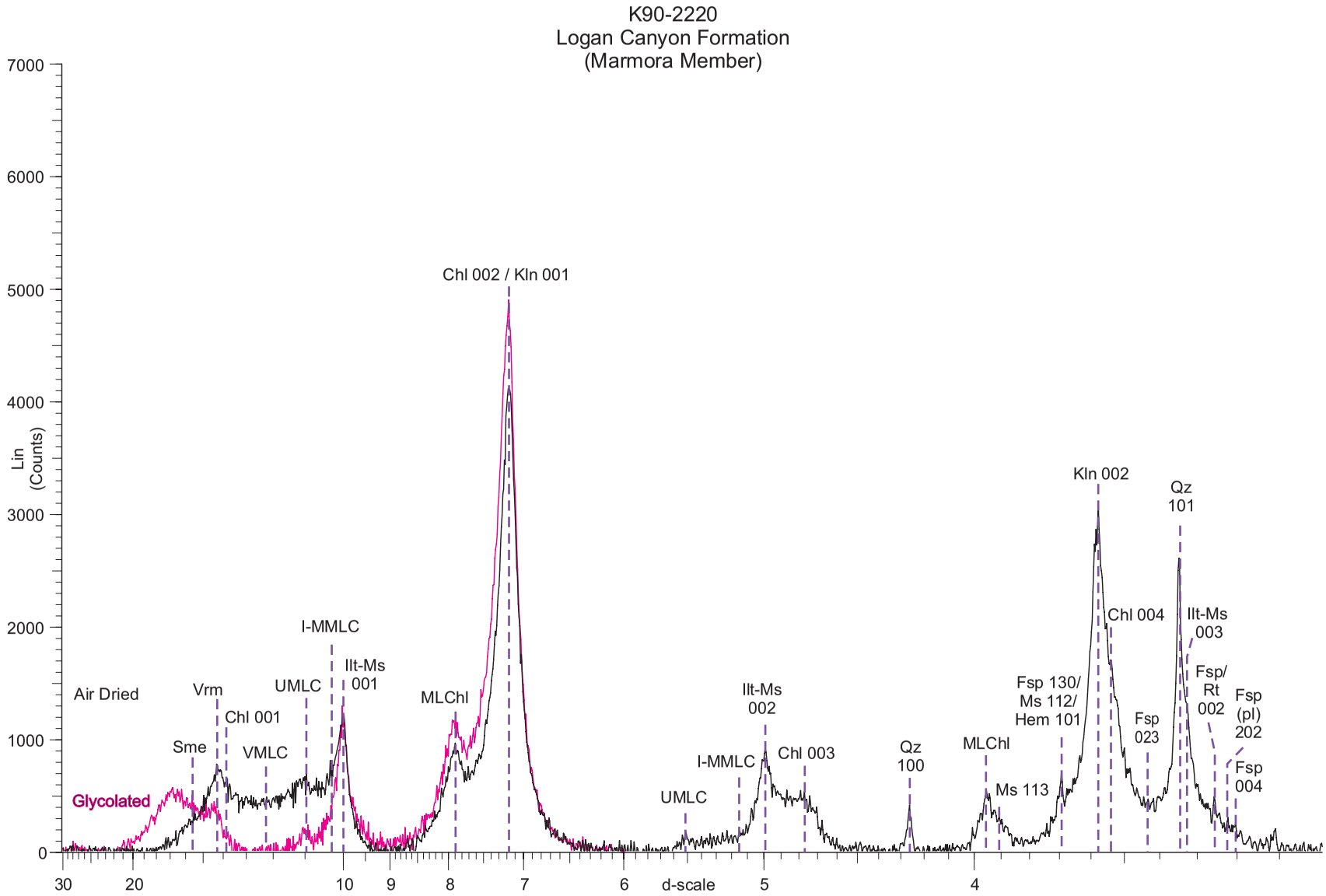
K90-2220
Logan Canyon Formation
(Marmora Member)
Lin (Counts)
7000
6000
5000
4000
3000
2000
1000
0
Air Dried
Glycolated
Sme
Vrm
Chl 001
VMLC
UMLC
I-MMLC
Ilt-Ms 001
MLChl
Chl 002 / Kln 001
UMLC
I-MMLC
Ilt-Ms 002
Chl 003
Qz 100
MLChl
Ms 113
Fsp 130/ Ms 112/ Hem 101
Kln 002
Chl 004
Fsp 023
Qz 101
Ilt-Ms 003
Fsp/ Rt 002
Fsp (pl) 202
Fsp 004
30
20
10
9
8
7
6
d-scale
5
4

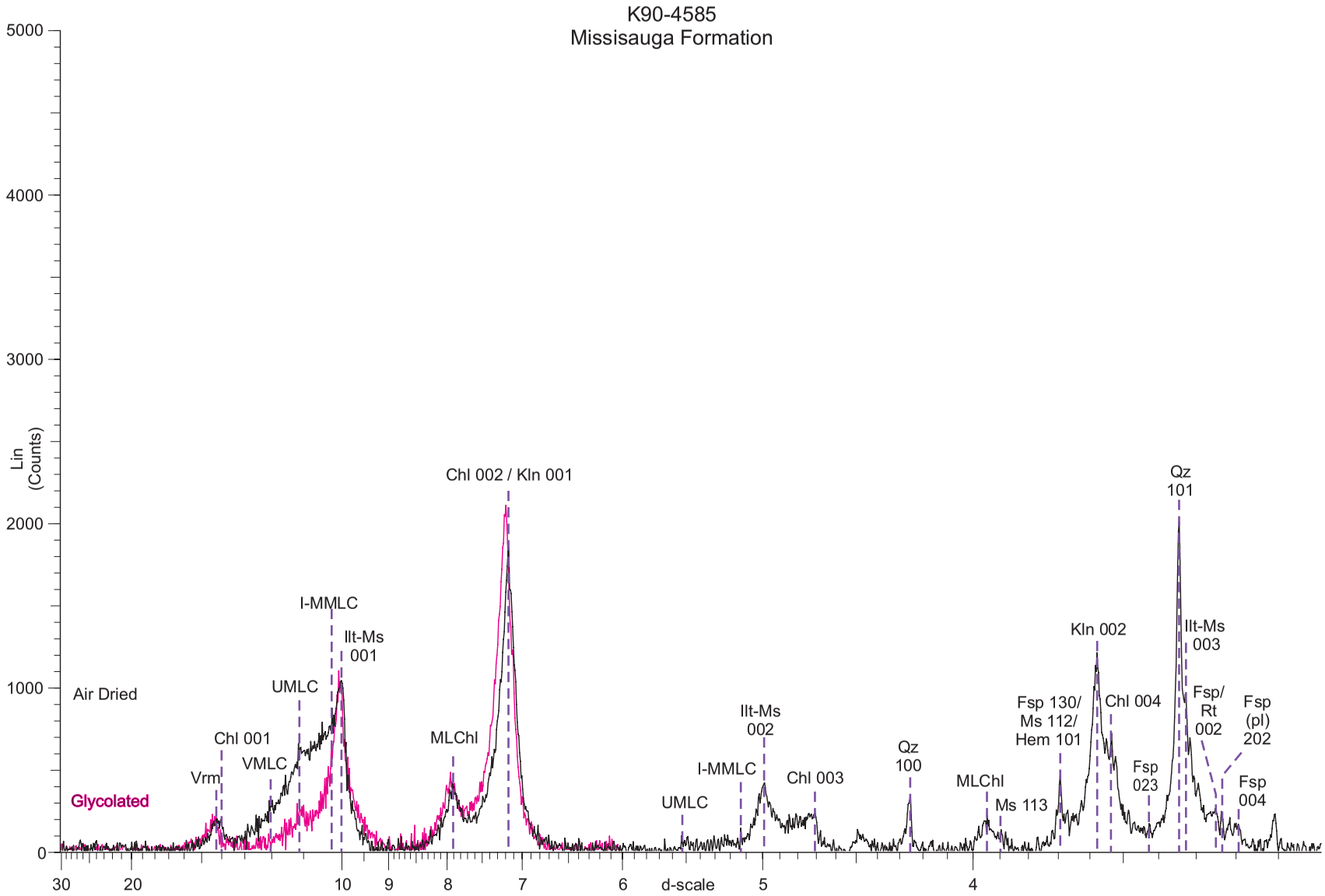
K90-4585
Missisauga Formation
Lin (Counts)
5000
4000
3000
2000
1000
0
Air Dried
Glycolated
Vrm
Chl 001
VMLC
UMLC
I-MMLC
Ilt-Ms 001
MLChl
Chl 002 / Kln 001
UMLC
I-MMLC
Ilt-Ms 002
Chl 003
Qz 100
MLChl
Ms 113
Fsp 130/ Ms 112/ Hem 101
Kln 002
Chl 004
Fsp 023
Qz 101
Ilt-Ms 003
Fsp/ Rt 002
Fsp (pl) 202
Fsp 004
30
20
10
9
8
7
6
d-scale
5
4

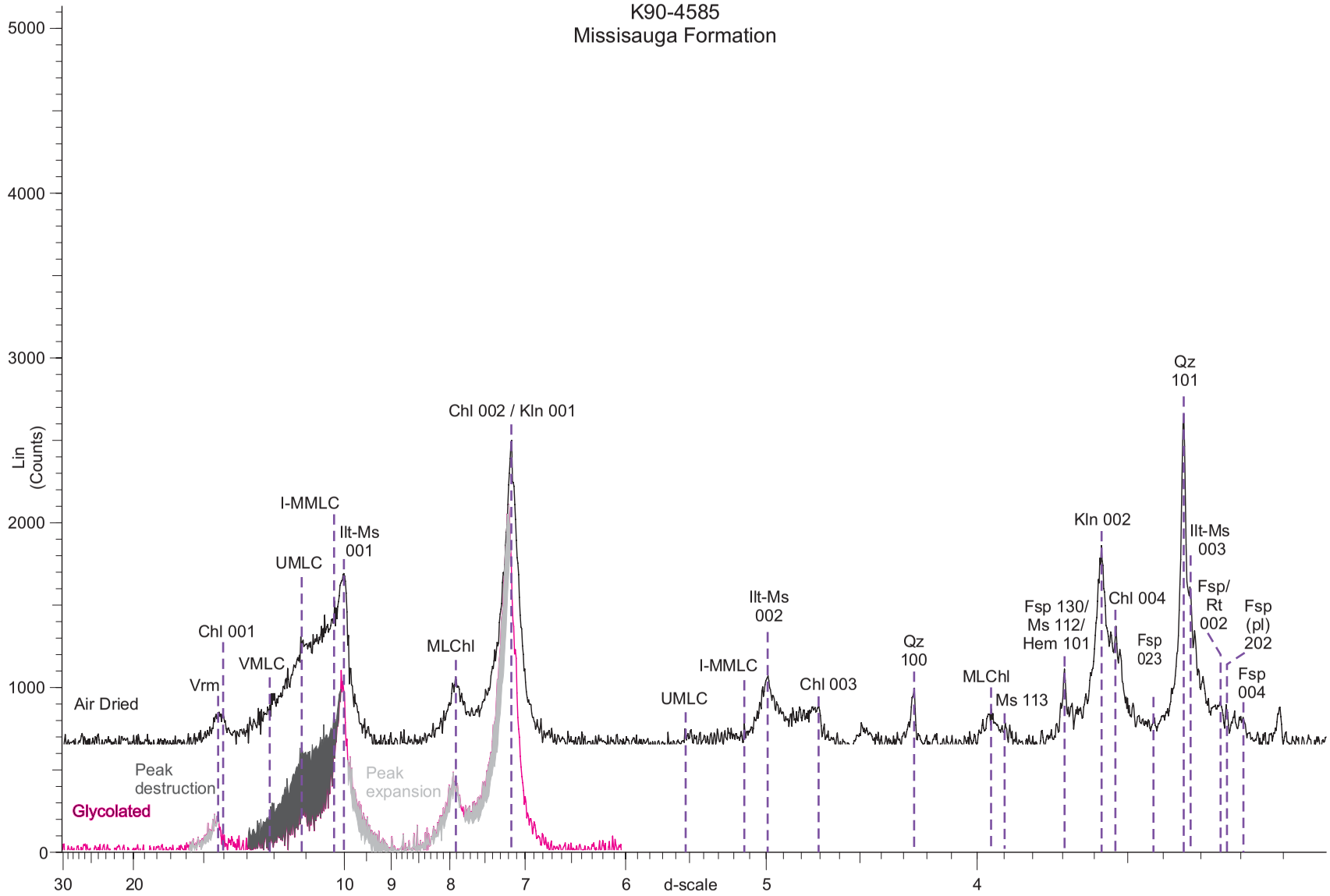
K90-4585
Missisauga Formation
Lin (Counts)
5000
4000
3000
2000
1000
0
30
20
10
9
8
7
6
d-scale
5
4
Air Dried
Vrm
Chl 001
VMLC
UMLC
I-MMLC
Ilt-Ms 001
MLChl
Chl 002 / Kln 001
UMLC
I-MMLC
Ilt-Ms 002
Chl 003
Qz 100
MLChl
Ms 113
Fsp 130/ Ms 112/ Hem 101
Kln 002
Chl 004
Fsp 023
Qz 101
Ilt-Ms 003
Fsp/ Rt 002
Fsp (pl) 202
Fsp 004
Peak destruction
Glycolated
Peak expansion

K90-5120
Missisauga Formation

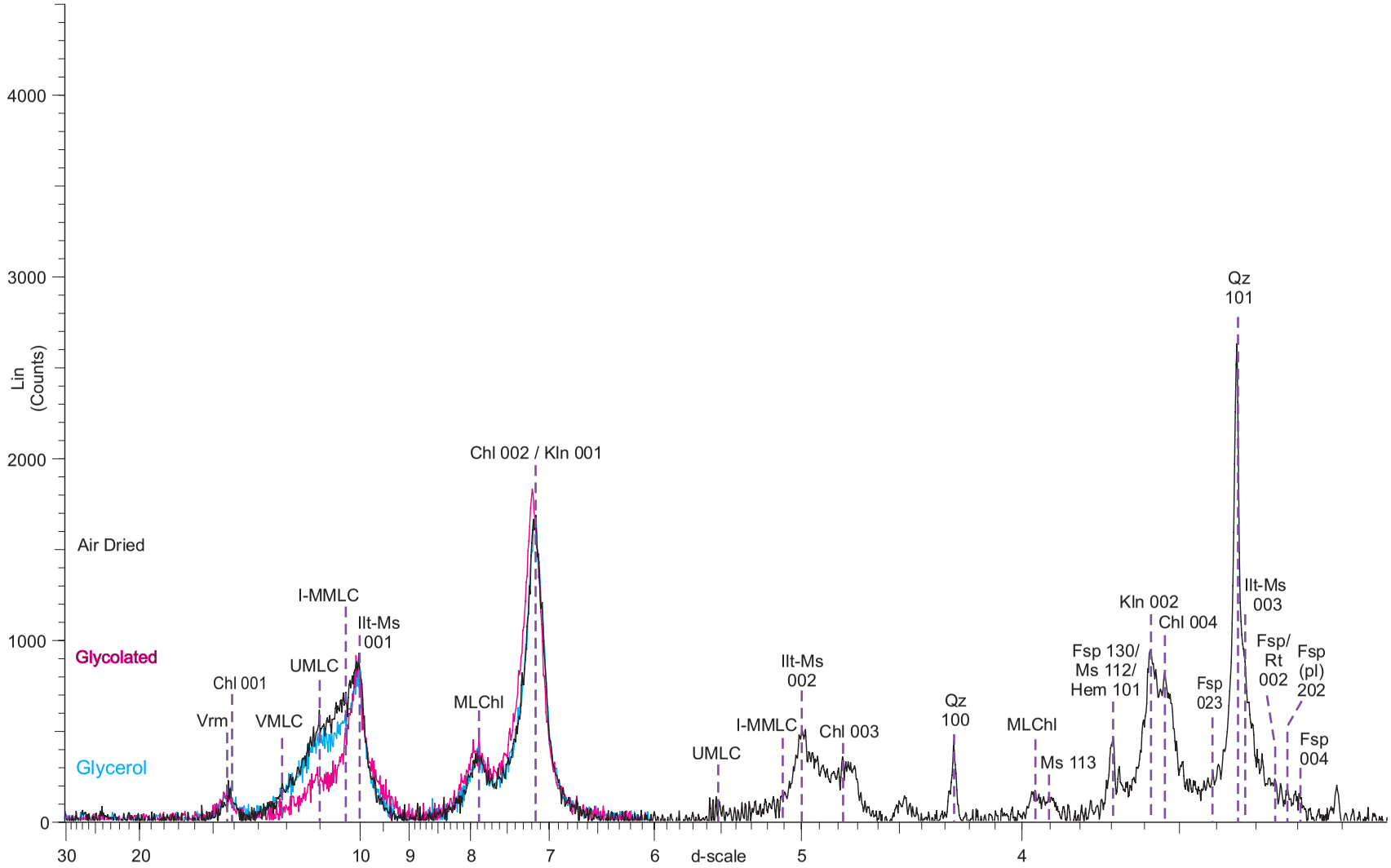

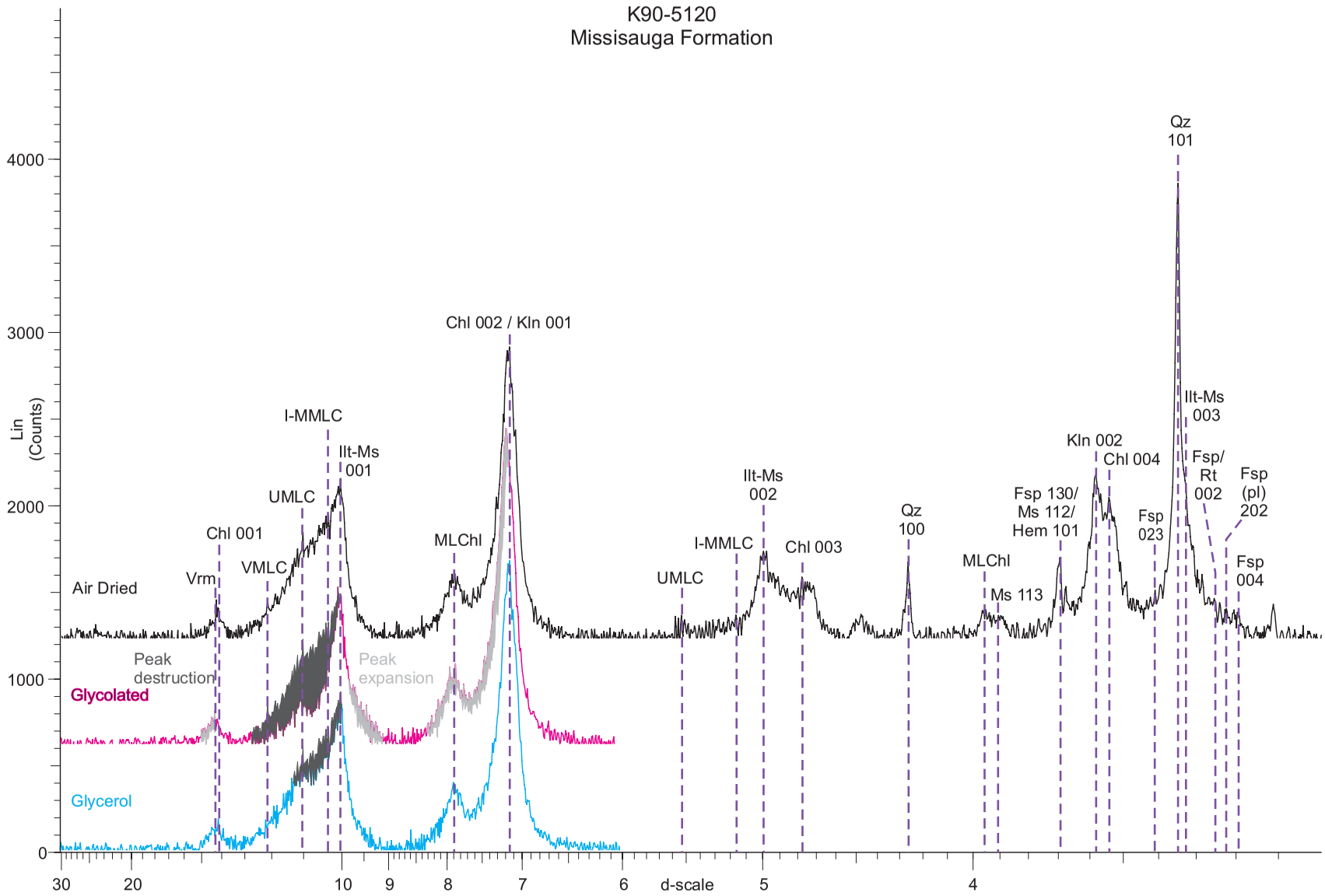
K90-5120
Missisauga Formation
Lin (Counts)
4000
3000
2000
1000
0
Air Dried
Vrm
Chl 001
VMLC
UMLC
I-MMLC
Ilt-Ms 001
MLChl
Chl 002 / Kln 001
UMLC
I-MMLC
Ilt-Ms 002
Chl 003
Qz 100
MLChl
Ms 113
Fsp 130/ Ms 112/ Hem 101
Kln 002
Chl 004
Fsp 023
Qz 101
Ilt-Ms 003
Fsp/ Rt 002
Fsp (pl) 202
Fsp 004
Peak destruction
Glycolated
Peak expansion
Glycerol
30
20
10
9
8
7
6
d-scale
5
4

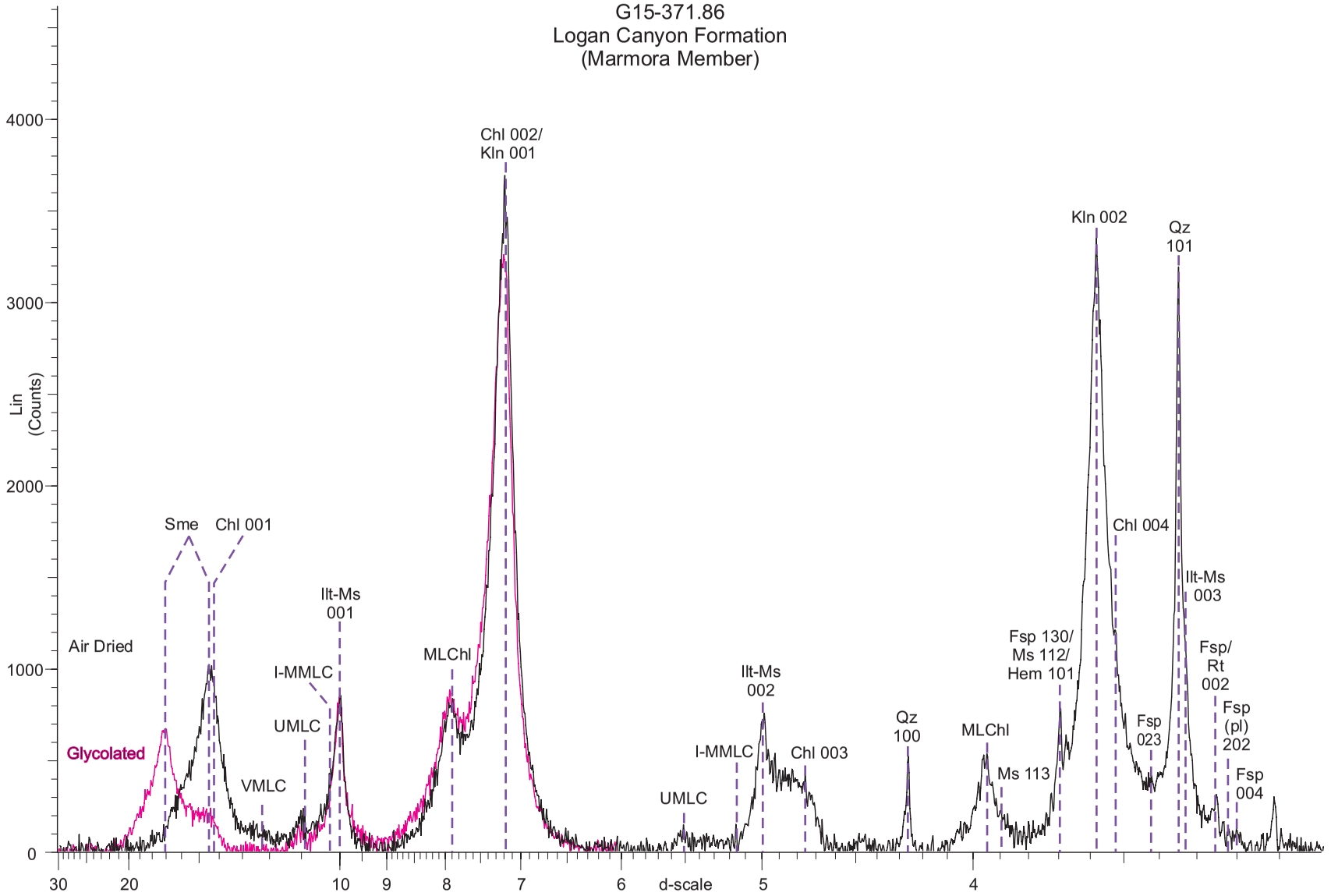
G15-371.86
Logan Canyon Formation
(Marmora Member)
Lin (Counts)
4000
3000
2000
1000
0
Air Dried
Glycolated
Sme
Chl 001
VMLC
I-MMLC
UMLC
Ilt-Ms 001
MLChl
Chl 002/ Kln 001
UMLC
I-MMLC
Ilt-Ms 002
Chl 003
Qz 100
MLChl
Ms 113
Fsp 130/ Ms 112/ Hem 101
Kln 002
Fsp 023
Chl 004
Qz 101
Ilt-Ms 003
Fsp/ Rt 002
Fsp (pl) 202
Fsp 004
30
20
10
9
8
7
6
d-scale
5
4

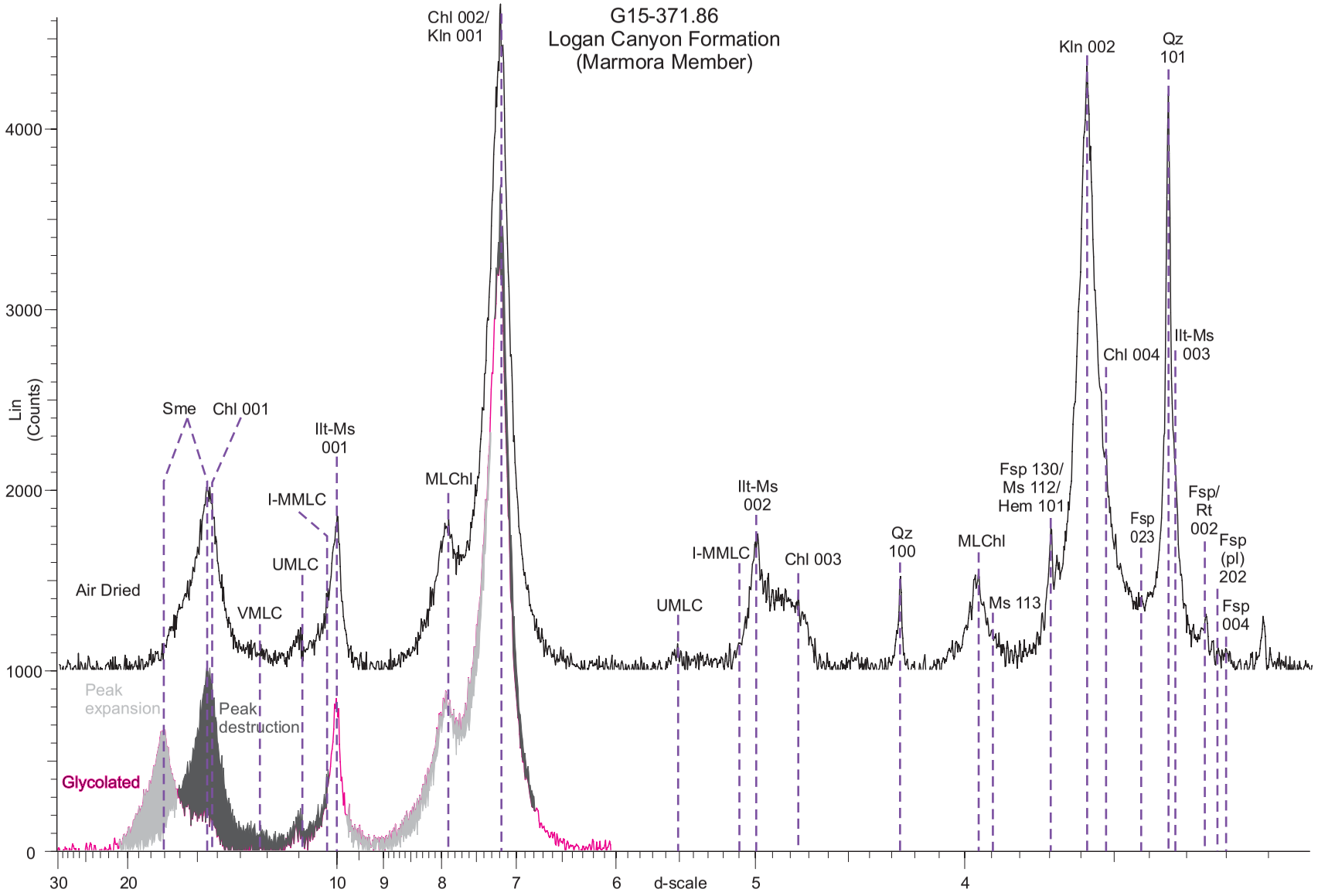
G15-371.86
Logan Canyon Formation
(Marmora Member)
Lin
(Counts)
4000
3000
2000
1000
0
Chl 002/
Kln 001
Kln 002
Qz
101
Sme
Chl 001
Ilt-Ms
001
MLChl
I-MMLC
Ilt-Ms
002
Fsp 130/
Ms 112/
Hem 101
Chl 004
Ilt-Ms
003
Fsp/
Rt
002
Fsp
023
Fsp
(pl)
202
Fsp
004
Air Dried
UMLC
VMLC
I-MMLC
Chl 003
Qz
100
MLChl
Ms 113
UMLC
Peak
expansion
Peak
destruction
Glycolated
30
20
10
9
8
7
6
d-scale
5
4

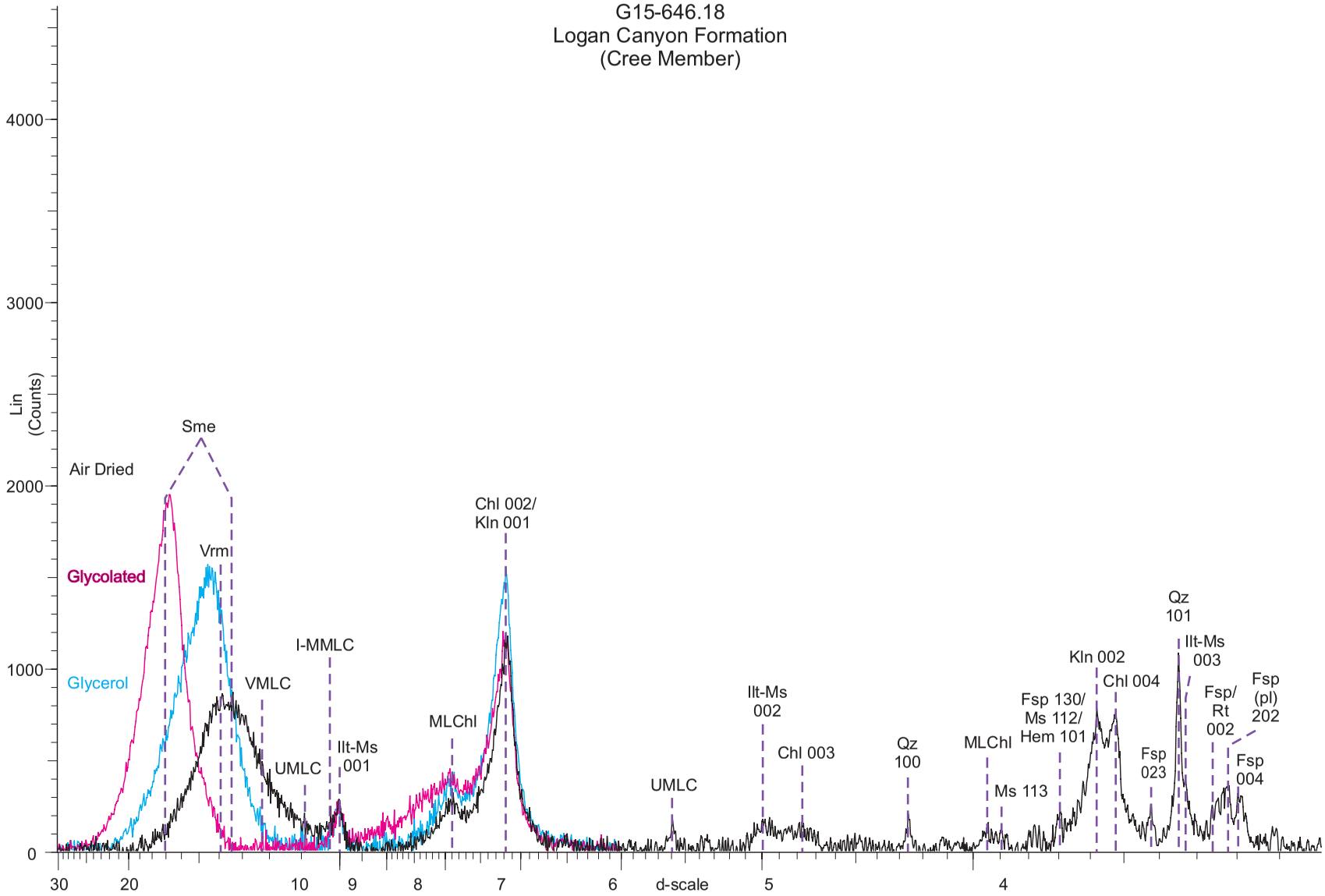
G15-646.18
Logan Canyon Formation
(Cree Member)
Lin (Counts)
4000
3000
2000
1000
0
Air Dried
Glycolated
Glycerol
Sme
Vrm
VMLC
UMLC
I-MMLC
Ilt-Ms 001
MLChl
Chl 002/ Kln 001
UMLC
Ilt-Ms 002
Chl 003
Qz 100
MLChl
Ms 113
Fsp 130/ Ms 112/ Hem 101
Kln 002
Chl 004
Fsp 023
Qz 101
Ilt-Ms 003
Fsp/ Rt 002
Fsp (pl) 202
Fsp 004
30
20
10
9
8
7
6
d-scale
5
4

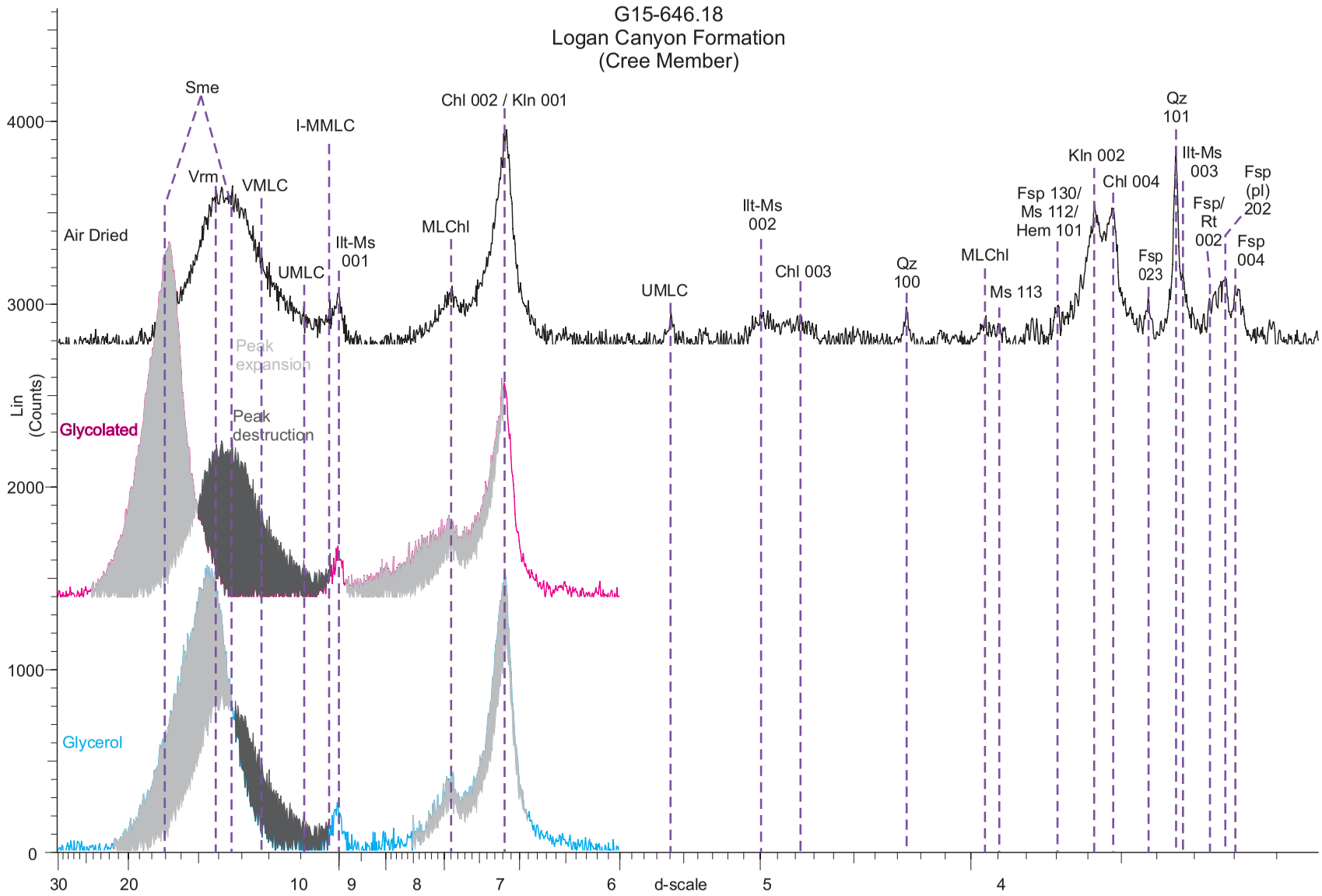
G15-646.18
Logan Canyon Formation
(Cree Member)
Air Dried
Glycolated
Glycerol
Lin (Counts)
4000
3000
2000
1000
0
Sme
Vrm
VMLC
I-MMLC
Chl 002 / Kln 001
UMLC
Ilt-Ms 001
MLChl
Peak expansion
Peak destruction
UMLC
Ilt-Ms 002
Chl 003
Qz 100
MLChl
Ms 113
Fsp 130/ Ms 112/ Hem 101
Kln 002
Chl 004
Fsp 023
Qz 101
Ilt-Ms 003
Fsp/ Rt 002
Fsp (pl) 202
Fsp 004
30
20
10
9
8
7
6
d-scale
5
4

N30-1469.1
Missisauga Formation
(Upper Member)

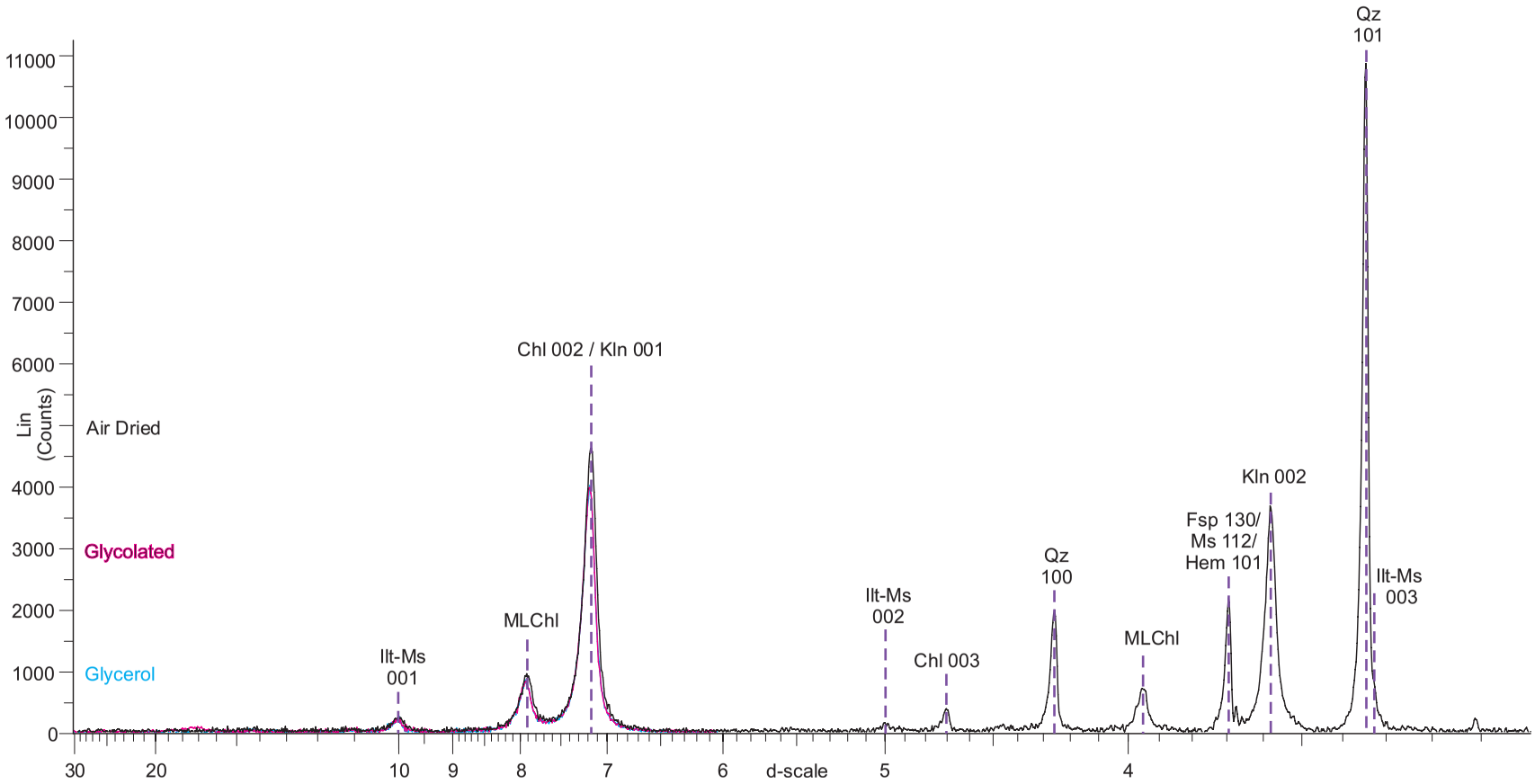

I13-3248.8
Logan Canyon Formation
(Naskapi Member)

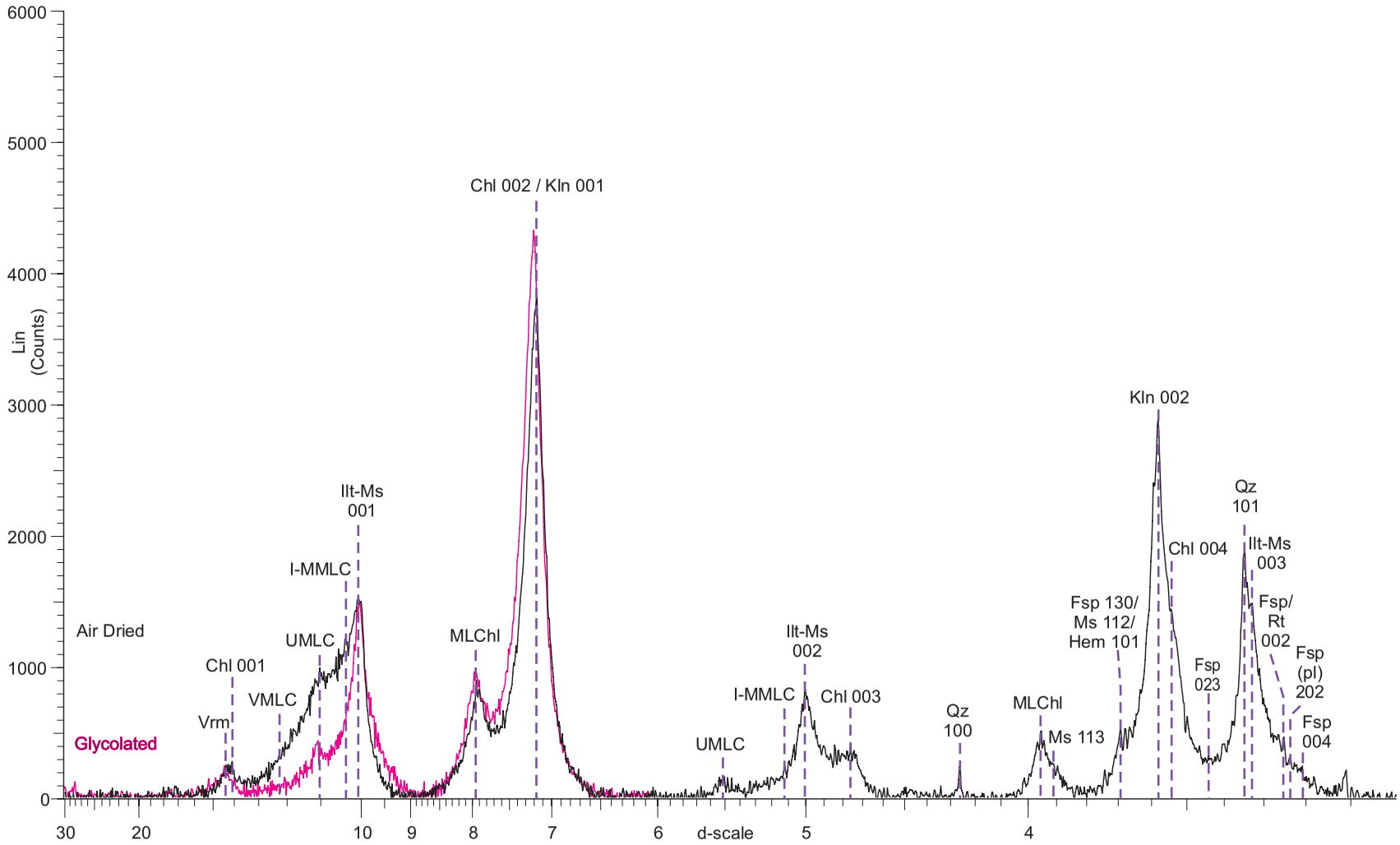

A99-2209.25
Logan Canyon Formation
(Cree Member)

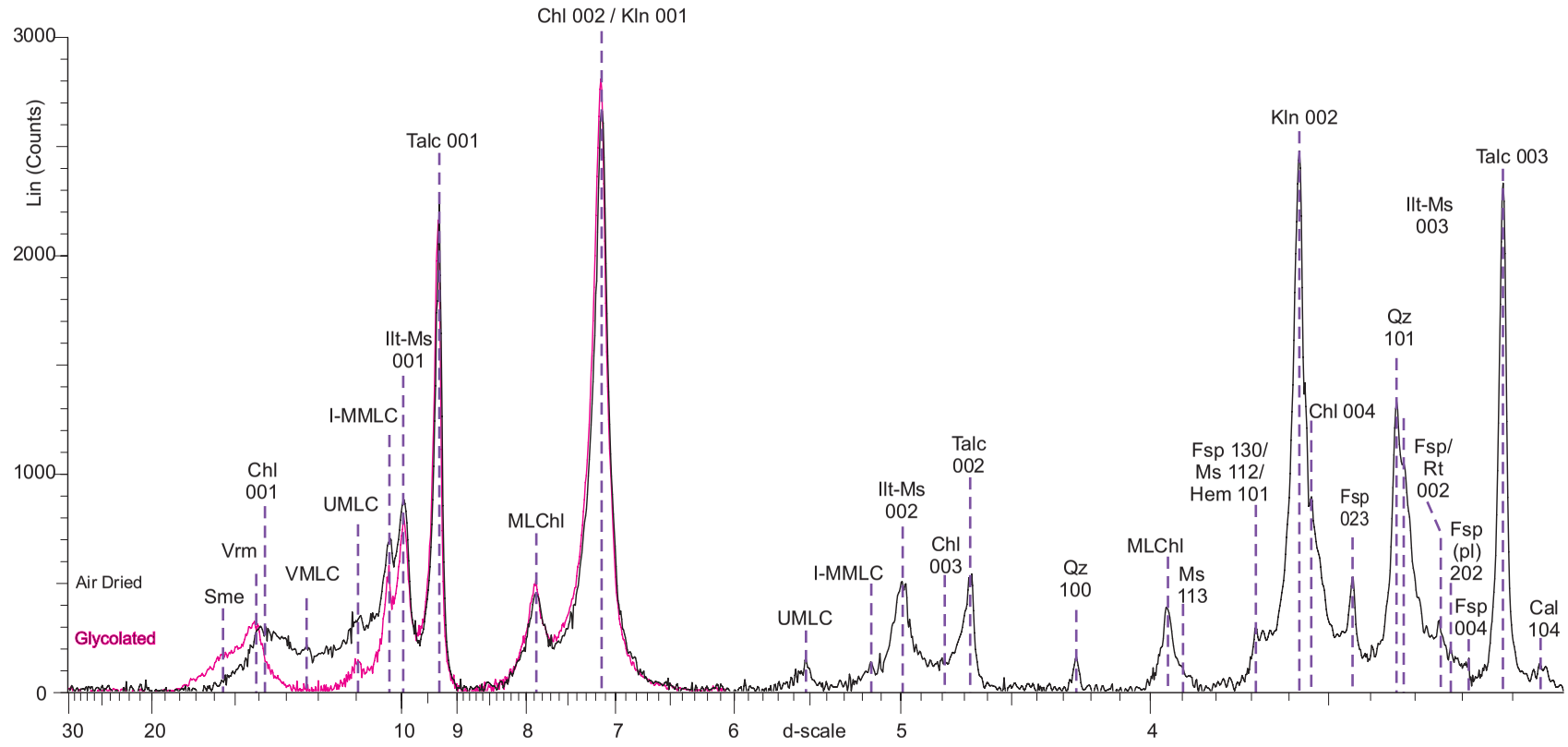

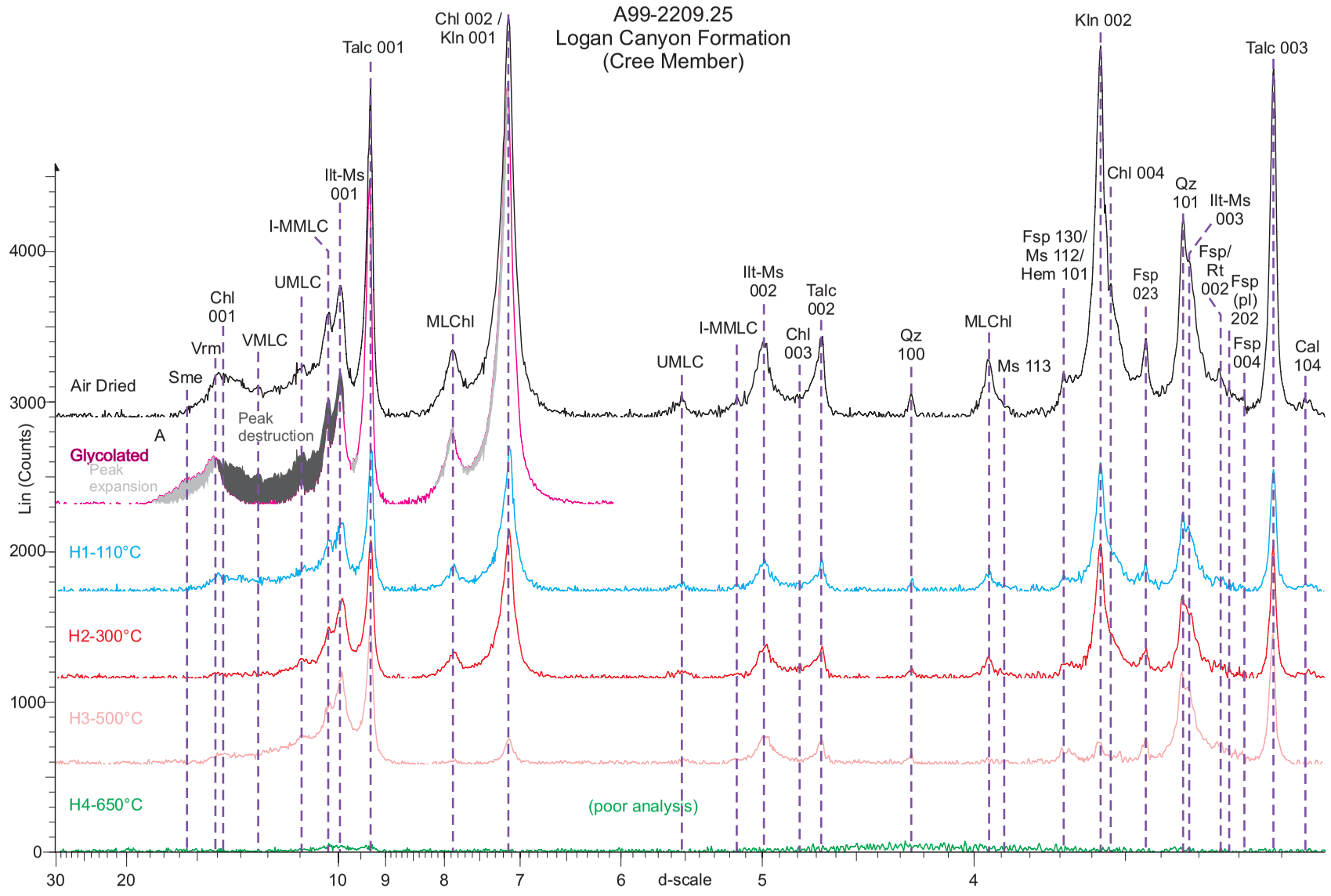
A99-2209.25
Logan Canyon Formation
(Cree Member)
Air Dried
Glycolated
Peak expansion
Peak destruction
H1-110°C
H2-300°C
H3-500°C
H4-650°C
(poor analysis)
Lin (Counts)
d-scale
Chl 002 / Kln 001
Talc 001
Ilt-Ms 001
I-MMLC
UMLC
Chl 001
Vrm
Sme
VMLC
MLChl
Ilt-Ms 002
I-MMLC
Chl 003
Talc 002
UMLC
Qz 100
MLChl
Ms 113
Fsp 130/ Ms 112/ Hem 101
Kln 002
Chl 004
Fsp 023
Qz 101
Ilt-Ms 003
Fsp/ Rt 002
Fsp (pl) 202
Fsp 004
Talc 003
Cal 104

A99-2209.25
Logan Canyon Formation
(Cree Member)

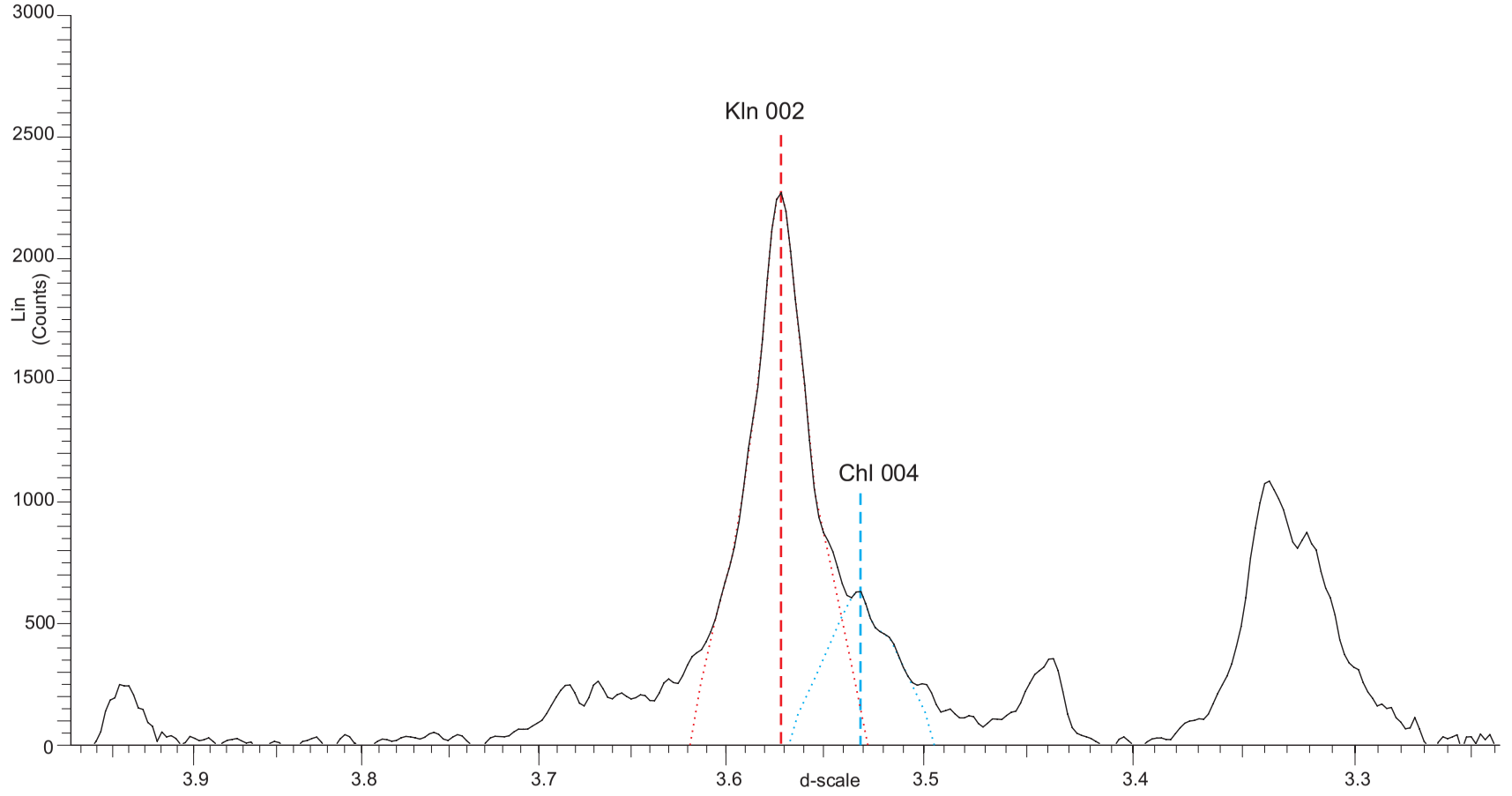

A99-2479.35
Missisauga Formation
(Upper Member)

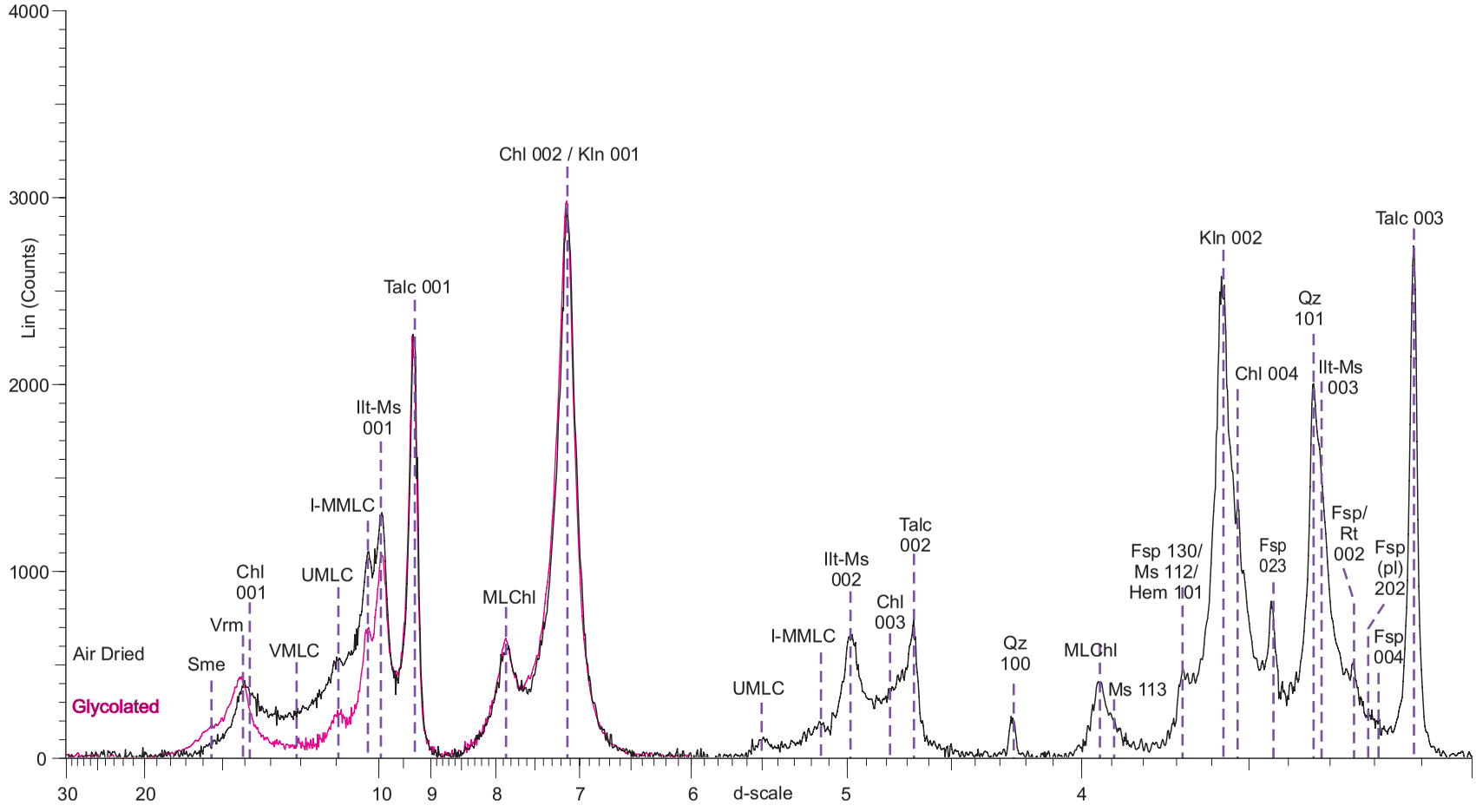

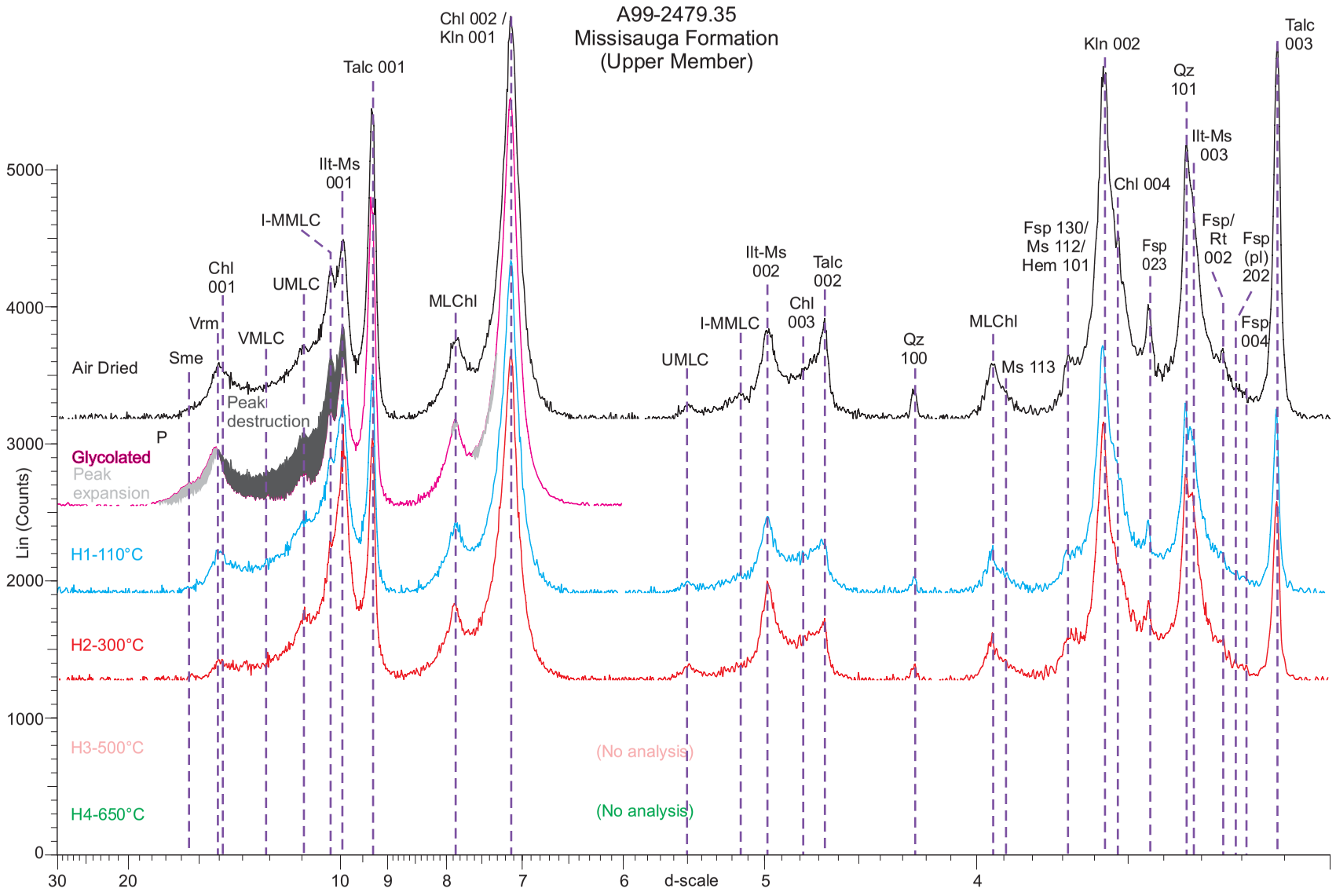
A99-2479.35
Missisauga Formation
(Upper Member)
Air Dried
Glycolated
Peak expansion
H1-110°C
H2-300°C
H3-500°C
H4-650°C
(No analysis)
(No analysis)
Peak destruction
P
Sme
Vrm
Chl 001
VMLC
UMLC
I-MMLC
Ilt-Ms 001
Talc 001
Chl 002 / Kln 001
MLChl
UMLC
I-MMLC
Ilt-Ms 002
Chl 003
Talc 002
Qz 100
MLChl
Ms 113
Fsp 130/ Ms 112/ Hem 101
Kln 002
Chl 004
Fsp 023
Qz 101
Ilt-Ms 003
Fsp/ Rt 002
Fsp (pl) 202
Fsp 004
Talc 003
Lin (Counts)
5000
4000
3000
2000
1000
0
30
20
10
9
8
7
6
d-scale
5
4

A99-2479.35
Missisauga Formation
(Upper Member)

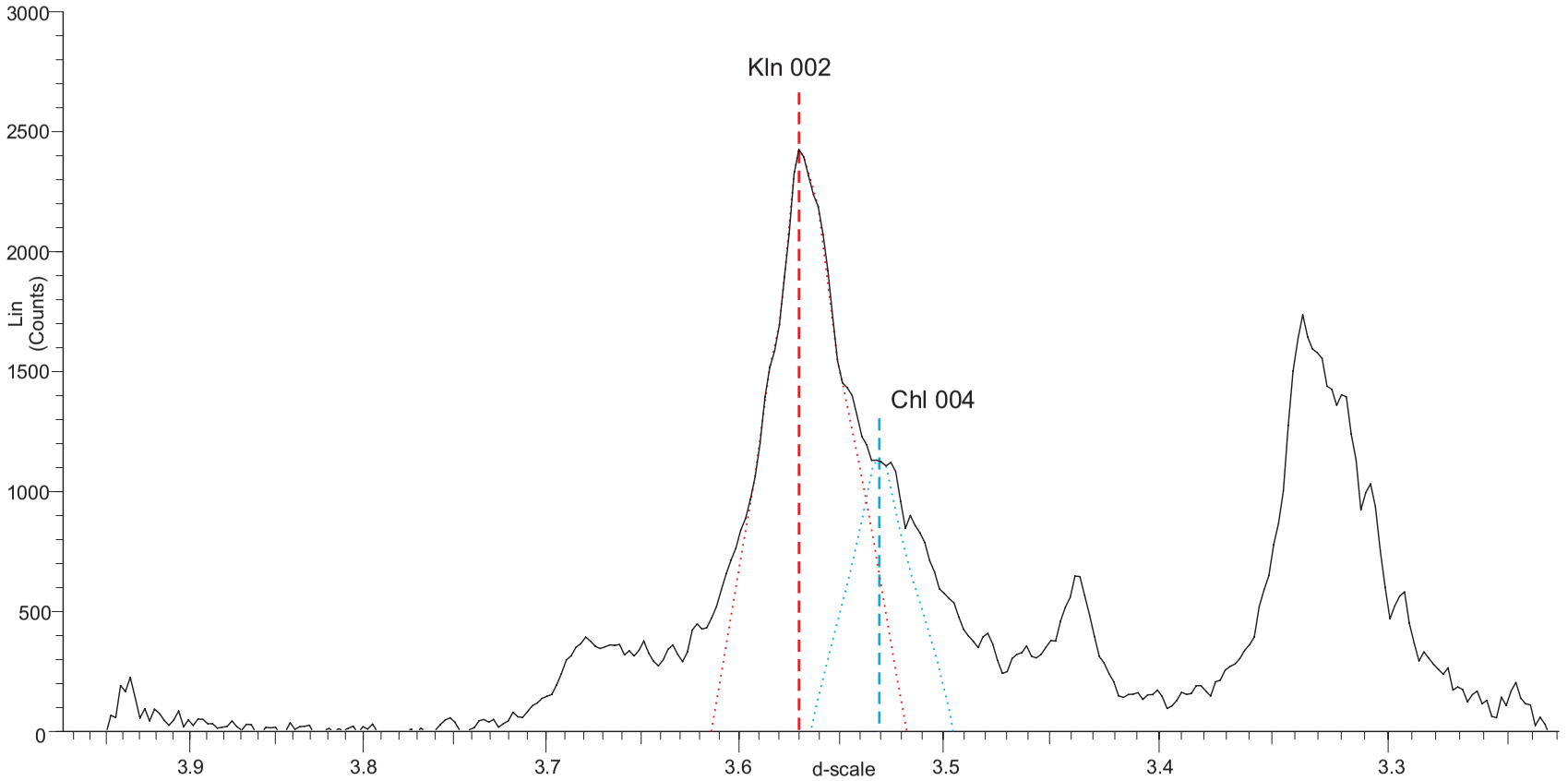

A99-2927.36
Missisauga Formation
(Middle Member)

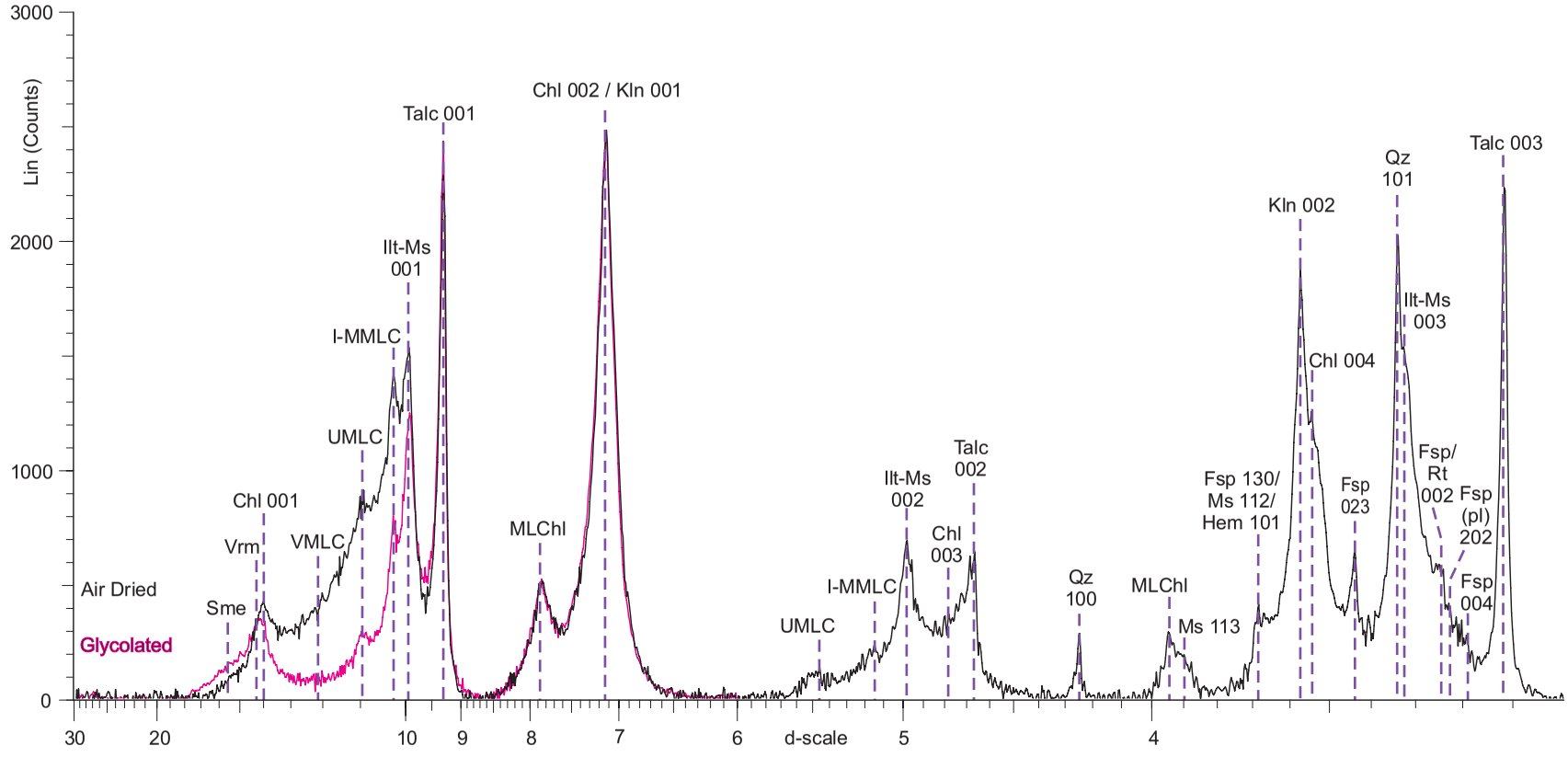

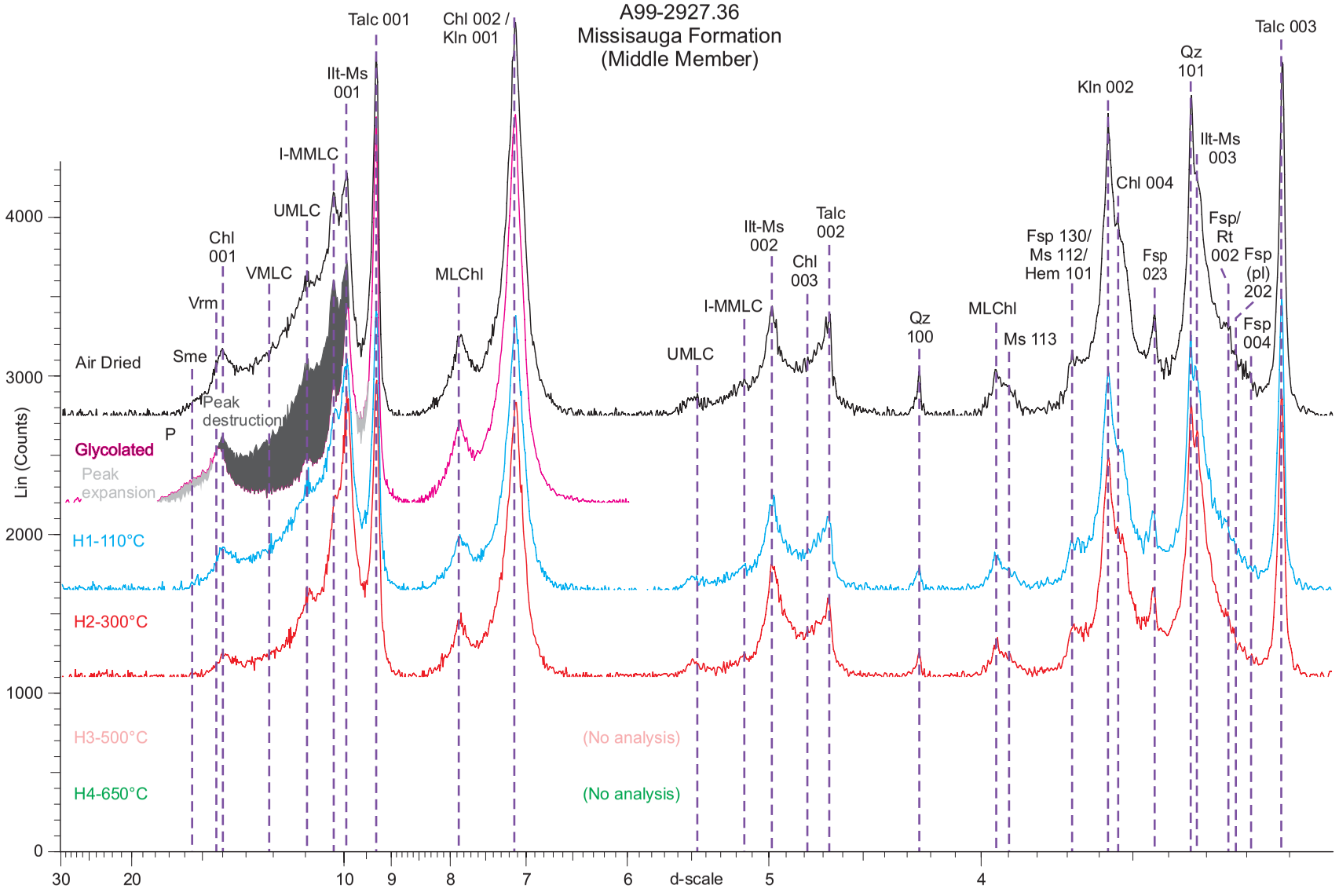
A99-2927.36
Missisauga Formation
(Middle Member)
Talc 001
Chl 002 /
Kln 001
Ilt-Ms
001
I-MMLC
UMLC
Chl
001
VMLC
Vrm
Sme
Air Dried
Peak
destruction
P
Glycolated
Peak
expansion
MLChl
Ilt-Ms
002
Talc
002
Chl
003
I-MMLC
UMLC
Qz
100
MLChl
Ms 113
Fsp 130/
Ms 112/
Hem 101
Kln 002
Chl 004
Fsp
023
Qz
101
Ilt-Ms
003
Fsp/
Rt
002
Fsp
(pl)
202
Fsp
004
Talc 003
H1-110°C
H2-300°C
H3-500°C
H4-650°C
(No analysis)
(No analysis)
Lin (Counts)
4000
3000
2000
1000
0
30
20
10
9
8
7
6
d-scale
5
4

A99-2927.36
Missisauga Formation
(Middle Member)

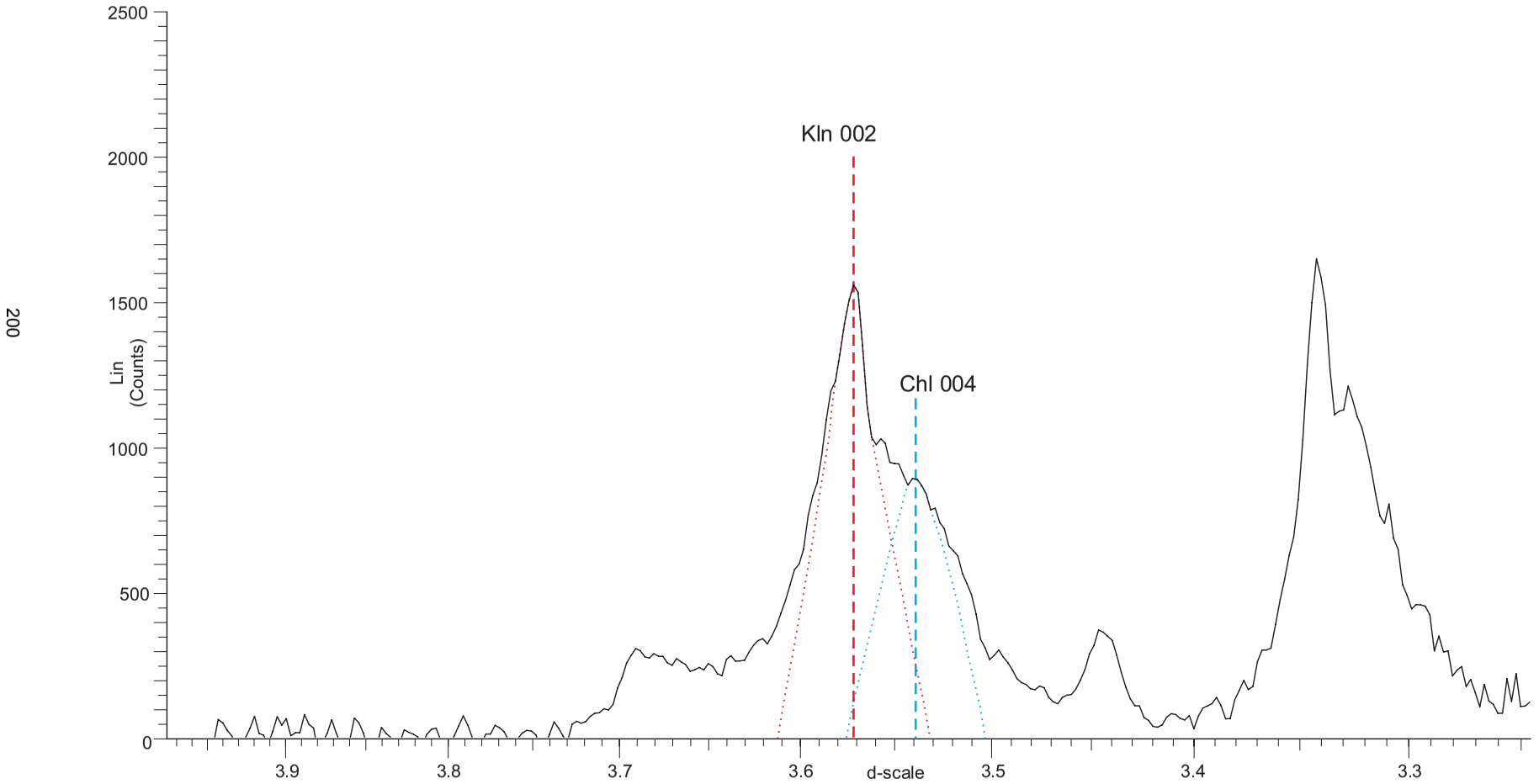

200

A99-3812.64
Mic Mac Formation

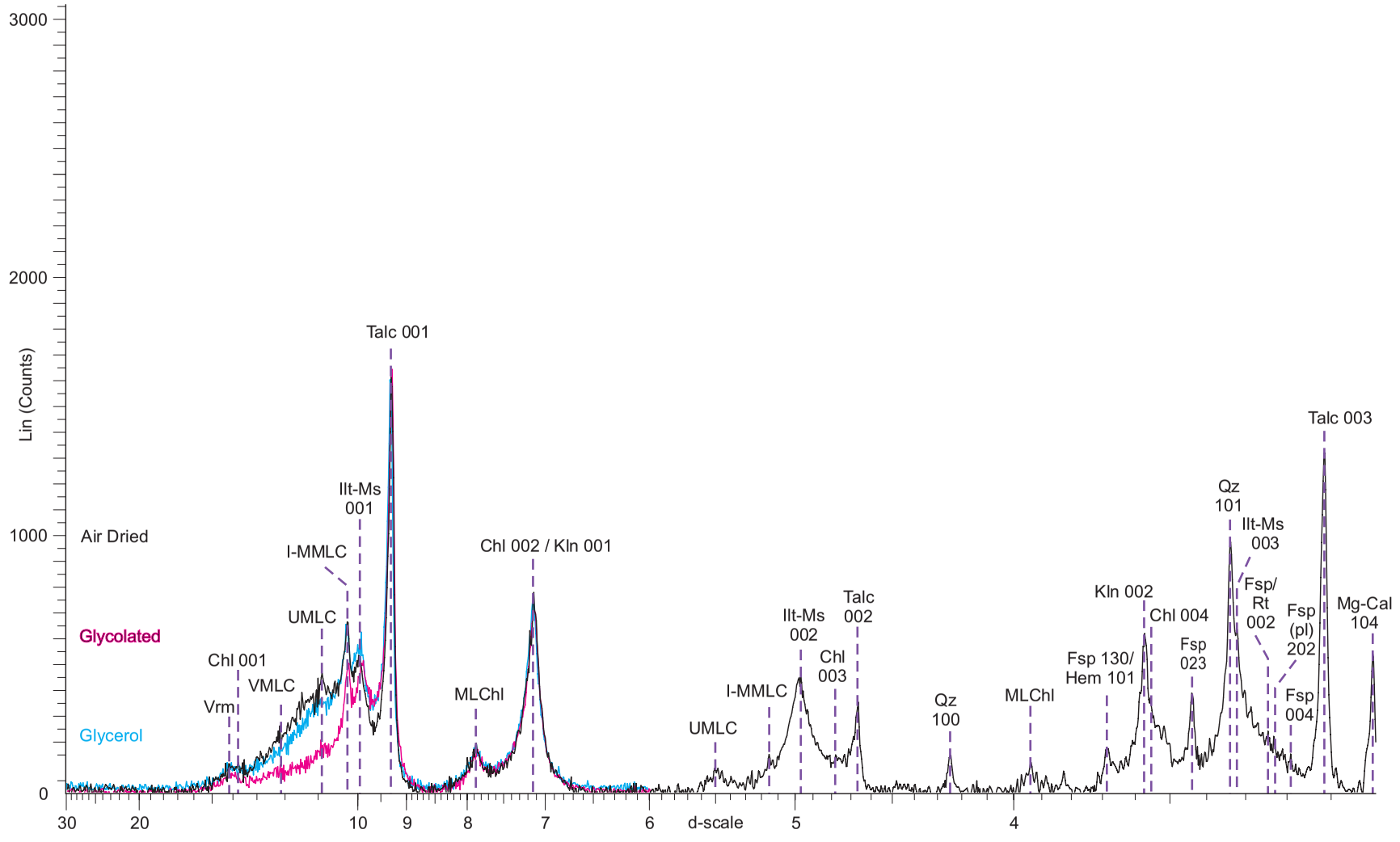

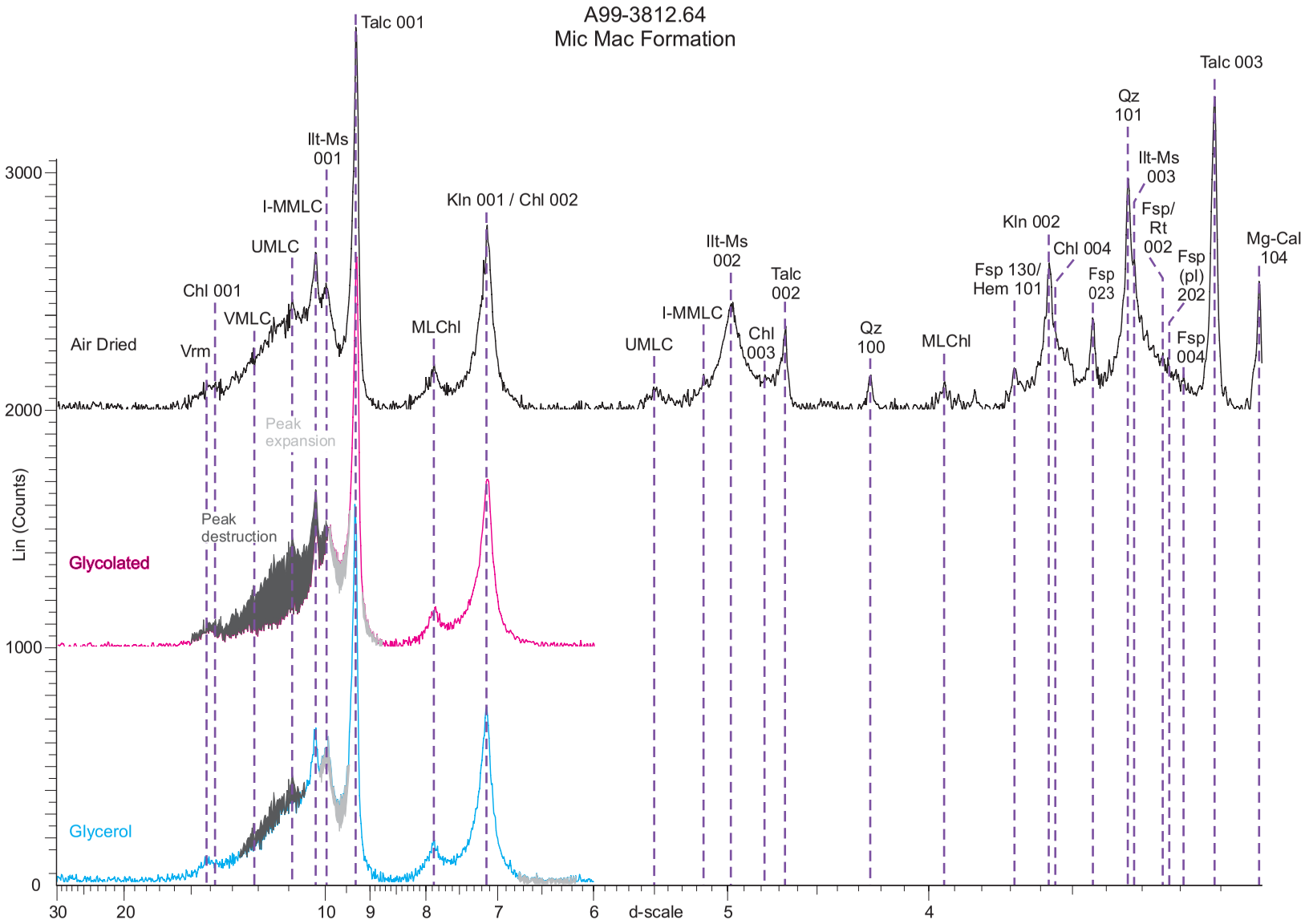
A99-3812.64
Mic Mac Formation
Talc 001
Ilt-Ms 001
I-MMLC
UMLC
Chl 001
VMLC
Vrm
Air Dried
MLChl
Kln 001 / Chl 002
UMLC
I-MMLC
Ilt-Ms 002
Chl 003
Talc 002
Qz 100
MLChl
Fsp 130/ Hem 101
Kln 002
Chl 004
Fsp 023
Qz 101
Ilt-Ms 003
Fsp/ Rt 002
Fsp (pl) 202
Fsp 004
Talc 003
Mg-Cal 104
Peak expansion
Peak destruction
Glycolated
Glycerol
Lin (Counts)
3000
2000
1000
0
30
20
10
9
8
7
6
d-scale
5
4

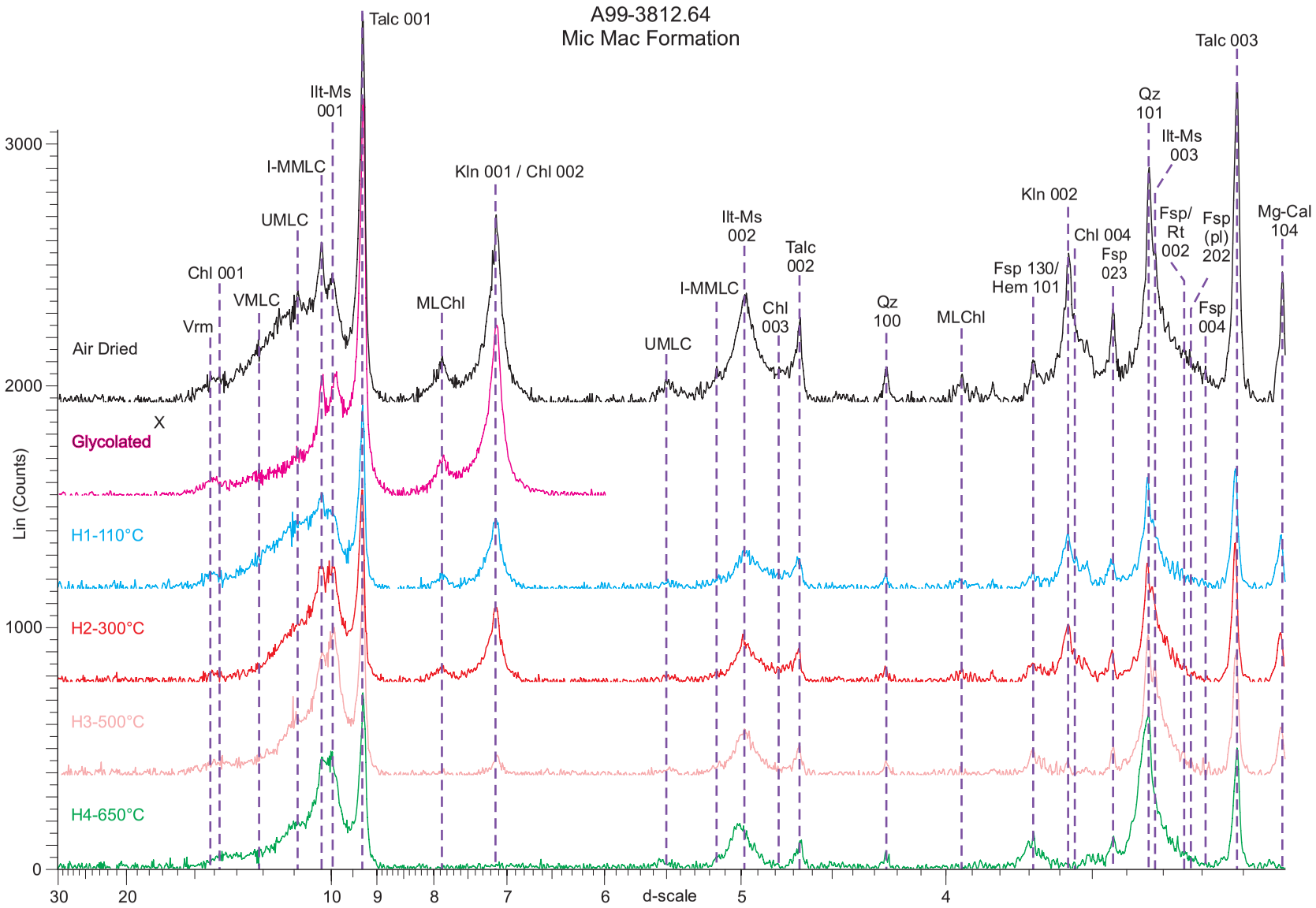
A99-3812.64
Mic Mac Formation
Talc 001
Ilt-Ms 001
I-MMLC
UMLC
Chl 001
VMLC
Vrm
Air Dried
X
Glycolated
H1-110°C
H2-300°C
H3-500°C
H4-650°C
MLChl
Kln 001 / Chl 002
UMLC
I-MMLC
Ilt-Ms 002
Chl 003
Talc 002
Qz 100
MLChl
Fsp 130/ Hem 101
Kln 002
Chl 004 Fsp 023
Qz 101
Ilt-Ms 003
Fsp/ Rt 002
Fsp (pl) 202
Fsp 004
Talc 003
Mg-Cal 104
Lin (Counts)
3000
2000
1000
0
30
20
10
9
8
7
6
d-scale
5
4

A99-3812.64
Mic Mac Formation

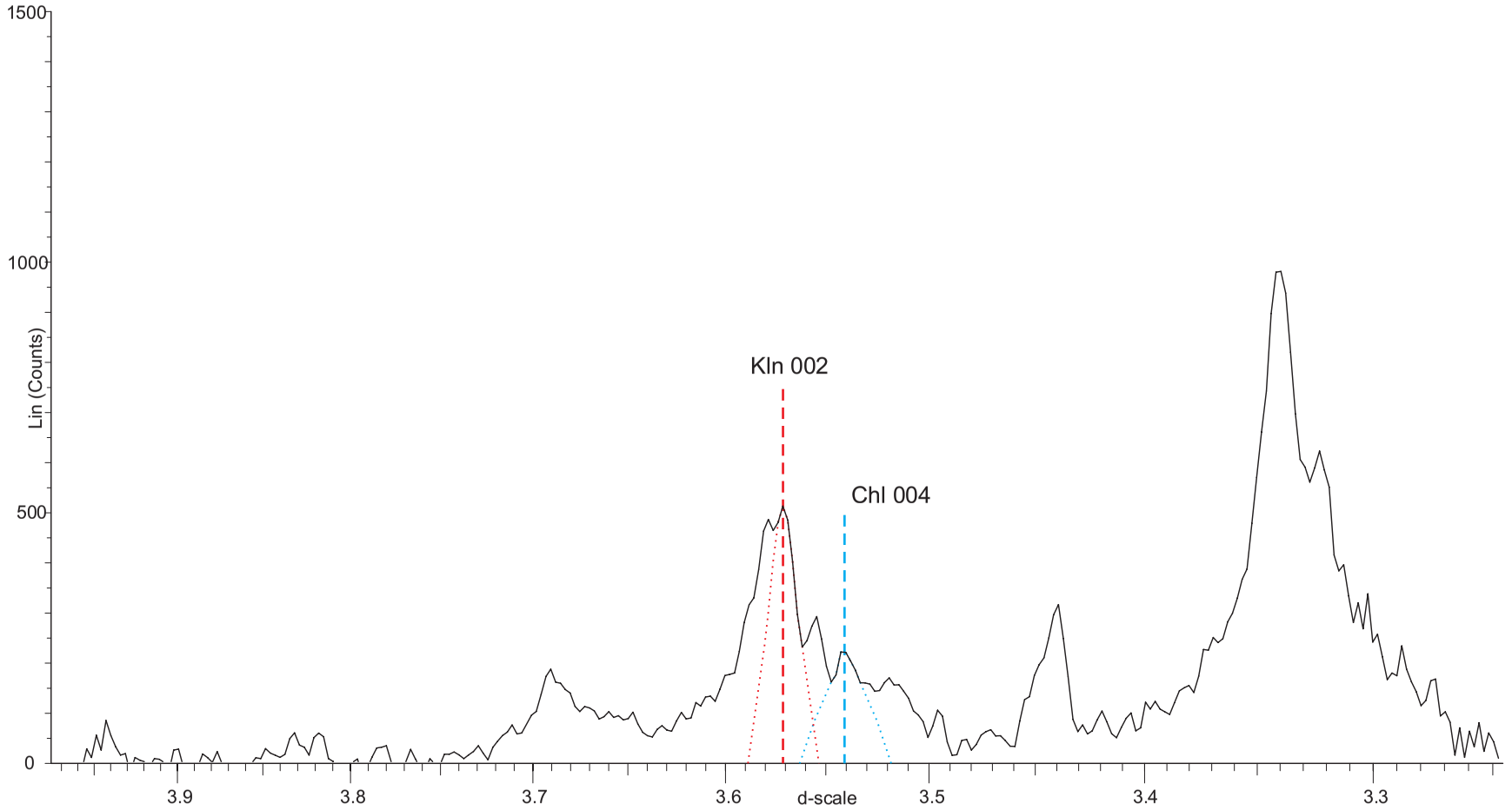

C67-3373.45
Missisauga Formation
(Middle Member)

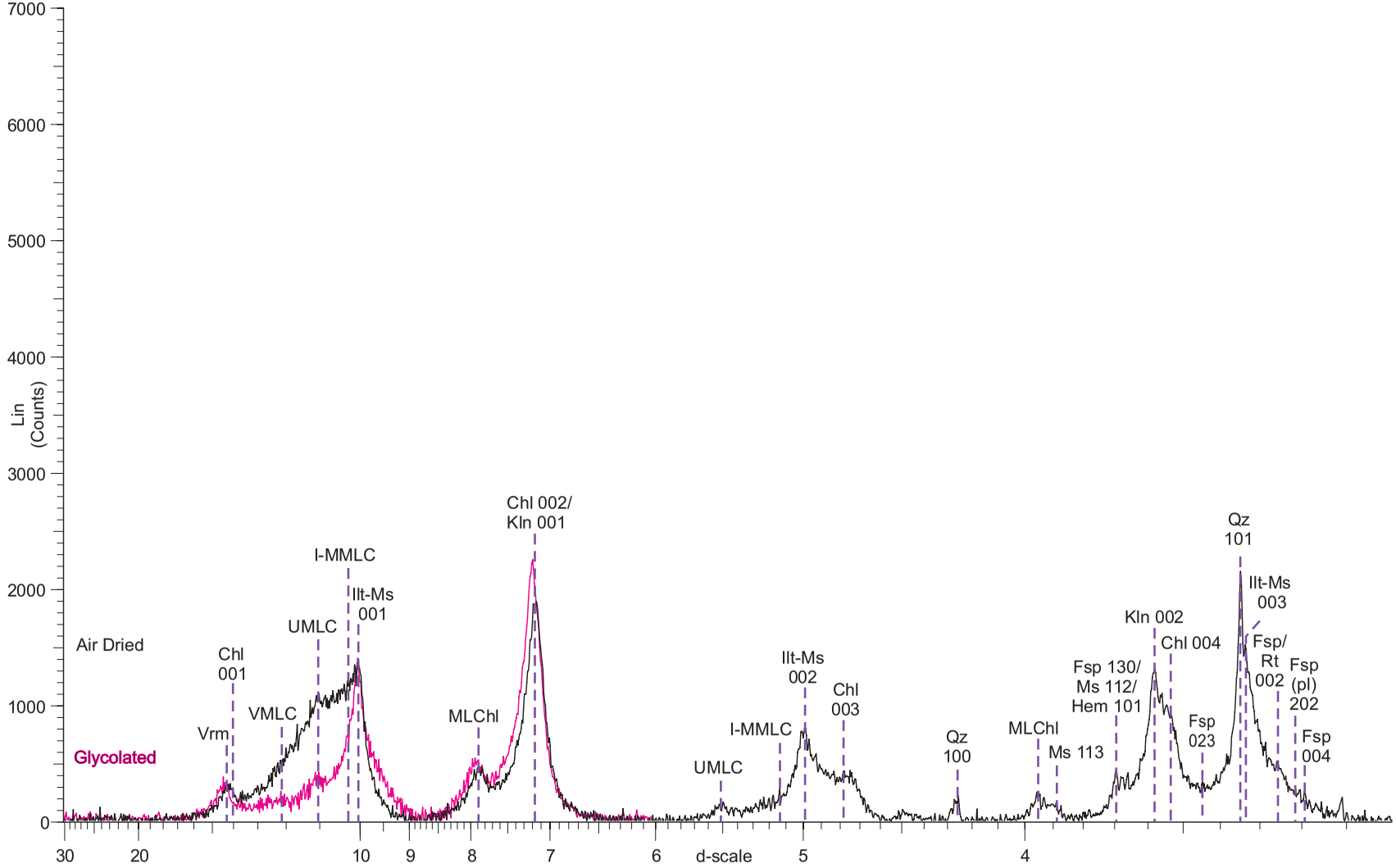

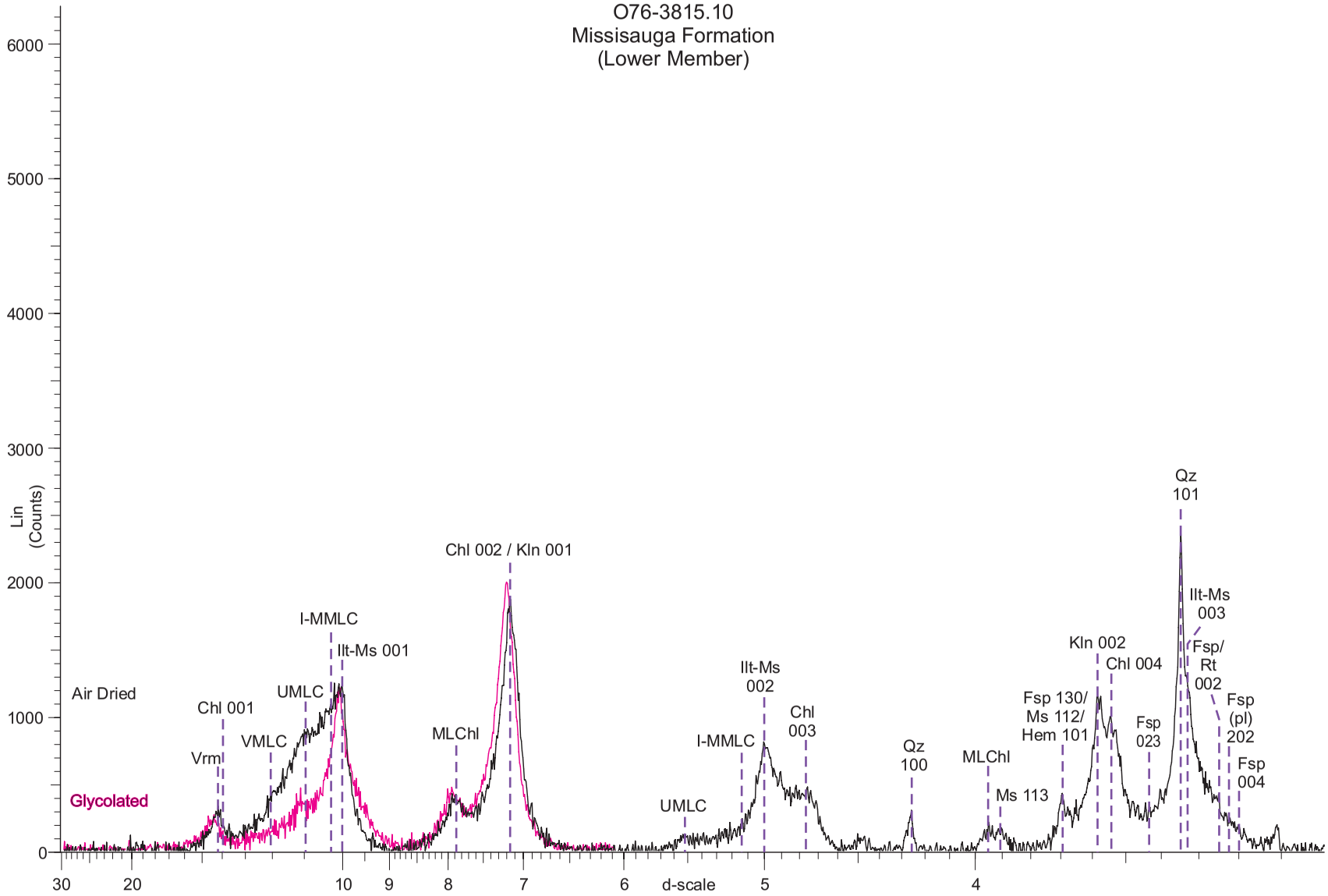
O76-3815.10
Missisauga Formation
(Lower Member)
Lin (Counts)
6000
5000
4000
3000
2000
1000
0
Air Dried
Glycolated
Chl 001
Vrm
VMLC
UMLC
I-MMLC
Ilt-Ms 001
MLChl
Chl 002 / Kln 001
UMLC
I-MMLC
Ilt-Ms 002
Chl 003
Qz 100
MLChl
Ms 113
Fsp 130/ Ms 112/ Hem 101
Kln 002
Chl 004
Fsp 023
Qz 101
Ilt-Ms 003
Fsp/ Rt 002
Fsp (pl) 202
Fsp 004
30
20
10
9
8
7
6
d-scale
5
4

O76-5956.80
Mic Mac

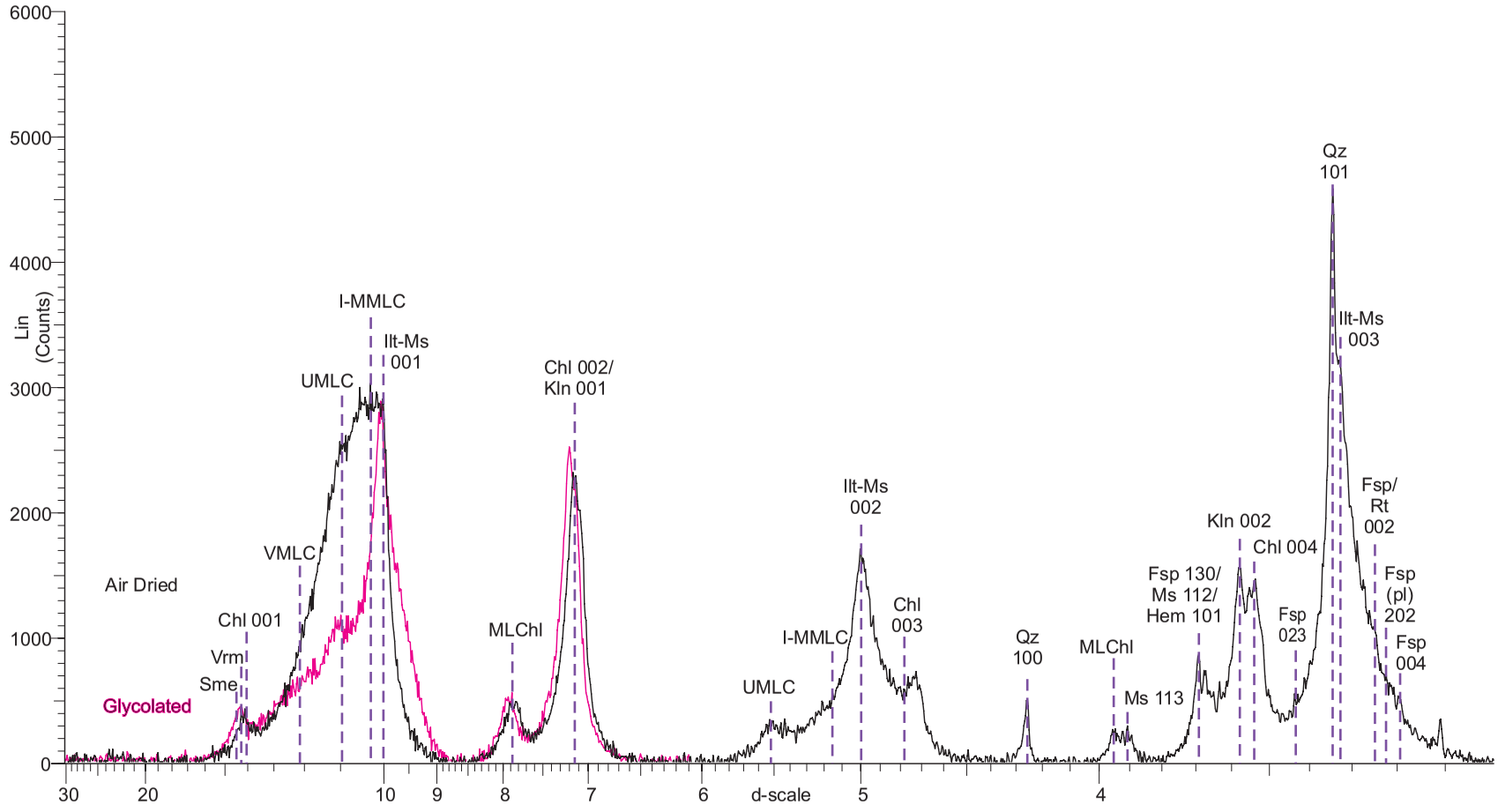

C74-1825
Logan Canyon Formation
(Sable Member)

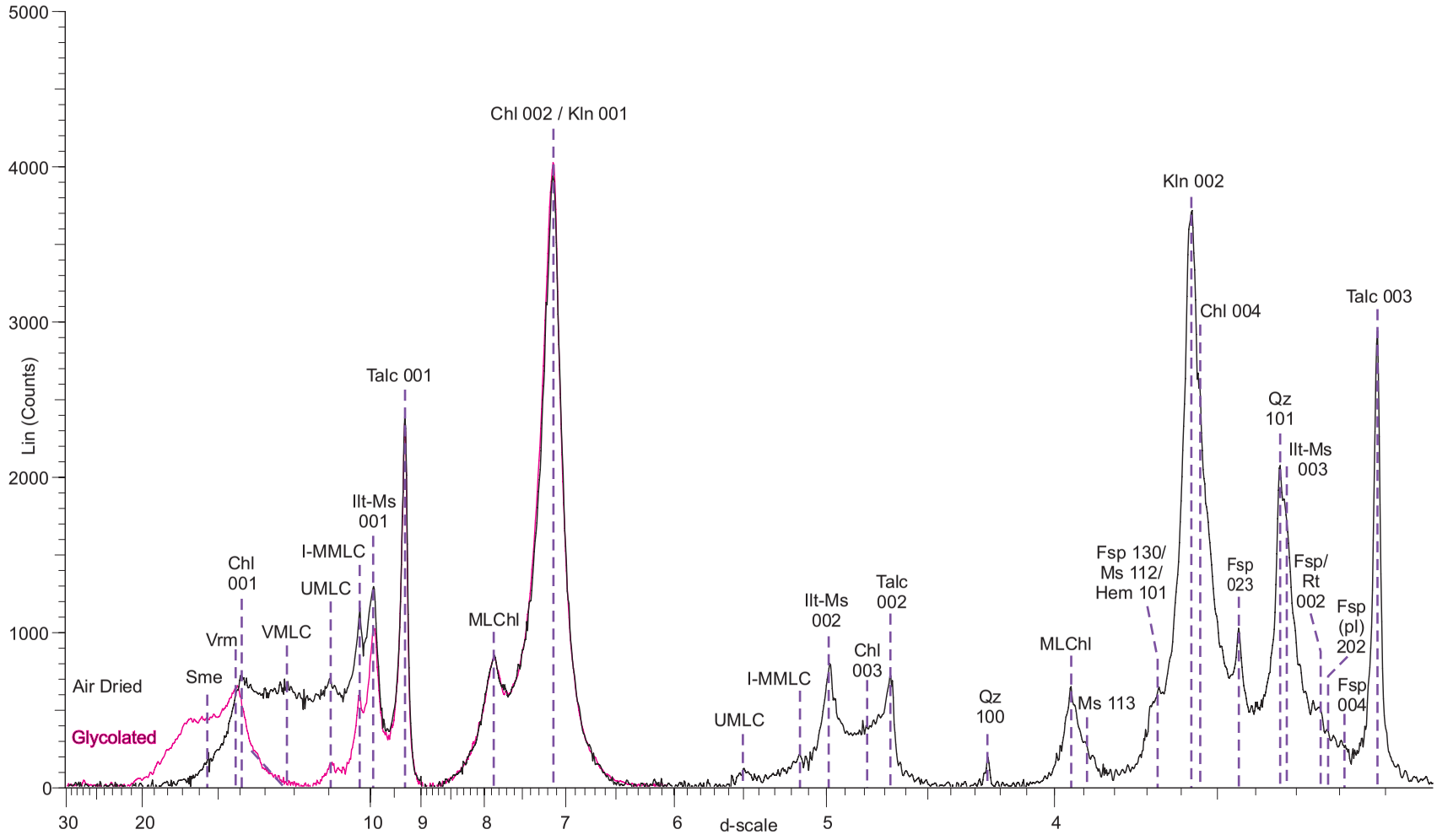

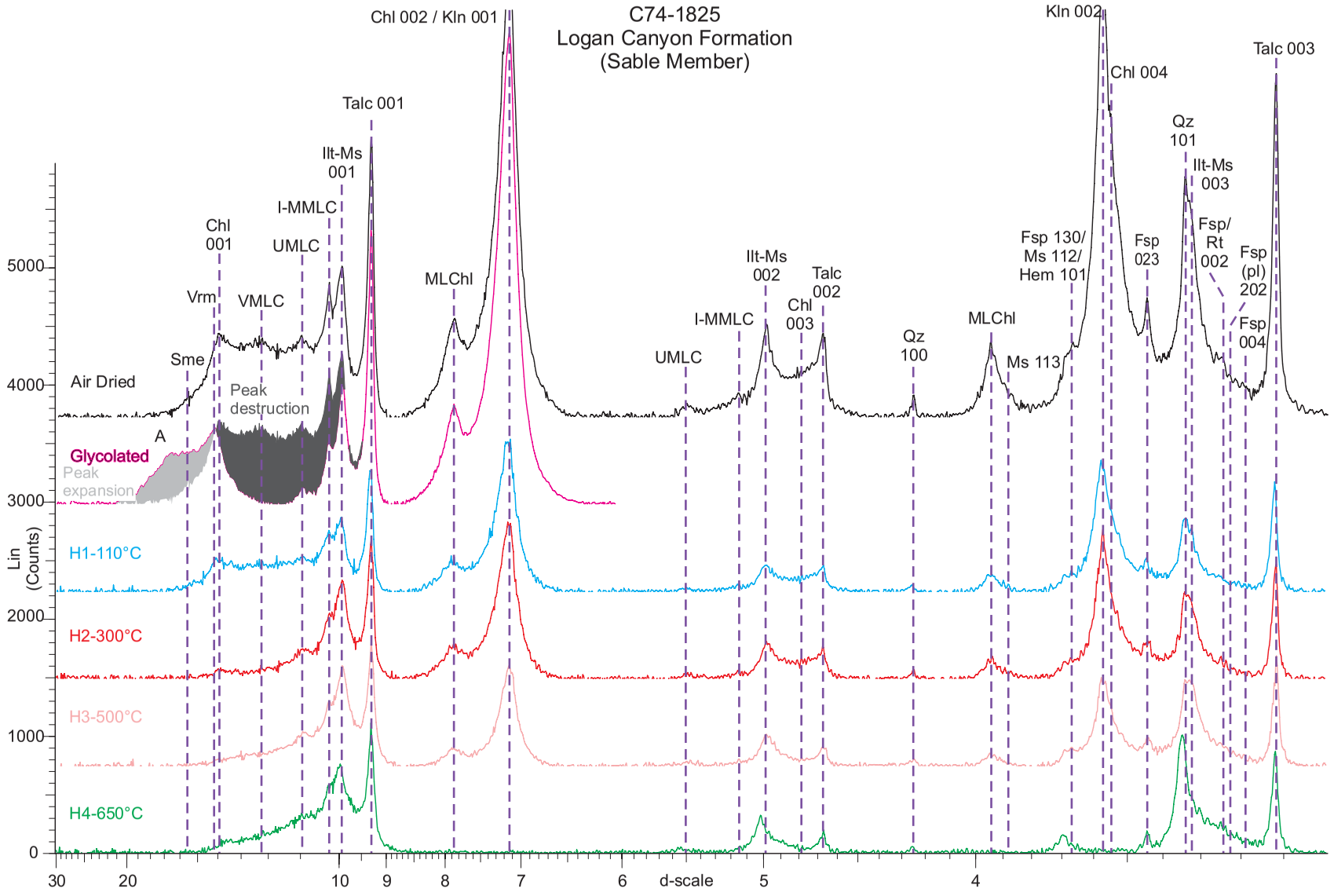
C74-1825
Logan Canyon Formation
(Sable Member)
Air Dried
Glycolated
Peak expansion
Peak destruction
A
H1-110°C
H2-300°C
H3-500°C
H4-650°C
Lin (Counts)
d-scale
Chl 002 / Kln 001
Talc 001
Ilt-Ms 001
I-MMLC
Chl 001
UMLC
Vrm
VMLC
Sme
MLChl
Ilt-Ms 002
Talc 002
Chl 003
I-MMLC
UMLC
Qz 100
MLChl
Ms 113
Fsp 130/ Ms 112/ Hem 101
Kln 002
Chl 004
Fsp 023
Qz 101
Ilt-Ms 003
Fsp/ Rt 002
Fsp (pl) 202
Fsp 004
Talc 003

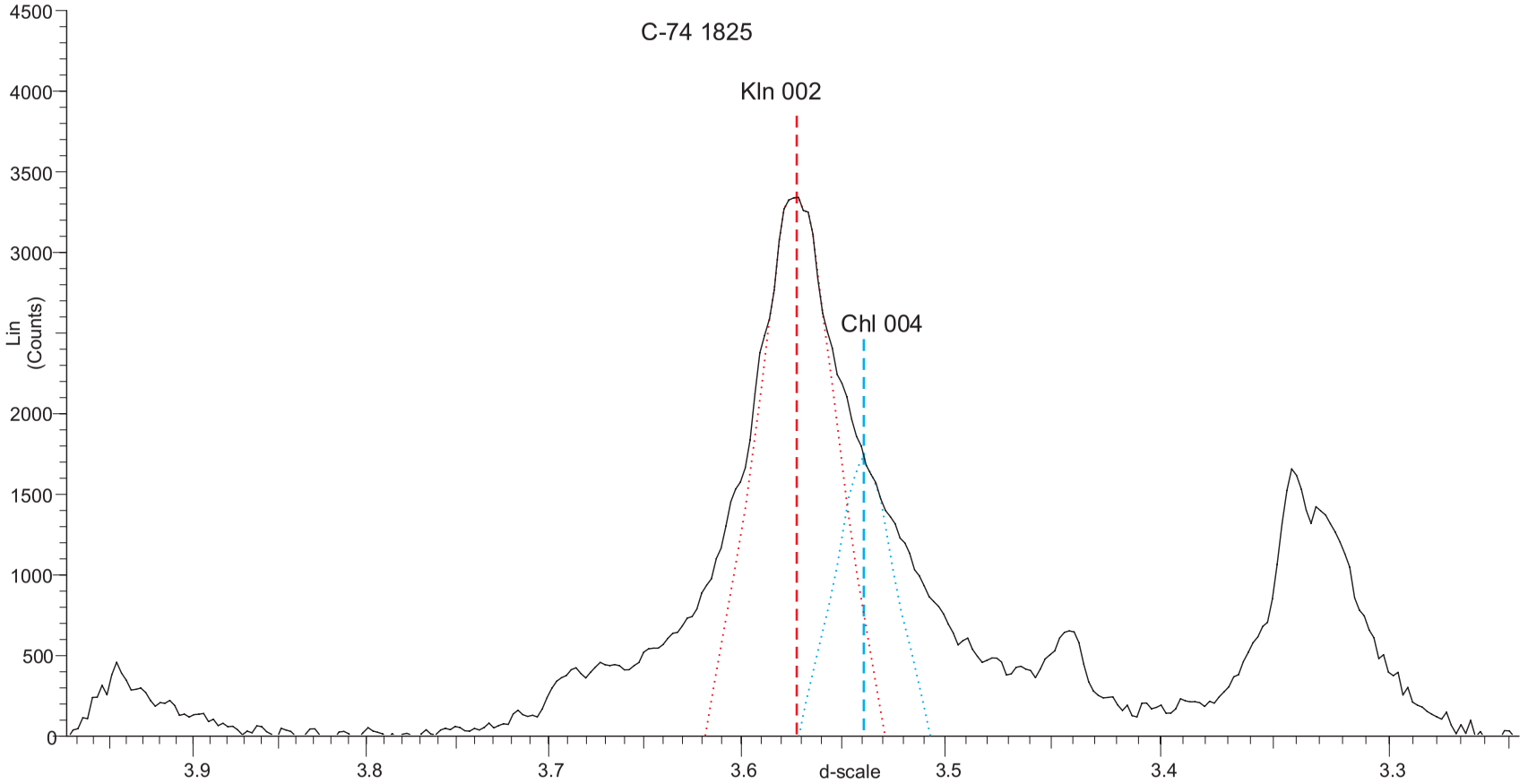
C-74 1825
Kln 002
Chl 004
Lin
(Counts)
4500
4000
3500
3000
2000
1500
1000
500
0
3.9
3.8
3.7
3.6
d-scale
3.5
3.4
3.3

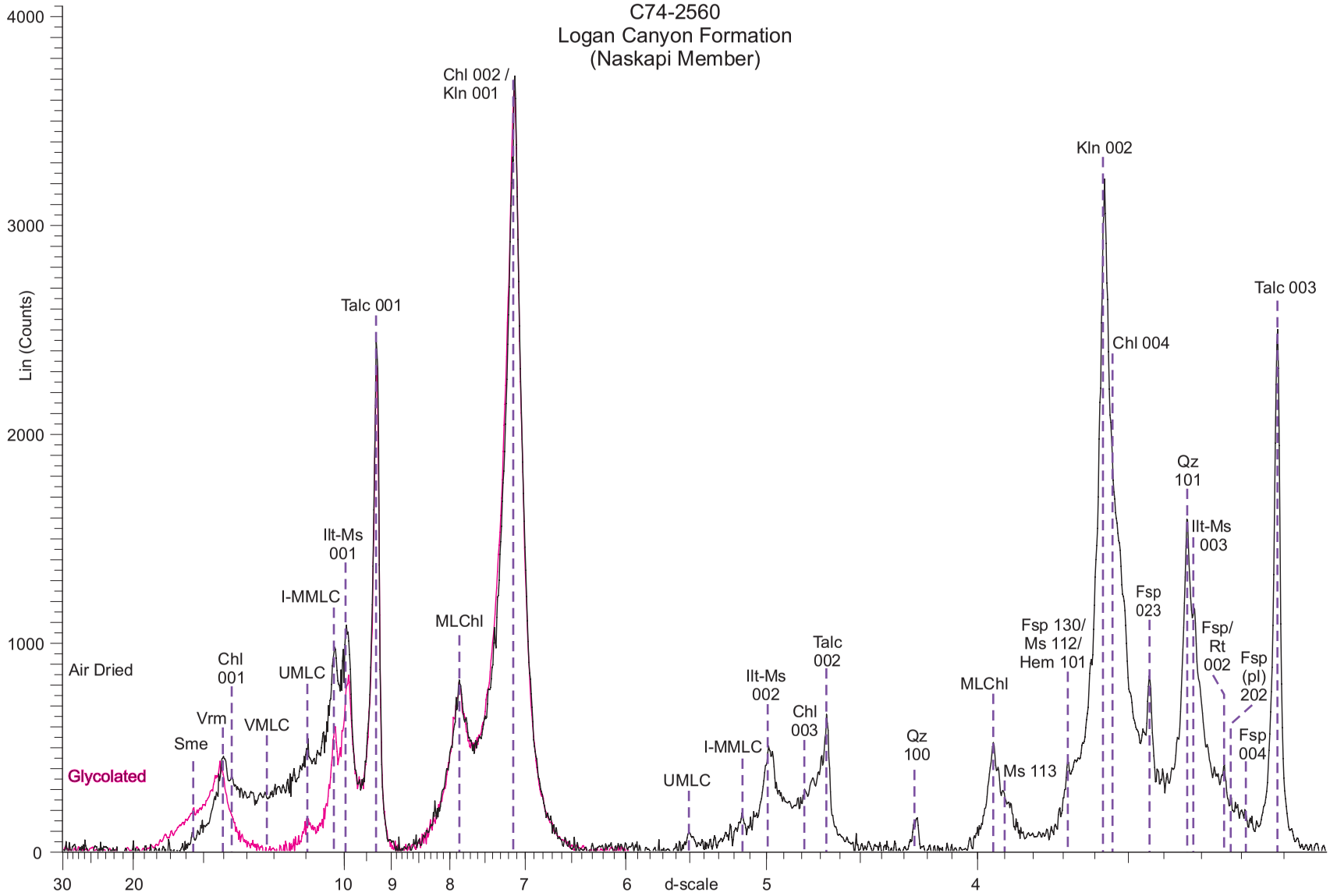
C74-2560
Logan Canyon Formation
(Naskapi Member)
Lin (Counts)
4000
3000
2000
1000
0
Air Dried
Glycolated
Sme
Vrm
Chl 001
VMLC
UMLC
I-MMLC
Ilt-Ms 001
Talc 001
MLChl
Chl 002 / Kln 001
UMLC
I-MMLC
Ilt-Ms 002
Chl 003
Talc 002
Qz 100
MLChl
Ms 113
Fsp 130/ Ms 112/ Hem 101
Kln 002
Chl 004
Fsp 023
Qz 101
Ilt-Ms 003
Fsp/ Rt 002
Fsp (pl) 202
Fsp 004
Talc 003
30
20
10
9
8
7
6
d-scale
5
4

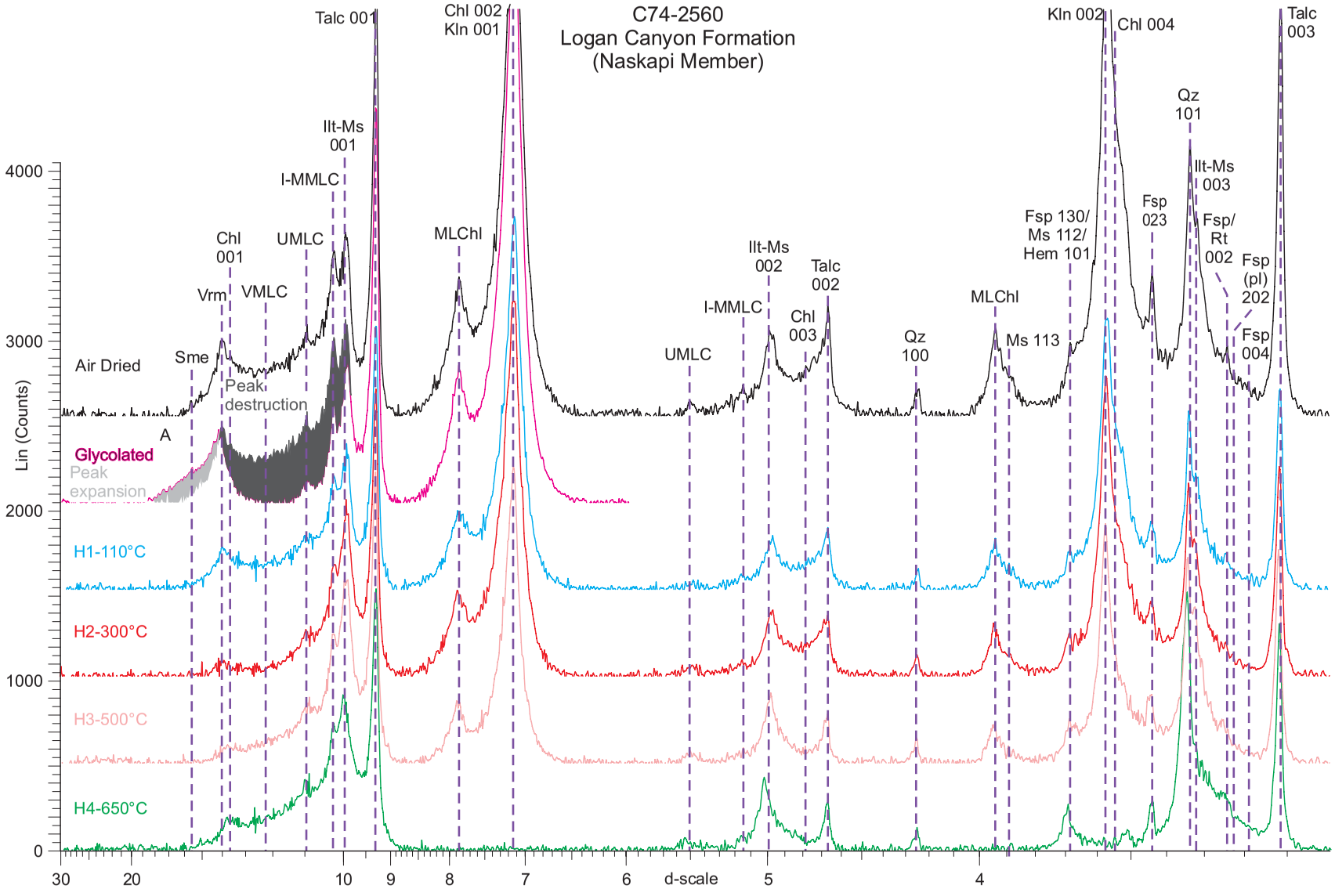
C74-2560
Logan Canyon Formation
(Naskapi Member)
Talc 001
Chl 002
Kln 001
Kln 002
Chl 004
Talc 003
Qz 101
Ilt-Ms 001
I-MMLC
Ilt-Ms 003
Fsp 023
Fsp/ Rt 002
Fsp (pl) 202
Fsp 004
Chl 001
UMLC
MLChl
Ilt-Ms 002
Talc 002
Fsp 130/ Ms 112/ Hem 101
Vrm
VMLC
Chl 003
Qz 100
MLChl
Ms 113
Sme
Air Dried
Peak destruction
A
Glycolated
Peak expansion
H1-110°C
H2-300°C
H3-500°C
H4-650°C
Lin (Counts)
4000
3000
2000
1000
0
30
20
10
9
8
7
6
d-scale
5
4

C74-2560
Logan Canyon Formation
(Naskapi Member)

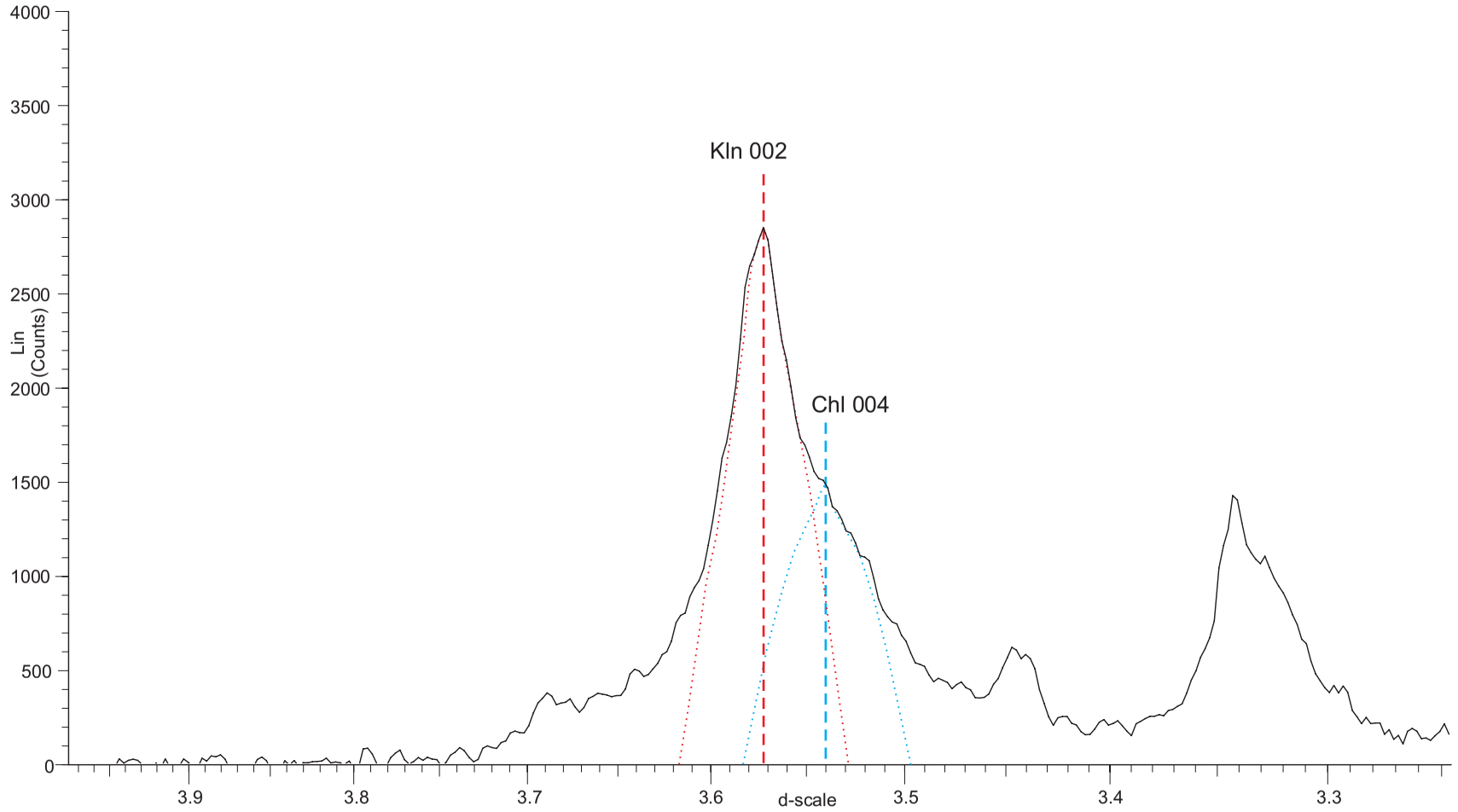

C74-3780
Missisauga Formation
(Lower Member)

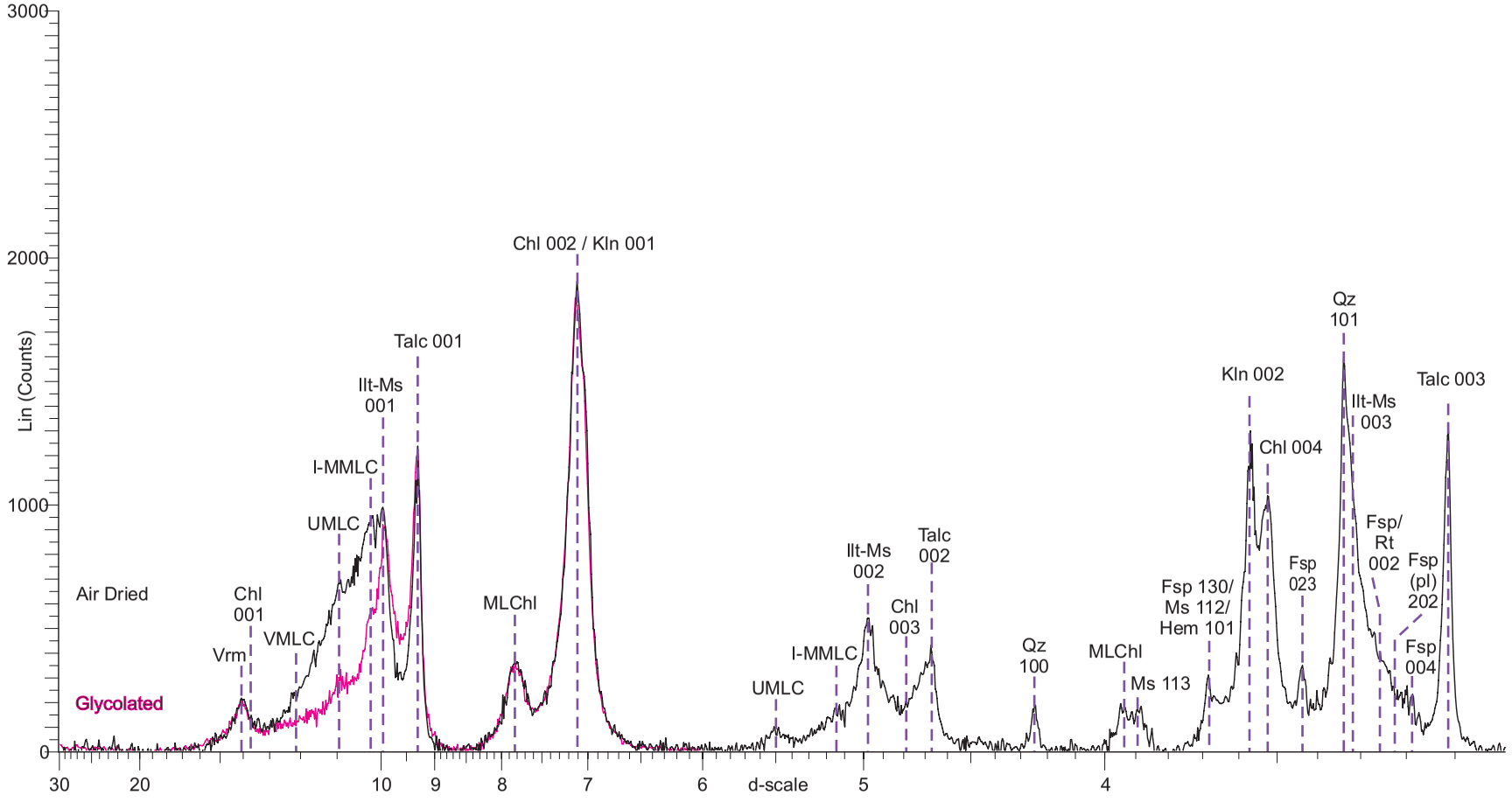

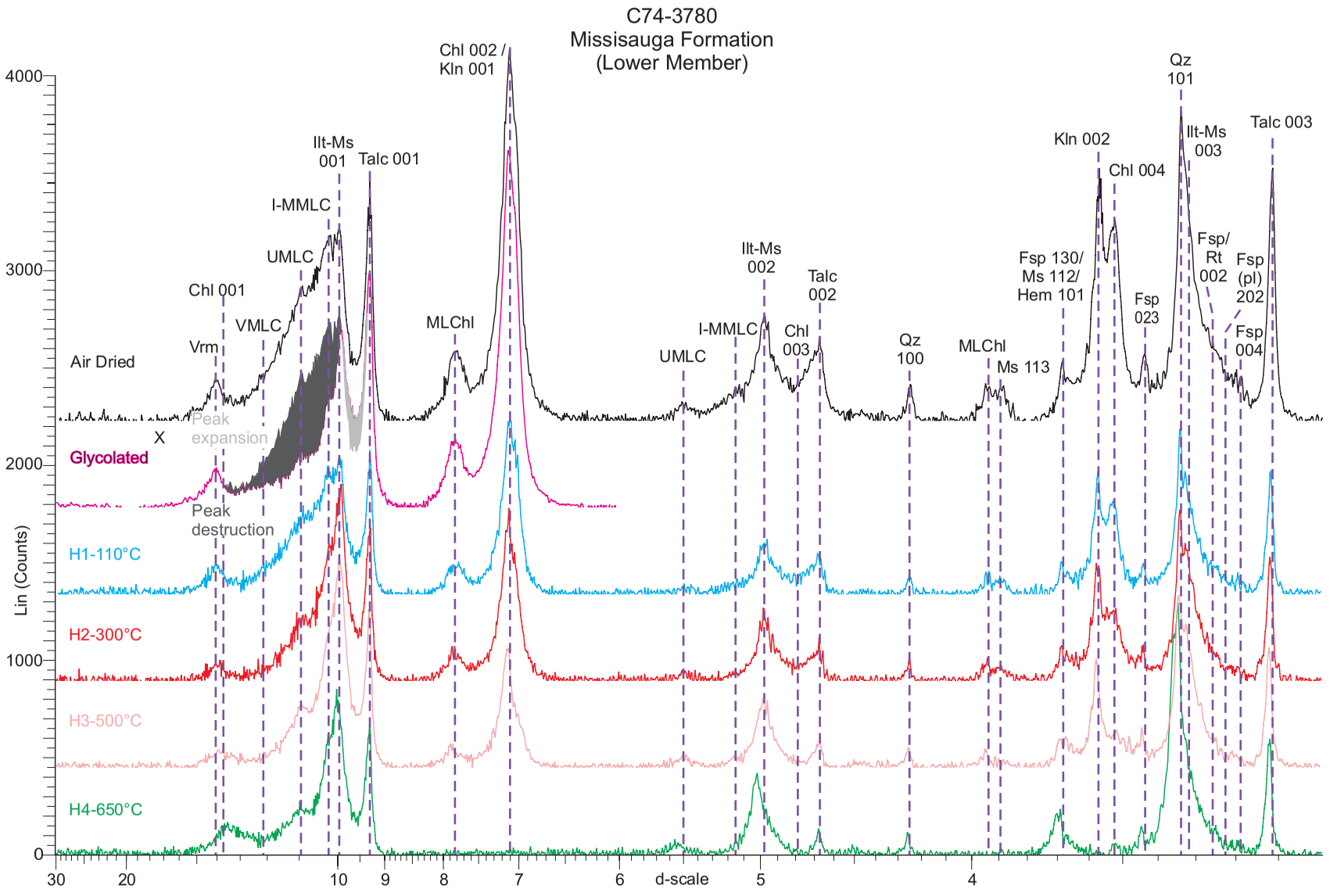
C74-3780
Missisauga Formation
(Lower Member)
Air Dried
Glycolated
H1-110°C
H2-300°C
H3-500°C
H4-650°C
Lin (Counts)
d-scale
Chl 001
Vrm
VMLC
UMLC
I-MMLC
Ilt-Ms 001
Talc 001
Chl 002 / Kln 001
MLChl
Ilt-Ms 002
I-MMLC
UMLC
Chl 003
Talc 002
Qz 100
MLChl
Ms 113
Fsp 130/ Ms 112/ Hem 101
Kln 002
Chl 004
Fsp 023
Qz 101
Ilt-Ms 003
Fsp/ Rt 002
Fsp (pl) 202
Fsp 004
Talc 003
Peak expansion
Peak destruction
X

C74-3780
Missisauga Formation
(Lower Member)

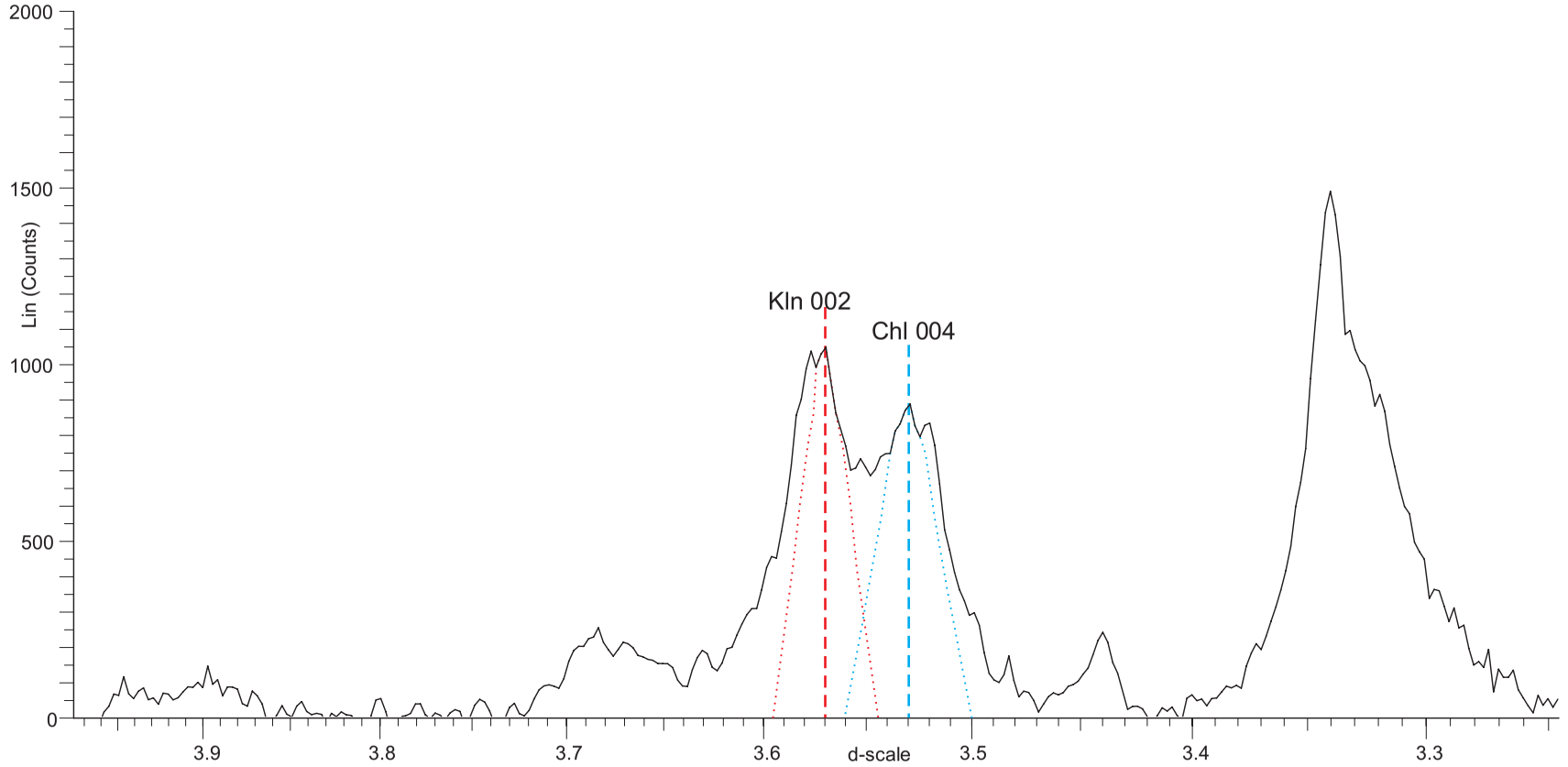

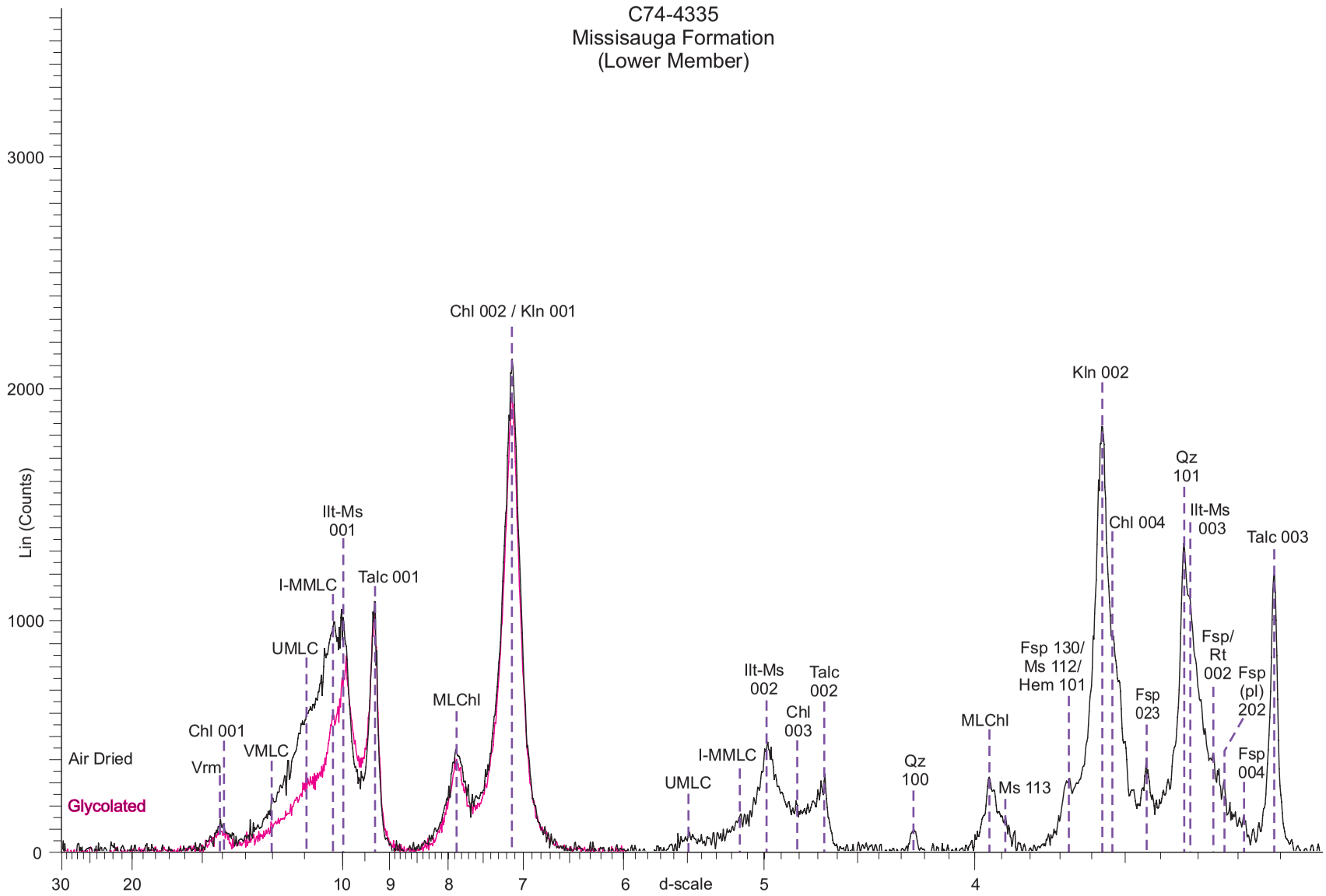
C74-4335
Missisauga Formation
(Lower Member)
Lin (Counts)
3000
2000
1000
0
Air Dried
Glycolated
Chl 001
Vrm
VMLC
UMLC
I-MMLC
Ilt-Ms
001
Talc 001
MLChl
Chl 002 / Kln 001
UMLC
I-MMLC
Ilt-Ms
002
Chl
003
Talc
002
Qz
100
MLChl
Ms 113
Fsp 130/
Ms 112/
Hem 101
Kln 002
Chl 004
Fsp
023
Qz
101
Ilt-Ms
003
Fsp/
Rt
002
Fsp
(pl)
202
Fsp
004
Talc 003
30
20
10
9
8
7
6
d-scale
5
4

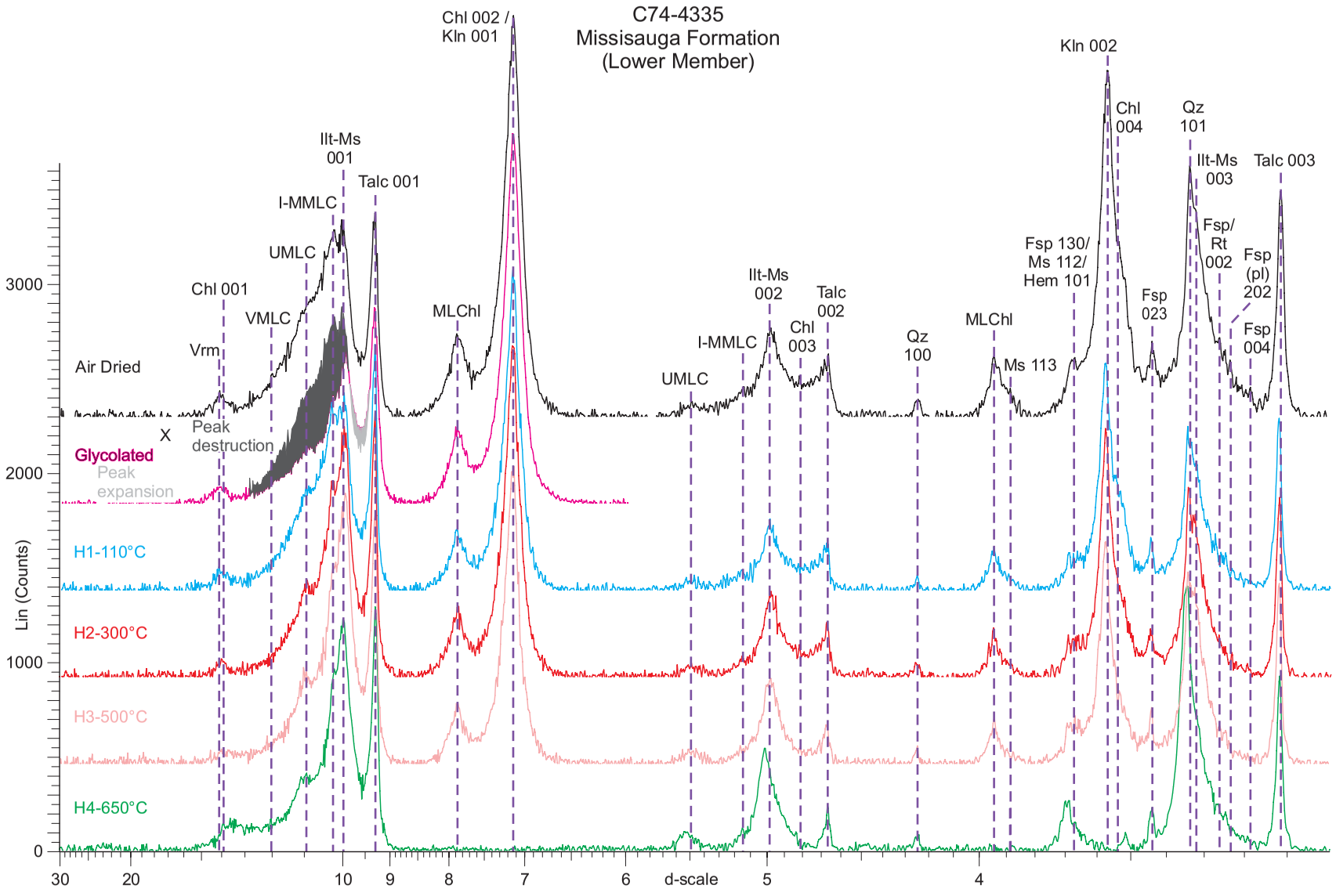
C74-4335
Missisauga Formation
(Lower Member)
Chl 002 /
Kln 001
Kln 002
Chl
004
Qz
101
Ilt-Ms
001
Talc 001
I-MMLC
UMLC
Ilt-Ms
003
Talc 003
Fsp/
Rt
002
Fsp
(pl)
202
Fsp
004
Fsp 130/
Ms 112/
Hem 101
Fsp
023
Ilt-Ms
002
Talc
002
Chl
003
Qz
100
MLChl
Ms 113
Chl 001
VMLC
MLChl
Vrm
Air Dried
X
Peak
destruction
Glycolated
Peak
expansion
H1-110°C
H2-300°C
H3-500°C
H4-650°C
Lin (Counts)
3000
2000
1000
0
30
20
10
9
8
7
6
d-scale
5
4

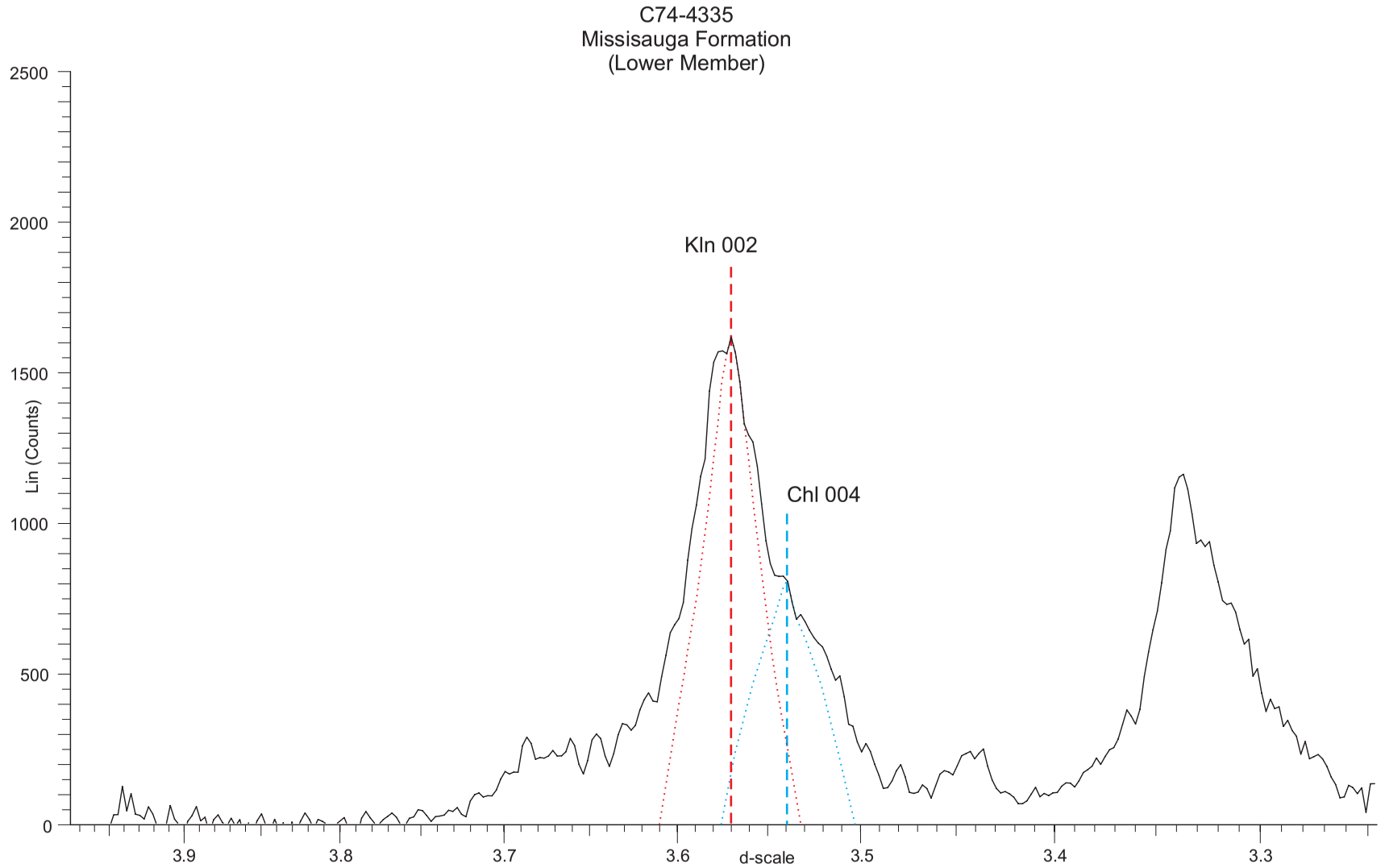
C74-4335
Missisauga Formation
(Lower Member)
Kln 002
Chl 004
Lin (Counts)
2500
2000
1500
1000
500
0
3.9
3.8
3.7
3.6
d-scale
3.5
3.4
3.3

I93-3080.38
Missisauga Formation
(Middle Member)

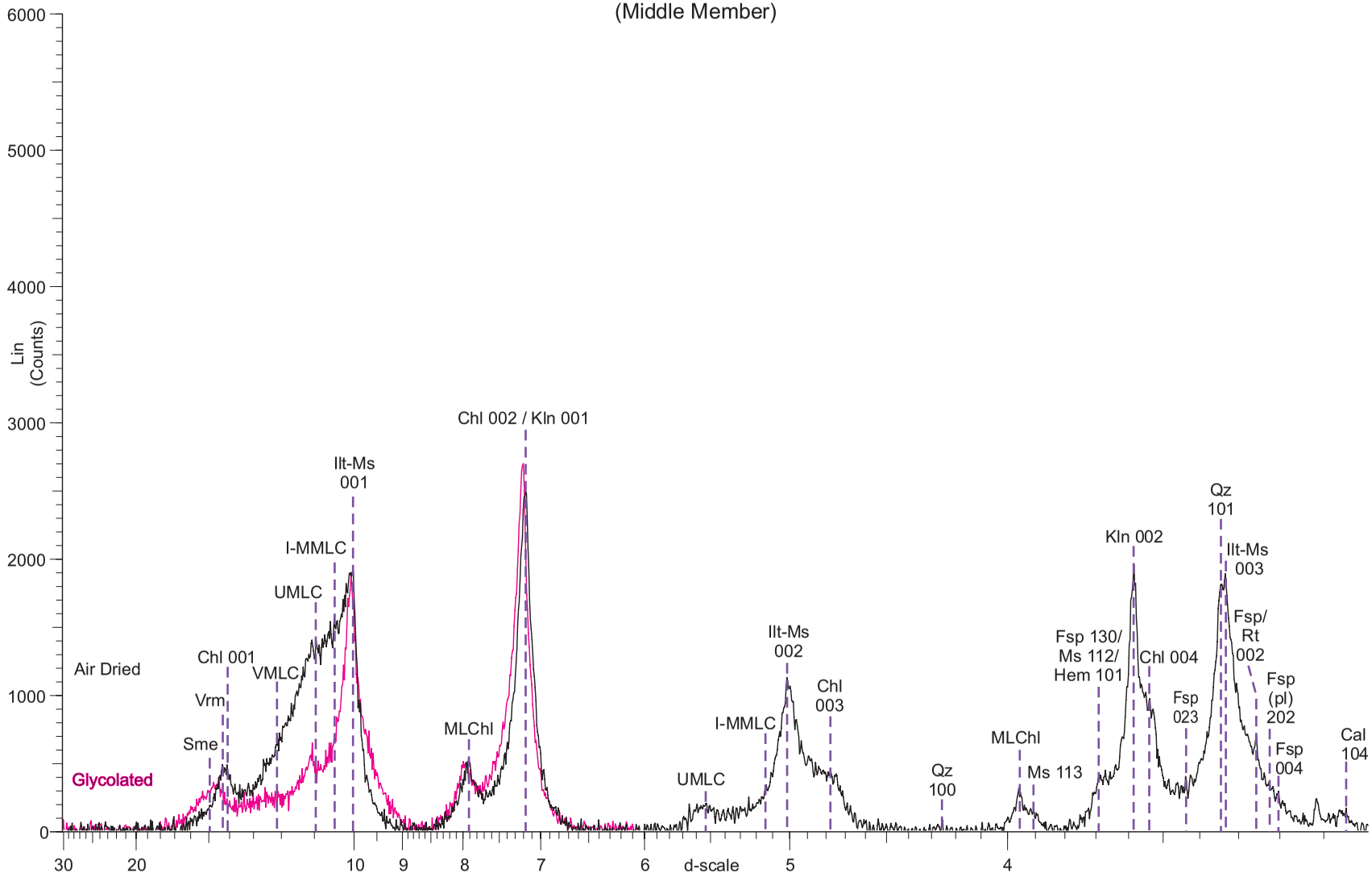

APPENDIX 2:
X-RAY DIFFRACTION OF KEY CLAY MINERALS FROM SIDEPACK SAMPLES VS DEPTH

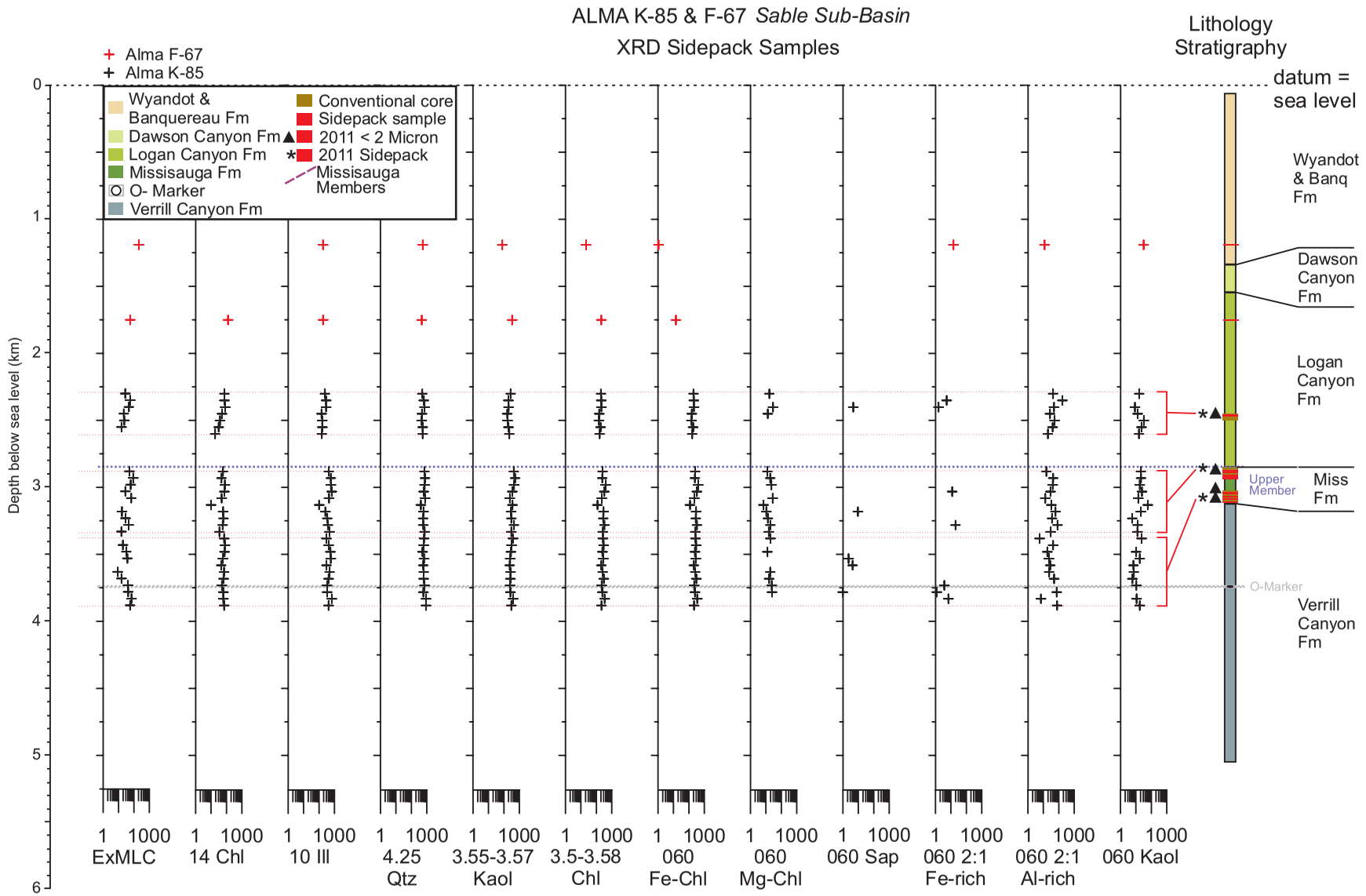
ALMA K-85 & F-67 Sable Sub-Basin
XRD Sidepack Samples
Alma F-67
Alma K-85
Wyandot & Banquereau Fm
Dawson Canyon Fm
Logan Canyon Fm
Missisauga Fm
O- Marker
Verrill Canyon Fm
Conventional core
Sidepack sample
2011 < 2 Micron
2011 Sidepack
Missisauga Members
Depth below sea level (km)
0
1
2
3
4
5
6
1 1000 ExMLC
1 1000 14 Chl
1 1000 10 Ill
1 1000 4.25 Qtz
1 1000 3.55-3.57 Kaol
1 1000 3.5-3.58 Chl
1 1000 060 Fe-Chl
1 1000 060 Mg-Chl
1 1000 060 Sap
1 1000 060 2:1 Fe-rich
1 1000 060 2:1 Al-rich
1 1000 060 Kaol
Lithology Stratigraphy
datum = sea level
Wyandot & Banq Fm
Dawson Canyon Fm
Logan Canyon Fm
Upper Member
Miss Fm
O-Marker
Verrill Canyon Fm

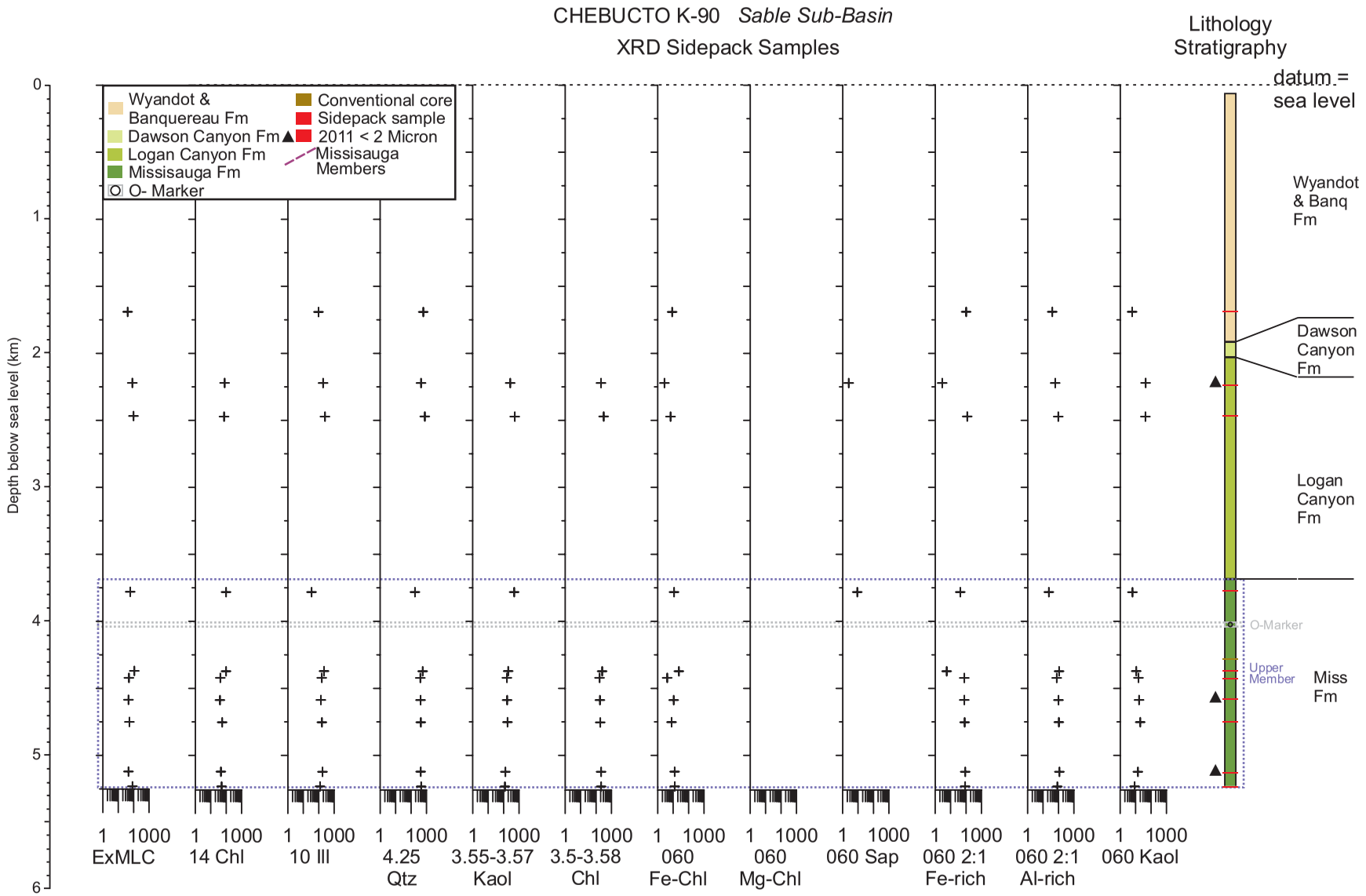
CHEBUCTO K-90 *Sable Sub-Basin*
XRD Sidepack Samples
Lithology
Stratigraphy
datum = sea level
Depth below sea level (km)
Wyandot & Banquereau Fm
Dawson Canyon Fm
Logan Canyon Fm
Missisauga Fm
O- Marker
Conventional core
Sidepack sample
2011 < 2 Micron
Missisauga Members
Wyandot & Banq Fm
Dawson Canyon Fm
Logan Canyon Fm
O-Marker
Upper Member
Miss Fm
1 1000 ExMLC
1 1000 14 Chl
1 1000 10 Ill
1 1000 4.25 Qtz
1 1000 3.55-3.57 Kaol
1 1000 3.5-3.58 Chl
1 1000 060 Fe-Chl
1 1000 060 Mg-Chl
1 1000 060 Sap
1 1000 060 2:1 Fe-rich
1 1000 060 2:1 Al-rich
1 1000 060 Kaol

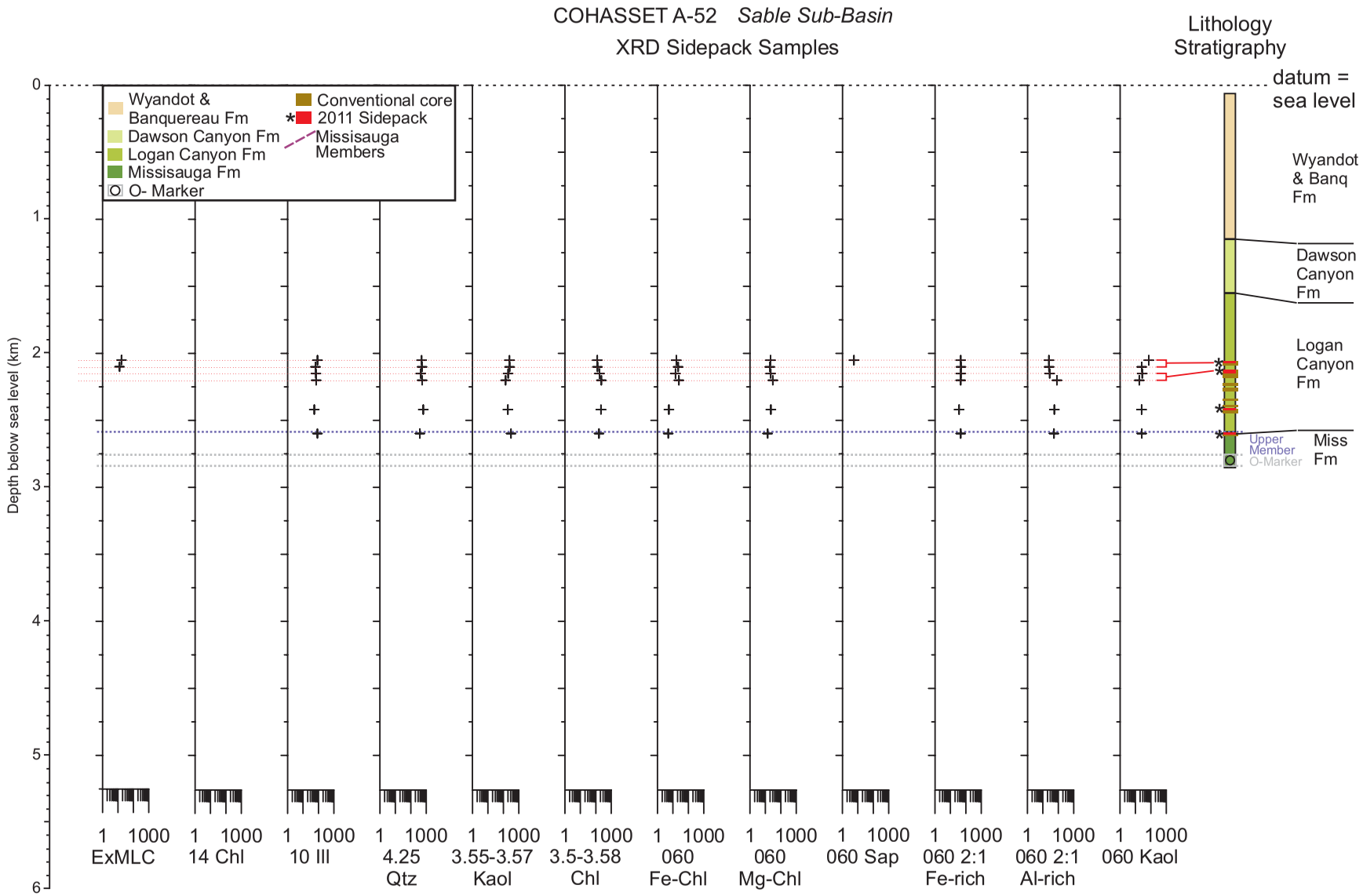
COHASSET A-52 *Sable Sub-Basin*
XRD Sidepack Samples
Lithology
Stratigraphy
datum =
sea level
Depth below sea level (km)
0
1
2
3
4
5
6
Wyandot &
Banquereau Fm
Dawson Canyon Fm
Logan Canyon Fm
Missisauga Fm
O- Marker
Conventional core
2011 Sidepack
Missisauga
Members
Wyandot
& Banq
Fm
Dawson
Canyon
Fm
Logan
Canyon
Fm
Upper
Member
Miss
Fm
O-Marker
1 1000
ExMLC
1 1000
14 Chl
1 1000
10 Ill
1 1000
4.25
Qtz
1 1000
3.55-3.57
Kaol
1 1000
3.5-3.58
Chl
1 1000
060
Fe-Chl
1 1000
060
Mg-Chl
1 1000
060 Sap
1 1000
060 2:1
Fe-rich
1 1000
060 2:1
Al-rich
1 1000
060 Kaol

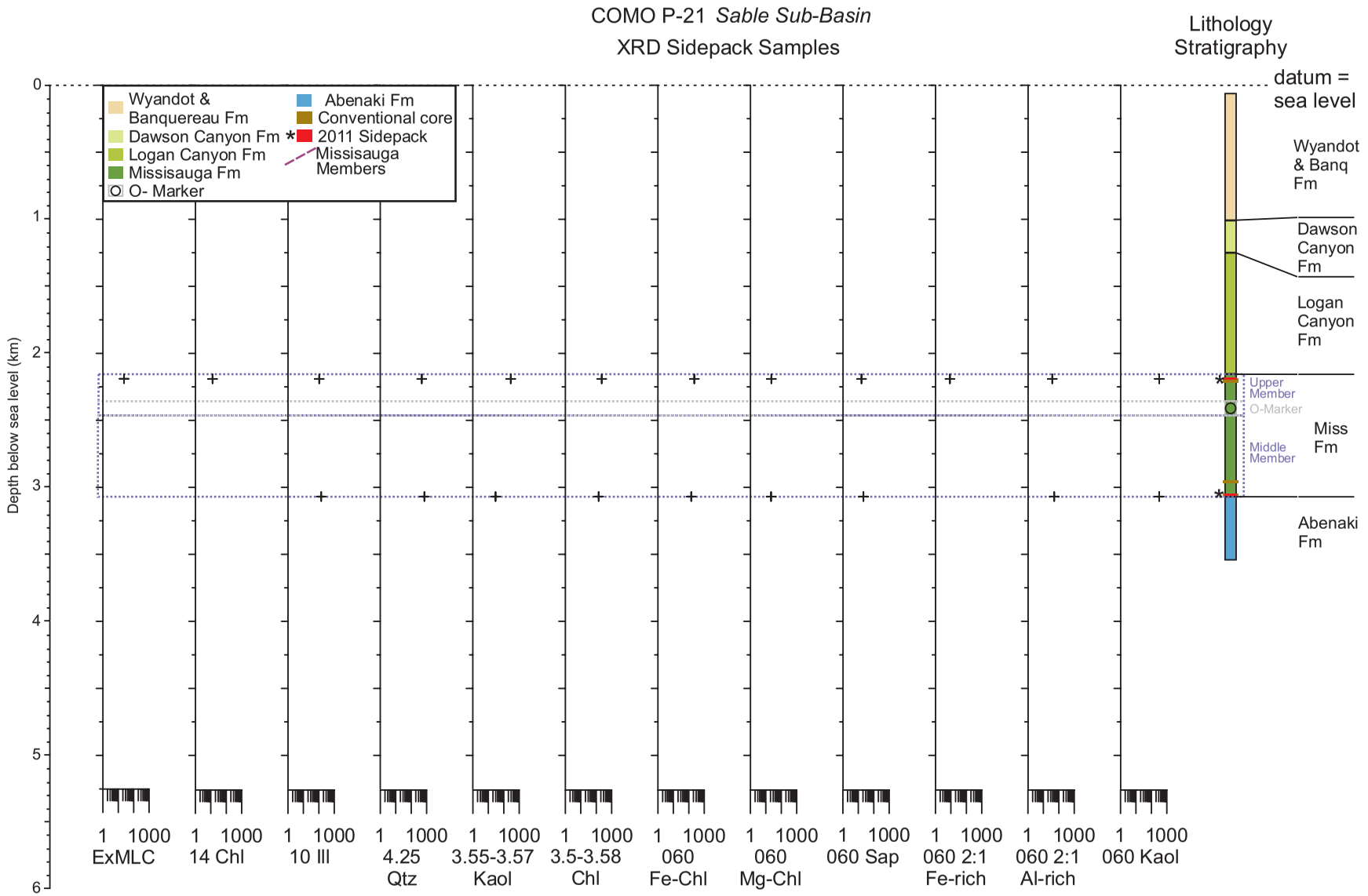
COMO P-21 Sable Sub-Basin
XRD Sidepack Samples
Lithology
Stratigraphy
datum =
sea level
Depth below sea level (km)
Wyandot &
Banquereau Fm
Dawson Canyon Fm
Logan Canyon Fm
Missisauga Fm
O- Marker
Abenaki Fm
Conventional core
2011 Sidepack
Missisauga
Members
Wyandot
& Banq
Fm
Dawson
Canyon
Fm
Logan
Canyon
Fm
Upper
Member
O-Marker
Middle
Member
Miss
Fm
Abenaki
Fm
0
1
2
3
4
5
6
1 1000
ExMLC
1 1000
14 Chl
1 1000
10 Ill
1 1000
4.25
Qtz
1 1000
3.55-3.57
Kaol
1 1000
3.5-3.58
Chl
1 1000
060
Fe-Chl
1 1000
060
Mg-Chl
1 1000
060 Sap
1 1000
060 2:1
Fe-rich
1 1000
060 2:1
Al-rich
1 1000
060 Kaol

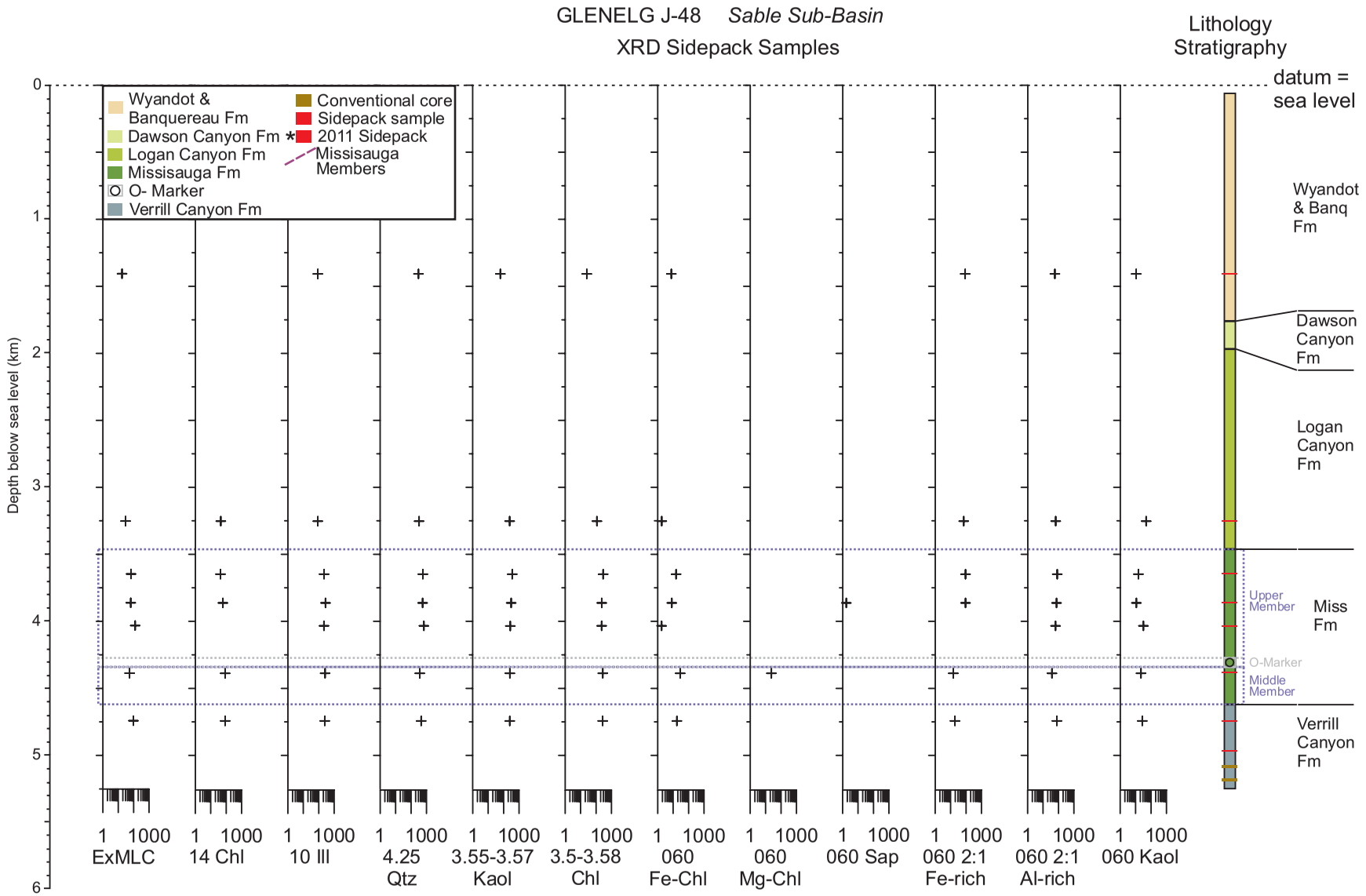
GLENELG J-48 *Sable Sub-Basin*
XRD Sidepack Samples
Lithology Stratigraphy
datum = sea level
Depth below sea level (km)
Wyandot & Banquereau Fm
Dawson Canyon Fm
Logan Canyon Fm
Missisauga Fm
O- Marker
Verrill Canyon Fm
Conventional core
Sidepack sample
2011 Sidepack
Missisauga Members
Wyandot & Banq Fm
Dawson Canyon Fm
Logan Canyon Fm
Upper Member
Miss Fm
O-Marker
Middle Member
Verrill Canyon Fm
1 1000 ExMLC
1 1000 14 Chl
1 1000 10 Ill
1 1000 4.25 Qtz
1 1000 3.55-3.57 Kaol
1 1000 3.5-3.58 Chl
1 1000 060 Fe-Chl
1 1000 060 Mg-Chl
1 1000 060 Sap
1 1000 060 2:1 Fe-rich
1 1000 060 2:1 Al-rich
1 1000 060 Kaol

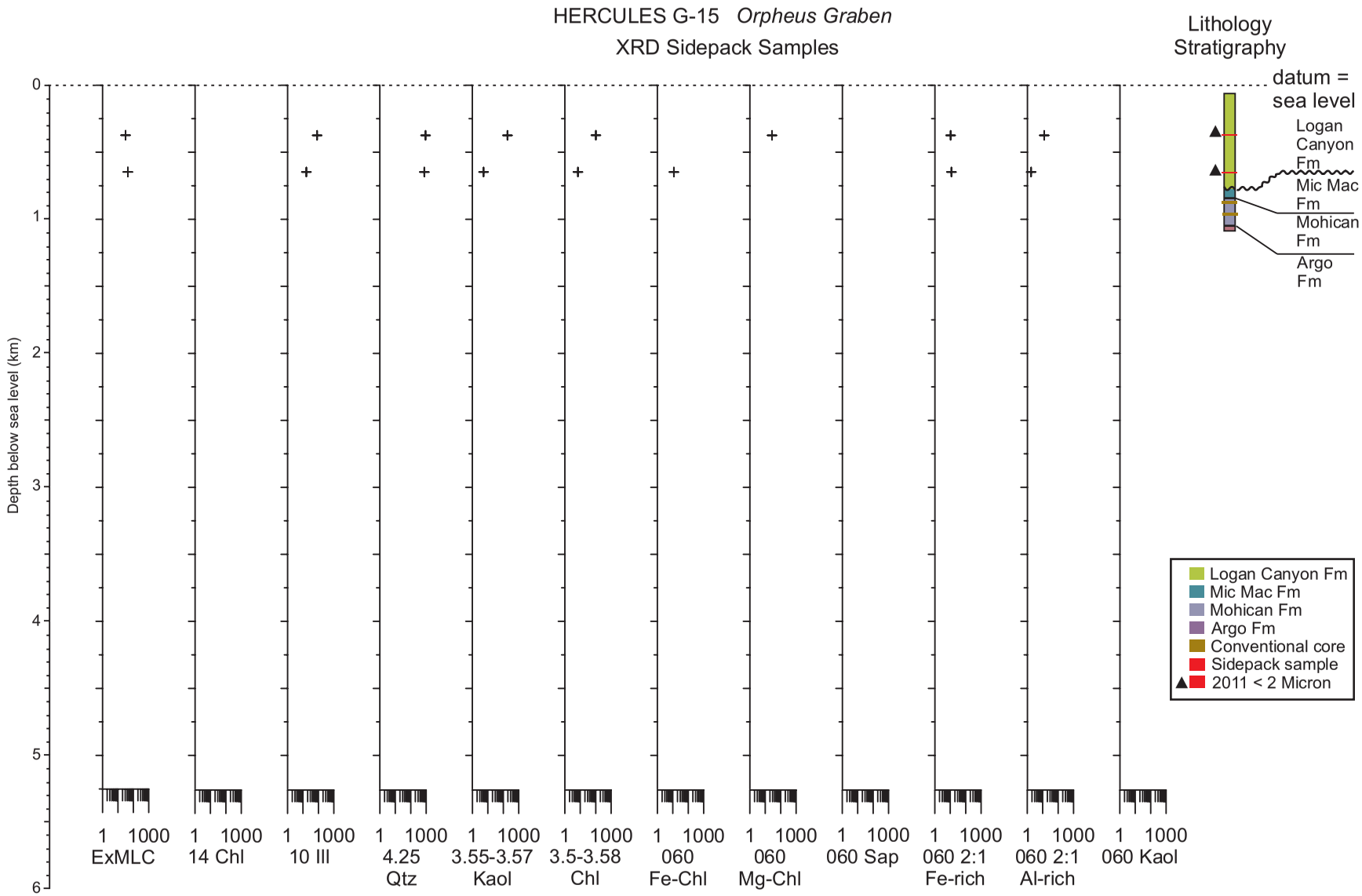
HERCULES G-15 *Orpheus Graben*
XRD Sidepack Samples
Lithology
Stratigraphy
datum =
sea level
Logan
Canyon
Fm
Mic Mac
Fm
Mohican
Fm
Argo
Fm
Depth below sea level (km)
0
1
2
3
4
5
6
1 1000
ExMLC
14 Chl
10 Ill
4.25
Qtz
3.55-3.57
Kaol
3.5-3.58
Chl
060
Fe-Chl
060
Mg-Chl
060 Sap
060 2:1
Fe-rich
060 2:1
Al-rich
060 Kaol
Logan Canyon Fm
Mic Mac Fm
Mohican Fm
Argo Fm
Conventional core
Sidepack sample
2011 < 2 Micron

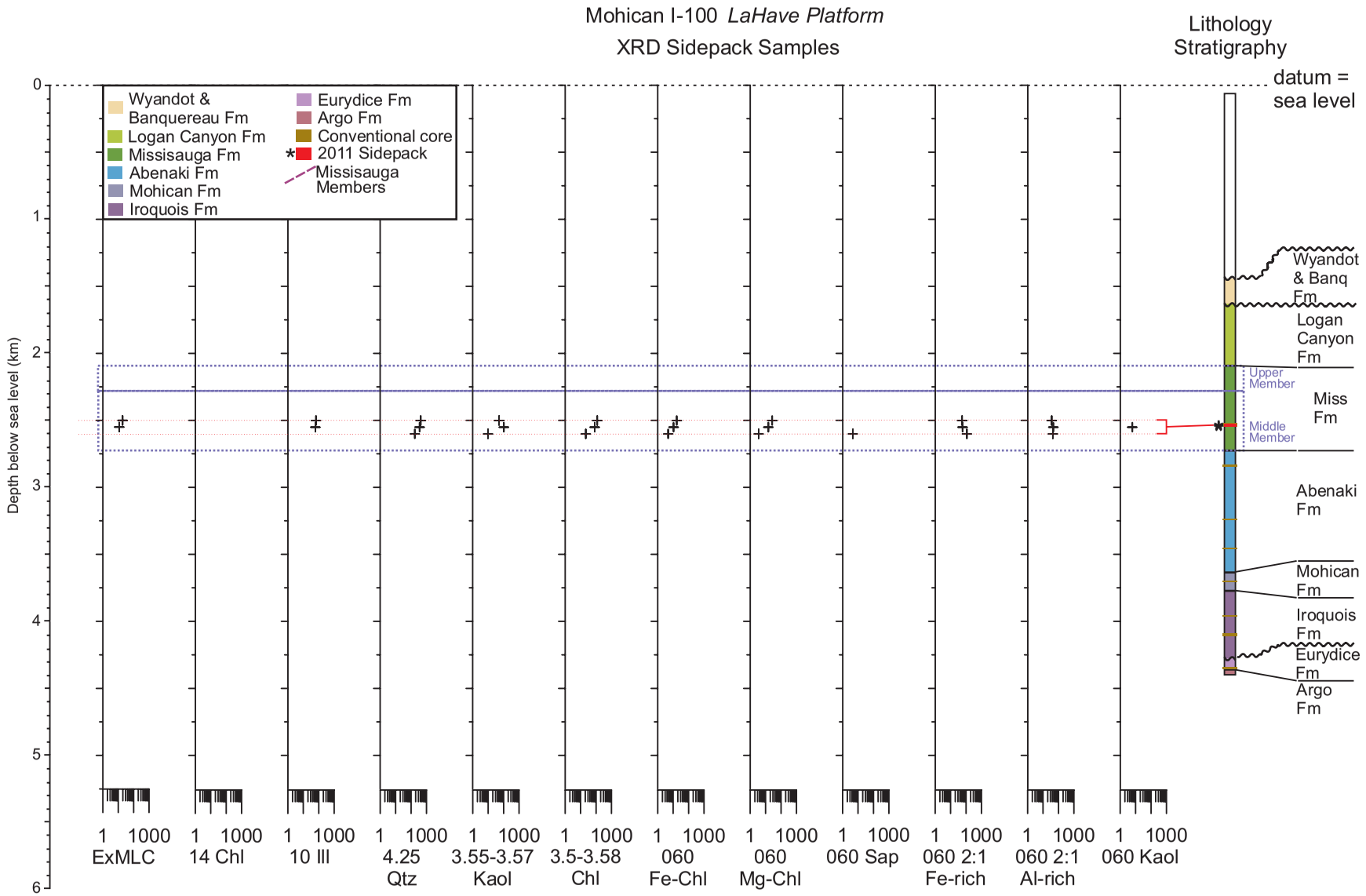
Mohican I-100 *LaHave Platform*
XRD Sidepack Samples
Lithology
Stratigraphy
datum =
sea level
Depth below sea level (km)
0
1
2
3
4
5
6
Wyandot &
Banquereau Fm
Logan Canyon Fm
Missisauga Fm
Abenaki Fm
Mohican Fm
Iroquois Fm
Eurydice Fm
Argo Fm
Conventional core
2011 Sidepack
Missisauga
Members
1 1000
ExMLC
1 1000
14 Chl
1 1000
10 Ill
1 1000
4.25
Qtz
1 1000
3.55-3.57
Kaol
1 1000
3.5-3.58
Chl
1 1000
060
Fe-Chl
1 1000
060
Mg-Chl
1 1000
060 Sap
1 1000
060 2:1
Fe-rich
1 1000
060 2:1
Al-rich
1 1000
060 Kaol
Wyandot
& Banq
Fm
Logan
Canyon
Fm
Upper
Member
Miss
Fm
Middle
Member
Abenaki
Fm
Mohican
Fm
Iroquois
Fm
Eurydice
Fm
Argo
Fm

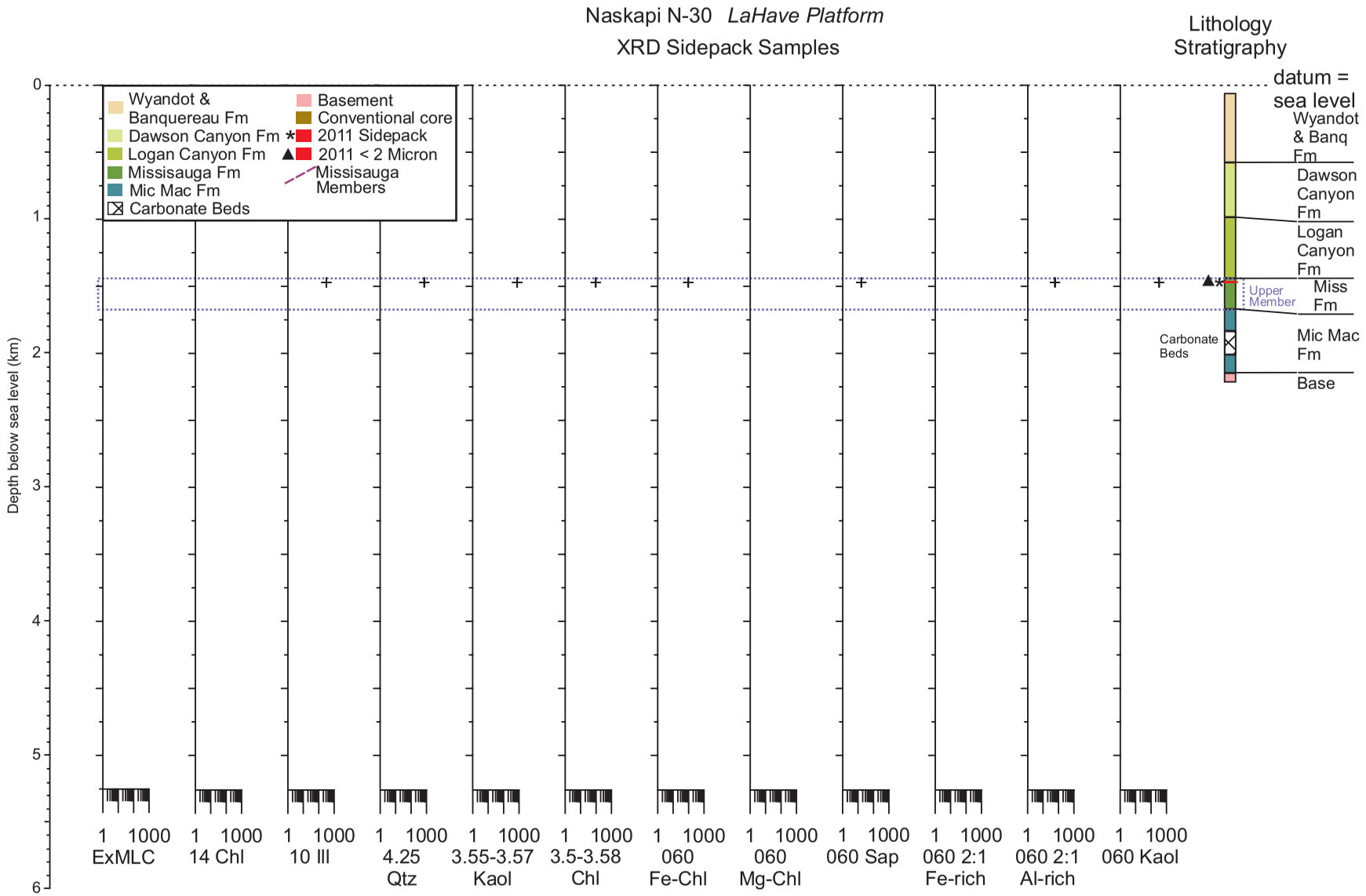
Naskapi N-30 *LaHave Platform*
XRD Sidepack Samples
Lithology
Stratigraphy
datum = sea level
Depth below sea level (km)
Wyandot & Banquereau Fm
Dawson Canyon Fm
Logan Canyon Fm
Missisauga Fm
Mic Mac Fm
Carbonate Beds
Basement
Conventional core
2011 Sidepack
2011 < 2 Micron
Missisauga Members
Wyandot & Banq Fm
Dawson Canyon Fm
Logan Canyon Fm
Upper Member
Miss Fm
Carbonate Beds
Mic Mac Fm
Base
1 1000 ExMLC
1 1000 14 Chl
1 1000 10 Ill
1 1000 4.25 Qtz
1 1000 3.55-3.57 Kaol
1 1000 3.5-3.58 Chl
1 1000 060 Fe-Chl
1 1000 060 Mg-Chl
1 1000 060 Sap
1 1000 060 2:1 Fe-rich
1 1000 060 2:1 Al-rich
1 1000 060 Kaol

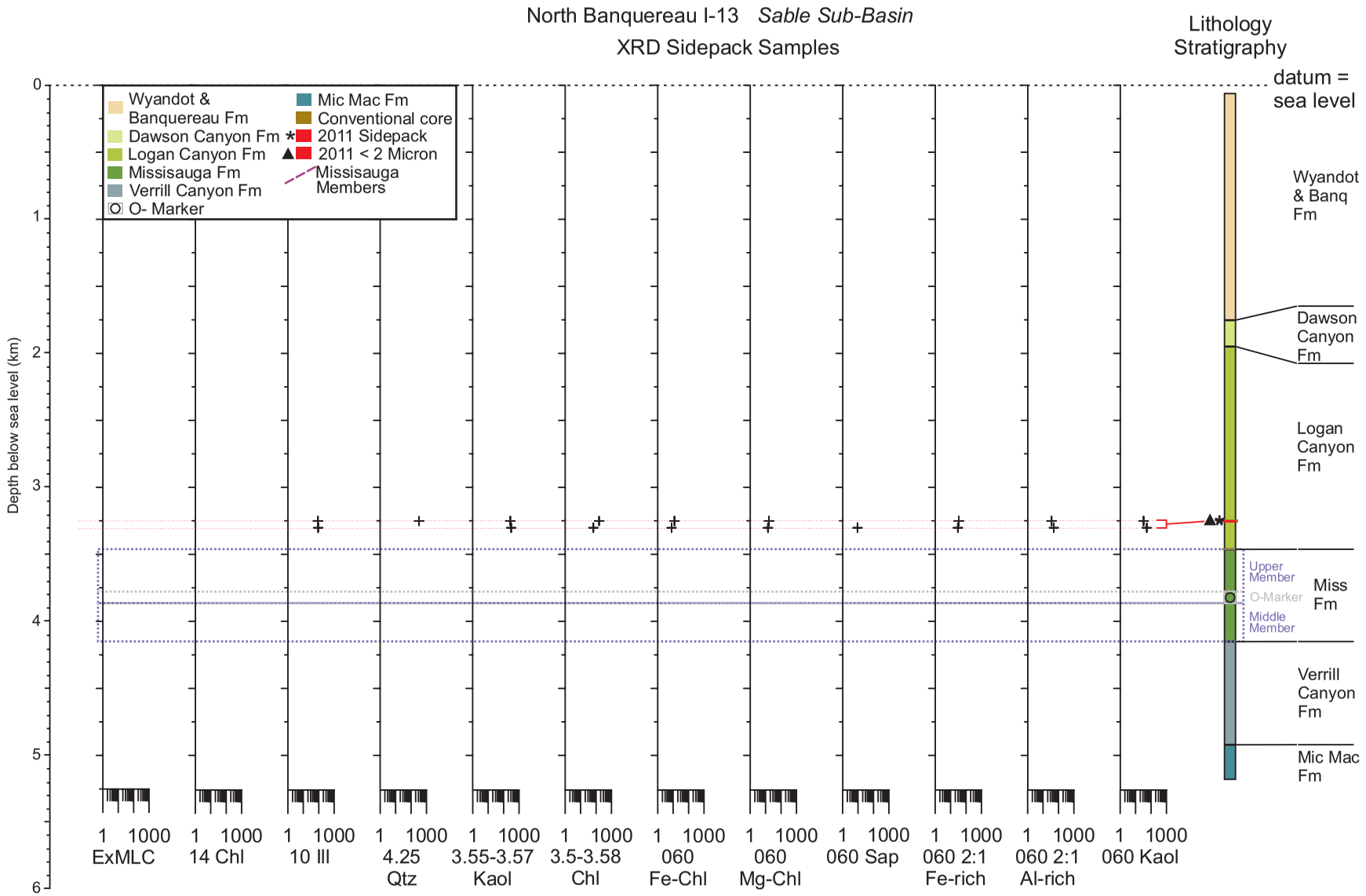
North Banquereau I-13 *Sable Sub-Basin*
XRD Sidepack Samples
Lithology
Stratigraphy
datum =
sea level
Depth below sea level (km)
Wyandot &
Banquereau Fm
Dawson Canyon Fm
Logan Canyon Fm
Missisauga Fm
Verrill Canyon Fm
O- Marker
Mic Mac Fm
Conventional core
2011 Sidepack
2011 < 2 Micron
Missisauga
Members
Wyandot
& Banq
Fm
Dawson
Canyon
Fm
Logan
Canyon
Fm
Upper
Member
O-Marker
Middle
Member
Miss
Fm
Verrill
Canyon
Fm
Mic Mac
Fm
1 1000
ExMLC
1 1000
14 Chl
1 1000
10 Ill
1 1000
4.25
Qtz
1 1000
3.55-3.57
Kaol
1 1000
3.5-3.58
Chl
1 1000
060
Fe-Chl
1 1000
060
Mg-Chl
1 1000
060 Sap
1 1000
060 2:1
Fe-rich
1 1000
060 2:1
Al-rich
1 1000
060 Kaol

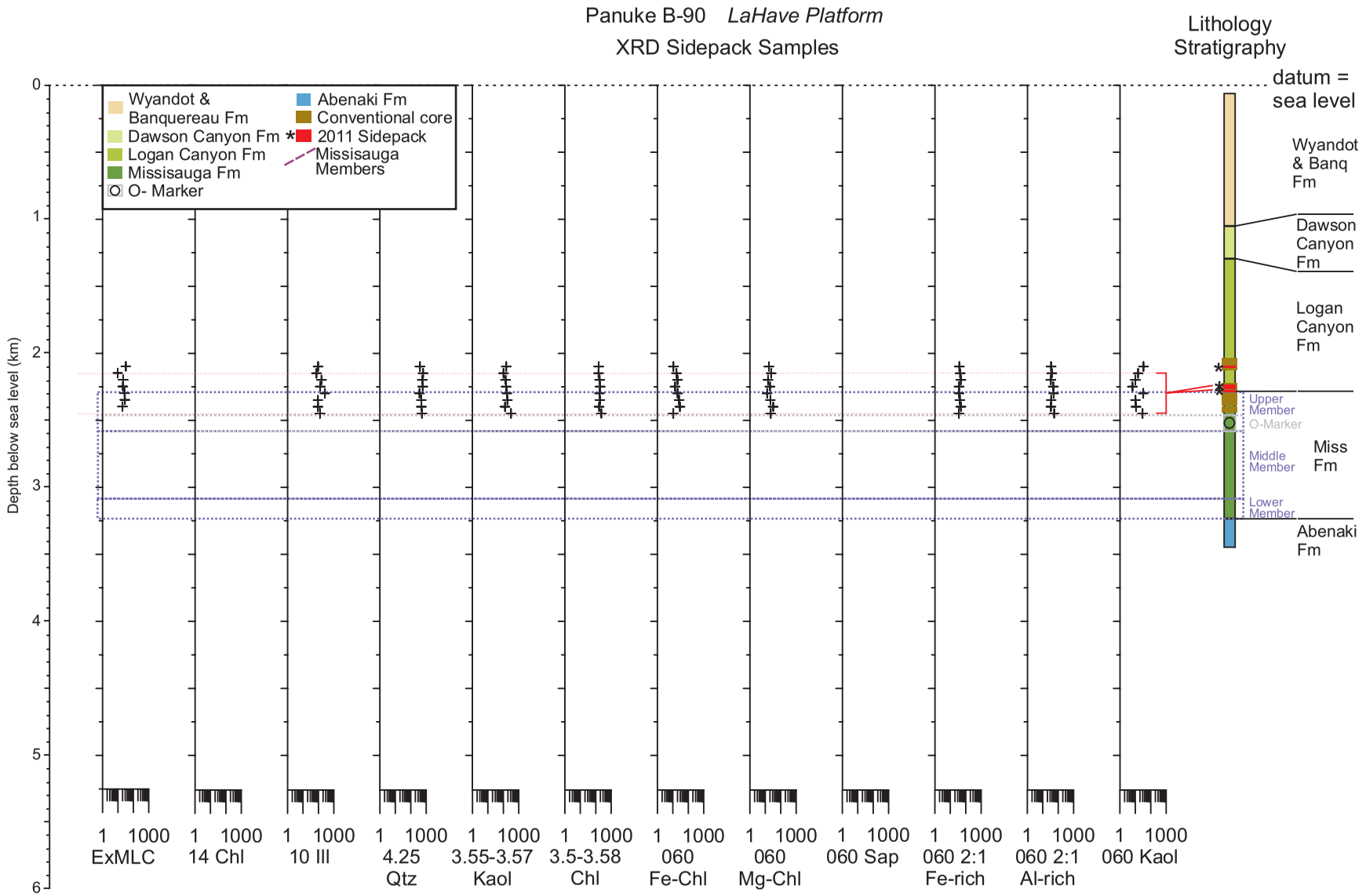
Panuke B-90 *LaHave Platform*
XRD Sidepack Samples
Lithology
Stratigraphy
datum =
sea level
Depth below sea level (km)
0
1
2
3
4
5
6
Wyandot &
Banquereau Fm
Dawson Canyon Fm
Logan Canyon Fm
Missisauga Fm
O- Marker
Abenaki Fm
Conventional core
2011 Sidepack
Missisauga
Members
Wyandot
& Banq
Fm
Dawson
Canyon
Fm
Logan
Canyon
Fm
Upper
Member
O-Marker
Middle
Member
Miss
Fm
Lower
Member
Abenaki
Fm
1 1000
ExMLC
1 1000
14 Chl
1 1000
10 Ill
1 1000
4.25
Qtz
1 1000
3.55-3.57
Kaol
1 1000
3.5-3.58
Chl
1 1000
060
Fe-Chl
1 1000
060
Mg-Chl
1 1000
060 Sap
1 1000
060 2:1
Fe-rich
1 1000
060 2:1
Al-rich
1 1000
060 Kaol

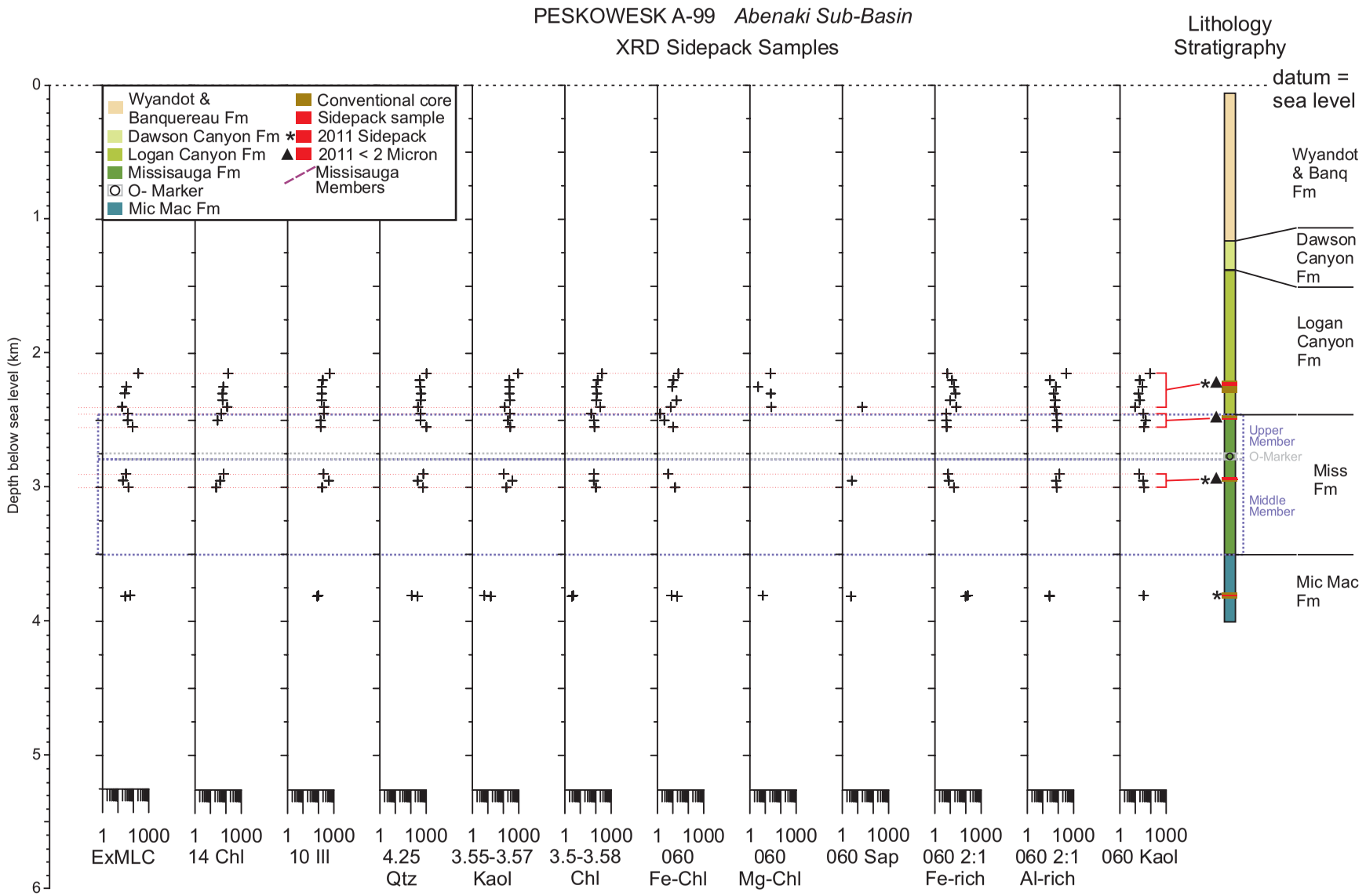
PESKOWESK A-99 *Abenaki Sub-Basin*
XRD Sidepack Samples
Lithology Stratigraphy
datum = sea level
Depth below sea level (km)
Wyandot & Banquereau Fm
Dawson Canyon Fm
Logan Canyon Fm
Missisauga Fm
O- Marker
Mic Mac Fm
Conventional core
Sidepack sample
2011 Sidepack
2011 < 2 Micron
Missisauga Members
Wyandot & Banq Fm
Dawson Canyon Fm
Logan Canyon Fm
Upper Member
O-Marker
Miss Fm
Middle Member
Mic Mac Fm
1 1000 ExMLC
1 1000 14 Chl
1 1000 10 Ill
1 1000 4.25 Qtz
1 1000 3.55-3.57 Kaol
1 1000 3.5-3.58 Chl
1 1000 060 Fe-Chl
1 1000 060 Mg-Chl
1 1000 060 Sap
1 1000 060 2:1 Fe-rich
1 1000 060 2:1 Al-rich
1 1000 060 Kaol

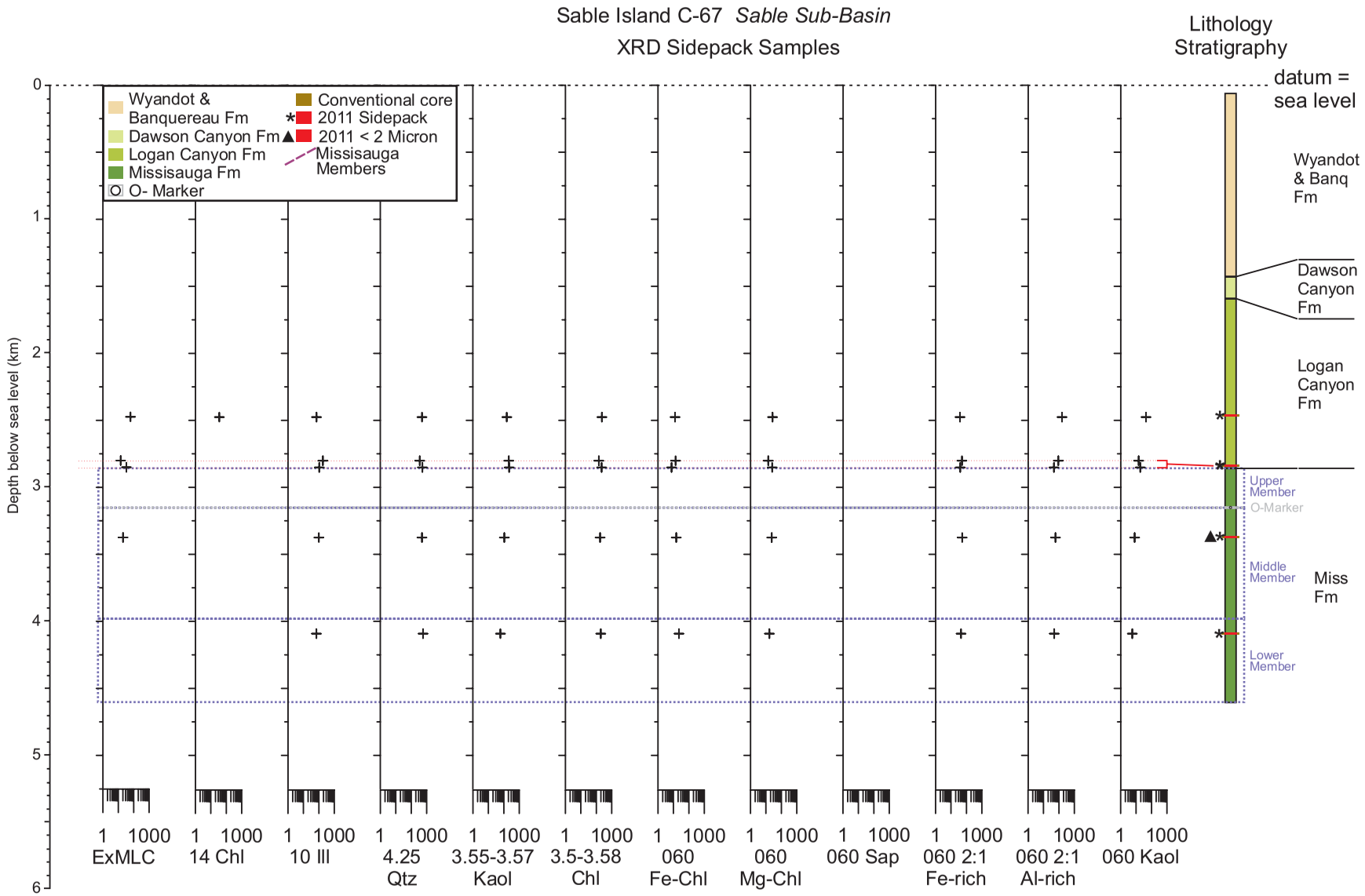
Sable Island C-67 *Sable Sub-Basin*
XRD Sidepack Samples
Lithology
Stratigraphy
datum =
sea level
Depth below sea level (km)
0
1
2
3
4
5
6
Wyandot &
Banquereau Fm
Dawson Canyon Fm
Logan Canyon Fm
Missisauga Fm
O- Marker
Conventional core
2011 Sidepack
2011 < 2 Micron
Missisauga
Members
Wyandot
& Banq
Fm
Dawson
Canyon
Fm
Logan
Canyon
Fm
Upper
Member
O-Marker
Middle
Member
Miss
Fm
Lower
Member
1 1000
ExMLC
1 1000
14 Chl
1 1000
10 Ill
1 1000
4.25
Qtz
1 1000
3.55-3.57
Kaol
1 1000
3.5-3.58
Chl
1 1000
060
Fe-Chl
1 1000
060
Mg-Chl
1 1000
060 Sap
1 1000
060 2:1
Fe-rich
1 1000
060 2:1
Al-rich
1 1000
060 Kaol

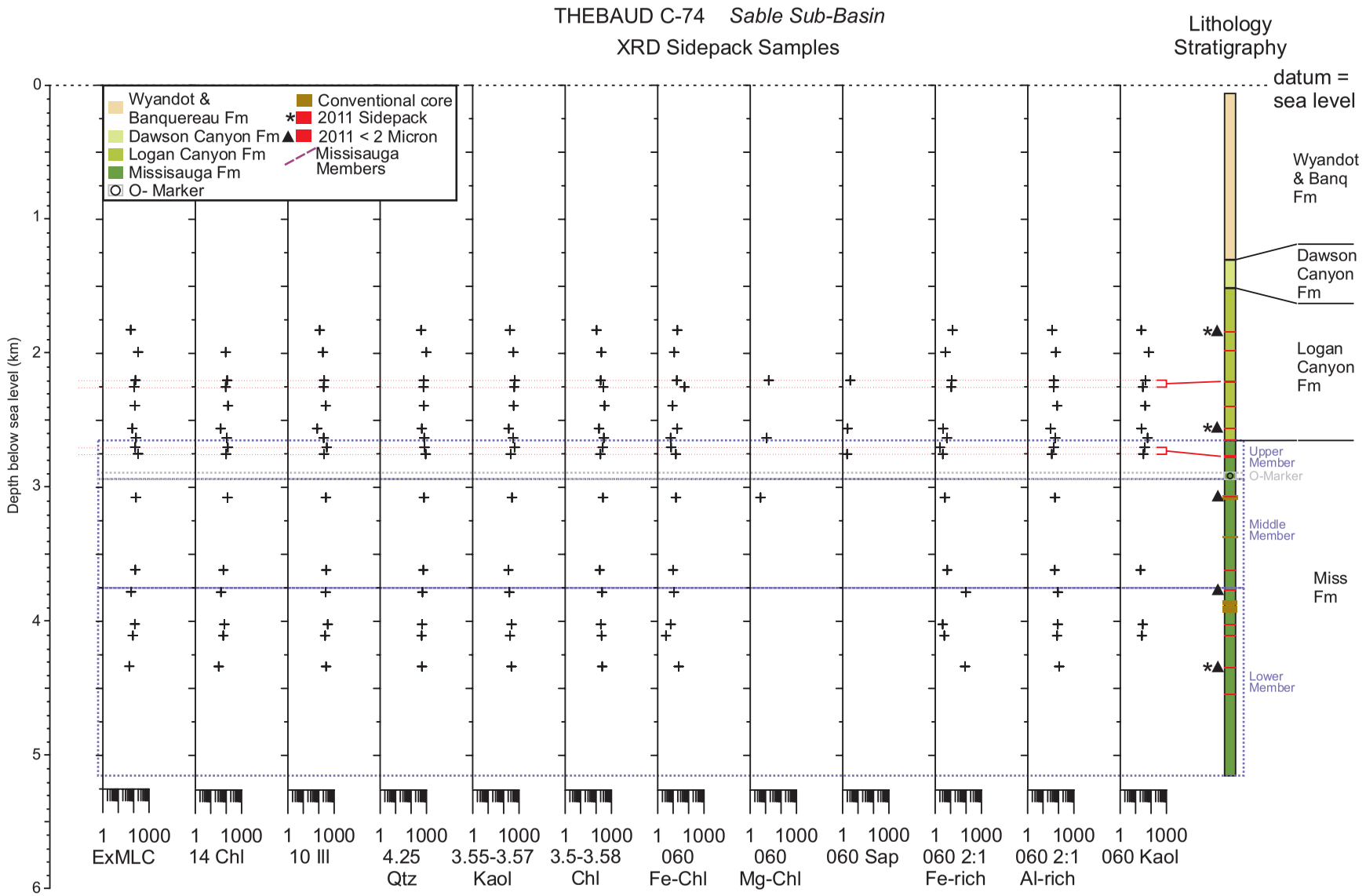
THEBAUD C-74 *Sable Sub-Basin*
XRD Sidepack Samples
Lithology
Stratigraphy
datum = sea level
Depth below sea level (km)
Wyandot & Banquereau Fm
Dawson Canyon Fm
Logan Canyon Fm
Missisauga Fm
O- Marker
Conventional core
2011 Sidepack
2011 < 2 Micron
Missisauga Members
Wyandot & Banq Fm
Dawson Canyon Fm
Logan Canyon Fm
Upper Member
O-Marker
Middle Member
Miss Fm
Lower Member
1 1000 ExMLC
1 1000 14 Chl
1 1000 10 Ill
1 1000 4.25 Qtz
1 1000 3.55-3.57 Kaol
1 1000 3.5-3.58 Chl
1 1000 060 Fe-Chl
1 1000 060 Mg-Chl
1 1000 060 Sap
1 1000 060 2:1 Fe-rich
1 1000 060 2:1 Al-rich
1 1000 060 Kaol

APPENDIX 3

X-RAY DIFFRACTION METHODS AND PEAK PICKING

SAMPLE PREPARATION METHOD:

1. If using large rock samples: Break off a small piece place it in the crusher and hammer on it until it is coarse (approx. 5-10 Min). If starting out with finer grained samples skip to step 2. If using clays move to step 3 or 4 depending on if a zincite standard is being used.

2. Place the crushed sample in the mortar and pestle and grind for approximately ten minutes.

3. Zero the scale with the vial on it. Measure out appropriate amount of sample into the vial then zero again and add ZnO standard. When measuring the samples try to ensure that if there are any larger pieces they are left out.

4. Mix thoroughly in the vial to ensure a representative sample is used and take enough to fill one slide and put it into the mortar and pestle.

5. Add a small amount of Methanol to the sample and grind for 2-10 minutes depending on the hardness of the sample

6. Score the back of a slide with the sample number using a glass cutter. Use a pipette to transfer the sample + Methanol onto the slide (enough to totally cover the slide).

7. Be sure to completely cover the slide with the prepared sample, however, do not overfill the slide, if it is too thick it may be damaged in the XRD.

8. Place the slide in a slightly warm oven (60°C) to dry.

9. Check slides for cracks in the samples after drying. If the samples have cracked too much then steps 5-7 may need to be repeated.

When making standards, after the sample has been weighed and mixed in the vial the entire amount of the sample should be placed in the mortar and pestle with methanol to be crushed.

Make an excel file with sample names, who prepared them, who picked the peaks, depths, type, mount, processes and any other information that may be useful with regards to the samples. Ensure that someone can come along in five years and pick up where you left off.

Mill Grinding Sample Preparation Method:

1. Crush sample with mortar and pestle to pass through a 0.4 mm sieve. Scrape powder in the beaker with a clean spatula.

2. Pass powder through a 0.4 mm sieve.

3. Add ZnO: 10% by weight of sample if standard is desired (0.3 g ZnO to 3 g sample and 4 ml methanol).

4. Insert sample into spaces between the rollers in the grinding jar and for every 3 g of sample add 4 ml of methanol to the sample. Grind for five minutes.

5. After grinding, remove grinding jar and replace lid with closure containing two pore holes (6 mm diameter) pour sample into beaker. Rinse jar with methanol several times to remove any remaining sample.

6. Dry samples then gently force through a 0.4 mm sieve with a pestle to produce a fine powder, and then load sidepack sample holders.

7. Transfer leftover powder in a clean labeled bottle.

8. After the sample is run, transfer it into the bottle with the leftovers.

9. Rinse rollers, grinding jar and lid with tap water and place in ultrasonic bath for two minutes.

10. Rinse rollers, grinding jar and lid with tap and then distilled water. Use acetone on the alumina rollers to accelerate drying while using compressed air on the jar and lid.

Mounts

<2 µm Preparation Method: (SP)

1. Take the freeze dried sample and add a few drops of water to make a paste (The zincite standard and initial sample processing is complete at this point).

2. Score the back of a slide with the sample number using a glass cutter.

3. Using a spatula, place a dollop of the sample paste on a glass slide.

4. Use a piece of photographic film (or something of similar sixe and texture) to smear the paste across the slide to give a thin even film. Ensure movement is unidirectional to properly orient the clays.

5. Let the sample dry in dust free environment such as a fume hood or oven (60°C max).

Sidepack Preparation Method: (SP)

1. If the sample contains water, place the sample on a tray and place in the oven (60°C) to dry.

2. If a zincite standard (or any other standard) is being used, measure and mix in the desired amount (typically 10% ZnO by weight of sample).

3. With the use of methanol and using a mortar and pestle or a mill grinder, grind the sample to a fine powder. Then dry the sample.

4. Pass dried sample through a 0.4 mm sieve (may need to crush again or use a pestle to gently force through the sieve).

5. Cover the sidepack slide with a glass slide and using a paper funnel or spatula; carefully pour the sample into the sidepack slide. Tap on countertop to compact to ensure no voids in the mount.

Smear Preparation Method: (Sm)

1. After the clays are centrifuged, add sufficient water or methanol (if needed) to make a paste (not a soup).

2. If a zincite standard (or any other standard) is being used, measure and mix in the desired amount (typically 10% ZnO by weight of sample).

3. Score the back of a slide with the sample number using a glass cutter.

4. Mix the sample well and transfer approx. 0.3 cc to the edge of a glass slide.

5. Use a piece of photographic film (or something of similar sixe and texture) to smear the paste across the slide to give a thin even film. Allow the mount to dry.

Methanol Preparation Method: (Me)

1. If a standard is needed, add ZnO: 10% by weight of sample.

2. Place sample in a mortar and pestle, add enough methanol to the sample so the crushed sample can be transferred with a pipette. Crush sample thoroughly.

3. Score the back of a slide with the sample number using a glass cutter. Use a pipette to transfer the sample + Methanol onto the slide (enough to totally cover the slide).

4. Dry samples in an oven at 60°C and run them in the XRD.

Bulk Preparation Method: (B)

1. If a standard is needed, add ZnO: 10% by weight of sample.

2. Place sample in a mortar and pestle, add enough methanol to the sample so the crushed sample can be transferred with a pipette. Crush sample thoroughly.

3. Score the back of a slide with the sample number using a glass cutter. Use a pipette to transfer the sample + Methanol onto the slide (enough to totally cover the slide).

4. Dry samples in an oven at 60°C and run them in the XRD.

Treatments

Heat Treatment: (H)

Using the <2 µm preparation steps, replace the glass slide with a high temperature glass slide. Run the samples once after letting them air dry. Then place the samples in an oven and heat to first desired temperature, after which the samples are to be analyzed. Continue heating and analyzing the samples until the maximum desired temperature has been achieved.

Glycolation Treatment: (Gly)

1. Typically used on <2 micron slide, however, can be used on other mounts.

2. Place the slides in a desiccator with ethylene glycol in its base for a minimum of 5 hours. If a vacuum can not be created in the desiccator then place it in an oven at 60°C.

Glycerol Treatment: (Cerol)

1. Typically used on <2 micron slide, however, can be used on other mounts.

2. Place the slides in a desiccator with glycerol in its base for a minimum of five hours. If a vacuum can not be created in the desiccator then place it in an oven at 60°C.

Short Scan Analysis: (SS)

1. This can be done with any type of mount/slide preparation. It is run at 27.5 - 30° 2θ with a step size of 1/4° 2θ per minute.

MEASURING X-RAY DIFFRACTION PEAKS IN THE XRD EVALUATION PROGRAM (EVA) (Non-Sidpack)

1. With the scan open; open the search by name or # box (on toolbar or F5), the box that opens will be called pattern (if it is not already open). From there you type the name of the minerals you are interested in and hit search. This will provide a list of slightly differently spaced standardized peaks, pick the one that is best for your work, either from the search code columns listed in Table 1 or ones you know and are comfortable using. If you are not looking for any specific minerals you can search Quartz so you can align the defractogram to the standard quartz peak in 2-Theta or do not use any standards for d-spacing.

Table 1: Mineral d-spacing.

Peak Priority	d-spacing Å	Intensity	Mineral (miller indicies)
Measure all peaks greater then 10Å (See below for posible mineral type)			
1	**24.800**	**10**	**Smectite (Aliettite)**
	~24.000	10	Mixed clay layer*
	17.700		Kaolinite/expandable mixed layered clay
1	**17.600**	**10**	**Smectite (Montmorillonite)**
	17.000	10	Smectite
1	**17.000**	**10**	**Smectite (Saponite)**
	16.900 - 17.400		Kaolinite/expandable
	15.800	8	Smectite (Hectorite)
1	**15.400**		**Smectite (Nontronite)**
	15.000 - 15.500	10	Chlorite-Smectite
1	**14.000 - 14.600**	**10**	**Vermiculite**
	13.600-14.300	3--10	Chlorite
	13.000	3	Expandable Mixed Layered Clay
1	**12.800**	**10**	**Sepiolite**
	12.400	6.5	Smectite (Aliettite)
	12.000	10	Mica/vermiculite mixed layered clay
	11.000		Vermiculite
1	**10.440**	**10**	**Palygorskite**
1	**10.260**	**10**	**muscovite/illite mixed layer**
1	**10.250**	**10**	**Halloysite-10Å**
	10.100	10	**Glauconite**
	10.100	10	**Biotite**
1	**10.100**		**Illite**
	10.000	10	**Muscovite**
1	**9.300**	**10**	**Talc**
	9.000	5	Smectite (Montmorillonite)
	8.500	5	Smectite (Saponite)
	8.270	1	Smectite (Aliettite)
	7.880		Mixed Layer chlorite
1	**7.630**	**10**	**Gypsum (020)**
	7.600	2	Sepiolite
Note: if small peak at 7.6-7.9Å measure			
Note: if there is a shoulder on the 7.2Å kaolinite note which side.			
1	**7.500**	**10**	**Halloysite-7Å**
1	**7.160-7.200**	**10**	**Kaolinite**/Chlorite Mg (Clinochlore)
1	**7.120-7.150**	**10**	Chlorite Mg (Clinochlore)/**Dickite**
1	**7.050**	**10**	**Chlorite Fe (Chamosite)**
1	**7.040 - 7.120**	**10**	**Berthierine, ferrous**
	5.690	4	Smectite (Saponite)
	5.520		Vermiculite
2	5.150	4	muscovite/illite mixed layer
	5.150	10	Halloysite
	5.050 - 5.020	5	Muscovite
	5.000		Illite (For clays offshore NS)
	4.960	1	Smectite (Aliettite)
	4.780		Chlorite Mg (Clinochlore)
	4.690	6	Plagioclase (oligoclase)
	4.670	9	Talc
1	**4.580**	**10**	**Smectite (Hectorite)**
	4.580	5	Smectite (Saponite)
	4.560		Smectite (Nontronite)
	4.530	9	Glauconite/Celadonite
1	**4.498**	**10**	**Chloritoid**
	4.490	8	Smectite (Montmorillonite)
	4.480		Illite
	4.480	8	Kaolinite (disordered)
	4.500 - 4.466	2	Palygorskite
2	4.449	10	**Chloritoid**
	4.440	9	Halloysite
	4.360	7	Kaolinite/Dickite
2	4.280	5	**Gypsum**
1	**4.260**	**3**	**Quartz (100)**

Note: the presence of feldspars maybe confirmed by peaks for plagioclase at 4.2-4.23Å and K-feldspars at 4.03-4.02Å.			
	4.235	5	K-Feldspar (sanidine)
	4.210 - 4.230	7	K-feldspar (orthoclase)
1	**4.220**	**10**	**K-Feldspar (microcline)**
	4.220	7	K-Feldspar (orthoclase)
1	**4.150 - 4.180**	**10**	**Goethite**
	4.106	1.6	K-Feldspar (anorthoclase)
	4.040	8	Plagioclase (andesine)
	4.040	5	Plagioclase (anorthite)
	4.030	1.6	Plagioclase (albite)
	4.030	8	Plagioclase (labradorite)
	4.020	8	Plagioclase (oligoclase)
	3.940		Mixed Layer Chlorite
	3.890	4	Muscovite (2M)
	3.860	1	Calcite
	3.686	3	Hematite
	3.684	3	Plagioclase (albite)
	3.660	6	Muscovite (1M)
	3.580	4	Smectite (Montmorillonite)
2	3.570	7	**Kaolinite**
1	**3.550**	**7--10**	**Chlorite Fe**
	3.540	1	Smectite (Aliettite)
	3.520	10	**Chlorite Fe (Chamosite)**
	3.510	10	Berthierine
1	**3.490**	**10**	**Anhydrite (020)**
1	**3.445**	**10**	**Barite**
	3.400	5	Halloysite-10Å
1	**3.370**	**10**	**Biotite**
	3.370	8	Smectite (Saponite)
1	**3.350**	**10**	**Muscovite (2M)**
2	3.340	10	**Quartz (101) (for carbonates)**
	3.320		Illite (For clays offshore NS)
1	**3.310**	**10**	**K-feldspar (orthoclase)**
	3.290	6	K-Feldspar (microcline)
	3.290	6	K-Feldspar (orthoclase)
	3.284	6	K-Feldspar (sanidine)
	3.260	5	Plagioclase (anorthite)
	3.260	8	K-Feldspar (microcline)
	3.250	8	K-Feldspar (microcline)
1	**3.250**	**10**	**Rutile**
	3.243	9	K-Feldspar (anorthoclase)
	3.240	4	K-Feldspar (microcline)
	3.240	6.5	K-Feldspar (orthoclase)
	3.240	5	Palygorskite
	3.225	5	K-Feldspar (sanidine)
1	**3.211**	**10**	**K-Feldspar (anorthoclase)**
1	**3.210**	**10**	**Plagioclase (andesine)**
	3.210	6	Plagioclase (anorthite)
1	**3.200**	**10**	**Plagioclase (labradorite)**
1	**3.200**	**10**	**Plagioclase (oligoclase)**
1	**3.196**	**10**	**Plagioclase (albite)**
1	**3.190**	**10**	**Plagioclase (anorthite)**
	3.180	9	Plagioclase (andesine)
	3.180	9	Plagioclase (anorthite)
	3.170	8	Plagioclase (labradorite)
	3.170	8	Plagioclase (oligoclase)
	3.140	7	Plagioclase (andesine)
	3.120	4	Pyrite
2	3.110		**Talc**
	3.100	10	Barite
	3.100	1	Smectite (Aliettite)
1	**3.040**	**10**	**Calcite (104)**
1	3.000	4-7	**Mg-calcite (104)**
	2.992	5	K-feldspar (orthoclase)
	2.990	3	Smectite (Montmorillonite)

	2.963	9	Chloritoid
	2.94-2.93	7	Plagioclase (albite/ andesine/ labradorite)
1	**2.900**	**10**	**Ankerite (104)**
1	**2.890**	**10**	**Dolomite (104)**
1	**2.820**	**10**	**Halite (200)**
	2.810	7	Zincite internal standard (100) (If halite and siderite are absent)
1	**2.790**	**10**	**Siderite (104) (overlaps with ZnO)**
1	**2.740**	**10**	**Magnesite**
1	**2.710**	**9**	**Pyrite (200)**
1	**2.700**	**10**	**Hematite**
	2.660	8	Biotite
	2.660	8	Smectite (Hectorite)
	2.640		Smectite (Nontronite)
	2.639	5	Chloritoid
	2.600	5	Zincite internal standard (002) (for carbonates)
1	**2.587**	**10**	**Glauconite**
1	**2.580**	**10**	**Celadonite**
	2.580	5	Sepiolite
	2.580	4	Smectite (Saponite)
	2.570	9	Muscovite (1M)
	2.570	4	Smectite (Montmorillonite)
	2.560	6/4	Kaolinite/Dickite
	2.560		Smectite (Nontronite)
	2.530	10	Berthierine
	2.510	7	Hematite
	2.487	5	Rutile
	2.480	6	Smectite (Hectorite)
	2.480	1	Smectite (Aliettite)
1	**2.470**	**10**	**Zincite internal standard (highest intensity should be measured for qualitative reasons)**
	2.457	1	Quartz
	2.450	5	Goethite
	2.450	5	Serpentines
	2.430		Smectite (Nontronite)
	2.400		Quartz
	2.367	7	Chloritoid
	2.340	9	Kaolinite (not influenced by chlorite)
	2.340	2	Siderite
	2.330	2	Anhydrite (202) (for preferred orientation)
	2.326	9	Dickite
1	**2.315**	**10**	**Cookeite**
	2.306	7	Chloritoid
	2.289		Kaolinite
	2.280	2	Calcite
	2.280		Quartz
	2.260	2	Sepiolite
	2.240	2	Calcite
	1.990	5	Halite (220) (when ZnO standard is used)
	1.797	6	Ankerite
	1.790	3	Dolomite (018, 116) (when ZnO standard is used)
	1.736	2	Siderite (018) (116) (when ZnO standard is used)
	1.720		Smectite (Nontronite)
	1.687	6	Rutile
2	1.633	10	**Pyrite**
Range2			
Before measuring peaks in range 2 the a quartz standard must be imported, aligned scaled and subtracted. See sidepack instructions for details.			
Then import the zincite standard and align, scale and subtract. If the product looks unrealistic then repeat after adjusting the scale of the standard until a smooth slope for the kaolinite 006 peak is obtained.			
Import the illite standard, align, scale and subtract.			
	1.581	8	Chloritoid
	1.560		Palygorskite **(060)**
	1.550 - 1.560	2--7	Fe-Chlorite **(060)**
	1.552	1	Fe-Chlorite **(060)** Orthochamosite
	1.551	9	Fe-Chlorite **(060)** Chamosite
	1.540 - 1.550		Sepiolite **(060)**

	1.538 - 1.549	2--7	Mg-Chlorite **(060)**
	1.541	2	Quartz
	1.541		Vermiculite **(060)**
	1.540	8	Biotite **(060)**
	1.539	10	Mg-Chlorite **(060)** Clinochlore
	1.537	5	Vermiculite **(060)**
	1.535	7	Smectite (Saponite)
	1.531 - 1.538		Serpentines **(060)**
	1.530	10	Smectite (Hectorite) **(060)**
	1.530	7	Smectite (Saponite) **(060)**
	1.510 - 1.530	2-10	2:1 Fe rich clays (glauconite or celadonite) **(060)**
	1.528	1	Vermiculite **(060)**
	1.527	5	Talc **(060)**
	1.520	5	Berthierine **(060)**
	1.520		Smectite (Nontronite)
	1.511		Glauconite **(060)**
	1.505	6	Clintonite **(060)**
	1.500	6	Smectite (Montmorillonite) **(060)**
	1.499 - 1.505		2:1 Al-rich clays (smectite-illite) **(060)**
Note: the kaolinite peak must be measured from the scan before it was removed.			
Now import the kaolinite standard and align, scale and subtract.			
	1.492	2-3	Pyrophyllite **(060)**
	1.489	8	Kaolinite **(060)**
	1.489	1	Al-Chlorite **(060)** Cookeite
	1.485	5	Clintonite (060)
	1.484	2	Hematite
	1.484	5	Halloysite
	1.477	3	Zincite (103) (for mudstone)
	1.452	4	Kaolinite (060)

Brown and Brindley, 1980; Anthony et al., 2001

2. Before measuring the peak areas the diffractogram needs to be aligned and adjusted. This takes several steps.

a) Open the toolbox. This can be done by pressing F2 on the keyboard or clicking on the hammer and screwdriver icon at the top of the screen. This opens a smaller window within the main window (if it is not already open).

b) Within this window under the tab SCANS, select the first scan (range 1) in the list of diffractograms. Click the 'Backgnd' button towards the bottom and then the 'Append' button in the bottom right. This will produce a new scan that has been zeroed to the baseline. You can now turn off the original scans (likely the first one in the list) by double clicking the checked box from the list of scans.

c) Now click on the 'Strip KA2' and then the 'Replace' button above the 'Append' button in the bottom right.

d) Due to variations in slide thicknesses peaks will vary in their positions along the X-axis. The next step is to correctly position the scans along the X-axis. This is achieved by aligning the scan to the quartz standards or other common standards.

To adjust the X-offset, select 'X-Offset' button within the toolbox window. The previously selected standards are displayed as vertical lines at the location of key peaks for Zincite (2.81 Å, 2.60 Å and 2.47 Å) and for quartz (4.26 Å, 3.34 Å/24.24 2-theta, Co radiation). Once you are happy with the position of the scan then click the "Replace" button.

(**Note:** If you are comfortable with the program you can use the replace button instead of the append button every time. This will reduce the amount of scans in the

list. It is advisable to append the first adjustment performed to the scan to preserve the original unaltered scan).

Measuring non-sidepack peak areas

1. Within the main window zoom to the desired area to be measured.

2. Now, within the toolbox click on the AREA tab at the top.

3. Select the 'Create' button from the bottom right.

4. Moving back to the main window you will notice that the mouse icon has changed to a downward pointing arrow. Position this at the edge and base of the desired peak and click & drag to the other side of the peaks base. This will provide the area measurement for the peak. It is best to follow a logical progression, i.e. starting at one end of the scan working your way to the other in this way the measurements will be placed in order. Use Table 1 to aid in mineral peak identification.

5. After reaching the last peak to be measured select all the measurement within the tool box window and copy/paste into an excel spread sheet.

MEASURING X-RAY DIFFRACTION PEAKS IN THE XRD EVALUATION PROGRAM (EVA) (Sidepack)

Introduction to sidepack XRD

Sidepack XRD slides are randomly oriented powder mounts. The slides produce diffractograms containing two ranges. The first range is from approximately 24 Å to 1.60 Å and it records measurements from 5° 2-theta to 69.5° 2-theta with a step interval of 0.02° 2-theta every two seconds. The second range is from approximately 1.60 Å to

1.43Å and it records measurements from 69.5° 2-theta to 77° 2-theta with a step interval of 0.01° 2-theta every 5 seconds. The second range resolves the 060 reflections peak.

Typically, an internal standard of zincite is added during the sample preparation. These internal standards are needed for quantitative measurements and alignment of diffractogram peaks. Alternatively, samples often contain enough naturally occurring quartz that it may also be used for alignment of peaks along the x-axis.

It is best to use the zincite .dif standard file to match up with the added internal standard, when performing the x-offset, because it is a control. The quartz peak can be used as a secondary source of accuracy in alignment. Table 1 provides some key peak locations.

Instructions for measuring sidepack XRD peak areas using the XRD Evaluation Program (EVA)

For range 1: follow the previous instructions. Remove the background, K2a and X-offset for Range 2.

The X-offset of range 2 does not need to match that of range 1; however, there should not be a drastic difference. Look at the value of offset applied to range 1. Try entering this value in for range 2 (to see the adjustment click on one of the other text boxes and then click on the slider on the slider bar, trying not to move it). Does the zincite peak align with the standards position? If so great if not make the needed corrections to align this scan, but if there is drastic differences in the degree of offset

between the two scans then there is something is wrong with your offsets and you will need to re-evaluate the positioning of both scans.

Measuring peak areas in range 1

Refer to instructions beginning on page 7.

Measuring peak areas in range 2

1. Measuring these peaks involves a little more work and judgment.

2. It first requires some of the peaks to be removed from the scan as that the underlining peaks may be calculated. Import the raw files for the standard scans for zincite, quartz, illite, and kaolinite (if you have them, if not they will need to be made). Starting with zincite and moving through the list in order each one should be imported, adjusted and subtracted individually prior to importing the next one on the list.

3. Both ranges for these scans should have already undergone the same initial processing, removing background, aligning on the x-axis to the zincite and quartz peaks, and stripping of the K-alpha. However, you may need to make minor adjustments with the x-axis.

- **Zincite** peak should be at 1.477 Å
- **Quartz** peak should be at 1.541 Å
- **Illite** peak should be at 1.499-1.505 Å
- **Kaolinite** peak should be at 1.489 Å

4. Once these steps are completed concentration is now given to 'range 2' where the 060 peaks are located.

5. First the Zincite standard peak is scaled to fit the zincite peak of the sample. To do this select the Y-scale button in the tool box and use the slider on the left to scale the peak. The blue arrow buttons can be used to increase or decrease the range of movement. These are useful in the fine tuning of the peak height. Attention should be place to the over all fit of the peak not just height.

6. Within the tool box in EVA there is an 'ADD/Sudt.' Button, which allows for scans to be added, subtracted and merged. By subtracting the peaks of zincite, quartz, kaolinite and illite the lesser 060 peaks can become easier to measure.

The steps to removing peaks are as follows:

a) Click the 'add/subt.' button.

b) On the left select 'A-B'.

c) From the list of scans select the 'range 2' pattern for the sample.

d) Click 'change' A.

e) Select the zincite standard scan from the list.

f) Click 'change' B.

g) This should show a new scan without the zincite standard peak at 1.47 Å.

h) If this scan looks reasonable keep it by clicking "Append". This will produce a new scan without the zincite peak at 1.477 Å. This will be your new scan from which the quartz peak at 1.544 Å will be subtracted using the same methods as above.

i) If the subtracted peak looks unreasonable then re-assess the overlay. It likely requires some tweaking by adjusting the peak height through the Y-scale button or peak position through the X-shift button. This holds true for all subtracted peaks and many

often require several attempts before the desired subtraction is made. Once you are happy with the produced scan move on to the quartz repeat the above steps (remember step c now uses the newest scan created after removing the last peak), then remove illite.

j) After removing illite measure the 1.489 Å kaolinite peak, before removing it.

k) In many of the Nova Scotia samples, the illite and kaolinite peaks are sufficiently small that they do not need to be removed.

SUMMARY RECIPE FOR PICKING SIDEPACK SLIDES:

-**For Range 1 and 2:**

- Background--Then Append
- Strip KA_2-- Then Replace
- Smooth—Then Replace
- Import zincite (zincite.spk1 [001].dif) and quartz (quartz.spk1 [001].dif) .dif standards
    - Adjust X-offset-- Then Replace

-Change scan colour to guard against confusion.

-Try to make sure the X-offset for each scan is not drastically different.

-Measure Peaks on range 1

-**For Range 2 (060):**

- Smooth--Then Append
- Import zincite standard peak Zincite1spk_Adj_Align (x-scale should be 1.477Å)

- Smooth--Then Append
- Y-Scale-- Adjust, then Append
- X-offset-- Adjust, then Append
- Add./Subt-- Select 'A-B'
  - Select range 2-- change A
  - Select zincite standard-- change B

-Make sure the standard peak and the sample peak line up, if not, repeat the process.

-Change scan colour to guard against confusion.

- Import quartz standard peak Quartz1spk_Adj_Align (x-scale should be 1.541Å)
  - Smooth--Then Append
  - Y-Scale-- Adjust, then Append
  - X-offset-- Adjust, then Append
  - Add./Subt-- Select 'A-B'
    - Select range 2-- change A
    - Select zincite standard-- change B

-Make sure the standard peak and the sample peak line up, if not, repeat the process.

-Change scan colour to guard against confusion.

- Import illite standard peak illite_no_qzt_Adj_Align (x-scale should be 1.499-1.505Å)
  - Smooth--Then Append
  - Y-Scale-- Adjust, then Append
  - X-offset-- Adjust, then Append

- Add./Subt-- Select ‘A-B’
    - Select range 2-- change A
    - Select zincite standard-- change B

-Make sure the standard peak and the sample peak line up, if not, repeat the process.

-Change scan colour to guard against confusion.

-Prior to removing the kaolinite peak, pick the kaolinite peak located at 1.489Å.

- Import kaolinite standard peak Kaolinite2spk_Adj_Align (x-scale should be 1.489Å)
    - Smooth--Then Append
    - Y-Scale-- Adjust, then Append
    - X-offset-- Adjust, then Append
    - Add./Subt-- Select ‘A-B’
        - Select range 2-- change A
        - Select zincite standard-- change B

-Make sure the standard peak and the sample peak line up, if not, repeat the process.

-Change scan colour to guard against confusion.

-Pick any other desired peaks.